Springer Series in

OPTICAL SCIENCES **147**

founded by H.K.V. Lotsch

Springer Series in

OPTICAL SCIENCES

The Springer Series in Optical Sciences, under the leadership of Editor-in-Chief *William T. Rhodes*, Georgia Institute of Technology, USA, provides an expanding selection of research monographs in all major areas of optics: lasers and quantum optics, ultrafast phenomena, optical spectroscopy techniques, optoelectronics, quantum information, information optics, applied laser technology, industrial applications, and other topics of contemporary interest.
With this broad coverage of topics, the series is of use to all research scientists and engineers who need up-to-date reference books.
The editors encourage prospective authors to correspond with them in advance of submitting a manuscript. Submission of manuscripts should be made to the Editor-in-Chief or one of the Editors. See also www.springer.com/series/624

Rosario Martínez-Herrero · Pedro M. Mejías · Gemma Piquero

Characterization of Partially Polarized Light Fields

Springer

Prof. Rosario Martínez-Herrero
Universidad Complutense de Madrid
Faculty of Physics
Optics Department, 28040 Madrid
Spain
r.m-h@fis.ucm.es

Prof. Pedro M. Mejías
Universidad Complutense de Madrid
Faculty of Physics
Optics Department, 28040 Madrid
Spain
pmmejias@fis.ucm.es

Dr. Gemma Piquero
Universidad Complutense de Madrid
Faculty of Physics
Optics Department, 28040 Madrid
Spain
piquero@fis.ucm.es

ISSN 0342-4111 e-ISSN 1556-1534
ISBN 978-3-642-01326-3 e-ISBN 978-3-642-01327-0
DOI 10.1007/978-3-642-01327-0
Springer Dordrecht Heidelberg London New York

Library of Congress Control Number: 2009927003

Cover design: eStudio Calamar S.L., Gerona, Spain

Printed on acid-free paper

Springer is part of Springer Science+Business Media (www.springer.com)

Preface

Polarization involves the vectorial nature of light. In theoretical topics and technological applications of current interest in optical science, the electromagnetic description of the light disturbance and polarization-related phenomena have turned out to be crucial. In fact, they have gained importance in recent years, attracting the attention of numerous scientists in the last decade. Photonics devices, biological optics, optical communications, atmospheric optics, and sensor technologies are examples of research areas where the vectorial features of light are relevant.

In practice, optical radiation exhibits randomness and spatial nonuniformity of the polarization state. These kinds of realistic and general situations are most frequently encountered in the literature, and drastically depart from the simplest model of harmonic plane waves. Keeping in mind the framework of classical optics, this book deals with the analytical problem of describing and characterizing the polarization and spatial structure of nonuniformly polarized fields, along with their evolution when light propagates through optical systems. This is the aim of this work.

In particular, the scope and the contents of the book are essentially focused on the contributions of the authors to four main issues, which correspond to approaching the problem under study from different angles. Thus, in Chap. 1, after a short introduction to the main standard representations of the polarization, we analyze in some detail several recently proposed measurable parameters, of practical use for characterizing, in a global way, the polarization of nonuniformly polarized beam-like fields. Chapter 2 also proposes an overall description, but now the alternative formalism allows a characterization of the polarization distribution and the shape of partially polarized, partially coherent beams. A family of measurable and meaningful parameters is defined, whose determination involves certain averages over the region of the transverse profile where the beam irradiance is significant.

On the other hand, in recent years, the coherence theory, well established for scalar beams, has been investigated with regard to partially polarized fields. It has been shown that, for stochastic electromagnetic beams, the properties concerning coherence and polarization features are, in general, connected with each other. Consequently, fundamental concepts, such as the degree of coherence and the fringe visibility in Young interferometers, should be revisited. This is done in some detail in Chap. 3.

Finally, Chap. 4 is devoted to nonparaxial electromagnetic fields, which arise when light is strongly focused and the beam reaches a waist size even smaller than the wavelength. The theoretical analysis deals with certain kinds of nonparaxial exact solutions of the Maxwell equations. Their polarization features are discussed and, in those cases in which the evanescent waves are significant (highly nonparaxial regime), their field structure is also described.

Although short surveys are provided to review some basic formalisms, the reader is assumed to be familiar with well-known concepts treated in many optics textbooks.

The research work leading to the results reported in this book have been obtained in collaboration with a number of researchers. We would like to acknowledge here their fundamental contribution. We also thank Prof. H. Weber for his interest, helpful suggestions and continuous kindness, which include support during all the experimental work described in Sect. 2.4.3 and performed at the Optisches Institut of the Technische Universität in Berlin. We are indebted to Prof. F. Gori, Dr. M. Santarsiero and Dr. R. Borghi, at the University of Rome 3, for helpful discussions concerning partially polarized Gaussian Schell-model beams. In addition, we are also grateful to Dr. M. Santarsiero and Profs. S. Bosch and A. Carnicer, at Barcelona University, for their kind reading of Chaps. 3 and 4.

This work was supported by the Ministerio de Educación y Ciencia of Spain, Project FIS2007-63396, and by the Comunidad de Madrid, Project: CCG07-UCM/ESP-3070.

Contents

Notation

Symbol	Name	First appearance in the text (Subsection)
$[\alpha\beta]_{ij}, i,j = s,p;$ $\alpha,\beta = x,y,u,v$		2.3.2
Det	determinant of a matrix	1.2.1
$\boldsymbol{E}$	electric field vector	1.2.1
$\tilde{\boldsymbol{E}},\tilde{\boldsymbol{H}}$	spatial Fourier transform of $\boldsymbol{E}$ and $\boldsymbol{H}$	4.2.1
$\boldsymbol{e}_1(\phi),\boldsymbol{e}_2(\rho,\phi)$		4.2.3
$\tilde{\boldsymbol{E}}_0(\rho,\phi)$		4.2.1
$\boldsymbol{E}_{azim}$	azimuthally polarized field	4.3.3
$\boldsymbol{E}_{closest},\boldsymbol{H}_{closest}$	closest electric and magnetic fields	4.4.2
$\boldsymbol{e}_{ev}(\rho,\phi)$		4.5.1
$\boldsymbol{E}_{pr},\boldsymbol{E}_{ev}$	propagating and evanescent terms of $\boldsymbol{E}$	4.2.2
$\boldsymbol{E}_R,\boldsymbol{E}_\theta$	radial and azimuthal components of $\boldsymbol{E}$	1.5.1
$\boldsymbol{E}_{rad}$	radially polarized field	4.3.2
$\boldsymbol{E}_s,\boldsymbol{E}_p$	transverse components of $\boldsymbol{E}$	1.2.1
$\boldsymbol{E}_{TE},\boldsymbol{E}_{TM}$	transverse-electric and transverse-magnetic terms of $\boldsymbol{E}$	4.2.3
$\Gamma(\boldsymbol{r}_1,\boldsymbol{r}_2,\tau)$	mutual coherence function	1.2.2
$\hat{\Gamma}(\boldsymbol{r}_1,\boldsymbol{r}_2,\tau)$		1.2.2
$g_{12} \equiv g(\boldsymbol{r}_1,\boldsymbol{r}_2)$		3.4
$\boldsymbol{H}$	magnetic field vector	4.2.1
$\boldsymbol{H}_{TE},\boldsymbol{H}_{TM}$	transverse-electric and transverse-magnetic terms of $\boldsymbol{H}$	4.2.3
$h(\boldsymbol{r},\boldsymbol{\eta},z)$	Wigner distribution function	2.2.1
$\hat{\boldsymbol{H}}(\tilde{\boldsymbol{r}},\tilde{\boldsymbol{\eta}},z)$	Wigner matrix	2.3.1
$\hat{\mathfrak{J}}$	Jones matrix	1.2.1
$\hat{J}(\boldsymbol{r}_1,\boldsymbol{r}_2,z)$	coherence-polarization matrix	1.2.2
$j(\boldsymbol{r}_1,\boldsymbol{r}_2)$	complex degree of coherence	1.6.1
$J_{sc}(\boldsymbol{r}_1,\boldsymbol{r}_2)$	mutual intensity	1.6.1
k	wavenumber	1.2.1
K	Kurtosis parameter	2.9
λ	wavelength	1.2.1
M^2	beam propagation factor	2.5

Symbol	Name	First appearance in the text (Subsection)
$\hat{\mathcal{M}}$	Müller matrix	1.2.3
$\mu(\boldsymbol{r}_1,\boldsymbol{r}_2)$	spectral degree of coherence (scalar case)	3.2.1
μ_s and μ_I	intrinsic degrees of coherence	3.3.2
μ^2_{STF}	electromagnetic degree of coherence	3.3.2
μ_w	Wolf's spectral degree of coherence	3.3.2
$\tilde{P}$	weighted degree of polarization	1.3
P_G	generalized degree of polarization	2.4.1
$P(\boldsymbol{r})$	local degree of polarization	1.2.4
P_{st}	standard degree of polarization	1.2.4
Q	beam quality parameter	2.5
$\tilde{\boldsymbol{r}} \equiv \boldsymbol{r}k$	dimensionless position vector	2.3.1
$\tilde{\rho}$	linear/circular polarization content	1.4.1
$\tilde{\rho}_R,\tilde{\rho}_\theta$	radial and azimuthal polarization content	1.5.1
$\boldsymbol{S}$	Stokes vector	1.2.3
$\boldsymbol{s}(\rho,\phi)$		4.2.3
$\boldsymbol{s}_{ev}(\rho,\phi)$		4.5.1
$s_i, i = 0,1,2,3$	Stokes parameters	1.2.3
$\hat{S}_i, i = 0,1,2,3$	Stokes matrices	2.3.2
$\hat{\sigma}_i, i = 0,1,2,3$	Pauli matrices	1.2.1
$\tilde{\sigma}_p$	variance associated to $\tilde{P}$	1.3
σ_ρ	variance associated to $\tilde{\rho}$	1.4.1
σ_R,σ_θ	variance associated to $\tilde{\rho}_R,\tilde{\rho}_\theta$	1.5.1
$\langle\cdot\rangle_t$	temporal average	1.2.2
Tr	trace of a matrix	1.2.1
$\boldsymbol{u}_R,\boldsymbol{u}_\theta$	radial and azimuthal unitary vector	1.5.1
$\mathcal{V}$	visibility	3.2.2
ω	angular frequency	1.2.1
$W(\boldsymbol{r}_1,\boldsymbol{r}_2)$	cross-spectral density function	2.1
$\hat{W}(\boldsymbol{r}_1,\boldsymbol{r}_2)$	cross-spectral density matrix	2.3.1
$\langle x^m y^n u^p v^q \rangle$	beam irradiance moments	2.2.1
$\hat{\zeta}_i, i = 0,1,2,3$		2.3.4
z_R	Rayleigh length	2.7

List of Acronyms

Acronym	Name
APF	azimuthally polarized field
APP	anisotropic pure phase plate
BCP matrix	beam coherence-polarization matrix
CDT	cross-spectral density tensor
CSD	cross-spectral density
GSM field	Gaussian Schell-model field
MSC field	mean-square coherent field
MZT system	Mach-Zehnder-type system
NP field	nonpolarized field
NUPP field	nonuniformly partially polarized field
NUTP field	nonuniformly totally polarized field
PGSM field	partially polarized Gaussian Schell-model field
RPF	radially polarized field
RPM field	radially-polarized-maintained field
SA	spherical aberration
SDC	spectral degree of coherence
SDT	spectral density tensor
SPE	spiral phase element
SUPA system	spatially-uniform polarization altering system
UP field	uniformly polarized field
UPP field	uniformly partially polarized field
UTP field	uniformly totally polarized field
WDF	Wigner distribution function

Chapter 1
Representations of the Polarization of Beamlike Fields

1.1 Introduction

This chapter deals with the problem of characterizing the polarization of light waves behaving as beamlike fields, i.e., fields whose electric vector $\boldsymbol{E}$ essentially lies in planes orthogonal to the direction of propagation. This occurs within the so-called paraxial approach, in which the longitudinal component of $\boldsymbol{E}$ is negligible to good accuracy. A major simplification can then be introduced to the calculations.

As will become apparent later, information about the polarization can be given through position-dependent functions, vectors and matrices, as well as by means of global parameters and figures of merit. The specific choice of one of these representations depends on each particular problem, including possible experimental limitations.

This chapter reviews such representations. Thus, in the next section, a short survey is given of several existing formalisms, extensively reported in textbooks, and commonly used to describe the polarization of light beams. Section 1.3 introduces the local degree of polarization but now averaged over the regions where the beam irradiance is significant. Such a measurable figure of merit enables a simple characterization of the overall polarization and its cross-sectional uniformity. This idea also applies in Sects. 1.4 and 1.5, which consider recently proposed measurable parameters that provide information about the transverse polarization distribution of totally polarized fields. Finally, Sect. 1.6 studies the particular case of partially polarized Gaussian Schell-model beams, which has received special attention in the literature.

1.2 Standard Representations of the Polarization

In this section we will briefly summarize the main standard formalisms applied to describe and handle the polarization of a light beam, namely, those based on the Jones matrices, the Müller calculus and, more recently, on the so-called beam coherence-polarization matrix (Gori, 1998a; Gori et al., 1998b). By means of vectors or matrices, all these treatments provide information about the local polarization of

R. Martínez-Herrero et al., *Characterization of Partially Polarized Light Fields*, Springer Series in Optical Sciences 147, DOI 10.1007/978-3-642-01327-0_1,

the field. This is the key conceptual difference with respect to the formalism we will introduce in the next chapter, in which the polarization will be characterized by means of global parameters that take into account the overall spatial structure of the beam in the near- and the far-field regimes.

Let us also remark that, in the following, the polarization state will be represented by the electric field vector associated with the electromagnetic disturbance (the magnetic field vector will be disregarded). This simplification should be understood as a consequence of the nature of the detection process usually involved in the experiments.

1.2.1 The Jones Calculus

To begin with, let us consider a monochromatic plane wave propagating along the z-axis. The associated electric field vector $\boldsymbol{E}$ can then be written in the form

$$\boldsymbol{E} = \begin{pmatrix} E_s \\ E_p \end{pmatrix} = \begin{pmatrix} a_s \exp\left[i\left(kz - \omega t + \delta_s\right)\right] \\ a_p \exp\left[i\left(kz - \omega t + \delta_p\right)\right] \end{pmatrix}, \tag{1.1}$$

where the subscripts s and p refer to the Cartesian components transverse to the direction of propagation z (see Fig. 1.1), $k = 2\pi/\lambda$ is the wavenumber of the light field (λ being the wavelength), ω the angular frequency of the light, and the coefficients a_j, δ_j, $j = s, p$, denote the amplitudes and phases associated with the transverse components. Note that the real (measurable) field would be given by $\boldsymbol{E}_{real} = \frac{1}{2}(\boldsymbol{E} + \boldsymbol{E}^*)$. We adopt, however, complex notation because, throughout this book, linear optics is considered. Of course, no physical difference should arise if one uses the notation $\exp[\mathrm{i}(\omega t - kz)]$ rather than its conjugate (see Eq. (1.1)). The choice can be selected for convenience.

It should also be remarked that the monochromatic plane wave used in the following discussions cannot be realized experimentally. The Jones formalism, however, holds also for quasi-monochromatic fields in the paraxial approach. More specifically, the following restrictions are assumed:

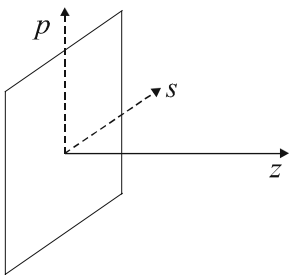

Fig. 1.1 Schematic of the Cartesian coordinate system. The plane wave propagates along the z-direction

– spectral bandwidth << mean angular frequency,
– divergence at the far field << 1,
– $\partial E/\partial z << kE$, where E refers to the magnitude of the field components.

As is well known in the literature (Azzam and Bashara, 1987; Born and Wolf, 1999; Brosseau, 1998; Chipman, 1994; Collett, 1992; Goldstein, 2003; Shurcliff, 1962), the so-called Jones vector that represents this field at some plane z is defined as

$$\boldsymbol{E} = \begin{pmatrix} a_s \exp(i\delta_s) \\ a_p \exp(i\delta_p) \end{pmatrix}. \tag{1.2}$$

Within the framework of the Jones calculus, the behavior of polarizing deterministic optical systems can be characterized by means of 2×2 matrices (the Jones matrices), which relate the input to the output fields travelling along the optical element. This is expressed in the form

$$\boldsymbol{E}_{output} = \hat{\mathfrak{J}}\,\boldsymbol{E}_{input} = \begin{pmatrix} \mathfrak{J}_{11} & \mathfrak{J}_{12} \\ \mathfrak{J}_{21} & \mathfrak{J}_{22} \end{pmatrix} \begin{pmatrix} E_s \\ E_p \end{pmatrix}_{input} \tag{1.3}$$

where $\mathfrak{J}_{mn}$, $m, n = 1, 2$, are complex numbers, and letters with a caret will denote matrices from now on. In general, the optical elements change the polarization state of the incident field by modifying its amplitude and/or phase, thus altering the components of the associated Jones vector.

It is also interesting to point out that any 2×2 matrix does not represent, in general, a realizable Jones matrix. Conditions for physical realisability of deterministic Jones matrices are (Brosseau, 1998)

$$0 \leq \mathrm{Tr}(\hat{\mathfrak{J}}\hat{\mathfrak{J}}^{\dagger}) \leq 2, \tag{1.4a}$$

and

$$\left|\mathrm{Det}\hat{\mathfrak{J}}\right|^2 \leqslant 1, \tag{1.4b}$$

where Tr and Det stand for trace and determinant, respectively, and the dagger symbolizes the adjoint (transposed conjugate) matrix.

The propagation law through cascaded optical systems follows from the product of the successive Jones matrices, i.e.,

$$\boldsymbol{E}_{output} = \hat{\mathfrak{J}}\,\boldsymbol{E}_{input} = \hat{\mathfrak{J}}_M \hat{\mathfrak{J}}_{M-1} \cdots \hat{\mathfrak{J}}_2 \hat{\mathfrak{J}}_1 \boldsymbol{E}_{input}, \tag{1.5}$$

where $\hat{\mathfrak{J}}_p$, $p = 1, \ldots, M$, denote the Jones matrices of the optical elements.

In general, a Jones matrix has two eigenvectors, $\boldsymbol{E}_a$ and $\boldsymbol{E}_b$, which obey the eigenvalue equations

$$\hat{\mathfrak{J}}\boldsymbol{E}_a = a\boldsymbol{E}_a, \tag{1.6a}$$

$$\hat{\mathfrak{J}}\boldsymbol{E}_b = b\boldsymbol{E}_b. \tag{1.6b}$$

These fields should be understood as eigenpolarization states, which retain their character after propagation through the system represented by the Jones matrix.

Let us also note that a Jones matrix can be written as a linear combination of the Pauli spin matrices (O'Neill, 1963; Whitney, 1971):

$$\hat{\mathfrak{J}} = \sum_{m=0}^{3} c_m \hat{\sigma}_m, \tag{1.7}$$

where $\hat{\sigma}_0$ represents the 2×2 identity matrix,

$$\hat{\sigma}_1 = \begin{pmatrix} 1 & 0 \\ 0 & -1 \end{pmatrix}, \tag{1.8a}$$

$$\hat{\sigma}_2 = \begin{pmatrix} 0 & 1 \\ 1 & 0 \end{pmatrix}, \tag{1.8b}$$

$$\hat{\sigma}_3 = \begin{pmatrix} 0 & -i \\ i & 0 \end{pmatrix}, \tag{1.8c}$$

and the coefficients c_m are complex numbers given by

$$c_n = \frac{\mathrm{Tr}(\hat{\mathfrak{J}}\hat{\sigma}_n)}{2}. \tag{1.9}$$

It is important to note that, in this introductory example, both the amplitude and the polarization state of this field are uniform across any transverse plane. In a general case, however, $\boldsymbol{E}$ would be a position-dependent function at each beam cross section. Moreover, the Jones matrices can also be position dependent (see, in this connection, Chap. 3).

To end this short survey of the Jones theory we recall that the transversality condition for the electric vector $\boldsymbol{E}$ implies that the fields are assumed to exhibit a typically small divergence. Precise studies demonstrate that, in this paraxial approach, the longitudinal field component is two or three orders of magnitude smaller than the global field amplitude itself (Mejías et al., 2002; Simon et al., 1987). Light beams beyond the paraxial approximation will be considered later, in Chap. 4.

A more detailed and rigorous treatment of the Jones calculus can be found, for example, in (Brosseau, 1998).

1.2.2 Coherence-Polarization Matrices

A description of the vectorial properties of a random electromagnetic light field, assumed to be stationary and ergodic (at least up to second-order), is provided by four coherence matrices, whose elements are (Beran and Parrent, 1967; Perina, 1971; Wolf, 1959)

$$\mathcal{E}_{jk} = \langle E_j^* (\boldsymbol{r}_1,t)\, E_k (\boldsymbol{r}_2,t+\tau)\rangle_t, \tag{1.10a}$$

$$\mathcal{H}_{jk} = \langle H_j^* (\boldsymbol{r}_1,t)\, H_k (\boldsymbol{r}_2,t+\tau)\rangle_t, \tag{1.10b}$$

$$\mathcal{M}_{jk} = \langle E_j^* (\boldsymbol{r}_1,t)\, H_k (\boldsymbol{r}_2,t+\tau)\rangle_t, \tag{1.10c}$$

$$\mathcal{N}_{jk} = \langle H_j^* (\boldsymbol{r}_1,t)\, E_k (\boldsymbol{r}_2,t+\tau)\rangle_t \tag{1.10d}$$

where E_j and H_k , $j, k = s, p, z$, denote the three Cartesian components of the electric and magnetic fields, respectively. In these equations $\boldsymbol{r}_1$ and $\boldsymbol{r}_2$ are position vectors, t is the temporal variable, τ a time interval, and the symbol $\langle\ \rangle_t$ represents a temporal average. In this sense, note that, since the field is ergodic, temporal and ensemble averages are equivalent.

The elements of the above coherence matrices give the correlations between the components of the electric and magnetic fields at two points, $\boldsymbol{r}_1$ and $\boldsymbol{r}_2$, evaluated at different times, t_1 and t_2, separated by the time interval $t_1 - t_2 = \tau$. It should be noted that the matrix elements do not depend on the time origin but only on the time difference τ because of the stationarity assumption. In addition, since

$$\mathcal{M}_{kj} (\boldsymbol{r}_1,\boldsymbol{r}_2,\tau) = \mathcal{N}_{jk}^* (\boldsymbol{r}_2,\boldsymbol{r}_1,-\tau), \tag{1.11}$$

the information contained in matrices $\hat{\mathcal{M}}$ and $\hat{\mathcal{N}}$ is equivalent, so that a set of 3×3 independent matrices would then suffice to characterize up to second order the electromagnetic disturbance.

Let us now restrict ourselves to a electric-vector description within the transverse approximation. In such a case, a single 2×2 matrix, $\hat{\Gamma}$, is required instead of the previous 3×3 coherence matrices. If we choose the z-axis as the effective direction of propagation of the beamlike field, the matrix $\hat{\Gamma}$ takes the form

$$\hat{\Gamma} (\boldsymbol{r}_1,\boldsymbol{r}_2,z;\tau) = \begin{pmatrix} \Gamma_{ss} (\boldsymbol{r}_1,\boldsymbol{r}_2,z;\tau) & \Gamma_{sp} (\boldsymbol{r}_1,\boldsymbol{r}_2,z;\tau) \\ \Gamma_{ps} (\boldsymbol{r}_1,\boldsymbol{r}_2,z;\tau) & \Gamma_{pp} (\boldsymbol{r}_1,\boldsymbol{r}_2,z;\tau) \end{pmatrix}, \tag{1.12}$$

where $\boldsymbol{r}_1$ and $\boldsymbol{r}_2$ denote now position vectors lying in a transverse plane $z =$ constant, and

$$\Gamma_{lm} (\boldsymbol{r}_1,\boldsymbol{r}_2,z;\tau) = \langle E_l^* (\boldsymbol{r}_1,z;\tau)\, E_m (\boldsymbol{r}_2,z;t+\tau)\rangle_t; \quad l,m = s,p. \tag{1.13}$$

As is quite apparent from Eq. (1.12), matrix $\hat{\Gamma}$ is the natural vectorial generalization of the well-known scalar mutual coherence function

$$\Gamma (\boldsymbol{r}_1,\boldsymbol{r}_2,\tau) = \langle E^* (\boldsymbol{r}_1,t)\, E (\boldsymbol{r}_2,t+\tau)\rangle_t. \tag{1.14}$$

In the present book we will focus attention on quasi-monochromatic light whose effective spectral width is $\Delta\nu$ (around a central frequency ν). If we further assume that any time delay is small compared with the coherence time $1/\Delta\nu$ (Mandel and

Wolf, 1995; Perina, 1971; Wolf, 2007) the matrix $\hat{\Gamma}$ becomes

$$\hat{\Gamma}\left(\boldsymbol{r}_1,\boldsymbol{r}_2,z;\tau\right) = \hat{J}\left(\boldsymbol{r}_1,\boldsymbol{r}_2,z\right)\exp\left(-2\pi i\nu\tau\right), \tag{1.15}$$

where

$$\hat{J}\left(\boldsymbol{r}_1,\boldsymbol{r}_2,z\right) = \begin{pmatrix} J_{ss}\left(\boldsymbol{r}_1,\boldsymbol{r}_2,z\right) & J_{sp}\left(\boldsymbol{r}_1,\boldsymbol{r}_2,z\right) \\ J_{ps}\left(\boldsymbol{r}_1,\boldsymbol{r}_2,z\right) & J_{pp}\left(\boldsymbol{r}_1,\boldsymbol{r}_2,z\right) \end{pmatrix}, \tag{1.16}$$

is called the beam coherence-polarization (BCP) matrix (Gori, 1998a; Gori et al., 1998b). In the above equation

$$J_{lm}\left(\boldsymbol{r}_1,\boldsymbol{r}_2,z\right) = \langle E_l^*\left(\boldsymbol{r}_1,z;t\right)E_m\left(\boldsymbol{r}_2,z;t\right)\rangle_t,\ l,m = s,p. \tag{1.17}$$

The BCP matrix constitutes a useful tool that provides a joint description of the polarization and spatial coherence properties of a partially polarized, partially coherent beam. Its diagonal elements, J_{ss} and J_{pp}, could then be understood as the mutual intensities of the beam after propagating through ideal linear polarizers whose transmission axes are the s-axis and the p-axis, respectively. Actually, $\hat{J}$ has only three independent elements, due to the relation between its nondiagonal elements

$$J_{sp}\left(\boldsymbol{r}_1,\boldsymbol{r}_2,z\right) = J_{ps}^*\left(\boldsymbol{r}_2,\boldsymbol{r}_1,z\right). \tag{1.18}$$

Finally, it should be remarked that all the elements of the BCP matrix are measurable functions, which can be experimentally determined, for example, through certain Young interference experiments (Gori et al., 1998b).

1.2.3 The Stokes-Müller Calculus

The local structure of the polarization of a beam-like field can be inferred from the BCP matrix with equal arguments $\boldsymbol{r}_1 = \boldsymbol{r}_2 = \boldsymbol{r}$. However, from a practical point of view, at each transverse plane z, an alternative four-parameter representation of polarized light is given in terms of the Stokes vector $\boldsymbol{S} = (s_0,s_1,s_2,s_3)$, whose components are the well-known Stokes parameters, defined in terms of the elements of matrix $\hat{J}$ in the form

$$s_0\left(\boldsymbol{r}\right) = J_{ss}\left(\boldsymbol{r}\right) + J_{pp}\left(\boldsymbol{r}\right), \tag{1.19a}$$

$$s_1\left(\boldsymbol{r}\right) = J_{ss}\left(\boldsymbol{r}\right) - J_{pp}\left(\boldsymbol{r}\right), \tag{1.19b}$$

$$s_2\left(\boldsymbol{r}\right) = 2\mathrm{Re}[J_{sp}(\boldsymbol{r})], \tag{1.19c}$$

$$s_3\left(\boldsymbol{r}\right) = 2\mathrm{Im}\left[J_{sp}\left(\boldsymbol{r}\right)\right], \tag{1.19d}$$

where Re[ ] and Im[ ] denote the real and imaginary parts, respectively, and $\hat{J}(\boldsymbol{r})$ means $\hat{J}(\boldsymbol{r},\boldsymbol{r})$. In addition, since

$$J_{ss}J_{pp} - J_{sp}J_{ps} \geq 0, \tag{1.20}$$

the Stokes parameters satisfy the general relation

$$s_0^2(\boldsymbol{r}) \geq s_1^2(\boldsymbol{r}) + s_2^2(\boldsymbol{r}) + s_3^2(\boldsymbol{r}). \tag{1.21}$$

In a similar way to that occurs for the Jones matrices, the matrix $\hat{J}$ can be written in terms of the Pauli matrices:

$$\hat{J}(\boldsymbol{r}) = \frac{1}{2}\left[s_0(\boldsymbol{r})\,\hat{\sigma}_0 + s_1(\boldsymbol{r})\,\hat{\sigma}_1 + s_2(\boldsymbol{r})\,\hat{\sigma}_2 + s_3(\boldsymbol{r})\,\hat{\sigma}_3\right]. \tag{1.22}$$

Taking this into account, the two eigenvalues, α_s and β_s, of matrix $\hat{J}$ are written as a combination of the Stokes parameters, namely,

$$\alpha_s = \frac{1}{2}\left[s_0 + \left(s_1^2 + s_2^2 + s_3^2\right)^{1/2}\right], \tag{1.23a}$$

$$\beta_s = \frac{1}{2}\left[s_0 - \left(s_1^2 + s_2^2 + s_3^2\right)^{1/2}\right]. \tag{1.23b}$$

One of the main advantages of the Stokes parameters arises from the fact of that they are measurable quantities. To determine them at each point of the transverse wavefront, a simple method consists of using, for example, a CCD camera placed at the observation plane, together with a polarizer at different orientations and a quarter-wave plate. The textbooks show that the Stokes parameters are found in a six-step procedure from the six measured values of the irradiance for different configurations of polarizer and retarder, namely,

$$s_0(\boldsymbol{r}) = I_{0^\circ}(\boldsymbol{r}) + I_{90^\circ}(\boldsymbol{r}), \tag{1.24a}$$

$$s_1(\boldsymbol{r}) = I_{0^\circ}(\boldsymbol{r}) - I_{90^\circ}(\boldsymbol{r}), \tag{1.24b}$$

$$s_2(\boldsymbol{r}) = I_{45^\circ}(\boldsymbol{r}) - I_{135^\circ}(\boldsymbol{r}), \tag{1.24c}$$

$$s_3(\boldsymbol{r}) = I_{\lambda/4,45^\circ}(\boldsymbol{r}) - I_{\lambda/4,135^\circ}(\boldsymbol{r}), \tag{1.24d}$$

where I denotes the irradiance at each point of the beam cross-section, the subscripts appearing in Eqs. (1.24a–c) refer to the angle that the transmission axis of the polarizer makes with the s-axis, and the subscripts in Eq. (1.24d) indicate that the beam propagates successively through a quarter-wave plate (where the fast axis is oriented along the s-axis) and a polarizer whose transmission axis makes angles 45° and 135° with the fast axis.

Within the framework of the Stokes parameters, the effect of an optical system on the polarization of a light field can be represented by a 4×4 matrix $\hat{\mathcal{M}}$ (Müller matrix), which transform the Stokes vector of the incident beam into the Stokes vector of the output field, i.e.,

$$\boldsymbol{S}_{out} = \hat{\mathcal{M}}\boldsymbol{S}_{in} = \begin{pmatrix} m_{00} & m_{01} & m_{02} & m_{03} \\ m_{10} & m_{11} & m_{12} & m_{13} \\ m_{20} & m_{21} & m_{22} & m_{23} \\ m_{30} & m_{31} & m_{32} & m_{33} \end{pmatrix} \begin{pmatrix} s_0 \\ s_1 \\ s_2 \\ s_3 \end{pmatrix}_{in} , \tag{1.25}$$

where m_{ij}, $i, j = 0, 1, 2, 3$, are real valued elements, and the subscript *in* and *out* stand for the input and output fields, respectively. The Müller matrix associated to a sequence of cascaded instruments is given by the product of the matrices of the individual optical devices. In addition, the most frequently encountered optical systems in practice involve polarization-altering properties which are uniform across the beam profile. Accordingly, the elements of the conventional Müller matrices are not position-dependent.

It is interesting to remark that, although all Jones matrices have a corresponding Müller matrix, it cannot be established a one-to-one mapping between these two kind of matricial representation. The correspondence relationships between matrices $\hat{\mathcal{M}}$ and $\hat{\mathfrak{J}}$ can be found, for example, in (Chipman, 1994; Simon, 1982). They provide necessary conditions for physical realizability. The interested reader can also see, for instance, (Azzam and Bashara, 1987; Brosseau, 1998; Chipman, 1994; Gil, 2000; Goldstein, 2003). Let us finally mention that the special and interesting case of nonreciprocal optical systems (e.g., optical diodes, optical insulators) has been investigated for partially polarized light in, for example, (Gevorgyan, 2003).

For illustrative purposes, Table 1.1 gives the Müller matrices associated with the most common polarization-altering (ideal) elements (see, for example, (Goldstein, 2003; Hecht, 1998)).

1.2.4 Local Degree of Polarization

It would be useful to characterize the polarization state of a light field by means of a single parameter or figure of merit. This is done in the literature by using the so-called standard degree of polarization, P_{st}: Since the Stokes vector of any quasimonochromatic beam can be considered as a sum of completely polarized and completely unpolarized fields, independent each other, the standard degree of polarization is usually introduced as the ratio of the irradiance of the polarized part to the global irradiance of the light wave (Brosseau, 1998). It should be remarked that, even for unpolarized laser beams, light becomes polarized in time intervals approaching the resonator decay time. Consequently, it will be implicitly considered in the experiments averaging over a time interval large compared with the internal fluctuation time of the system.

The determination of P_{st} at a certain transverse plane involves measurements of the integrated power over the full detection area. But this is of practical use only when the light field has uniform polarization across the beam profile.

Table 1.1 Müller matrices of basic polarization-altering (ideal) optical devices

Optical element	Müller matrix
Linear polarizer (transmission axis along x)	$\frac{1}{2}\begin{pmatrix} 1 & 1 & 0 & 0 \\ 1 & 1 & 0 & 0 \\ 0 & 0 & 0 & 0 \\ 0 & 0 & 0 & 0 \end{pmatrix}$
Linear polarizer (transmission axis along y)	$\frac{1}{2}\begin{pmatrix} 1 & -1 & 0 & 0 \\ -1 & 1 & 0 & 0 \\ 0 & 0 & 0 & 0 \\ 0 & 0 & 0 & 0 \end{pmatrix}$
Linear polarizer at +45°	$\frac{1}{2}\begin{pmatrix} 1 & 0 & 1 & 0 \\ 0 & 0 & 0 & 0 \\ 1 & 0 & 1 & 0 \\ 0 & 0 & 0 & 0 \end{pmatrix}$
Linear polarizer at –45°	$\frac{1}{2}\begin{pmatrix} 1 & 0 & -1 & 0 \\ 0 & 0 & 0 & 0 \\ -1 & 0 & 1 & 0 \\ 0 & 0 & 0 & 0 \end{pmatrix}$
Quarter-wave plate (fast axis along x)	$\begin{pmatrix} 1 & 0 & 0 & 0 \\ 0 & 1 & 0 & 0 \\ 0 & 0 & 0 & 1 \\ 0 & 0 & -1 & 0 \end{pmatrix}$
Quarter-wave plate (fast axis along y)	$\begin{pmatrix} 1 & 0 & 0 & 0 \\ 0 & 1 & 0 & 0 \\ 0 & 0 & 0 & -1 \\ 0 & 0 & 1 & 0 \end{pmatrix}$
Half-wave plate	$\begin{pmatrix} 1 & 0 & 0 & 0 \\ 0 & 1 & 0 & 0 \\ 0 & 0 & -1 & 0 \\ 0 & 0 & 0 & -1 \end{pmatrix}$

In general, however, such ratio differs from one point to another across the wavefront. In such a case, the polarization state is better described by the local degree of polarization $P(\boldsymbol{r})$, where $\boldsymbol{r}$ is, again, a position vector lying in a transverse plane. It has a similar meaning to parameter P_{st}, but now referred to each point at the beam cross-section. Function $P(\boldsymbol{r})$ has been written in many equivalent forms in the literature, for example,

$$\begin{aligned} P(\boldsymbol{r}) &= \left\{ 1 - \frac{4\mathrm{Det}[\hat{J}(\boldsymbol{r})]}{\left(\mathrm{Tr}[\hat{J}(\boldsymbol{r})]\right)^2} \right\}^{1/2} \\ &= \frac{\alpha_s(\boldsymbol{r}) - \beta_s(\boldsymbol{r})}{\alpha_s(\boldsymbol{r}) + \beta_s(\boldsymbol{r})} \\ &= \frac{[s_1^2(\boldsymbol{r}) + s_2^2(\boldsymbol{r}) + s_3^2(\boldsymbol{r})]^{1/2}}{s_0(\boldsymbol{r})}. \end{aligned} \tag{1.26}$$

Of course, $P(\boldsymbol{r})$ is constant for fields uniformly polarized throughout the beam profile.

Two main properties make useful this function:

(i) Its value is independent of the choice of the transverse s- and p-axis.
(ii) It satisfies

$$0 \leq P(\boldsymbol{r}) \leq 1. \tag{1.27}$$

In particular, the maximum value $P(\boldsymbol{r}) = 1$, for every $\boldsymbol{r}$, corresponds to uniformly totally polarized beams, and the minimum value, $P(\boldsymbol{r}) = 0$, for every $\boldsymbol{r}$, refers to unpolarized (natural) light.

Here we do not proceed further into the analysis of this function, which will be extensively handled in subsequent sections and chapters.

1.3 Weighted Degree of Polarization

As we pointed out earlier, light exhibits, in general, a polarization that is a function of the position at the beam profile. It would then be useful to handle measurable parameters that allow to globally characterize in a simple way both, the polarization and its uniformity across the transverse section.

Accordingly, let us introduce a parameter $\tilde{P}$ in the form (Piquero et al., 1999)

$$\tilde{P} = \frac{\iint I(x,y)P(x,y)\,dx\,dy}{\iint I(x,y)\,dx\,dy}, \tag{1.28}$$

where $I(x,y)$ is the irradiance distribution at a plane $z =$ constant. We call $\tilde{P}$ the weighted degree of polarization. Note that $\tilde{P}$ computes mainly those regions where the beam irradiance is significant. Moreover, the appearance of the factor $I(x,y)$ in the definition of $\tilde{P}$ minimizes the contribution of the beam wings, thus reducing harmful effects such as camera offset, small signal-to-noise ratio and background. Also note that, for uniformly partially-polarized beams, the standard parameter P_{st} and the weighted degree of polarization have the same value. It should also be remarked that, in general, $\tilde{P}$ is not invariant upon propagation through ABCD optical systems.

It can be shown that the above parameter $\tilde{P}$ satisfies the inequality

$$0 \leq \tilde{P} \leq 1. \tag{1.29}$$

Those beams whose parameter $\tilde{P}$ approaches 1 will be mostly totally polarized (at least in the regions with significant irradiance), even though they have spatially distributed polarization states. The opposite case $\tilde{P} = 0$ means that the field is non-polarized over the whole profile. Intermediate values of $\tilde{P}$ indicate, of course, that the beam is partially polarized.

Consequently, parameter $\tilde{P}$ allow to roughly classify the beams as totally ($\tilde{P} = 1$), partially ($0 < \tilde{P} < 1$) or non-polarized ($\tilde{P} = 0$) fields, and this classification scheme applies for non-uniform polarization distributions.

The dispersion of the values of the local degree of polarization $P(x,y)$ across wavefront can be easily evaluated by means of the following parameter:

$$\tilde{\sigma}_p^2 = \frac{\iint I(x,y)\left[P(x,y) - \tilde{P}\right]^2 dx\,dy}{\iint I(x,y)\,dx\,dy}, \tag{1.30}$$

similar to the variance of $P(x,y)$ (the irradiance $I(x,y)$ acting as a density function).

It can also be shown that (Piquero et al., 1999)

$$0 \leq \tilde{\sigma}_p \leq 1/2. \tag{1.31}$$

This parameter provides a simple overall characterization of the uniformity of the local degree of polarization over the beam cross-section. For example, for radially totally polarized fields, $\tilde{\sigma}_p = 0$, which is consistent with the fact of that these beams are totally polarized everywhere.

Let us finally remark that the above two parameters, $\tilde{P}$ and $\tilde{\sigma}_p$, can be experimentally determined following the standard procedure used to measure the Stokes parameters, with a final CCD array to get the irradiance at each point of the observation plane.

1.4 Linear and Circular Polarization Content of Totally Polarized Beams

As is well known, the electric field associated to an electromagnetic disturbance should, in general, be considered as a position-dependent stochastic process. Thus, the equations involving the field vector should be understood in an average sense. Note, however, that, in the present section, we will be concerned with totally polarized beams, so that, for simplicity, symbols referring to the statistical character of the field will not be explicitly shown in the notation. A description of the stochastic behavior of a light field in the space-frequency domain will be studied later in subsequent chapters.

In the present section, the attention will be focused on non-uniformly totally polarized beams. In particular, we are here interested on the global characterization of the so-called linear or circular polarization content at the transverse profile of this kind of beams.

1.4.1 Key Definitions and Physical Meaning

As customary, we represent the electric field vector, $\boldsymbol{E}(\boldsymbol{r})$, propagating essentially along the z-axis, by means of the Jones vector associated to its transverse components at a certain plane z:

$$\boldsymbol{E}(\boldsymbol{r}) = \begin{pmatrix} E_s(\boldsymbol{r}) \\ E_p(\boldsymbol{r}) \end{pmatrix}. \tag{1.32}$$

Let us now introduce two orthogonal unitary vectors, $\boldsymbol{u}_r = \frac{1}{\sqrt{2}} \begin{pmatrix} 1 \\ i \end{pmatrix}$ and $\boldsymbol{u}_l = \frac{1}{\sqrt{2}} \begin{pmatrix} 1 \\ -i \end{pmatrix}$, where the subscripts r and l refer to right-handed and left-handed circularly polarized fields, respectively. In terms of these unitary vectors, the field $\boldsymbol{E}(\boldsymbol{r})$ can be written in the form

$$\boldsymbol{E}(\boldsymbol{r}) = (\boldsymbol{E} \cdot \boldsymbol{u}_r)\boldsymbol{u}_r + (\boldsymbol{E} \cdot \boldsymbol{u}_l)\boldsymbol{u}_l, \tag{1.33}$$

where the dot symbolizes the inner product, i.e., $\boldsymbol{a} \cdot \boldsymbol{b} = a_x b_x^* + a_y b_y^*$. The vector $\boldsymbol{E}_r = (\boldsymbol{E} \cdot \boldsymbol{u}_r)\boldsymbol{u}_r$ would then represent the field at the output of an optical device that only transmits the right-handed circularly-polarized component of the input field. Consequently, the quantity

$$\|\boldsymbol{E}_r\|^2 \equiv \int |\boldsymbol{E}_r(\boldsymbol{r})|^2 d\boldsymbol{r}, \tag{1.34}$$

where the integration extends throughout the beam cross-section, can be understood as the beam power associated to the "right-handed circular content" $\boldsymbol{E}_r$ of the field. Moreover, this quantity also reads

$$\|\boldsymbol{E}_r\|^2 = \frac{1}{2} \int s_0(\boldsymbol{r}) d\boldsymbol{r} + \frac{1}{2} \int s_3(\boldsymbol{r}) d\boldsymbol{r}, \tag{1.35}$$

where s_0 and s_3 are the Stokes parameters defined earlier. On the other hand, the total power can be written in the form

$$\|\boldsymbol{E}\|^2 \equiv \int \left[|\boldsymbol{E}_s(\boldsymbol{r})|^2 + \left|\boldsymbol{E}_p(\boldsymbol{r})\right|^2 \right] d\boldsymbol{r} = \int s_0(\boldsymbol{r}) d\boldsymbol{r}, \tag{1.36}$$

so that the ratio between the power associated to the right-handed circular content of the beam and its total power reads

$$\frac{\|\boldsymbol{E}_r\|^2}{\|\boldsymbol{E}\|^2} = \frac{1}{2} + \frac{1}{2} \frac{\int s_3(\boldsymbol{r}) d\boldsymbol{r}}{\int s_0(\boldsymbol{r}) d\boldsymbol{r}}. \tag{1.37}$$

It should be remarked that the above ratio can also be interpreted as the percentage of the power transmitted through a right-handed circular polarizer

(averaged over the transverse region of the beam profile where the irradiance is significant).

Let us now introduce the following parameters, evaluated at a transverse plane z (Martínez-Herrero et al., 2006):

$$\tilde{\rho} = \frac{\int \rho(\boldsymbol{r}) s_0(\boldsymbol{r}) d\boldsymbol{r}}{\int s_0(\boldsymbol{r}) d\boldsymbol{r}} \tag{1.38}$$

and

$$\sigma_\rho = \frac{\int (\rho(\boldsymbol{r}) - \tilde{\rho})^2 s_0(\boldsymbol{r}) d\boldsymbol{r}}{\int s_0(\boldsymbol{r}) d\boldsymbol{r}}, \tag{1.39}$$

where

$$\rho(\boldsymbol{r}) \equiv \frac{s_3(\boldsymbol{r})}{s_0(\boldsymbol{r})}. \tag{1.40}$$

We see that the overall parameter $\tilde{\rho}$ computes mainly in those regions where the irradiance is significant enough, and ranges from –1 (pure left-handed circularly polarized light) to +1 (pure right-handed circularly polarized light). The value $\tilde{\rho} = 0$ corresponds to a pure (in general, non-uniformly) linearly polarized field.

As it is quite apparent from the definition, $\tilde{\rho}$ can be determined by measuring the Stokes parameters s_0 and s_3 integrated over the full detection area, even though the beam is non-uniformly polarized. This is a useful property from an experimental point of view.

On the other hand, the parameter σ_ρ gives the dispersion of the values of $\rho(\boldsymbol{r})$ across the beam section. It represents the variance of $\rho(\boldsymbol{r})$, where the local value of the Stokes parameter $s_0(\boldsymbol{r})$ behaves as a density function. Accordingly, this parameter globally characterizes the uniformity of the ratio $\rho(\boldsymbol{r})$ over the beam profile. In particular, the values $\tilde{\rho} = 0 = \sigma_\rho$, indicate that the field is linearly polarized throughout its transverse section.

1.4.2 Application to an Example

To get further insight into the physical meaning of $\tilde{\rho}$, let us consider a non-uniformly totally polarized beam whose electric field vector $\boldsymbol{E}$ at the plane $z = 0$ is given by the Jones vector (Martínez-Herrero et al., 2006)

$$\mathbf{E}(r) = E_0 \exp\left(-\frac{r^2}{w_0^2}\right) \begin{pmatrix} 1 \\ \exp(-ig(r)) \end{pmatrix}, \tag{1.41}$$

with

$$g(r) = \frac{\pi}{2} \exp\left[-(b\,r)^n\right],\ n = 4, \tag{1.42}$$

where E_0 is an amplitude factor, r denotes the radial polar coordinate, and w_0 and b are constants (w_0 is proportional to the transverse dimension of the beam size, and

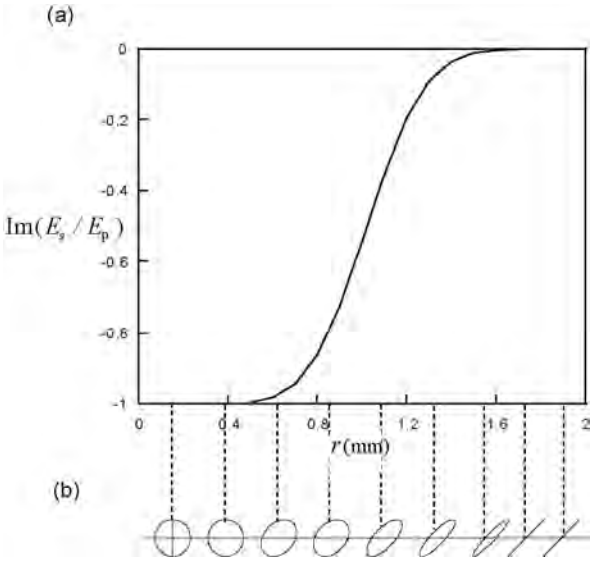

Fig. 1.2 (**a**) Ratio $\mathrm{Im}(E_\mathrm{s}(r)/E_\mathrm{p}(r))$ versus the radial distance r to the origin. (**b**) Schematic diagram of the polarization state in the range $r \in [0,2]$ mm. See also (Martínez-Herrero et al., 2006)

b^{-1} is a measure of the width of the function $g(r)$). Note that the whole beam shows a Gaussian irradiance profile, together with an abrupt transition from a circularly-polarized state near the beam center to a 45°-azimuth linearly-polarized state outside this region. This is shown in Fig. 1.2a, where the ratio $\mathrm{Im}(E_\mathrm{s}(r)/E_\mathrm{p}(r))$ has been given for the value $b = 1\,\mathrm{mm}^{-1}$. A representation of the change from circular to linear polarization is sketched in Fig 1.2b. Of course, sharper transitions can be computed for higher values of n in Eq. (1.42).

In Fig. 1.3 the parameters $\tilde{\rho}$ and σ_ρ have been plotted in terms of the ratio w_0/b. When $w_0/b << 1$, we have $\tilde{\rho} \approx -1$ and $\sigma_\rho \approx 0$, so that the beam essentially behaves

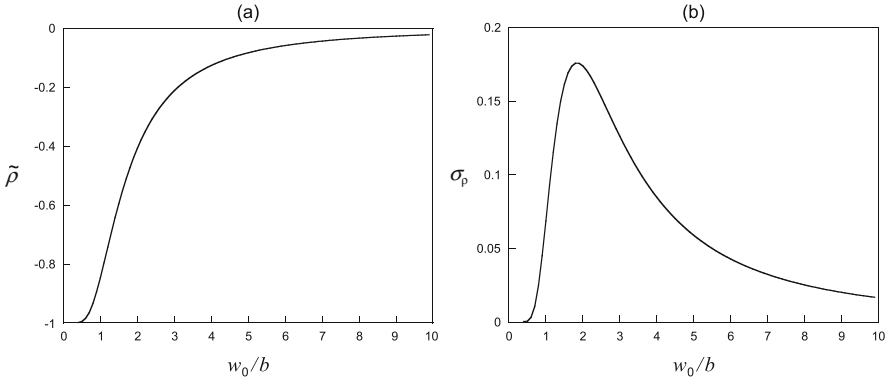

Fig. 1.3 Parameters $\tilde{\rho}$ and σ_ρ for the field given by Eq. (1.41): (**a**) $\tilde{\rho}$ versus the ratio w_0/b; (**b**) σ_ρ versus the ratio w_0/b. See also (Martínez-Herrero et al., 2006)

as a left-handed circularly-polarized field inside the region where the irradiance takes significant values. For $w_0/b >> 1$, we obtain $\tilde{\rho} \approx 0$ and the beam becomes linearly polarized over the whole beam profile except over a small region close to its center. The intermediate case $w_0/b = 2$ gives $\tilde{\rho} = -0.41$ and $\sigma_\rho = 0.17$, and a mixture of both states of polarization (linear and left-handed circular) appears.

1.4.3 Measurability

To check the measurability of the above parameters, we can make use of the beam emitted by a He-Ne laser source Spectra Physics 117A (intensity and frequency-stabilized mode), linearly (> 1000:1) and uniformly polarized.

The images are taken with a CCD camera Pulnix TM-765 and a laser beam analizer from Spiricon. Further details about the experimental set-up can be found in (Martínez-Herrero et al., 2006). For this beam, we get $\tilde{\rho} = 0.0043$ and $\sigma_\rho = 0.0001$. In addition, when left and right-handed circularly polarized beams are synthesized by means of a quarter-wave plate, one obtains $\tilde{\rho} = -1.008$, $\sigma_\rho = 0.001$ and $\tilde{\rho} = 1.081$, $\sigma_\rho = 0.001$, respectively. All these measured values show a reasonable agreement with the manufacturers' data.

Let us now consider a second test that measures the parameters $\tilde{\rho}$ and σ_ρ in a more involved case, namely, a non-uniformly totally polarized beam generated after propagation through a uniaxial anisotropic material. In the experiments, the He-Ne laser beam of the previous example was used. The anisotropic medium is a calcite crystal whose optic axis is oriented along the propagation direction (Piquero and Vargas-Balbuena, 2004; Provenziani et al., 2002). To synthesize a nonuniformly totally polarized (NUTP) beam, we employ a slightly convergent or divergent beam impinging on the crystal. This can be implemented by means of a microscope objective in front of the calcite plate (see Fig. 1.4). A convergent lens is used to focus the

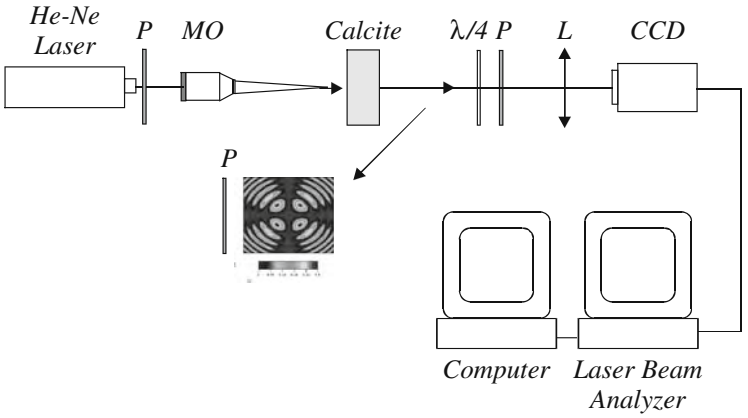

Fig. 1.4 Experimental set-up used to measure the parameters $\tilde{\rho}$ and σ_ρ at the output of a calcite crystal. *MO* denotes a microscope objective, *L* is a convergent lens, *P* represents a polarizer, and $\lambda/4$ symbolizes a quarter-wave plate. See also (Martínez-Herrero et al., 2006)

beam into the CCD camera. We get $\tilde{P} = 1.036$, $\tilde{\rho} = 0.044$ and $\sigma_\rho = 0.22$. From the value of the weighted degree of polarization, it is concluded that the output field essentially behaves as a totally polarized beam throughout its transverse section, as expected. This value of parameter $\tilde{\rho}$ means that the average polarization is linear over the significant region of the beam profile. In addition, since σ_ρ clearly differs from zero, we infer that the output beam is not uniformly polarized. It should finally be noted that this behavior agrees with the values calculated at the output of a calcite crystal on the basis of the Jones formalism. (Piquero and Vargas-Balbuena, 2004).

1.5 Radial and Azimuthal Polarization Content of Totally Polarized Beams

Beams with radial or azimuthal polarization distributions have receiving increasing attention in the literature (see, for instance, (Bomzon et al., 2002; Deng et al., 2007; Diehl et al., 2006; Dorn et al., 2003; Gupta et al., 2007; Kozawa and Sato, 2007; Lumer et al., 2008; Meier et al., 2007; Moshe et al., 2003, 2007; Moser et al., 2005; Nieminen et al., 2008; Niziev and Nesterov, 1999; Oron et al., 2000; Pasilly and Denis, 2005; Phua and Lai, 2007; Quabis et al., 2005; Qiu et al., 2009; Roth et al., 2005; Sheppard and Choudhury, 2004; Tidwell et al., 1990; Tovar, 1998; Volpe and Petrov, 2004; Wu et al., 2007; Yonezawa et al., 2008; Zhan, 2004) and Chap. 4 of the present book). This is a consequence of their potential applications: For example, it has been shown that a radially polarized field can be focused into a spot region significantly smaller that for uniform linear polarization. This leads to interesting possibilities in confocal microscopy, lithography, and optical trapping, as well as optical data storage. Moreover, radially polarized light may also increase the efficiency and cutting speed in material processing by laser, and this kind of beams have even been used (see also Chap. 2) to reduce cumbersome thermally-induced effects in solid-state lasers.

In addition, radial and azimuthal polarizers are now commercially available (they have been implemented by using, for example, dichroic and liquid-crystal-based devices) (Erdelyi and Bor, 2006; Erdelyi and Gajdatsy 2008; Stalder and Schadt, 1996).

In the present section we will extend the overall characterization given in the previous section by introducing several new global parameters, which are useful to describe the radial and azimuthal polarization content of non-uniformly totally polarized beams. As it will next be apparent, such figures of merit can be obtained in terms of the Stokes parameters, and measured from the data collected at the output of either a radial or an azimuthal dichroic polarizer, integrated throughout the beam cross-section.

1.5.1 Key Definitions

Let us consider a paraxial beam propagating along the z-axis. Since fields will be assumed totally polarized, for simplicity, we again disregard in the notation their

stochastic character. The electric field vector, $\boldsymbol{E}$, associated to a non-uniformly totally polarized beam (at a certain transverse plane), is then written in planar polar coordinates in the form

$$\boldsymbol{E}(r,\theta) = \begin{pmatrix} E_s \\ E_p \end{pmatrix} = \begin{pmatrix} f(r,\theta) \\ g(r,\theta) \end{pmatrix}, \tag{1.43}$$

where f and g denote position-dependent functions, and r and θ are the polar coordinates. Let $\boldsymbol{u}_R$ and $\boldsymbol{u}_\theta$ be orthogonal unitary vectors in the radial and azimuthal directions, respectively, i.e.,

$$\boldsymbol{u}_R = (\cos\theta, \sin\theta)\,, \tag{1.44a}$$

$$\boldsymbol{u}_\theta = (-\sin\theta, \cos\theta)\,. \tag{1.44b}$$

In terms of these vectors, the electric field $\boldsymbol{E}$ reads

$$\boldsymbol{E}(r,\theta) = \boldsymbol{E}_R(r,\theta) + \boldsymbol{E}_\theta(r,\theta), \tag{1.45}$$

where

$$\boldsymbol{E}_R(r,\theta) = (\boldsymbol{E}\cdot\boldsymbol{u}_R)\boldsymbol{u}_R, \tag{1.46a}$$

$$\boldsymbol{E}_\theta(r,\theta) = (\boldsymbol{E}\cdot\boldsymbol{u}_\theta)\boldsymbol{u}_\theta. \tag{1.46b}$$

the dot symbolizing the inner product, as usual. In Eq. (1.45), the terms $\boldsymbol{E}_R$ and $\boldsymbol{E}_\theta$ would represent the field at the output of an optical device that only transmits radial or azimuthal components of the input field, respectively. Accordingly, $\boldsymbol{E}_R$ is a radially polarized field and $\boldsymbol{E}_\theta$ is azimuthally polarized. At each point of the transverse beam profile, the percentage of the (local) irradiance associated to the radial component can be evaluated by means of the following ratio

$$\rho_R(r,\theta) = \frac{|\boldsymbol{E}_R(r,\theta)|^2}{|\boldsymbol{E}(r,\theta)|^2}, \tag{1.47a}$$

and analogously for the azimuthal component,

$$\rho_\theta(r,\theta) = \frac{|\boldsymbol{E}_\theta(r,\theta)|^2}{|\boldsymbol{E}(r,\theta)|^2}. \tag{1.47b}$$

Therefore, the radial and azimuthal polarization content of a non-uniformly totally polarized field could be characterized by averaging the expressions (1.47a)

and (1.47b) over the region of the beam cross-section where the irradiance is significant, i.e., (Martínez-Herrero et al., 2008; Lumer and Moshe, 2009)

$$\tilde{\rho}_R = \frac{\int_0^{\infty}\int_0^{2\pi} \rho_R(r,\theta)\ |\boldsymbol{E}(r,\theta)|^2\ r\ dr\ d\theta}{\int_0^{\infty}\int_0^{2\pi} |\boldsymbol{E}(r,\theta)|^2\ r\, dr\, d\theta} = \frac{\int_0^{\infty}\int_0^{2\pi} \rho_R\,(r,\theta)\ I(r,\theta)\, r\, dr\, d\theta}{\int_0^{\infty}\int_0^{2\pi} I(r,\theta)\, r dr d\theta}, \tag{1.48a}$$

$$\tilde{\rho}_\theta = \frac{\int_0^{\infty}\int_0^{2\pi} \rho_\theta(r,\theta)\ |\boldsymbol{E}(r,\theta)|^2\ r\, dr\, d\theta}{\int_0^{\infty}\int_0^{2\pi} |\boldsymbol{E}(r,\theta)|^2\, r\, dr\, d\theta} = \frac{\int_0^{\infty}\int_0^{2\pi} \rho_\theta\,(r,\theta)\, I(r,\theta)\ \ r\, dr\, d\theta}{\int_0^{\infty}\int_0^{2\pi} I(r,\theta)\, r\, dr\, d\theta}. \tag{1.48b}$$

where $I(r, \theta)$ denotes the irradiance at each point of the beam profile. The dispersion of the values ρ_R and ρ_θ would then be determined from the expressions (Martínez-Herrero et al., 2008):

$$\sigma_R^2 = \frac{\int_0^{\infty}\int_0^{2\pi} \left(\rho_R\,(r,\theta) - \tilde{\rho}_R\right)^2 I(r,\theta)\ r\, dr\, d\theta}{\int_0^{\infty}\int_0^{2\pi} I(r,\theta)\, r\, dr\, d\theta}, \tag{1.49a}$$

$$\sigma_\theta^2 = \frac{\int_0^{\infty}\int_0^{2\pi} \left(\rho_\theta\,(r,\theta) - \tilde{\rho}_\theta\right)^2 I(r,\theta)\ r\, dr\, d\theta}{\int_0^{\infty}\int_0^{2\pi} I(r,\theta)\, r\, dr\, d\theta}. \tag{1.49b}$$

Of course, when σ_R^2 (or σ_θ^2) equals to zero means that the beam is uniformly polarized. Also note that σ_R^2 and σ_θ^2 globally characterize the uniformity of the radial and azimuthal polarization content over the wavefront. They represent the variance of ρ_R and ρ_θ, where the local value of the irradiance behaves as a density function.

In addition, it can be shown that

$$0 \leq \tilde{\rho}_R \leq 1, \tag{1.50a}$$

$$0 \leq \tilde{\rho}_\theta \leq 1, \tag{1.50b}$$

where the value 1 corresponds to a pure radial (or azimuthal) beam. Moreover, these parameters satisfy the relation

$$\tilde{\rho}_R + \tilde{\rho}_\theta = 1. \tag{1.51}$$

This property implies that the radial and the azimuthal polarization content of a beam should be understood as complementary properties. In practice, it would then

suffice to determine one of these parameters. Let us finally remark that the above parameters depend, in general, on the plane z we are considering.

1.5.2 Relations with the Stokes Parameters

We will next show that the degrees of radial and azimuthal polarization, $\tilde{\rho}_R$ and $\tilde{\rho}_\theta$, can be written in a simple way in terms of the conventional Stokes parameters. To see this, note first that

$$\boldsymbol{E}_R(\boldsymbol{r},\theta) = (\boldsymbol{E}\cdot\boldsymbol{u}_R)\,\boldsymbol{u}_R = f\cos\theta + g\sin\theta, \tag{1.52a}$$

$$\boldsymbol{E}_\theta(\boldsymbol{r},\theta) = (\boldsymbol{E}\cdot\boldsymbol{u}_\theta)\,\boldsymbol{u}_\theta = -f\sin\theta + g\cos\theta, \tag{1.52b}$$

so that

$$|\boldsymbol{E}_R|^2 = \cos^2\theta\,|f|^2 + \sin^2\theta\,|g|^2 + 2\,\sin\theta\cos\theta\,\mathrm{Re}\left\{f^* g\right\}, \tag{1.53a}$$

$$|\boldsymbol{E}_\theta|^2 = \sin^2\theta\,|f|^2 + \cos^2\theta\,|g|^2 - 2\,\sin\theta\cos\theta\,\mathrm{Re}\left\{f^* g\right\}. \tag{1.53b}$$

Taking this into account, one obtains

$$|\boldsymbol{E}_R|^2 = \frac{1}{2}s_0 + \frac{\cos 2\theta}{2}s_1 + \frac{\sin 2\theta}{2}s_2, \tag{1.54a}$$

$$|\boldsymbol{E}_\theta|^2 = \frac{1}{2}s_0 - \frac{\cos 2\theta}{2}s_1 - \frac{\sin 2\theta}{2}s_2, \tag{1.54b}$$

where s_0, s_1 and s_2 denote the standard Stokes parameters at each point (r,θ) of the beam cross-section. From their definitions, parameters $\tilde{\rho}_R$ and $\tilde{\rho}_\theta$ finally read

$$\tilde{\rho}_R = \frac{1}{2} + \frac{1}{2P}\int_0^\infty\int_0^{2\pi}\left[\cos(2\theta)\;s_1(r,\theta) + \sin(2\theta)\;s_2(r,\theta)\right]\;r\,dr\,d\theta, \tag{1.55a}$$

$$\tilde{\rho}_\theta = \frac{1}{2} - \frac{1}{2P}\int_0^\infty\int_0^{2\pi}\left[\cos(2\theta)\;s_1(r,\theta) + \sin(2\theta)\;s_2(r,\theta)\right]\;r\,dr\,d\theta, \tag{1.55b}$$

with

$$P = \int_0^\infty\int_0^{2\pi} s_0(r,\theta)\,r\,dr\,d\theta. \tag{1.55c}$$

It is clear from Eqs. (1.55) that $\tilde{\rho}_R$ and $\tilde{\rho}_\theta$ do not depend on the local Stokes parameter s_3, so that no information about s_3 is required to describe the radial

or azimuthal polarization content of a beam. This behavior should physically be expected because s_3 equals zero for any radially (or azimuthally) polarized field. This also applies for the particular but interesting case of a radially polarized beam with vortex wavefront (see, for example, (Machavariani et al., 2007) and references therein). In such a case, the global phase factor that defines the topological charge does not alter the relative phase term between the transverse components and, therefore, the parameter s_3 remains equal to zero. One would naively expect this independence on s_3 because this Stokes parameter gives the "circularity" of the polarization state: the extreme values $s_3 = \pm 1$ correspond to a circularly totally polarized beam (see Sect. 1.4).

1.5.3 Relations with the Output of Radial and Azimuthal Polarizers

Instead of measuring and computing the local values of the Stokes parameters, it would be of more practical use to infer the parameters $\tilde{\rho}_R$ and $\tilde{\rho}_\theta$ from the integrated data over the full detection area: In fact, we do not need to perform detailed (local) detections but a global single irradiance measurement. This can be attained in a simple way by using either a radial or an azimuthal commercially available polarizer. To show this, note first that

$$\tilde{\rho}_R = \frac{1}{P} \int_0^\infty \int_0^{2\pi} |P_R \{\boldsymbol{E}(r,\theta)\}|^2 \, r \, dr \, d\theta, \tag{1.56}$$

where

$$P_R \{\boldsymbol{E}(r,\theta)\} = (\boldsymbol{E} \cdot \boldsymbol{u}_R) \, \boldsymbol{u}_R \tag{1.57}$$

represents the (point-dependent) output of the polarizer. We thus see that the integral in Eq. (1.56) would just give the overall irradiance (integrated throughout the wavefront) collected at the output of the polarizer. Also note that, to implement the operation described by Eq. (1.57), the polarizer should eliminate the azimuthal component $\boldsymbol{E}_\theta$ of the input field. Accordingly, a dichroic polarizer should be employed.

In an analogous way, $\tilde{\rho}_\theta$ can be written as follows

$$\tilde{\rho}_\theta = \frac{1}{P} \int_0^\infty \int_0^{2\pi} |P_\theta \{\boldsymbol{E}(r,\theta)\}|^2 \, r \, dr \, d\theta, \tag{1.58}$$

where now

$$P_\theta \{\boldsymbol{E}(r,\theta)\} = (\boldsymbol{E} \cdot \boldsymbol{u}_\theta) \, \boldsymbol{u}_\theta \tag{1.59}$$

denotes the output of an azimuthal dichroic polarizer. In this kind of devices, each tiny area of the polarizer behaves like a linear polarizer with the transmission axis orthogonal to the radial direction. Such dichroic polarizers are well known in the literature, used, for example, as polarization axis finders. Let us finally recall that both parameters, $\tilde{\rho}_R$ and $\tilde{\rho}_\theta$, satisfy Eq. (1.51).

1.5.4 Measurability

To test the measurability of parameters $\tilde{\rho}_R$ and $\tilde{\rho}_\theta$, we will employ two commercial optical devices, namely, a conventional linear polarizer and a liquid-crystal polarization converter based on a nematic liquid-crystal cell, which can be switched to obtain either radial or azimuthal polarization distribution from a linearly polarized input beam (Stalder and Schadt, 1996).

In all the measurements, $\tilde{\rho}_R$ and $\tilde{\rho}_\theta$ are found by calculating the local Stokes parameters. The set-up is depicted in Fig. 1.5a and b. For a more detailed description of the experiment, the interested reader can see, for example, (Martínez-Herrero et al., 2008).

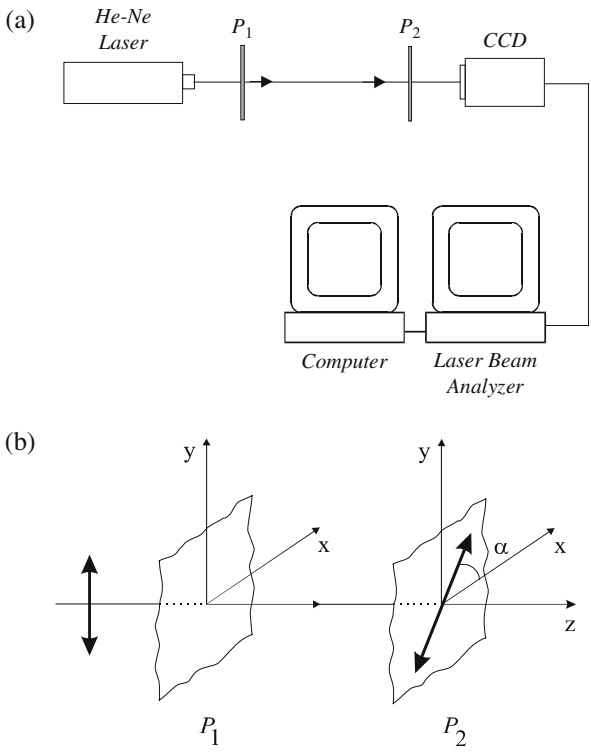

Fig. 1.5 (**a**) Experimental set-up used in the measurements. P_1 denotes either the linear polarizer or the liquid-crystal polarization converter tested in the experiments, and P_2 represents the linear polarizer handled to evaluate the Stokes parameters. (**b**) Cartesian reference axes considered in the experiments. In all the cases, the beam emerging from the laser cavity is linearly polarized along the *y*-axis. To determine the Stokes parameters, the transmission axis of the polarizer P_2 (analizer) makes angles $\alpha(0°, 90°, 45°, 135°)$ with respect to the *x*-axis. See also (Martínez-Herrero et al., 2008)

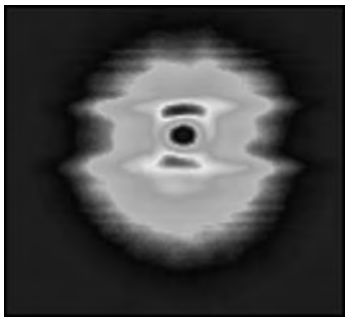

Fig. 1.6 Irradiance distribution after the polarization converter in the radial mode, without P_2 (see the main text). After (Martínez-Herrero et al., 2008), with permission

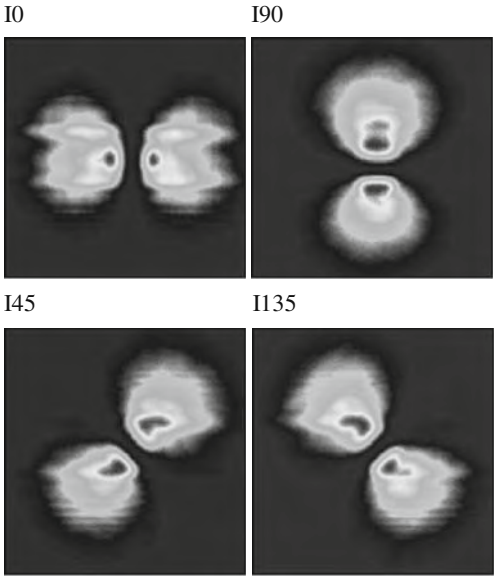

Fig. 1.7 Irradiance distributions after P_2 for several orientations of its transmission axis (0°, 90°, 45° and 135°). The beam emerges from the polarization converter operating in the radial mode. After (Martínez-Herrero et al., 2008), with permission

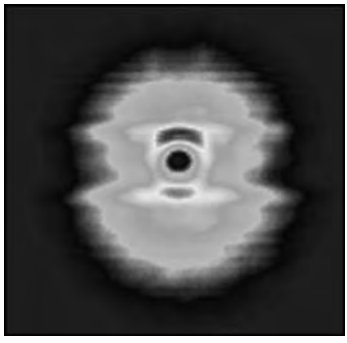

Fig. 1.8 Irradiance distribution after the polarization converter in the azimuthal mode, without P_2 (see the main text). After (Martínez-Herrero et al., 2008), with permission

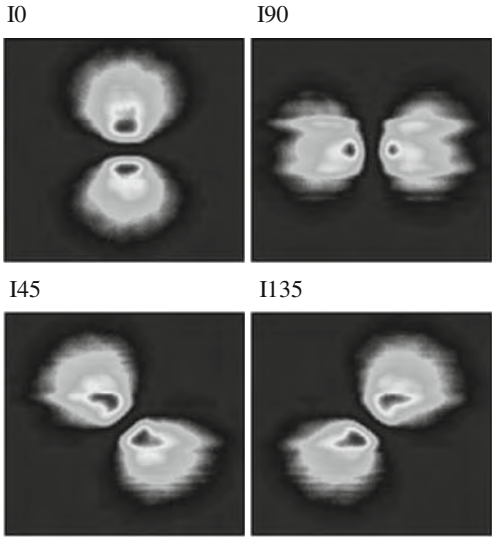

Fig. 1.9 Irradiance distributions after P_2 for several orientations of its transmission axis (0°, 90°, 45° and 135°). Now, the beam emerges from the polarization converter operating in the azimuthal mode. After (Martínez-Herrero et al., 2008), with permission

The light source used to test the linear polarizer is a linearly polarized Gaussian beam emitted by a Spectra Physics He-Ne laser device. The experimental result is $\tilde{\rho}_R = \tilde{\rho}_\theta = 0.499$, showing an excellent agreement with the expected theoretical value $\tilde{\rho}_R = \tilde{\rho}_\theta = 0.5$ (according with the manufacturer specifications).

In the other test, when the above He-Ne laser beam impinges on the polarization converter switched to obtain radial polarization, we find for the output beam $\tilde{\rho}_R = 0.986$ and $\tilde{\rho}_\theta = 0.014$, with $\sigma_R^2 = \sigma_\theta^2 = 0.009$, showing good agreement with the values $\tilde{\rho}_R = 1$, $\tilde{\rho}_\theta = 0$, $\sigma_R^2 = \sigma_\theta^2 = 0$ associated to an (ideal) pure radially polarized beam. Figure 1.6 plots the irradiance distributions at the output of the polarization converter, driven in the radial mode. In this figure, around to the center of symmetry we see a small (about 400 microns) region (a central hole) with undefined liquid-crystal orientation. This arises from the construction principle of the cell (for details, see, for example, (Stalder and Schadt, 1996)). Note, however, that the influence of this hole on $\tilde{\rho}_R$ and $\tilde{\rho}_\theta$ is negligible for the propagation distances considered in the experiments.

Figure 1.7 provides the irradiance distributions at the output of the linear polarizer P_2 for different orientations of its transmittance axis (the angles 0°, 90°, 45° and 135° are associated to the values required to measure the Stokes parameters). In the figures, the number and position of the lobes agree with the theoretical predictions for the beam emerging from the polarization converter.

The experiments can also be performed in the azimuthal mode of the liquid-crystal device. We get $\tilde{\rho}_R = 0.012$ and $\tilde{\rho}_\theta = 0.988$, with $\sigma_R^2 = \sigma_\theta^2 = 0.007$. This shows again an excellent agreement with the values $\tilde{\rho}_R = 0$, $\tilde{\rho}_\theta = 1$, $\sigma_R^2 = \sigma_\theta^2 = 0$ that characterize a pure (ideal) azimuthally polarized beam. For the sake of completeness, Fig. 1.8 shows the irradiance profile (quite similar to that of Fig. 1.6) at the output of the polarization converter, and Fig. 1.9 represents the irradiance

distributions at the output of P_2, driven in the azimuthal mode. The experimental results confirm the measurability of the proposed global parameters.

1.6 Partially Polarized Gaussian Schell-Model Beams

The last two sections have been concerned with totally polarized fields. However, light in nature is, in general, partially polarized. Therefore, before finishing this chapter devoted to the representations of the polarization, it seems appropriate to spend some time in the characterization of this kind of fields.

We will briefly analyze in the present section the so-called partially polarized Gaussian Schell-model (PGSM) fields, which is a physically meaningful example of partially coherent, partially polarized beam with peculiar characteristics of its transverse section. This model of electromagnetic beams was proposed in (Gori et al., 2001) some time ago, and since then considerable literature has been published on this topic, including the study of the propagation through different type of systems (e.g., turbulent atmosphere, gradient index fibers, spherically aberrated lenses, diffractive apertures). In this connection, see, for example, (Eyyuboglu et al., 2007; Ge et al., 2004; Gori et al., 2008; Hanson et al., 2008; Korotkova et al., 2004; Lu and Pan, 2002; Pan and Lu, 2003; Piquero et al., 2001a, b, 2002; Roychowdhury and Korotkova, 2005; Santarsiero, et al., 2009; Shirai, 2005a, Shirai et al. 2005b; Wang et al., 2007; Zhao, 2006). In addition, PGSM fields represent an adequate model to describe real beams, such as those emitted by certain class of multimode lasers (Gori and Palma, 1978, Gori, 1980; Santis et al., 1979).

We will first recall some characteristics of Gaussian Schell-model fields in the scalar case, and we will next continue with the study of (vectorial) PGSM beams and the behavior of their local degree of polarization.

1.6.1 Gaussian Schell-Model Beams: Scalar Case

Within the scalar framework, Gaussian Schell-model (GSM) beams (see, for example, (Mandel and Wolf, 1995) and references therein) have been very useful in coherence theory, in particular, in radiometric characterization of partially coherent sources. This type of fields exhibits a Gaussian irradiance distribution, but they differ from the conventional Gaussian TEM00 beams in which they are not spatially fully coherent. In fact, they can be written as an incoherent superposition of Gaussian-Hermite laser modes. The partial coherence involves, however, an important advantage of these beams, which arises, on the one hand, from the reduction of speckle and ringing effects, associated to completely coherent sources, and on the other hand, from its high directionally.

Let us now recall the mutual coherence function $\Gamma(\boldsymbol{r}_1,\boldsymbol{r}_2,\tau)$ introduced in Eq. (1.14). This function provides a measure of the correlation between light disturbances at two separated points, $\boldsymbol{r}_1$ and $\boldsymbol{r}_2$, at different times, t and $t+\tau$, respectively.

When the cross-correlation is evaluated at the same time ($\tau = 0$), the resulting function is referred in the literature as the mutual intensity (Born and Wolf, 1999). In the particular case of GSM fields, their mutual intensity, $J_{\rm sc}$, between points $\boldsymbol{r}_1$ and $\boldsymbol{r}_2$ at some transverse plane (say, $z = 0$) takes the form (Wolf, 2007)

$$J_{\rm sc}\,(\boldsymbol{r}_1,\boldsymbol{r}_2,0) = A_0 \exp\left[\frac{r_1^2 + r_2^2}{4\sigma^2} - \frac{(\boldsymbol{r}_1 - \boldsymbol{r}_2)^2}{2\mu^2}\right], \tag{1.60}$$

where the subscript "sc" indicates that we are considering the scalar case, and A_0 is a constant factor. Note that the irradiance at $z = 0$ is

$$J_{sc}(\boldsymbol{r},\boldsymbol{r},0) = A_0 \exp\left(-\frac{r^2}{2\sigma^2}\right). \tag{1.61}$$

Accordingly, σ represents here the width of the Gaussian irradiance profile. To understand the physical meaning of parameter μ, let us consider the so-called complex degree of coherence of the field, defined from the mutual intensity as (Mandel and Wolf, 1995)

$$j\,(\boldsymbol{r}_1,\boldsymbol{r}_2) = \frac{J(\boldsymbol{r}_1,\boldsymbol{r}_2)}{[J\,(\boldsymbol{r}_1,\boldsymbol{r}_1)]^{1/2}\,[J\,(\boldsymbol{r}_2,\boldsymbol{r}_2)]^{1/2}}. \tag{1.62}$$

For GSM beams, $j\,(\boldsymbol{r}_1,\boldsymbol{r}_2)$ takes the form

$$j\,(\boldsymbol{r}_1,\boldsymbol{r}_2) = \exp\left[-\frac{(\boldsymbol{r}_1 - \boldsymbol{r}_2)^2}{2\mu^2}\right]. \tag{1.63}$$

We thus see that μ is a measure of the distance for which two points of the transverse section of the beam are considered correlated. The coherence properties of this kind of sources range from the incoherent limit ($\mu = 0$), to the fully coherent case ($\mu = \infty$). In general, they behave as partially coherent.

As is well known, when a GSM beam freely propagates (in the paraxial approach), its mutual intensity at each plane z obeys the law (Gori, 1983)

$$J_{sc}\,(\boldsymbol{r}_1,\boldsymbol{r}_2,z) = \frac{A_0}{F^2\,(z)} \exp\left[-\frac{ik}{2R(z)}\left(r_1^2 - r_2^2\right)\right] \times$$
$$\times \exp\left[-\frac{r_1^2 + r_2^2}{4\sigma^2 F^2(z)}\right] \exp\left[-\frac{(\boldsymbol{r}_1 - \boldsymbol{r}_2)^2}{2\,\mu^2 F^2(z)}\right], \tag{1.64}$$

where

$$F^2(z) = 1 + \frac{(\lambda z/\pi)^2}{4\sigma^2}\left(\frac{1}{4\sigma^2} + \frac{1}{4\mu^2}\right), \tag{1.65a}$$

and

$$R(z) = z\left(1 + \frac{1}{F^2(z)}\right). \tag{1.65b}$$

It is clear from Eq. (1.64), that such a source exhibits a Gaussian transverse profile whose waist is placed at plane $z = 0$.

1.6.2 Gaussian Schell-Model Beams: Vectorial Case

The scalar approach can be applied to uniformly totally polarized beams in those cases in which the state of polarization does no affect to the phenomena under study. However, since beams are, in general, non-uniformly partially polarized, it seems of interest to extend the GSM model to a vectorial framework.

This generalization was introduced in (Gori et al., 2001) by writing the elements of the BCP matrix at plane $z = 0$ (assumed to be the waist plane) in a form that closely resembles the scalar regime

$$J_{\alpha\beta}(\boldsymbol{r}_1,\boldsymbol{r}_2,z=0) = A_{\alpha\beta}\exp\left[-\frac{r_1^2 + r_2^2}{4\sigma_{\alpha\beta}^2} - \frac{(\boldsymbol{r}_1 - \boldsymbol{r}_2)^2}{2\mu_{\alpha\beta}^2}\right], \qquad (\alpha,\beta = s,p), \tag{1.66}$$

where $\sigma_{\alpha\beta}$ and $\mu_{\alpha\beta}$ are positive constants. In particular, $\sigma_{\alpha\alpha}$, $\mu_{\alpha\alpha}$ and $A_{\alpha\alpha} \equiv A_\alpha$, are related, respectively, to the beam width, the transverse coherence length and the beam power associated to each field component. From the mathematical conditions to be satisfied by the BCP matrix, some constrains are inferred, namely, (Gori et al., 2001, 2008)

$$A_{sp}^* = A_{ps};\ \sigma_{sp} = \sigma_{ps};\ \mu_{sp} = \mu_{ps}. \tag{1.67}$$

In addition, from a physical point of view, the argument of the coefficients A_{sp} accounts for a constant phase shift between the s- and p-components of the field. Since such a phase difference could be readily eliminated using a suitable wave-plate, for the sake of simplicity, the argument of A_{sp} will be set equal to zero. In summary, within this formalism, a partially polarized Gaussian Schell-model beam is characterized by nine parameters.

In the following, we will be concerned with a particular type of PGSM beams, namely, those that are undistinguishable from the scalar Gaussian Schell-model fields when no polarizing elements are used. This means that its equivalent mutual intensity at $z = 0$, J_{eq}, defined as

$$J_{eq}(\boldsymbol{r}_1,\boldsymbol{r}_2,0) = J_{ss}(\boldsymbol{r}_1,\boldsymbol{r}_2,0) + J_{pp}(\boldsymbol{r}_1,\boldsymbol{r}_2,0), \tag{1.68}$$

is identical to that of a GSM beam in the scalar case. We then have

$$\sigma_{ss} = \sigma_{pp}; \mu_{ss} = \mu_{pp}, \tag{1.69}$$

and the BCP matrix would be characterized by seven parameters.

The local degree of polarization $P(\boldsymbol{r}, z)$ of this kind of field can be calculated from the elements of the BCP matrix as follows (see Sect. 1.2.4) (Gori, 1998a; Gori et al.1998b)

$$P(\boldsymbol{r},z) = \sqrt{\frac{\left[J_{ss}(\boldsymbol{r},\boldsymbol{r},z) - J_{pp}(\boldsymbol{r},\boldsymbol{r},z)\right]^2 + 4J_{sp}(\boldsymbol{r},\boldsymbol{r},z)^2}{\left[J_{ss}(\boldsymbol{r},\boldsymbol{r},z) + J_{pp}(\boldsymbol{r},\boldsymbol{r},z)\right]^2}}. \tag{1.70}$$

After substituting Eq. (1.66) (with the constraints (1.67) and (1.69)) into Eq. (1.70), the local degree of polarization at the initial plane, $P(\boldsymbol{r}, 0)$, reads

$$P(r,0) = \sqrt{\left(\frac{A_{ss} - A_{pp}}{A_{ss} + A_{pp}}\right)^2 + \frac{4A_{sp}^2}{\left(A_{ss} + A_{pp}\right)^2} \exp\left[-\left(\frac{1}{\sigma_{sp}^2} - \frac{1}{\sigma_{ss}^2}\right) r^2\right]}. \tag{1.71}$$

Let us now further simplify the type of PGSM fields we are considering by making

$$\sigma_{sp} = \sigma_{ss} = \sigma. \tag{1.72}$$

We immediately see that these fields become uniformly partially polarized at z=0, and their BCP matrix, characterized now by six free parameters, takes the form

$$\hat{J}(\boldsymbol{r}_1,\boldsymbol{r}_2,z=0) = \exp\left(-\frac{r_1^2 + r_2^2}{4\sigma^2}\right) \begin{pmatrix} A_s \exp\left(-\frac{(\boldsymbol{r}_1-\boldsymbol{r}_2)^2}{2\mu^2}\right) & A_{sp} \exp\left(-\frac{(\boldsymbol{r}_1-\boldsymbol{r}_2)^2}{2\mu_{sp}^2}\right) \\ A_{sp} \exp\left(-\frac{(\boldsymbol{r}_1-\boldsymbol{r}_2)^2}{2\mu_{sp}^2}\right) & A_s \exp\left(-\frac{(\boldsymbol{r}_1-\boldsymbol{r}_2)^2}{2\mu^2}\right) \end{pmatrix} \tag{1.73}$$

where $A_s = A_{ss}$, $A_p = A_{pp}$, $\mu_{ss} = \mu$, together with the constraints (Gori et al., 2001)

$$A_{sp}^2 \leq A_s A_p, \tag{1.74a}$$

$$\mu \leq \mu_{sp} \leq \mu \left(\frac{\sqrt{A_s A_p}}{A_{sp}}\right)^{1/2}, \tag{1.74b}$$

which are derived by applying the non-negativity condition to the BCP matrix.

In order to analyze how the polarization characteristics of these beams change upon propagation, we have to write the BCP matrix at any distance z. By applying

to each matrix element a similar law to that used for the propagated mutual intensity of a GSM beam in the scalar formalism, we get (Gori et al., 2001)

$$J_{\alpha\beta}(\boldsymbol{r}_1,\boldsymbol{r}_2,z) = \frac{A_{\alpha\beta}}{F^2_{\alpha\beta}(z)} \exp\left[-\frac{ik}{2R_{\alpha\beta}(z)}\left(r_1^2 - r_2^2\right)\right] \times , \\ \times \exp\left[-\frac{r_1^2 + r_2^2}{4\sigma^2 F^2_{\alpha\beta}(z)}\right] \exp\left[-\frac{(\boldsymbol{r}_1 - \boldsymbol{r}_2)^2}{2\mu^2_{\alpha\beta} F^2_{\alpha\beta}(z)}\right], \tag{1.75}$$

where

$$F^2_{\alpha\beta}(z) = 1 + \frac{\left(\lambda z/\pi\right)^2}{4\sigma^2}\left(\frac{1}{4\sigma^2} + \frac{1}{\mu^2_{\alpha\beta}}\right), \tag{1.76}$$

$$R_{\alpha\beta}(z) = z\left(1 + \frac{1}{F^2_{\alpha\beta}(z)}\right), \quad \alpha,\beta = s,p. \tag{1.77}$$

Note that $F_{ss}(z) = F_{sp}(z)$ when $\mu_{ss} = \mu_{sp} = \mu$.

In addition, from Eq. (1.70) we obtain at once the free propagation law for the local degree of polarization of this type of fields:

$$P(\boldsymbol{r},z) = \left\{\left(\frac{A_s - A_p}{A_s + A_p}\right)^2 + \frac{4A^2_{sp}}{\left(A_s + A_p\right)^2}\left[\frac{F_{ss}(z)}{F_{sp}(z)}\right]^4 \\ \exp\left[-\frac{r^2}{\sigma^2}\left(\frac{1}{F^2_{sp}(z)} - \frac{1}{F^2_{ss}(z)}\right)\right]\right\}^{1/2}. \tag{1.78}$$

This expression shows that, for this class of PGSM beams, the degree of polarization, which is uniform at the plane $z = 0$, will exhibit a position-dependence (Gaussian) at any cross-section (unless either $\mu_{ss} = \mu_{sp}$ or $A_{sp} = 0$). In particular, it can be shown that if the light field is totally polarized across the source plane ($P(\boldsymbol{r},0) = 1$), then the beam keeps such behavior upon propagation. It should also be noted that the condition $P(\boldsymbol{r},z) \leq 1$ for any choice of $(\boldsymbol{r},z)$ leads to further limitations for the values μ_{ss} and μ_{sp}.

More details about the behavior of the local degree of polarization upon free propagation and its dependence with the parameters of the light source can be found in (Gori et al., 2001).

1.6.3 The Van Cittert-Zernike Theorem

As is well known, within the scalar approach, the van Cittert-Zernike theorem is one of the most important results of the theory of partial coherence (Born and Wolf, 1999; Mandel and Wolf, 1995; Perina, 1971; Wolf, 2007). It is a fundamental tool in the study of the propagation of partially coherent fields. Moreover, the generalization of this theorem to partially polarized fields could be of practical use for

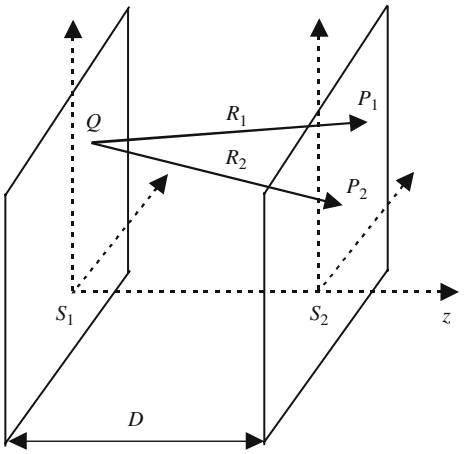

Fig. 1.10 The van Cittert-Zernike theorem: Notation

synthesizing the PGSM beams we have just considered. Let us then review this theorem, written in both, the scalar and the vectorial versions.

We first consider a planar quasi-monochromatic spatially-incoherent secondary source whose mutual intensity at a source plane S_1 is given by

$$J\left(\boldsymbol{\rho}_1,\boldsymbol{\rho}_2\right) = \lambda^2 A_0\left(\boldsymbol{\rho}_1\right)\delta\left(\boldsymbol{\rho}_1 - \boldsymbol{\rho}_2\right) \tag{1.79}$$

where λ represents here the mean wavelength, $\boldsymbol{\rho}_1$ and $\boldsymbol{\rho}_2$ are two points of the source plane, δ denotes the two-dimensional Dirac delta function and $A_0\left(\boldsymbol{\rho}_1\right)$ is proportional to the irradiance at point $\boldsymbol{\rho}_1$. Equation (1.79) implies that any two arbitrary distinct points across the source plane are uncorrelated. For an arbitrary couple of points (P_1 and P_2) at a certain transverse plane S_2 (see Fig. 1.10), the mutual intensity can be shown to read

$$J\left(\boldsymbol{r}_1,\boldsymbol{r}_2\right) = \iint_{S_1} A_0\left(\boldsymbol{\rho}\right)\frac{e^{ik(R_1-R_2)}}{R_1 R_2}\cos\theta_1\cos\theta_2\, d\boldsymbol{\rho}, \tag{1.80}$$

where $\boldsymbol{\rho}$ is the position vector of a generic point Q of S_1, $\boldsymbol{r}_i$, $i = 1,2$, denote the position vectors of points P_i, R_i are the distances from Q to P_i, and θ_i are the angles that forms QP_i with the z-axis.

Equation (1.80) represents the well-known expression of the van Cittert-Zernike theorem in the scalar case. It should be remarked that we are assuming that the dimensions of the source are large compared with the mean wavelength. In turns, the source size and the distance between P_1 and P_2 are considered to be small compared with the distance D between S_1 and S_2. Taking this into account, the van Cittert-Zernike theorem can also be written in the form (Mandel and Wolf, 1995)

$$J\left(\boldsymbol{r}_1,\boldsymbol{r}_2\right) = \frac{\exp\left[\frac{ik}{2D}\left(r_1^2 - r_2^2\right)\right]}{D^2}\iint_{S_1} A_0\left(\boldsymbol{\rho}\right)\exp\left[\frac{-ik}{D}\boldsymbol{\rho}\cdot\left(\boldsymbol{r}_1 - \boldsymbol{r}_2\right)\right]d\boldsymbol{\rho}. \tag{1.81}$$

We see that Eq. (1.81) represents (a quadratic factor apart) the Fourier transform of the beam irradiance at the source plane. Moreover, the complex degree of coherence at plane S_2 reads

$$j\left(\boldsymbol{r}_1,\boldsymbol{r}_2\right)=\exp\left[\frac{ik}{2D}\left(\boldsymbol{r}_1^2-\boldsymbol{r}_2^2\right)\right]\mathrm{G}(\boldsymbol{r}_1-\boldsymbol{r}_2), \tag{1.82}$$

where

$$G(\boldsymbol{r}_1-\boldsymbol{r}_2)=\frac{\iint\limits_{S_1}A_0\left(\boldsymbol{\rho}\right)\exp\left[\frac{-ik}{D}\boldsymbol{\rho}\cdot\left(\boldsymbol{r}_1-\boldsymbol{r}_2\right)\right]d\boldsymbol{\rho}}{\iint\limits_{S_1}A_0\left(\boldsymbol{\rho}\right)d\boldsymbol{\rho}}. \tag{1.83}$$

Equation (1.82) can be understood as the normalized amplitude one would observe at P_1 if a spherical wave, converging to P_2, illuminates an opening with identical shape and size as the source, and whose amplitude distribution over the diffracting aperture is proportional to the irradiance across the source. This meaningful interpretation makes of quite practical use the van Cittert-Zernike theorem applied to instrumental-optics problems (concerning, for instance, the resolving power in optical systems and image formation).

A second well-known consequence easily inferred from this theorem refers to the increment of coherence of the light field upon free propagation, even though the initial (planar) source is spatially incoherent.

In order to extend the van Cittert-Zernike theorem to the vectorial regime, some proposals have been reported in the literature (Alonso et al., 2006; Gori et al., 2000). Within the paraxial approach, we focus our attention to that introduced in (Gori et al., 2000): The BCP matrix of a partially polarized spatially-incoherent source at $z=0$ is written in the form

$$\hat{J}\left(\boldsymbol{\rho}_1,\boldsymbol{\rho}_2,0\right)=\lambda^2\begin{pmatrix}A_{ss}\left(\boldsymbol{\rho}_1\right)\delta\left(\boldsymbol{\rho}_1-\boldsymbol{\rho}_2\right) & A_{sp}\left(\boldsymbol{\rho}_1\right)\delta\left(\boldsymbol{\rho}_1-\boldsymbol{\rho}_2\right)\\ A_{ps}\left(\boldsymbol{\rho}_1\right)\delta\left(\boldsymbol{\rho}_1-\boldsymbol{\rho}_2\right) & A_{pp}\left(\boldsymbol{\rho}_1\right)\delta\left(\boldsymbol{\rho}_1-\boldsymbol{\rho}_2\right)\end{pmatrix}. \tag{1.84}$$

It can be shown that each element of the BCP in Eq. (1.84) obeys a propagation law analogous to Eq. (1.81), i.e.,

$$\begin{aligned}J_{\alpha\beta}\left(\boldsymbol{r}_1,\boldsymbol{r}_2,z\right)=&\frac{\exp\left[\frac{ik}{2z}\left(r_1^2-r_2^2\right)\right]}{z^2}\iint\limits_{S_1}A_{\alpha\beta}\left(\boldsymbol{\rho}\right)\\&\exp\left[\frac{-ik}{z}\boldsymbol{\rho}\cdot\left(r_1-r_2\right)\right]d\boldsymbol{\rho};\ \left(\alpha,\beta=s,p\right),\end{aligned} \tag{1.85}$$

which generalizes the van Cittert-Zernike theorem to partially polarized beams.

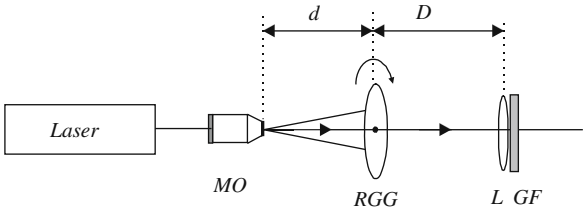

Fig. 1.11 Experimental set up used for the synthesis of a Gaussian Schell-model beam in the scalar case. MO: microscope objective; RGG: rotating ground glass; L: converging lens; GF: Gaussian filter.

1.6.4 Experimental Synthesis of GSM fields

As we mentioned earlier, the above theorem provides a useful tool for the synthesis of GSM beams in both the scalar and the vectorial treatments. For illustrative purposes, we next briefly describe the synthesis process in the scalar case (Santis et al., 1986) (the vectorial synthesis is a generalization of the scalar procedure).

The main goal would then be the generation of both Gaussian beam irradiance, $A(\boldsymbol{r})$, and Gaussian degree of coherence $j(\boldsymbol{r}_1,\boldsymbol{r}_2)$, namely,

$$A\,(\boldsymbol{r}) = A_0\,\exp\left(\frac{r^2}{\sigma^2}\right), \tag{1.86a}$$

$$j\,(\boldsymbol{r}_1,\boldsymbol{r}_2) = \exp\left[\frac{(\boldsymbol{r}_1-\boldsymbol{r}_2)^2}{2\mu^2}\right]. \tag{1.86b}$$

From Eq. (1.82), it follows that $j(\boldsymbol{r}_1, \boldsymbol{r}_2)$, given by Eq. (1.86b), can be understood (quadratic phase factors apart) as the complex degree of coherence of the field propagated (according with the van Cittert-Zernike theorem) from a planar spatially-incoherent secondary source. Such source with a Gaussian profile can be implemented by using the set-up shown in Fig. 1.11. We handle a TEM_{00} laser beam, a microscope objective, *MO*, to focus the field, and a rotating ground glass, *RGG*, placed at a distance d from the objective. The irradiance of the incoherent source, just after the rotating glass, is given by

$$A_i\,(\boldsymbol{r}) = A_0 \exp\left(\frac{r^2}{\sigma_i^2}\right), \tag{1.87}$$

where A_0 is a constant and σ_i denotes the transverse width of the beam. Note that this size can be modified by choosing the appropriate distance d.

After freely propagating a distance D from the glass, the partially coherent field distribution can be inferred making use of the van Cittert-Zernike theorem. In fact, a Gaussian degree of coherence is obtained whose transverse coherence length μ is given by

$$\mu = \frac{D}{\sqrt{2}}\frac{\lambda}{\pi\,\sigma_i}. \tag{1.88}$$

In order to cancel out the quadratic factor in Eq. (1.82), a lens with focal length D is used. The final step of the procedure consists of placing a Gaussian filter (GF) in front of the beam. We thus obtain a secondary source with a Gaussian profile of the required width, σ. The waist of the synthesized field is located at the GF plane. It should also be remarked that, on varying the distance D, we could control at will the degree of coherence of the source.

Partially polarized Gaussian Schell-model beams have been synthesized by using a similar method, but, in this case, by applying the vectorial van Cittert-Zernike theorem. We handle two incoherent primary sources, linearly polarized along orthogonal axes, which are superposed through a Mach-Zehnder interferometer. For further details, the interested reader could see (Piquero et al., 2002).

References

Alonso, M. A., Korotkova, O., Wolf, E. (2006): Propagation of the electric correlation matrix and the van Cittert-Zernike theorem for random electromagnetic fields, J. Mod. Opt. 53, 969–978.

Azzam, R. M. A., Bashara, N. M. (1987): *Ellipsometry and Polarized Light* (North-Holland, Amsterdam).

Beran, M. J., Parrent, G. B. (1967): *Theory of Partial Coherence* (Prentice Hall, Englewood Cliffs, NJ)

Bomzon, Z., Biener, G., Kleiner, V., Hasman, E. (2002): Radially and azimuthally polarized beams generated by space-variant dielectric subwavelength gratings, Opt. Lett. 27, 285–287.

Born, M., Wolf, E. (1999): *Principles of Optics*, 7th ed., (Cambridge University Press, Cambridge).

Brosseau, C. (1998): *Fundamentals of Polarized Light* (Wiley, New York).

Chipman, R. A. (1994): Polarimetry, Chap. 22, *Handbook of Optics*, vol. II (McGraw-Hill, New York).

Collett, E. (1992): *Polarized Light*, (Marcel Dekker, Inc. New York).

Deng, D., Guo, Q., Wu, L., Yang, X. (2007): Propagation of radially polarized elegant light beams, J. Opt. Soc. Am. B 24, 636–643.

Diehl, D. W., Schoonover, R. W., Visser, T. D. (2006): The structure of focused, radially polarized fields, Opt. Express 14, 3030–3038.

Dorn, R., Quabis, S., Lenchs, G. (2003): Sharper focus for a radially polarized light beam, Phys. Rev. Lett. 91, 233901 (1–4).

Erdelyi, M., Bor, Z. (2006): Radial and azimuthal polarizers, J. Opt. A: Pure Appl. Opt. 8, 737–742.

Erdelyi, M., Gajdatsy, G. (2008): Radial and azimuthal polarizer by means of a birefringent plate, J. Opt. A: Pure Appl. Opt. 10, 055007 (1–6).

Eyyuboglu, H. T., Baykal, Y., Cai, Y. (2007): Degree of polarization for partially coherent general beams in turbulent atmosphere, Appl. Phys. B 89, 91–97.

Ge, D., Cai, Y. J., Lin, Q. (2004): Propagation of partially polarized Gaussian Schell-model beams in dispersive and absorbing media, Opt. Commun. 229, 93–98.

Gevorgyan, A. H. (2003): Nonreciprocal waves in absorbing multilayer elements, Tech. Phys. Lett. 29, 819–823.

Gil, J. J. (2000): Characteristic properties of Mueller matrices, J. Opt. Soc. Am. A 17, 328–334.

Goldstein, D. (2003): *Polarized Light*, 2nd ed., Revised and Expanded (Optical Science and Engineering, Dekker).

Gori, F., Palma, C. (1978): Partially coherent sources which give rise to highly directional light beams, Opt. Commun. 27, 185–188.

Gori, F. (1980): Collett-Wolf sources and multimode lasers, Opt. Commun. 34, 301–305.

Gori, F. (1983): Mode propagation of the field generated by Collett-Wolf sources, Opt. Commun. 46, 149–154.

Gori, F. (1998a): Matrix treatment for partially polarized, partially coherent beams, Opt. Lett. 23, 241–243.
Gori, F., Santarsiero, M., Vicalvi, S., Borghi, R., Guattari, G. (1998b): Beam coherence-polarization matrix, J. Eur. Opt. Soc. A: Pure Appl. Opt. 7, 941–951.
Gori, F., Santarsiero, M., Borghi, R., Piquero, G. (2000): Use of the van Cittert-Zernike theorem for partially polarized sources, Opt. Lett 25, 1291–1293.
Gori, F., Santarsiero, M., Piquero, G., Borghi, R., Mondello, A., Simon, R. (2001): Partially polarized Gaussian Schell-model beams, J. Opt. A: Pure Appl. Opt. 3, 1–9.
Gori, F., Santarsiero, M., Borghi, R., Ramírez-Sánchez, V. (2008): Realizability condition for electromagnetic Schell-model sources, J. Opt. Soc. Am. A 25, 1016–1020.
Gupta, D. N., Kant, N., Kim, D. E., Suk, H. (2007): Electron acceleration to GeV energy by a radially polarized laser, Phys. Lett. A 368, 402–407.
Hanson, S. G., Wang, W., Jakobsen, M. L., Takeda, M. (2008): Coherence and polarization of electromagnetic beams modulated by random phase screens and their changes through complex ABCD optical systems, J. Opt. Soc. Am. A 25, 2338–46.
Hecht, E. (1998): *Optics* (Addison Wesley Longman, London).
Korotkova, O., Salem, M., Wolf, E. (2004): Beam conditions for radiation generated by an electromagnetic Gaussian Schell-model source, Opt. Lett. 29, 1173–1175.
Kozawa, Y., Sato, S. (2007): Sharper focal spot formed by higher-order radially polarized laser beams, J. Opt. Soc. Am. A 24, 1793–1798.
Lu, B. D., Pan, L. Z. (2002): Propagation of vector Gaussian-Schell-model beams through a paraxial optical ABCD system, Opt. Commun. 205, 7–16.
Lumer, Y., Moshe, I., Horovitz, Z., Jackel, S., Machavariani, G., Meir, A. (2008): Thermally induced birefringence in nonsymmetrically pumped laser rods and its implications for attainment of good beam quality in high-power, radially polarized lasers, Appl. Opt. 47, 3886–3891.
Lumer, Y., Moshe, I., (2009): Radial and azimuthal beam parameters, Opt. Lett. 34, 265–267.
Machavariani, G., Lumer, Y., Moshe, I., Meir, A., Jackel, S. (2007): Birefringence-induced bifocusing for selection of radially or azimuthally polarized laser modes, Opt. Lett. 32, 1468–1470.
Mandel, L., Wolf, E. (1995): *Optical Coherence and Quantum Optics* (Cambridge University Press, Cambridge).
Martínez-Herrero, R., Mejías, P. M., Piquero, G. (2006): Overall parameters for the characterization of non-uniformly totally polarized beams, Opt. Commun. 265, 6–10.
Martínez-Herrero, R., Mejías, P. M., Piquero, G. (2008): Global parameters for characterizing the radial and azimuthal polarization content of totally polarized beams, Opt. Commun. 281, 1976–1980.
Mejías, P. M., Martínez-Herrero, R., Piquero, G., Movilla, J. M. (2002): Parametric characterization of the spatial structure of non-uniformly polarized laser beams, Prog. Quantum Electron. 26, 65–130.
Meier, M., Romano, V., Feurer, T. (2007): Material processing with pulsed radially and azimuthally polarized laser radiation, Appl. Phys. 86, 329–334.
Moshe, I., Jackel, S., Meir, A. (2003): Production of radially or azimuthally polarized beams in solid-state lasers and the elimination of thermally induced birefringence effects, Opt. Lett. 28, 807–809.
Moshe, I., Jackel, S., Meir, A., Lumer, Y, Leibush, E. (2007): 2 kW, M2<10 radially polarized beams from aberration-compensated rod-based Nd:YAG lasers, Opt. Lett. 32, 47–49.
Moser, T., Glur, H., Romano, V., Pigeon, F., Parriaux, O., Ahmed, M. A., Graf, T. (2005): Polarization-selective grating mirrors used in the generation of radial polarization, Appl. Phys. B 80, 707–713.
Nieminen, T. A., Heckenberg, N. R., Rubinsztein-Dunlop, H. (2008): Forces in optical tweezers with radially and azimuthally polarized trapping beams, Opt. Lett. 33, 122–124.
Niziev, V. G., Nesterov, A. V. (1999): Influence of beam polarization on laser cutting efficiency, J. Phys. D: Appl. Phys. 32, 1455–1461.

O'Neill, E. L. (1963): *Introduction to Statistical Optics* (Addison-Wesley, Reading, Massachusetts).
Oron, R., Blit, S., Davidson, N., Fiesem, A. A. (2000): The formation of laser beams with pure azimuthal or radial polarization, Appl. Phys. Lett. 77, 3322–3324.
Pan, L., Lu, B. (2003): Propagation properties of partially polarized Gaussian Schell-model beams through an axis-unsymmetric paraxial ABCD system, Opt. Quantum Electron. 35, 129–138.
Pasilly, N., Denis, R. S. (2005): Aït-Ameur, K., Treussart, F., Hierle, R., Roch, J. F., Simple interferometric technique for generation of a radially polarized light beam, J. Opt. Soc. Am. A 22, 984–991.
Perina, J. (1971): *Coherence of Light* (Van Nostrand Reinhold Company, London).
Phua, P. B., Lai, W. J. (2007): Simple coherent polarization manipulation scheme for generating high power radially polarized beam, Opt. Express 15, 14251–14256.
Piquero, G., Movilla, J. M., Mejías, P. M., Martínez-Herrero, R. (1999): Degree of polarization of non-uniformly partially polarized beams: a proposal, Opt. Quant. Electron. 31, 223–225.
Piquero, G., Borghi, R., Santarsiero, M. (2001a): Gaussian Schell-model beams propagating through polarization gratings, J. Opt. Soc. Am. A 18, 1399–1405.
Piquero, G., Borghi, R., Mondello, A., Santarsiero, M. (2001b): Far field of beams generated by quasi-homogeneous sources passing through polarization gratings, Opt. Comm. 195, 339–350.
Piquero, G., Gori, F., Romanini, P., Santarsiero, M., Borghi, R., Mondello, A. (2002): Synthesis of partially polarized Gaussian Schell-model sources, Opt. Commun. 208, 9–16.
Piquero, G., Vargas-Balbuena, J. (2004): Non-uniformly polarized beams across their transverse profiles: an introductory study for undergraduate optics courses, Eur. J. Phys. 25, 793–800.
Provenziani, D., Ciattoni, A., Cincotti, G., Palma, C., Ravaccia, F., Sapia, C. (2002): Stokes parameters of a Gaussian beam in a calcite crystal, Opt. Express 10, 699–706.
Quabis, S., Dorn, R., Leuchs, G. (2005): Generation of a radially polarized doughnut mode of high quality, Appl. Phys. B 81, 597–600.
Qiu, Y., Liu, J., Chen, Z. (2009): Propagation properties of radially polarized partially coherent LG (0,1)* beams, Opt. Commun. 282, 69–73.
Roth, M. S., Wyss, E. W., Glur, H., Weber, H. P. (2005): Generation of radially polarized beams in a Nd:YAG laser with self-adaptive overcompensation of the thermal lens, Opt. Lett. 30, 1665–1667.
Roychowdhury, H., Korotkova, O. (2005): Realizability conditions for electromagnetic Gaussian Schell-model sources, Opt. Commun. 249, 379–385.
Santarsiero, M., Borghi, R., Ramírez-Sánchez, V. (2009): Synthesis of electromagnetic Schell-model sources, J. Opt. Soc. Am. A 26, 1437–1443.
Santis, P., Gori, F., Palma, C. (1979): Generalized Collett-Wolf sources, Opt. Commun. 28, 151–155.
Santis, P., Gori, F., Guattari, G., Palma, C. (1986): Synthesis of partially coherent fields, J. Opt. Soc. Am. A 3, 1258–1262.
Sheppard, C. J. R., Choudhury, A. (2004): Annular pupils, radial polarization, and superresolution, Appl. Opt. 43, 4322–4327.
Shirai, T. (2005a): Polarization properties of a class of electromagnetic Gaussian Schell-model beams which have the same far-zone intensity distribution as a fully coherent laser beam, Opt. Commun. 256, 197–209.
Shirai, T.; Korotkova, O.; Wolf, E. (2005b): A method of generating electromagnetic Gaussian Schell-model beams, J. Opt. A: Pure Appl. Opt 7, 232–237.
Shurcliff, W. A. (1962): *Polarized Light* (Harvard University Press, Cambridge, Mass.).
Simon, R. (1982): The connection between the Jones and Mueller matrices, Opt. Commun. 42, 293–297.
Simon, R., Sudarshan, E. C. G., Mukunda, N. (1987): Cross polarization in laser beams, Appl. Opt. 26, 1589–1593.
Stalder, M., Schadt, M. (1996): Linearly polarized light with axial symmetry generated by liquid-crystal polarization converters, Opt. Lett. 21, 1948–50.

Tidwell, S. C., Ford, D. H., Kimura, W. D. (1990): Generating radially polarized beams interferometrically, Appl. Opt. 29, 2334–2339.
Tovar, A. (1998): Production and propagation of cylindrically polarized Laguerre-Gaussian Laser beams, J. Opt. Soc. Am. A 15, 2705–2711.
Volpe, G., Petrov, D. (2004): Optical tweezers with cylindrical vector beams produced by optical fibers, Opt. Commun. 237, 89–95.
Wang, H., Wang, X., Zeng, A., Yang, K. (2007): Effects of coherence on anisotropic electromagnetic Gaussian-Schell model beams on propagation, Opt. Lett. 32, 2215–2217.
Whitney, C. (1971): Pauli-algebraic operators in polarization optics, J. Opt. Soc. Am. 61, 1207–1213.
Wolf, E. (1959): Coherence properties of partially polarized electromagnetic radiation, Il Nuovo Cimento 13, 1165–1181.
Wolf, E. (2007): *Introduction to the Theory of Coherence and Polarization of Light* (Cambridge University Press, Cambridge).
Wu, G., Lou, Q., Zhou, J., Dong, J., Wei, Y. (2007): Focal shift in focused radially polarized ultrashort pulsed laser beams, Appl. Opt. 46, 6251–6255.
Yonezawa, K., Kozawa, Y., Sato, S. (2008): Focusing of radially and azimuthally polarized beams through a uniaxial crystal, J. Opt. Soc. Am A 25, 469–472.
Zhan, Q. W. (2004): Trapping metallic Rayleigh particles with radial polarization, Opt. Express 12, 3377–3382.
Zhao, G. P. (2006): Spectral switches of vector Gaussian Schell-model beams passing through a spherically aberrated lens, J. Mod. Opt. 53, 1083–1092.

Chapter 2
Second-Order Overall Characterization of Non-uniformly Polarized Light Beams

2.1 Introduction

In the previous chapter, the light fields were represented in the space-time domain by means of the BCP matrix (or through the mutual coherence function in the scalar case). For convenience, we will now prefer to work in the space-frequency regime. Consequently, as is well known in the Optics textbooks (Born and Wolf, 1999; Mandel and Wolf, 1995; Perina, 1971; Wolf, 2007) the partially coherent scalar field would then be described (up to second-order) by the so-called cross-spectral density (CSD) $W(\boldsymbol{r}_1, \boldsymbol{r}_2, z; \omega)$, defined in the form

$$W(\boldsymbol{r}_1,\boldsymbol{r}_2,z;\omega) = \overline{E^*(\boldsymbol{r}_1,z;\omega)\, E(\boldsymbol{r}_2,z;\omega)}, \tag{2.1}$$

where E denotes the wide-sense stationary random field, $\boldsymbol{r}_1$ and $\boldsymbol{r}_2$ represent two points at the beam cross-section, orthogonal to the propagation direction z, and the overbar symbolizes the average over the ensemble of realizations. For the sake of simplicity, the explicit dependence on the angular frequency ω of the light beam will be omitted from now on. Although W enables us to propagate analytically the field through optical systems, the accurate experimental determination of the CSD function is not a simple task, and becomes especially difficult for multimode laser beams (for example, those emitted by high-power lasers).

Instead of such a local analysis, there are many situations in which a global characterization would be of more practical use. More specifically, in the present chapter, we are interested in a description of the spatial structure of light fields by means of overall parameters that

(i) are valid for arbitrary beams,
(ii) are defined analytically in a rigorous way,
(iii) are measurable,
(iv) propagate through common optical systems according to simple laws.

Thus, this chapter is arranged as follows. In the next section the overall scalar formalism is shown, and, in Sect. 2.3, a generalization to the vectorial case (i.e., to

R. Martínez-Herrero et al., *Characterization of Partially Polarized Light Fields*, Springer Series in Optical Sciences 147, DOI 10.1007/978-3-642-01327-0_2,

partially polarized beams) is provided. The generalized degree of polarization of non-uniformly polarized fields is introduced in Sect. 2.4. Section 2.5 is devoted to the so-called beam quality parameter of a light field, which provides a meaningful joint description of the focusing capabilities of the beam at the near- and far-field. Application of the above parameters to the particular but important case of partially-polarized Gauss Schell-model beams is analyzed in Sect. 2.6. The possibility of beam quality improvement is considered in Sect. 2.7, and the changes generated on this parameter by different types of optical phase devices are described in Sect. 2.8. Finally, an introductory example of global beam shaping of non-uniformly polarized fields is briefly discussed in Sect. 2.9.

2.2 Second-Order Overall Characterization: Scalar Case

We next provide a survey of the key spatial global characteristics that are commonly used in the scalar framework. They are based on the so-called irradiance moments of the field, which describe the overall spatial structure of the beam. It should be remarked that these scalar parameters and figures of merit have been accepted as current ISO standards for light fields (ISO, 1999, 2003, 2005). Furthermore, the scalar treatment constitutes an appropriate starting point to investigate, in subsequent sections, the polarization behavior in the more involved vectorial case.

2.2.1 Formalism and Key Definitions

To begin with, let us first define the Wigner distribution function (WDF), which is associated to the CSD function through a Fourier transform relationship (Bastiaans, 1989):

$$h(\boldsymbol{r},\boldsymbol{\eta},z) = \int_{-\infty}^{+\infty} W(\boldsymbol{r},\boldsymbol{s},z) \exp(ik\,\boldsymbol{\eta}\cdot\boldsymbol{s})\; d\boldsymbol{s}, \tag{2.2}$$

where $\boldsymbol{r} = (x,y)$ denotes the two-dimensional position vector at a transverse plane, $k\boldsymbol{\eta} = (ku, kv) = (k_x, k_y)$ gives the wavevector components along the Cartesian x and y axes, and $\boldsymbol{s}$ is a vectorial variable. Accordingly, u and v would represent angles of propagation (without taking evanescent waves into account). In Eq. (2.2) the CSD function is expressed in terms of the variables $\boldsymbol{r}$ and $\boldsymbol{s}$, which are related with $\boldsymbol{r}_1$ and $\boldsymbol{r}_2$ by the formulae (see Fig. 2.1):

$$\boldsymbol{r} = \frac{\boldsymbol{r}_1 + \boldsymbol{r}_2}{2}, \tag{2.3a}$$

$$\boldsymbol{s} = \boldsymbol{r}_1 - \boldsymbol{r}_2. \tag{2.3b}$$

The WDF was introduced by Wigner to describe the quantum-mechanics phenomena in the (position-momentum) phase space. Later Walther (1968) demonstrated the role of this function in Optics as a link between partial coherence and

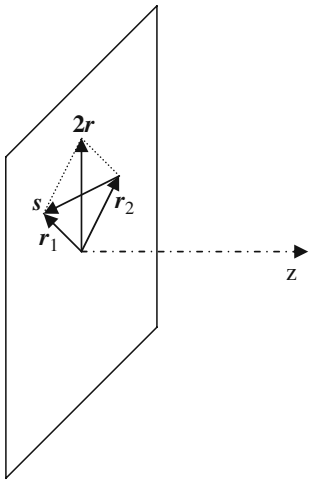

Fig. 2.1 Illustrating the geometrical representation of vectors $\boldsymbol{r}$ and $\boldsymbol{s}$

traditional radiometry: The WDF can physically be understood in Optics as the amplitude associated to a ray passing through a point along a certain direction. Some care, however, should be taken because the WDF could reach negative values in certain cases (Friberg, 1993; Marchand and Wolf, 1974) (unlike the positiveness of the energy content of a ray). Note that integration of $h(\boldsymbol{r},\boldsymbol{\eta},z)$ over the angular variables u and v is proportional to the beam irradiance. Moreover, integration over the spatial variables x and y gives the directional intensity, which is a proportional to the radiant intensity of the field (a factor $\cos^2\alpha$ apart, where α is the angle of observation with respect to the z-axis).

In terms of the WDF, a number of parameters can be defined, which provide an overall spatial description of the field upon propagation. Let us introduce the beam irradiance moments in the form

$$\langle x^m y^n u^p v^q \rangle \equiv \frac{1}{I_o} \iint_{-\infty}^{+\infty} x^m y^n u^p v^q h\,(\boldsymbol{r},\boldsymbol{\eta},z)\, d\boldsymbol{r}\, d\boldsymbol{\eta}, \tag{2.4}$$

where m, n, p, q are integer numbers, the sharp brackets $\langle\ \rangle$ are defined by Eq. (2.4) itself, and

$$I_0 = \iint_{-\infty}^{+\infty} h\,(\boldsymbol{r},\boldsymbol{\eta},z)\, d\boldsymbol{r}\, d\boldsymbol{\eta} \tag{2.5}$$

At each transverse plane, the four first-order beam moments, $\langle x\rangle$, $\langle y\rangle$, $\langle u\rangle$ and $\langle v\rangle$, characterize the center of the beam profile and the mean direction of the field. For simplicity, in what follows it will be assumed that these moments equal zero. This is not a true restriction, since it is equivalent to a shift of the Cartesian coordinate system. In summary, we consider that the z-axis coincides with the mean direction of propagation, and the beam center is placed on this axis at any plane z.

The resulting ten different second-order moments allow a global and meaningful characterization of the spatial structure of a partially coherent quasimonochromatic beam. In terms of them, we may introduce the following parametrization for scalar fields (see, for example, (Giesen and Morin, 1998; Giesen and Weber 2002; Kudryashov et al., 2006; Laabs and Weber, 2000; Mejías et al., 1993; Morin and Giesen, 1996; Weber et al., 1994; WLT, 2001)):

(i) $\langle r^2 \rangle = \langle x^2 + y^2 \rangle$: (Squared) *spatial size* of the beam cross-section, referred to the region where the irradiance takes significant values. In this expression, $\langle x^2 \rangle$ and $\langle y^2 \rangle$ represent (squared) transverse beam widths along the x and y-axes, respectively (see Fig. 2.2). In terms of the beam irradiance, $I(x,y)$, this moment reads

$$\langle x^2 + y^2 \rangle = \frac{\iint_{-\infty}^{+\infty} \left(x^2 + y^2\right) I\,(x,y)\,dxdy}{\iint_{-\infty}^{+\infty} I\,(x,y)\,dxdy}. \tag{2.6}$$

(ii) $\langle \eta^2 \rangle = \langle u^2 + v^2 \rangle$: (Squared) *far-field divergence*, which is connected with the energy distribution associated with each spatial frequency of the beam.

(iii) $\langle \boldsymbol{r} \cdot \boldsymbol{\eta} \rangle = \langle xu + yv \rangle$: This moment provides the position of the *beam waist*, i.e., the plane where the beam width takes its minimum value (see Fig. 2.2). At the

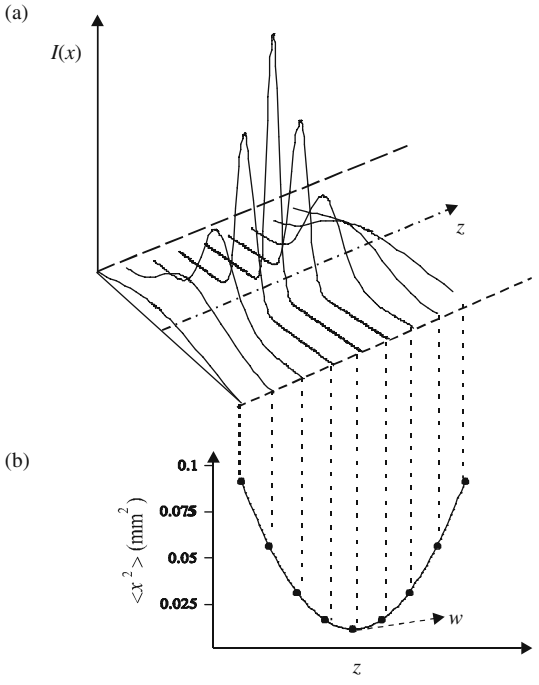

Fig. 2.2 Free propagation of a typical (one-dimensional) Gaussian beam (λ = 633 nm). (**a**) Irradiance profiles at different planes z = constant. (**b**) Parabolic dependence of the second-order moment $\langle x^2 \rangle$ on the propagation distance z. The value w denotes the position of the waist plane (minimum beam width). In the figure, the separation between the successive planes is 125 mm. See also (Mejías et al., 2002)

waist plane, $\langle xu + yv \rangle$ vanishes. It should be remarked that a general astigmatic beam would exhibit different minimum widths, $\langle x^2 \rangle_{\min}$ and $\langle y^2 \rangle_{\min}$ at different positions along z. The global beam waist, whose position z_w is given by the condition

$$\langle xu + yv \rangle = 0, \tag{2.7}$$

refers to the minimum value (under free propagation) of the global second-order moment $\langle r^2 \rangle$. Note, in addition, that $\langle xu \rangle$ and $\langle yv \rangle$ are related to the curvature radii of the beam wavefront by the formulae:

$$R_x = \frac{\langle x^2 \rangle}{\langle xu \rangle}, \tag{2.8}$$

$$R_y = \frac{\langle y^2 \rangle}{\langle yv \rangle}. \tag{2.9}$$

(iv) $\langle xy \rangle$: It gives the orientation (with regard to the laboratory axes) of the so-called *principal axis* of the beam through the condition $\langle xy \rangle = 0$ (Martínez-Herrero and Mejías, 2006a, b; Serna et al., 1991, 1992a, b). It should be noticed that the beam widths $\langle x^2 \rangle^{1/2}$ and $\langle y^2 \rangle^{1/2}$ reach their extreme (maximum and minimum) values along the principal axes (see Fig. 2.3). Since, for general beams, the transverse profile rotates as the field propagates into free space, these axes are used to determine the orientation of the beam profile.

(v) $\langle uv \rangle$: It provides the orientation of the so-called *absolute axes* of the beam (Serna et al., 1991, 1992a, b), defined by the condition $\langle uv \rangle = 0$. Unlike the principal axes, the absolute axes do not rotate upon free propagation, and they constitute an absolute transverse coordinate system with respect to which the orientation of the principal axes can be established.

(vi) $\langle xv \rangle - \langle yu \rangle$: It is related with the *orbital angular momentum* of the global beam (Alieva and Bastiaans, 2004; Allen et al., 2009; Bekshaev et al., 2003; Martínez-Herrero and Mejías, 2006b; Nemes and Siegman, 1994; Vasnetsov et al., 2003). The existence of angular momentum is a consequence of the beam structure and is responsible for the twisting spatial behavior of certain

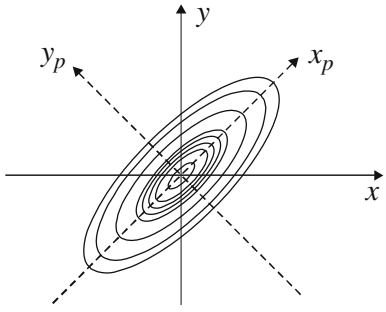

Fig. 2.3 Illustrating the second-order moment <*xy*>. The contour lines of equal irradiance (isophotes) correspond to an astigmatic Gaussian profile at a transverse plane. The principal axes are denoted by x_P,y_P

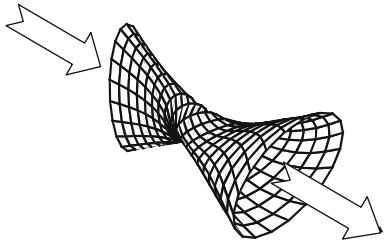

Fig. 2.4 Illustrating the spatial behavior of a twisted Gaussian beam (upon free propagation). The arrows show the propagation direction of the beam. See also (Mejías et al., 2002)

fields under free propagation (see Fig. 2.4). Note, in this sense, that the time-averaged orbital angular-momentum flux, J_z , transported by a beam through a transverse plane z reads

$$J_z = \frac{I_0}{c} \left(\langle xv \rangle - \langle yu \rangle \right). \tag{2.10}$$

where c is the speed of light in vacuum. In particular J_z equals zero for rotationally-symmetric Gaussian fields as well as for Hermite-Gauss beams, but it changes for twisted Gaussian fields (Gori et al., 1994; Nemes and Siegman, 1994; Simon and Mukunda, 1993) or for certain Laguerre-Gauss beams. The reader should realize that, in general, no plane wavefront exists in the waist region, but two cylindrical wavefronts separated by a certain distance. Hence, in a general case, there is no common waist along the orthogonal x- and y-axes.

It is interesting to note that, for deterministic beams represented by a well-defined electric field amplitude E, the above physical parameters can also be directly written in terms of E as follows:

$$\langle r^2 \rangle = \frac{1}{I} \iint r^2 |E(r,\theta)|^2 \, r \, dr \, d\theta, \tag{2.11a}$$

$$\langle \eta^2 \rangle = \frac{1}{k^2 I} \iint \left(\left| \frac{\partial E}{\partial r} \right|^2 + \frac{1}{r^2} \left| \frac{\partial E}{\partial \theta} \right|^2 \right) r \, dr \, d\theta, \tag{2.11b}$$

$$\langle \boldsymbol{r} \cdot \boldsymbol{\eta} \rangle = \frac{1}{k I} \iint r \, \mathrm{Im} \left[E^* \frac{\partial E}{\partial r} \right] r \, dr \, d\theta, \tag{2.11c}$$

$$\langle xy \rangle = \frac{1}{2I} \iint r^2 \, \sin 2\theta \, |E(r,\theta)|^2 \, r \, dr \, d\theta, \tag{2.11d}$$

$$\langle xv - yu \rangle = \frac{1}{k I} \iint \mathrm{Im} \left[E^* \frac{\partial E}{\partial \theta} \right] r \, dr \, d\theta, \tag{2.11e}$$

$$\langle uv \rangle = \frac{1}{k^2 I} \iint \left\{ \frac{\sin 2\theta}{2} \left(\left| \frac{\partial E}{\partial r} \right|^2 - \frac{1}{r^2} \left| \frac{\partial E}{\partial \theta} \right|^2 \right) + \frac{\cos 2\theta}{r} \mathrm{Re} \left[\frac{\partial E^*}{\partial r} \frac{\partial E}{\partial \theta} \right] \right\} r \, dr \, d\theta \tag{2.11f}$$

where $I = \iint |E|^2 r\, dr\, d\theta$ is a normalization factor, proportional to the beam power. For illustrative purposes, in these equations we have used planar polar coordinates r and θ, frequently encountered in the literature. Alternative expressions for the second-order moments can be found, for example, in (Alda et al., 1997; Weber, 1992). Finally, let us briefly remark that the second-order moment $\langle x^2 \rangle$ takes the value $\frac{w^2}{4}$ for a Gaussian amplitude $\exp\left(-\frac{x^2}{w^2}\right)$.

In this section we have focused the attention on the mathematical definition of the irradiance moments. Details for the practical use of the above parameters can be found in the ISO standard 11146.

2.2.2 Propagation and Measurement of the Irradiance Moments

To analytically handle in a compact form the second-order irradiance moments of a scalar beam, they are usually arranged in a 4×4 symmetric matrix, $\hat{M}$, defined, at a certain transverse plane, as follows

$$\hat{M} = \begin{pmatrix} \langle x^2 \rangle & \langle xy \rangle & \langle xu \rangle & \langle xv \rangle \\ \langle xy \rangle & \langle y^2 \rangle & \langle yu \rangle & \langle yv \rangle \\ \langle xu \rangle & \langle yu \rangle & \langle u^2 \rangle & \langle uv \rangle \\ \langle xv \rangle & \langle yv \rangle & \langle uv \rangle & \langle v^2 \rangle \end{pmatrix}. \tag{2.12}$$

We immediately see that all the moments introduced in (i)–(vi) can be written in terms of the elements of matrix $\hat{M}$. The usefulness of this matrix arises from the simple link between the values of $\hat{M}$ at the output and input planes of any first-order optical system. The general propagation law takes the form (Bastiaans, 1989; Serna et al., 1991)

$$\hat{M}_{out} = \hat{P}\, \hat{M}_{inp}\, \hat{P}^t, \tag{2.13}$$

where $\hat{P}$ is the 4×4 ABCD matrix representing the optical system (Siegman, 1986), and the subscripts *out* and *inp* refer to output and input planes, respectively.

It is also important to notice that the second-order moments are measurable quantities. The measurement procedure commonly employs CCD cameras or similar devices such as pyroelectric matrix arrays. Apart from the resolution limit defined by the pixel size of the camera, the main experimental limitation comes from the signal-to-noise ratio of the output signal. Defective pixels, background noise and electronic circuitry, among other noise sources, also reduce the performance of the measurement devices.

The standard method used to determine the second-order moments records the irradiance profile $I(x,y,z)$ at different transverse planes by means of a sensor array camera. From the data supplied by the camera (irradiance versus position), one computes the purely spatial moments $\langle x^2 \rangle$, $\langle y^2 \rangle$ and $\langle xy \rangle$. Since they propagate in free

space according to a parabolic law, by means of a fitting procedure of the experimental data to the parabolic curves we obtain all moments except $\langle xv \rangle$ and $\langle yu \rangle$, which are coupled. They can be determined through a pair of additional measurements by using an auxiliary cylindrical lens. Here we do not proceed further into the experimental procedure. Additional details can be found, for example, in (Mejías et al., 2002).

It should also be mentioned that the above formalism based on the second-order irradiance moments fails in certain cases (e.g., slit diffraction). The main problem arises when one tries to analytically determine the far-field divergence. One finds that this parameter becomes infinite. Any attempt to represent the sharp edge by smooth functions fails too because the second-order moment $\langle \eta^2 \rangle$ takes higher values as the fit improves, and, in the limit, tends to infinite again. Although, on the basis of the moments formalism, second-order characteristic beam parameters were generalized for fields crossing through hard-edge openings (Martínez-Herrero and Mejías, 1993b, Martínez-Herrero et al., 1995c; Martínez-Herrero et al., 2003b), this is a problem whose analytical solution deserves further study in the future.

Let us finally remark that generalization of the above scalar formalism to light pulses (nanoseconds) can be found in (Mejías and Martínez-Herrero, 1995; Encinas-Sanz et al., 1998).

2.3 Second-Order Overall Characterization: Vectorial Case

In Chap. 1 we pointed out that partially polarized beams and polarization-altering optical devices could be mathematically modelled by using the Stokes vectors and Müller matrices. It was implicitly assumed, however, a uniform polarization distribution across the beam profile. In the present section we will generalize the Stokes formalism in order to characterize the overall spatial structure of a polarized light field. The propagation laws through optical systems will also be investigated. This formalism extends the description based on the irradiance moments, reported in the previous section for the scalar case, to non-uniformly polarized beams.

2.3.1 The Wigner Matrix

Let us again consider an electromagnetic field propagating essentially along the z axis. Assuming that the longitudinal component of the field is negligible, the electric field vector reads (within the paraxial approach)

$$\boldsymbol{E}\left(\boldsymbol{r},z\right) = \left(E_s\left(\boldsymbol{r},z\right), E_p\left(\boldsymbol{r},z\right)\right). \tag{2.14}$$

For the sake of convenience, the position vector $\boldsymbol{r} = (x,y)$ is defined in the present section as the product of the wavenumber k by the transverse Cartesian coordinates of the point at which the field is determined. To avoid any confusion, we will write the dimensionless position vector $k\boldsymbol{r}$ in the form $\tilde{\boldsymbol{r}} \equiv k\boldsymbol{r}$.

For vectorial beamlike fields, it is customary to employ their cross-spectral density matrix (Born and Wolf, 1999; Mandel and Wolf, 1995; Perina, 1971; Wolf, 2007), namely,

$$\hat{W}(\tilde{\boldsymbol{r}}_1,\tilde{\boldsymbol{r}}_2) = \overline{\boldsymbol{E}^{\dagger}(\tilde{\boldsymbol{r}}_1,z)\,\boldsymbol{E}(\tilde{\boldsymbol{r}}_2,z)}, \tag{2.15}$$

where

$$\boldsymbol{E}^{\dagger} = \begin{pmatrix} E_s^* \\ E_p^* \end{pmatrix}. \tag{2.16}$$

In terms of $\hat{W}$, we can now introduce the so-called Wigner matrix, $\hat{H}$, defined in the form (Martínez-Herrero and Mejías, 1997b)

$$\hat{H}(\tilde{\boldsymbol{r}},\boldsymbol{\eta},z) = \frac{1}{k^2}\iint \hat{W}\left(\tilde{\boldsymbol{r}}+\frac{\boldsymbol{s}}{2},\tilde{\boldsymbol{r}}-\frac{\boldsymbol{s}}{2}\right)\exp(i\boldsymbol{\eta}\cdot\boldsymbol{s})d\boldsymbol{s}, \tag{2.17}$$

where $\tilde{\boldsymbol{r}} = (\tilde{\boldsymbol{r}}_1+\tilde{\boldsymbol{r}}_2)/2$ and $\boldsymbol{s} = \tilde{\boldsymbol{r}}_1-\tilde{\boldsymbol{r}}_2$ as in the previous section. No confusion should arise from the fact that the symbol H is also commonly used for the magnetic field, because the Wigner matrix always appears with a caret.

Matrix $\hat{H}$ can also be written in the form

$$\hat{H}(\tilde{\boldsymbol{r}},\boldsymbol{\eta},z) = \begin{pmatrix} h_{ss}(\tilde{\boldsymbol{r}},\boldsymbol{\eta},z) & h_{sp}(\tilde{\boldsymbol{r}},\boldsymbol{\eta},z) \\ h_{ps}(\tilde{\boldsymbol{r}},\boldsymbol{\eta},z) & h_{pp}(\tilde{\boldsymbol{r}},\boldsymbol{\eta},z) \end{pmatrix}, \tag{2.18}$$

where

$$h_{ij}(\tilde{\boldsymbol{r}},\boldsymbol{\eta},z) = \frac{1}{k^2}\iint \overline{E_i^*\left(\tilde{\boldsymbol{r}}+\frac{\boldsymbol{s}}{2},z\right)E_j\left(\tilde{\boldsymbol{r}}-\frac{\boldsymbol{s}}{2},z\right)}\exp(i\boldsymbol{s}\cdot\boldsymbol{\eta})d\boldsymbol{s}; \quad i,j = s,p. \tag{2.19}$$

It should be noted that the diagonal elements of $\hat{H}$ represent the WDF associated to each transverse component of the whole beam. In addition, the off-diagonal elements h_{sp} and h_{ps} accounts for the correlation between the two transverse components of the field. In the scalar framework, only the diagonal elements of the Wigner matrix would be considered.

2.3.2 The Stokes Matrices

Let us now define the so-called Stokes matrices in the form (Martínez-Herrero et al., 1997b)

$$\hat{S}_n = \iint \boldsymbol{R}^t\boldsymbol{R}\,\mathrm{Tr}\left(\hat{\sigma}_n\hat{H}(\tilde{\boldsymbol{r}},\boldsymbol{\eta})\right)d\tilde{\boldsymbol{r}}d\boldsymbol{\eta}, \quad n = 0,1,2,3, \tag{2.20}$$

where

$$\boldsymbol{R} = (\tilde{\boldsymbol{r}},\boldsymbol{\eta}) = (x,y,u,v) \tag{2.21}$$

is a 1×4 vector, $\hat{\sigma}_0$ denotes here the 2×2 identity matrix and $\hat{\sigma}_1$,$\hat{\sigma}_2$ y $\hat{\sigma}_3$ are again the Pauli matrices. For the sake of convenience, we introduce the following notation

$$[\alpha\beta]_{ij} = \iint \alpha\beta h_{ij}(\tilde{\boldsymbol{r}},\boldsymbol{\eta},z)d\tilde{\boldsymbol{r}}d\boldsymbol{\eta}; \qquad i,j = s,p;\ \alpha,\beta = x,\ y,\ u,\ v, \tag{2.22}$$

along with

$$[\alpha\beta]_0 \equiv [\alpha\beta]_{ss} + [\alpha\beta]_{pp}\,, \tag{2.23a}$$

$$[\alpha\beta]_1 \equiv [\alpha\beta]_{ss} - [\alpha\beta]_{pp} \tag{2.23b}$$

$$[\alpha\beta]_2 \equiv [\alpha\beta]_{sp} + [\alpha\beta]_{ps}\,, \tag{2.23c}$$

$$[\alpha\beta]_3 \equiv i\left([\alpha\beta]_{sp} - [\alpha\beta]_{ps}\right), \tag{2.23d}$$

where the subscripts 0, 1, 2 and 3 refer to the corresponding Stokes matrices.

As is quite apparent from Eq. (2.22), $[\alpha\beta]_{ij}$ are closely related with the second-order moments of the WDF defined for scalar fields (cf. Eq. (2.4)). Moreover, the quantities $[\alpha\beta]_n$, $n = 0, 1, 2, 3$, resembles the structure of the conventional Stokes parameters. It should also be noted that the present treatment reduces to the scalar one for the particular case of uniformly linearly-polarized beams. In particular, the standard Stokes parameters can be considered themselves as zero-order irradiance moments.

Let us now write matrix $\hat{S}_0$ as follows

$$\hat{S}_0 = \begin{pmatrix} \hat{\mathrm{W}}_0^2 & \hat{\boldsymbol{\Psi}}_0 \\ \hat{\boldsymbol{\Psi}}_0^{\,t} & \hat{\boldsymbol{\Phi}}_0^{\,2} \end{pmatrix}, \tag{2.24}$$

where

$$\hat{\mathrm{W}}_0^2 \equiv \begin{pmatrix} [x^2]_0 & [xy]_0 \\ [xy]_0 & [y^2]_0 \end{pmatrix}, \tag{2.25a}$$

$$\hat{\boldsymbol{\Phi}}_0^{\,2} \equiv \begin{pmatrix} [u^2]_0 & [uv]_0 \\ [uv]_0 & [v^2]_0 \end{pmatrix}, \tag{2.25b}$$

$$\hat{\boldsymbol{\Psi}}_0 \equiv \begin{pmatrix} [xu]_0 & [xv]_0 \\ [yu]_0 & [yv]_0 \end{pmatrix}. \tag{2.25c}$$

These 2×2 matrices contain the overall spatial characteristics of the beam, namely,

– the spatial structure of the transverse irradiance profile in the near field (matrix $\hat{\mathrm{W}}_0^2$).
– the divergence of the beam (beam spread) at the far field (matrix $\hat{\boldsymbol{\Phi}}_0^2$).
– the orbital angular moment of the beam (matrix $\hat{\boldsymbol{\Psi}}_0$).
– the averaged curvature radius (elements $[xu]_0$, $\left[yv\right]_0$).

In other words, matrix $\hat{S}_0$ gives, in the vectorial case, a similar information to that provided by the beam matrix, $\hat{M}$, in the scalar case. As a matter of fact, the elements of both matrices are related through the formulae

$$\langle x^2\rangle = \frac{\left[x^2\right]_0}{4\pi^2 k^2 I}; \quad \langle y^2\rangle = \frac{\left[y^2\right]_0}{4\pi^2 k^2 I}, \tag{2.26a}$$

$$\langle u^2\rangle = \frac{\left[u^2\right]_0}{4\pi^2 I}; \quad \langle v^2\rangle = \frac{\left[v^2\right]_0}{4\pi^2 I}, \tag{2.26b}$$

$$\langle xu\rangle = \frac{[xu]_0}{4\pi^2 kI}; \quad \langle yv\rangle = \frac{\left[yv\right]_0}{4\pi^2 kI}, \tag{2.26c}$$

$$\langle xv\rangle = \frac{[xv]_0}{4\pi^2 kI}; \quad \langle yu\rangle = \frac{\left[yu\right]_0}{4\pi^2 kI}, \tag{2.26d}$$

$$\langle xy\rangle = \frac{\left[xy\right]_0}{4\pi^2 k^2 I}; \quad \langle uv\rangle = \frac{[uv]_0}{4\pi^2 I}, \tag{2.26e}$$

where

$$I = \frac{1}{4\pi^2}\iint \mathrm{Tr}\,\hat{H}\, d\tilde{\boldsymbol{r}}\, d\boldsymbol{\eta}, \tag{2.27}$$

and $<\alpha\beta>$, $\alpha, \beta = x, y, u, v$, are the second-order irradiance moments defined for scalar fields in the previous section. It is important to note that, on the contrary to that occurs concerning the dimensionless squared brackets, the spatial variables inside the sharp brackets keep their usual dimensions (for example, $<xu>$ exhibits dimension of length).

Equations (2.26) allow to conclude that the spatial parameters introduced in the scalar case can be obtained from the knowledge of the elements of the Stokes matrix $\hat{S}_0$.

Let us finally remark the formal analogy between the well-known inequality satisfied by the standard Stokes parameters,

$$s_0^2 \geq s_1^2 + s_2^2 + s_3^2, \tag{2.28}$$

and the diagonal elements of the Stokes matrices:

$$\left(\mathrm{Tr}\,\hat{S}_0\right)^2 \geq \left(\mathrm{Tr}\,\hat{S}_1\right)^2 + \left(\mathrm{Tr}\,\hat{S}_2\right)^2 + \left(\mathrm{Tr}\,\hat{S}_3\right)^2. \tag{2.29}$$

On the basis of this condition, a rather rough but simple classification scheme of partially polarized beams can be outlined.

Any beam should belong to one of the following three categories:

(a) *Second-order totally polarized beams*.
These are beams fulfilling

$$\left(\mathrm{Tr}\,\hat{S}_0\right)^2 = \left(\mathrm{Tr}\,\hat{S}_1\right)^2 + \left(\mathrm{Tr}\,\hat{S}_2\right)^2 + \left(\mathrm{Tr}\,\hat{S}_3\right)^2. \tag{2.30}$$

Belong to this type of fields, those uniformly totally polarized (UTP) beams whose Cartesian components of the electric field vector are proportional, i.e.,

$$E_s(\boldsymbol{r}) = \alpha E_p(\boldsymbol{r}), \tag{2.31}$$

where α is a complex number.

(b) *Second-order non-polarized beams*.
These are beams fulfilling

$$\mathrm{Tr}\,\hat{S}_1 = \mathrm{Tr}\,\hat{S}_2 = \mathrm{Tr}\,\hat{S}_3 = 0. \tag{2.32}$$

Belong to this category those locally unpolarized beams (i.e., $P(\boldsymbol{r}) = 0$ everywhere) whose divergences along de s- and p- directions take the same value ($[\eta^2]_{ss} = [\eta^2]_{pp}$). Of course, this is not the only example. We could also mention, for instance, radial or azimuthally totally-polarized beams (see Chap. 1 and references therein).

(c) *Second-order partially polarized beams*.
These fields are defined through the inequality

$$\left(\mathrm{Tr}\,\hat{S}_0\right)^2 > \left(\mathrm{Tr}\,\hat{S}_1\right)^2 + \left(\mathrm{Tr}\,\hat{S}_2\right)^2 + \left(\mathrm{Tr}\hat{S}_3\right)^2. \tag{2.33}$$

Beams not included in the categories (a) and (b) belong to this type.

2.3.3 Propagation Laws and Measurement

Let us now report the propagation laws of the Stokes matrices through optical systems. Attention will be focused on three kind of devices.

i. *First-order optical (ABCD) systems*
It can be shown that the general propagation law for the Stokes matrices, propagating through first-order systems represented by 4×4 matrices $\hat{P} = \begin{pmatrix} \hat{A} & \hat{B} \\ \hat{C} & \hat{D} \end{pmatrix}$, reads

$$\hat{S}_n^{out} = \hat{P}'\hat{S}_n^{inp}(\hat{P}')^t \qquad n = 0,1,2,3\ , \tag{2.34}$$

which is formally identical to Eq. (2.13) for the scalar case. In this equation, the superscripts *out* and *inp* refer to the output and input planes of the ABCD system, and

$$\hat{P}' \equiv \begin{pmatrix} \hat{A}' & \hat{B}' \\ \hat{C}' & \hat{D}' \end{pmatrix} \tag{2.35}$$

where $\hat{A}' = \hat{A}$, $\hat{B}' = k\hat{B}$, $\hat{C}' = \frac{1}{k}\hat{C}$ and $\hat{D}' = \hat{D}$. The changes should be introduced because, in the Wigner-Stokes formalism, we are using dimensionless position variables. Thus, although $\hat{A}$ and $\hat{D}$ are dimensionless, the elements of matrix $\hat{B}$ are expressed in units of length and the elements of $\hat{C}$ are given in units of the inverse of length.

Two immediate consequences can be obtained from the propagation law (2.34):

(a) The Stokes matrices propagate through ABCD optical systems independently each other.
(b) There are two kinds of beams that retain the same character (with regard to the polarization) after propagation through ABCD systems:

– Uniformly totally polarized beams.
– Second-order non-polarized beams for which (Martínez-Herrero et al., 1997b; Mejías et al., 2002)

$$\hat{S}_1 = \hat{S}_2 = \hat{S}_3 = 0. \tag{2.36}$$

ii. *Spatially-uniform polarization-altering (SUPA) systems*
They are optical devices whose components modify the polarization state of the light in a uniform way throughout the beam cross-section. They are described by Müller matrices with constant elements.

In this case, the general propagation law for the Stokes matrices becomes (Martínez-Herrero et al., 1997b)

$$\hat{S}_n^{out} = \sum_{m=0}^{3} \hat{\mathcal{M}}_{nm} \hat{S}_m^{inp}, \quad n,m = 0,1,2,3, \tag{2.37}$$

where $\hat{\mathcal{M}}_{nm}$ denote the elements of the Müller matrix. It is important to notice that, unlike to that occurs for first-order optical systems, the Stokes matrices, in general, do not propagate through SUPA systems independently each other: Each Stokes matrix at the output of such kind of systems depends, in principle, on the values of the four Stokes matrices associated to the incident beam.

iii. *Mixed systems*
They should be understood as the combination of first-order optical systems and SUPA devices cascaded in an arbitrary way. This kind of systems exhibits two analytical properties:

(a) The ABCD matrix that represents a first-order optical component commutes with the Müller matrix associated to a SUPA device. Note, however,

that two ABCD matrices, in general, does not commute. The same applies for the Müller matrices.

(b) All the ABCD components of a mixed system, represented by the dimensionless matrices $\hat{P}_n$, $n = 1,2\ldots,N$, can be reduced to an equivalent first-order optical device whose ABCD matrix, $\hat{P}^{eq}$, is given by

$$\hat{P}^{eq} = \prod_{n=0}^{N} \hat{P}_n \tag{2.38}$$

In asimilar way, all the SUPA devices of a mixed system, represented by the Müller matrices $\hat{\mathcal{M}}_m$, $m = 1, 2\ldots, M$, can be reduced to an equivalent SUPA component whose Müller matrix $\hat{\mathcal{M}}^{eq}$ is

$$\hat{\mathcal{M}}^{eq} = \prod_{m=0}^{M} \hat{\mathcal{M}}_m. \tag{2.39}$$

Taking the above properties into account, it can be shown that the propagation law of the Stokes matrices of a general beam through mixed systems reads

$$\hat{S}_p^{out} = \hat{P}^{eq} \left(\sum_{q=0}^{3} \hat{\mathcal{M}}_{pq}^{eq} \hat{S}_q^{inp} \right) \left(\hat{P}^{eq} \right)^t, \; p,q = 0,1,2,3, \tag{2.40}$$

or, making use of the commutative property,

$$\hat{S}_p^{out} = \sum_{q=0}^{3} \hat{\mathcal{M}}_{pq}^{eq} \left(\hat{P}^{eq} \hat{S}_q^{inp} \right) \left(\hat{P}^{eq} \right)^t, \; p,q = 0,1,2,3. \tag{2.41}$$

Let us finally remark that all the elements of the four Stokes matrices are measurable quantities. The procedure to determine the Stokes matrices is based on the well-known procedure to get the conventional Stokes parameters. Accordingly, a mixed system composed of a quarter-wave plate, a free propagation distance and a linear polarizer is used. The key of the method is to link matrix

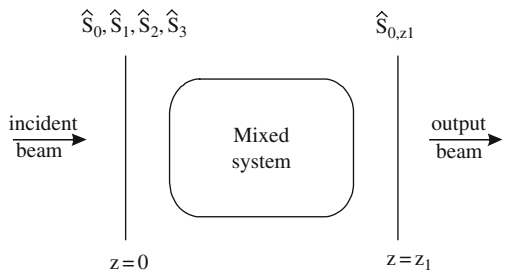

Fig. 2.5 Illustrating the basis of the procedure employed to determine the Stokes matrices

$\hat{S}_0$ at a plane $z = z_1$ with the Stokes matrices at the plane $z = 0$ where we want to measure their values (see Fig. 2.5).
Since the elements of $\hat{S}_0$ are connected with the second-order irradiance moments, our measurement problem reduces to obtain such moments. Here we do not proceed further into the details of the experimental methods used to find the Stokes matrices (see, in this connection, (Mejías et al., 2002) and references therein).

2.3.4 Invariant Parameters

In terms of the Wigner-Stokes formalism, we are now going to introduce certain overall parameters that remain invariant upon propagation through rotationally-symmetric first-order optical systems. In addition, these parameters do not change under rotation of the transverse Cartesian axes with respect to which the electric field components are given.

To begin with, let us first define a matrix $\hat{T}$ in the form

$$\hat{T} = \begin{pmatrix} \tilde{\boldsymbol{r}} \cdot \tilde{\boldsymbol{r}} & \tilde{\boldsymbol{r}} \cdot \boldsymbol{\eta} \\ \boldsymbol{\eta} \cdot \tilde{\boldsymbol{r}} & \boldsymbol{\eta} \cdot \boldsymbol{\eta} \end{pmatrix}, \tag{2.42}$$

where $\tilde{\boldsymbol{r}}$ is again the dimensionless position vector. In terms of the elements of matrix $\hat{T}$, the following 2×2 matrices can be introduced (Martínez-Herrero and Mejías, 2007):

$$\hat{\zeta}_n = \int \hat{T}\ \mathrm{Tr}\left(\hat{\sigma}_n \hat{H}\right) d\tilde{\boldsymbol{r}} d\boldsymbol{\eta},\ n = 0,1,2,3, \tag{2.43}$$

which are expressed in explicit form as follows:

$$\hat{\zeta}_0 = \begin{pmatrix} \left[\tilde{r}^2\right]_{ss} + \left[\tilde{r}^2\right]_{pp} & \left[\tilde{\boldsymbol{r}} \cdot \boldsymbol{\eta}\right]_{ss} + \left[\tilde{\boldsymbol{r}} \cdot \boldsymbol{\eta}\right]_{pp} \\ \left[\tilde{\boldsymbol{r}} \cdot \boldsymbol{\eta}\right]_{ss} + \left[\tilde{\boldsymbol{r}} \cdot \boldsymbol{\eta}\right]_{pp} & \left[\eta^2\right]_{ss} + \left[\eta^2\right]_{pp} \end{pmatrix}, \tag{2.44a}$$

$$\hat{\zeta}_1 = \begin{pmatrix} \left[\tilde{r}^2\right]_{ss} - \left[\tilde{r}^2\right]_{pp} & \left[\tilde{\boldsymbol{r}} \cdot \boldsymbol{\eta}\right]_{ss} - \left[\tilde{\boldsymbol{r}} \cdot \boldsymbol{\eta}\right]_{pp} \\ \left[\tilde{\boldsymbol{r}} \cdot \boldsymbol{\eta}\right]_{ss} - \left[\tilde{\boldsymbol{r}} \cdot \boldsymbol{\eta}\right]_{pp} & \left[\eta^2\right]_{ss} - \left[\eta^2\right]_{pp} \end{pmatrix}, \tag{2.44b}$$

$$\hat{\zeta}_2 = 2\mathrm{Re}\begin{pmatrix} \left[\tilde{r}^2\right]_{sp} & \left[\tilde{\boldsymbol{r}} \cdot \boldsymbol{\eta}\right]_{sp} \\ \left[\tilde{\boldsymbol{r}} \cdot \boldsymbol{\eta}\right]_{sp} & \left[\eta^2\right]_{sp} \end{pmatrix}, \tag{2.44c}$$

$$\hat{\zeta}_3 = 2\mathrm{Im}\begin{pmatrix} \left[\tilde{r}^2\right]_{sp} & \left[\tilde{\boldsymbol{r}} \cdot \boldsymbol{\eta}\right]_{sp} \\ \left[\tilde{\boldsymbol{r}} \cdot \boldsymbol{\eta}\right]_{sp} & \left[\eta^2\right]_{sp} \end{pmatrix}. \tag{2.44d}$$

It can be shown that $\hat{\zeta}_n$, $n = 0,1,2,3$, also read

$$\hat{\zeta}_n = \begin{pmatrix} \mathrm{Tr}\,(S_{11})_n & \mathrm{Tr}\,(S_{12})_n \\ \mathrm{Tr}\,(S_{21})_n & \mathrm{Tr}\,(S_{22})_n \end{pmatrix}, \tag{2.45}$$

where $(S_{11})_n$, $(S_{12})_n$, $(S_{21})_n$ and $(S_{22})_n$ denote the 2×2 matrices associated to the 4×4 Stokes matrix $\hat{S}_n$, namely

$$\hat{S}_n = \begin{pmatrix} (S_{11})_n & (S_{12})_n \\ (S_{21})_n & (S_{22})_n \end{pmatrix}. \tag{2.46}$$

For example,

$$(S_{11})_0 \equiv \hat{W}_0^2 \equiv \begin{pmatrix} [x^2]_0 & [xy]_0 \\ [xy]_0 & [y^2]_0 \end{pmatrix} \equiv \begin{pmatrix} [x^2]_{ss} + [x^2]_{pp} & [xy]_{ss} + [xy]_{pp} \\ [xy]_{ss} + [xy]_{pp} & [y^2]_{ss} + [y^2]_{pp} \end{pmatrix}, \tag{2.47a}$$

$$(S_{12})_0 \equiv (S_{21})_0^t \equiv \hat{\Psi}_0 \equiv \begin{pmatrix} [xu]_0 & [xv]_0 \\ [yu]_0 & [yv]_0 \end{pmatrix} \equiv \begin{pmatrix} [xu]_{ss} + [xu]_{pp} & [xv]_{ss} + [xv]_{pp} \\ [yu]_{ss} + [yu]_{pp} & [yv]_{ss} + [yv]_{pp} \end{pmatrix}, \tag{2.47b}$$

$$(S_{22})_0 \equiv \hat{\Phi}_0^2 \equiv \begin{pmatrix} [u^2]_0 & [uv]_0 \\ [uv]_0 & [v^2]_0 \end{pmatrix} \equiv \begin{pmatrix} [u^2]_{ss} + [u^2]_{pp} & [uv]_{ss} + [uv]_{pp} \\ [uv]_{ss} + [uv]_{pp} & [v^2]_{ss} + [v^2]_{pp} \end{pmatrix}, \tag{2.47c}$$

and so on.

Recall that the Stokes matrices $\hat{S}_n$ provide an overall description of non-uniformly partially-polarized beams through general optical systems (including polarization-altering devices). In a complementary way, the matrices $\hat{\zeta}_n$ can be of use to characterize such beams through rotationally-symmetric ABCD systems.

To further clarify this point, let us first report several properties of these polarization matrices:

(i) $\mathrm{Tr}\,\hat{\zeta}_n = \mathrm{Tr}\,\hat{S}_n$. This follows at once from Eqs. (2.45) and (2.46).

(ii) For matrices $\hat{\zeta}_n$, the propagation law through rotationally-symmetric first-order optical systems takes the form

$$\left(\hat{\zeta}_n\right)_{output} = \hat{P}' \left(\hat{\zeta}_n\right)_{input} (\hat{P}')^t \; n = 0,1,2,3, \tag{2.48}$$

where the 2×2 dimensionless matrix $\hat{P}'$ was defined in Eq. (2.35). Note that Eq.(2.48) is formally identical to the propagation law of the Stokes matrices through ABCD systems.

(iii) Under rotation of the transverse Cartesian axes around the propagation direction z, the matrices $\hat{\zeta}_n$ become

$$\hat{\zeta}_0' = \hat{\zeta}_0; \tag{2.49a}$$

$$\hat{\zeta}_3' = \hat{\zeta}_3, \tag{2.49b}$$

$$\hat{\zeta}_1' = \cos 2\theta \; \hat{\zeta}_1 + \sin 2\theta \; \hat{\zeta}_2, \tag{2.49c}$$

$$\hat{\zeta}_2' = -\sin 2\theta \; \hat{\zeta}_1 + \cos 2\theta \; \hat{\zeta}_2, \tag{2.49d}$$

where the primes denote the matrices after rotation, and θ is the rotation angle. To get this result we have taken into account that the electric field components read after rotation

$$E_s' = \cos\,\theta\, E_s + \sin\theta\, E_p \tag{2.50a}$$

$$E_p' = -\sin\theta\, E_s + \cos\theta\, E_p \tag{2.50b}$$

In terms of matrices $\hat{\zeta}_n$, a number of invariant overall parameters can be introduced:

(i) $\mathrm{Det}\hat{\zeta}_0$ (2.51)

(ii) $\mathrm{Det}\hat{\zeta}_3$ (2.52)

(iii) $\mathrm{Det}\hat{\zeta}_1 + \mathrm{Det}\hat{\zeta}_2$. (2.53)

It follows from the propagation law (2.48) that these three parameters remain constant when the beam propagates along rotationally-symmetric optical systems (which are the most frequently encountered in the literature). Accordingly, these invariant parameters can be used as suitable labels to characterize, in an analytical way, the spatial distribution of the polarization state of beams propagating through this type of systems. Moreover, since the elements of the Stokes matrices are measurable quantities, the same applies for these parameters. Note that they are also invariant upon rotation of the transverse Cartesian axes.

Let us finally point out that a family of additional invariants can easily be derived from the former ones. Here we only mention two of them:

(a) $$\mathfrak{M} = \mathrm{Det}\hat{\zeta}_0 - \sum_{i=1}^{3} \mathrm{Det}\hat{\zeta}_i, \tag{2.54}$$

(b) and

$$\mathfrak{N} = \frac{2\mathrm{Det}\hat{\zeta}_0 \left| \sum_{i=1}^{3} \mathrm{Det}\hat{\zeta}_i \right|}{\left(\mathrm{Det}\hat{\zeta}_0 + \left| \sum_{i=1}^{3} \mathrm{Det}\hat{\zeta}_i \right| \right)^2}, \tag{2.55}$$

with $0 \leq \mathfrak{N} \leq 1$.

As is clear from the invariance properties of parameters (2.51), (2.52), and (2.53), $\mathfrak{M}$ and $\mathfrak{N}$ inherit this behaviour, namely, $\mathfrak{M}$ and $\mathfrak{N}$ do not change upon both, propagation through rotationally-symmetric ABCD systems and rotation of the transverse coordinate axes. We do not proceed further into the applications of the invariant parameters. This point deserves more study in the future.

2.4 Generalized Degree of Polarization

As we pointed out earlier (see Chap. 1), when we deal with non-uniformly polarized beams, the point-dependent information about the polarization state is provided by the local degree of polarization, $P(\boldsymbol{r})$, defined in Sect. 1.2. However, $P(\boldsymbol{r})$ is not a parameter or figure of merit, but a function.

In the following, a global parameter will be considered in order to characterize both the polarization state and its uniformity across the transverse profile of a general partially polarized beam.

2.4.1 Definition and Properties of Generalized Degree of Polarization

Within the framework of the Wigner-Stokes formalism, let us introduce the so-called generalized degree of polarization, defined at a transverse plane in the form (Movilla et al., 1998)

$$P_G = \sqrt{\frac{\left(\mathrm{Tr}\ \hat{S}_1\right)^2 + \left(\mathrm{Tr}\ \hat{S}_2\right)^2 + \left(\mathrm{Tr}\ \hat{S}_3\right)^2}{\left(\mathrm{Tr}\ \hat{S}_0\right)^2}} = \sqrt{\frac{\left(\mathrm{Tr}\ \hat{\boldsymbol{\xi}}_1\right)^2 + \left(\mathrm{Tr}\ \hat{\boldsymbol{\xi}}_2\right)^2 + \left(\mathrm{Tr}\ \hat{\boldsymbol{\xi}}_3\right)^2}{\left(\mathrm{Tr}\ \hat{\boldsymbol{\xi}}_0\right)^2}}. \tag{2.56}$$

Note that the second equality follows from the property (i) of matrices $\hat{\boldsymbol{\xi}}_n$, n = 0,1,2,3 (see Sect. 2.3).

As is quite evident from this definition, P_{G} exhibits a similar analytical structure to the standard degree of polarization P. Furthermore, this formal similarity extends to two main properties, namely,

(i) $$0 \leq P_G \leq 1, \tag{2.57}$$

and

(ii) P_{G} is independent of the choice of the Cartesian s- and p-axis. Note, in this sense, that P_{G} is given in terms of the traces of symmetric matrices, which are rotationally invariant (around the z-axis).

It can also be shown that $P_G = 1$ for second-order totally polarized beams, and $P_G = 0$ for second-order non-polarized beams. Moreover, it follows at once that P_{G} remains invariant under propagation through ABCD systems for two kind of fields, namely, uniformly totally polarized beams, and second-order non-polarized beams fulfilling $\hat{S}_1 = \hat{S}_2 = \hat{S}_3 = 0$.

A final property concerns the propagation of P_{G}: this parameter satisfies the same law that governs to the Stokes matrices, restricted to their diagonal elements.

2.4.2 Physical Meaning and Measurement

For non-uniformly totally polarized beams, the generalized degree of polarization provides a measure of the uniformity of the polarization over the regions of the beam profile where the irradiance is not negligible. This can be illustrated by means of the following example.

Let us consider a non-uniformly totally-polarized beam whose electric field vector $\boldsymbol{E}$ at the plane $z = 0$ is given by the Jones vector (Movilla et al., 1998)

$$\mathbf{E}(r) = \begin{pmatrix} E_s(r) \\ E_p(r) \end{pmatrix} = E_o \exp\left[-\left(\frac{r}{w_0} \right)^2 \right] \begin{pmatrix} \cos\left[f(r) \right] \\ \sin\left[f(r) \right] \end{pmatrix}, \tag{2.58}$$

with

$$f(r) = \frac{\pi}{2} \exp\left[-(ar)^n \right], \; n = 16, \tag{2.59}$$

where E_0 is a constant amplitude factor, r denotes the radial polar coordinate, w_0 represents the beam size at the waist plane and a^{-1} is a measure of the width of the superGaussian function $f(r)$. Thus, the beam given by Eq. (2.58) exhibits a Gaussian irradiance profile and, at each point of its cross-section, the field is linearly polarized whose azimuth depends on the distance to the propagation axis z.

The spatially-distributed polarization of this beam is illustrated in Fig. 2.6a and c for three different values of the dimensionless product aw_0: Inside the circle whose radius is $\approx a^{-1}$ the beam closely behaves as a uniformly linearly polarized field with negligible s-component. Outside such a circle, the field remains uniformly polarized but now with $E_p \approx 0$. The abrupt transition between both regions is a direct consequence of the high superGaussian character ($n = 16$) of function $f(r)$.

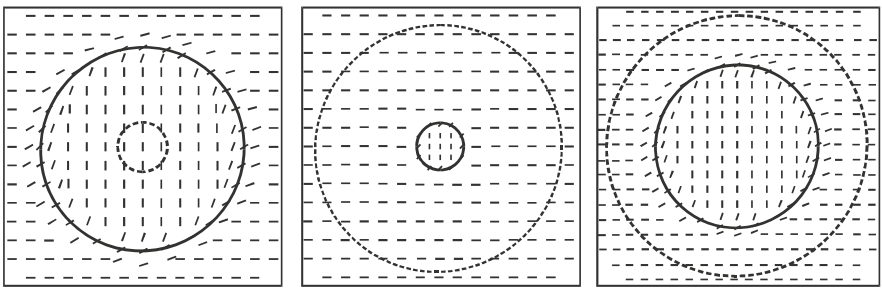

Fig. 2.6 Spatial distribution of the polarization state of the field $\boldsymbol{E}$ given by Eq. (2.58) at the transverse plane $z = 0$. The radii of the circles are $1/a$ (continuous line) and w_0 (dashed line). The small segments show the local orientation of the linearly polarized field. See also (Movilla et al., 1998)

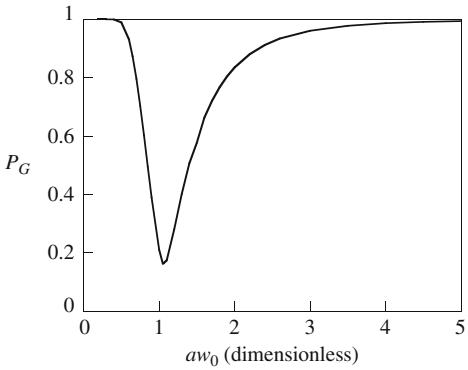

Fig. 2.7 Generalized degree of polarization P_G versus the dimensionless product aw_0. See also (Movilla et al., 1998)

In Fig. 2.6a (with aw_0<<1) the beam is nearly *p*-polarized inside the solid-line circle, which is the region where the irradiance takes significant values. On the other hand, in Fig. 2.6b (with aw_0>>1) the beam behaves as *s*-polarized over the whole transverse profile except over a small region around its center. Finally, in Fig. 2.6c (with $aw_0 \approx 1$) the overall irradiance associated to the *s*- and *p*-regions are balanced.

It is illustrative to calculate the generalized degree of polarization in terms of the product aw_0. This is represented in Fig. 2.7.

Parameter P_G approaches unity for the cases shown in Fig. 2.5a and b, butP_G drastically reduces ($P_G < 0.3$) when aw_0 approaches 1 (Fig. 2.5c).

In summary, we conclude for the example presented here (totally polarized field) that values of P_G nearly 1 means that the beam essentially behaves as uniformly polarized, at least across the region of the beam profile where the irradiance is significant. The opposite case, $P_G \approx 0$, would imply the lack of a global definite polarization over such peak irradiance.

The parameter P_G can be experimentally determined from the measurement of the traces of the Stokes matrices. In the following we briefly describe two procedures to determine them. Both methods involve the measurement of the total power together with the beam width and divergence for several orientations of a polarizer and a quarter-wave plate at an observation plane, which remains unchanged during the procedure.

Method A

It follows four steps (Movilla et al., 2000):

Step 1

Measurement of the global power, I, (squared) beam width $\langle r^2 \rangle$, and (squared) far-field divergence $\langle \eta^2 \rangle$ at the observation plane after free propagation. Here, the measurements are performed with no use of any polarizing element.

Step 2

Measurement of the same parameters as before but now the beam travels through a polarizer which accepts linear polarization in the azimuth $\alpha = 0°$, where α indicates the orientation of the transmission axis of the polarizer with respect to the *s*-axis.

Step 3

Same measurements as in step 2 but now with $\alpha = 45°$.

Step 4

Measurement of I, $\langle r^2 \rangle$ and $\langle \eta^2 \rangle$ after the beam propagates successively through a quarter-wave plate (whose fast axis makes an angle 0° with the *s*-axis) and a polarizer with $\alpha = 45°$.

In terms of the experimental data, the traces of the matrices $\hat{S}_i$ are given by the following equations:

$$\mathrm{Tr}\, S_0 \;=\; 4\pi^2 \left(k^2 \langle r^2 \rangle_{FP} + \langle \eta^2 \rangle_{FP} \right) I_{FP}, \tag{2.60a}$$

$$\mathrm{Tr}\, S_1 \;=\; \frac{1}{T_1 - T_2} \left[8\pi^2 I_{0°} \left(k^2 \langle r^2 \rangle_{0°} + \langle \eta^2 \rangle_{0°} \right) - (T_1 + T_2)\, \mathrm{Tr}\hat{S}_0 \right], \tag{2.60b}$$

$$\mathrm{Tr}\, S_2 \;=\; \frac{1}{T_1 - T_2} \left[8\pi^2 I_{45°} \left(k^2 \langle r^2 \rangle_{45°} + \langle \eta^2 \rangle_{45°} \right) - (T_1 + T_2)\, \mathrm{Tr}\hat{S}_0 \right], \tag{2.60c}$$

$$\mathrm{Tr}\, S_3 = \frac{1}{T_1 - T_2} \left[\frac{8\pi^2 I_{\frac{\lambda}{4},45°}}{T_{\frac{\lambda}{4}}} \left(k^2 \langle r^2 \rangle_{\frac{\lambda}{4},45°} + \langle \eta^2 \rangle_{\frac{\lambda}{4},45°} \right) - (T_1 + T_2)\, \mathrm{Tr}\hat{S}_0 \right], \tag{2.60d}$$

where the subscript *FP* means free propagation, the coefficients T_1 and T_2 are the major and minor principal transmittances of the polarizer, $T_{\frac{\lambda}{4}}$ is the transmittance of the quarter-wave plate and the subscripts 0°, 45°, and $\frac{\lambda}{4}$,45° refer to the value of α and to the presence of the quarter-wave plate.

Method B

In this case the first steps measure the total power, the beam width and the divergence after the beam propagates through a polarizer oriented so as to transmit the component in the azimuths (i) $\alpha = 0°$; (ii) $\alpha = 45°$; (iii) $\alpha = 90°$ and (iv) $\alpha = 135°$. The same parameters are then measured after the beam travels successively through a quarter-wave plate whose fast-axis makes an angle 0° with the *s*-axis, and a polarizer with azimuth α=45° and $\alpha = 135°$; respectively. Again, the observation plane is not changed during the process.

The traces of the Stokes matrices now become

$$\mathrm{Tr}\, S_0 = \frac{4\pi^2}{T_1 + T_2}\left[I_{0^\circ}\left(k^2\langle r^2\rangle_{0^\circ} + \langle \eta^2\rangle_{0^\circ}\right) + I_{90^\circ}\left(k^2\langle r^2\rangle_{90^\circ} + \langle \eta^2\rangle_{90^\circ}\right)\right] \tag{2.61a}$$

$$\mathrm{Tr}\, S_1 = \frac{4\pi^2}{T_1 - T_2}\left[I_{0^\circ}\left(k^2\langle r^2\rangle_{0^\circ} + \langle \eta^2\rangle_{0^\circ}\right) - I_{90^\circ}\left(k^2\langle r^2\rangle_{90^\circ} + \langle \eta^2\rangle_{90^\circ}\right)\right], \tag{2.61b}$$

$$\begin{aligned}\mathrm{Tr}\, S_2 = \frac{4\pi^2}{T_1 - T_2}\Big[& I_{45^\circ}\left(k^2\langle r^2\rangle_{45^\circ} + \langle \eta^2\rangle_{45^\circ}\right) \\ & - I_{135^\circ}\left(k^2\langle r^2\rangle_{135^\circ} + \langle \eta^2\rangle_{135^\circ}\right)\Big]\end{aligned} \tag{2.61c}$$

$$\begin{aligned}\mathrm{Tr}\, S_3 = \frac{4\pi^2}{T_{\frac{\lambda}{4}}(T_1 - T_2)}\Big[& I_{\frac{\lambda}{4},45^\circ}\left(k^2\langle r^2\rangle_{\frac{\lambda}{4},45^\circ} + \langle \eta^2\rangle_{\frac{\lambda}{4},45^\circ}\right) \\ & - I_{\frac{\lambda}{4},135^\circ}\left(k^2\langle r^2\rangle_{\frac{\lambda}{4},135^\circ} + \langle \eta^2\rangle_{\frac{\lambda}{4},135^\circ}\right)\Big].\end{aligned} \tag{2.61d}$$

Let us finally remark that the main difference between the above methods arises from the existence in the former case of measurements of the direct, freely propagating beam, without using any polarizing elements, whereas, in method B, all measurements involve the presence of a polarizer.

Although the procedures are analytically simple, some care, however, is required because the optical devices are not ideal and may exhibit certain harmful effects.

For example, special attention should be taken to align the system in order that the beam crosses through the center of the optical components. Thus, when these components rotate, the influence of their spatial inhomogeneities on the overall irradiance will be strongly reduced. In an ideal configuration, note also that P_{G} should be independent of the angle formed by the polarization plane of the input beam (fixed all along the experiment) and the *s*-axis.

Let us finally remark that the polarizer could introduce some distortion into the beam irradiance profile. In particular, although the beam size of a uniformly polarized field should not change after crossing an ideal polarizer, however, in practice, the total irradiance reduction caused by the polarizer alters the beam width due to the influence of background and offset noises.

2.4.3 Generalized Degree of Polarization of Beams Emerging from Optically-Pumped Nd:YAG Rods

As an illustrative example, we will now determine the generalized degree of polarization of the field at the output of an optically pumped Nd:YAG rod. We will see that P_{G} could be a useful tool to infer the behavior of certain parameters of the system.

As is well known, the active medium in high-power solid-state laser resonators (for example, cylindrical rod in Nd:YAG lasers), involves thermal processes produced by both absorption of radiation and cooling. These thermal effects give rise to changes in the temperature, which exhibit a spatial dependence on the radial polar coordinate r (assuming homogeneous pumping in the laser rod). Moreover, birefringent mechanical strains are also induced by the temperature gradient.

In the particular case of high-power Nd:YAG lasers, the thermal processes generate a refractive index with a parabolic dependence on r. In other words, the laser rod behaves as a thin lens (thermal lens). In addition, the rod becomes birefringent with two values of the refractive index, n_r and n_ϕ, associated to light polarized along radial and azimuthal directions, respectively, (Lü et al., 1995)

$$n_r(r) = n_0\left(1 - \frac{\alpha_r}{2}r^2\right), \tag{2.62}$$

$$n_\varphi(r) = n_0\left(1 - \frac{\alpha_\varphi}{2}r^2\right), \tag{2.63}$$

n_0 being the refractive index at the center of the rod and α_r and α_ϕ being functions of a number of parameters, namely, the total power absorbed by the rod, the radius and the length of the rod, the thermal conductivity, and the photoelastic coefficients associated to the radial and azimuthal components.(Hodgson and Weber, 1993; Martínez-Herrero et al., 1995b; Montmerle et al., 2006)

Assuming well-collimated beams traveling along the rod, the birefringent medium may be modelled by a Jones matrix (referred to the Cartesian s and p axes):

$$\hat{\mathfrak{J}} = \begin{pmatrix} \mathfrak{J}_{ss}(r,\theta) & \mathfrak{J}_{sp}(r,\theta) \\ \mathfrak{J}_{sp}(r,\theta) & \mathfrak{J}_{pp}(r,\theta) \end{pmatrix}, \tag{2.64}$$

with

$$\mathfrak{J}_{ss}(r,\theta) = e^{ikLn_r(r)}\cos^2\theta + e^{ikLn_\varphi(r)}\sin^2\theta, \tag{2.65a}$$

$$\mathfrak{J}_{sp}(r,\theta) = \left[e^{ikLn_r(r)} - e^{ikLn_\varphi(r)}\right]\sin\theta\cos\theta, \tag{2.65b}$$

$$\mathfrak{J}_{pp}(r,\theta) = e^{ikLn_r(r)}\sin^2\theta + e^{ikLn_\varphi(r)}\cos^2\theta, \tag{2.65c}$$

where L is the length of the rod and the angle θ is shown in Fig. 2.8.

The active medium would then modify the polarization state of the input beam in a spatially non-uniform way. Note, however, that incident beams with radial or azimuthal linear polarization do not alter their polarization state after propagating through the rod.

For simplicity, let us now consider a typical linearly-polarized rotationally-symmetric Gaussian beam whose waist coincides with the entrance plane of the

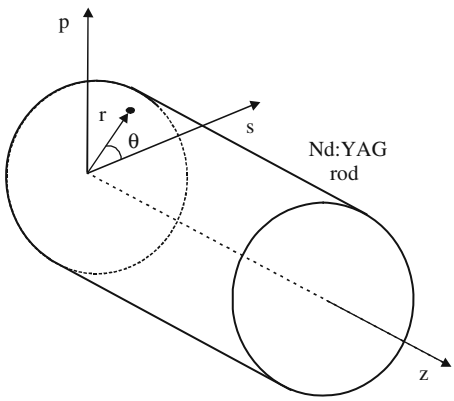

Fig. 2.8 Geometry and notation used to write the Jones matrix $\hat{\mathfrak{J}}$: r and θ denote polar coordinates at a plane orthogonal to the rod axis z

active medium. The amplitude of the electric field vector associated to such beam reads

$$\boldsymbol{E}\,(r,\theta) = E_0 \exp\left(-\frac{r^2}{w_0^2}\right)\begin{pmatrix}1\\0\end{pmatrix}, \tag{2.66}$$

where E_0 and w_0 are constants. By assuming the rod wide enough to neglect the border effects (diffraction and gain saturation effects are also ignored), the s- and p- components of the field at the output plane of de rod will then be obtained by applying the Jones matrix $\hat{\mathfrak{J}}$ to $\boldsymbol{E}\,(r,\theta)$, and one gets

$$E_s\,(r,\theta) = E_0\left[e^{ikLn_r(r)}\cos^2\theta + e^{ikLn_\varphi(r)}\sin^2\theta\right]\exp\left(-\frac{r^2}{w_0^2}\right), \tag{2.67a}$$

$$E_p\,(r,\theta) = E_0\sin\theta\cos\theta\left[e^{ikLn_\varphi(r)} - e^{ikLn_r(r)}\right]\exp\left(-\frac{r^2}{w_0^2}\right). \tag{2.67b}$$

From these equations, after lengthy but straightforward calculations, we find the following simple expression for the generalized degree of polarization at the output plane of the rod:

$$P_G = \frac{1}{2}\left[1 + \frac{1-\beta}{(1-\beta)^2}\right], \tag{2.68}$$

where the constant β contains information about the optical characteristics of the material, the beam size and the energy supplied to the medium (Movilla et al., 2000)

Equation (2.68) shows a one-to-one correspondence between P_G and β. Accordingly, the measurement of P_G would provide the value of β. The experimental set-up used to measure P_G is shown in Fig. 2.9, and P_G is plotted as a function of β in

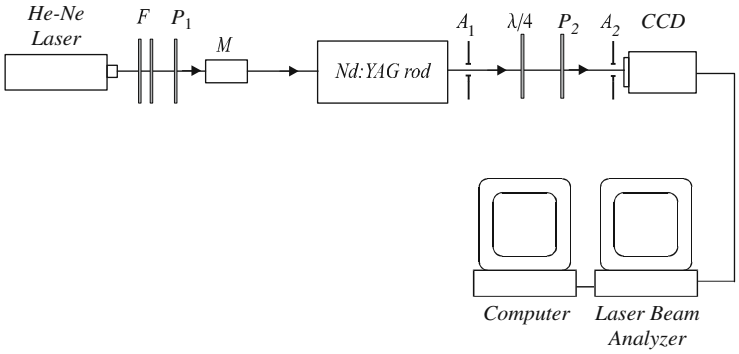

Fig. 2.9 Experimental setup used to measure the generalized degree of polarization, P_{G}, of an (initial) Gaussian beam crossing a birefringent optically-pumped Nd:YAG rod. *F* denotes neutral filters employed to attenuate the beam irradiance; P_1 represents a polarizer that controls the azimuth of the incident beam; *M* shows the presence of a magnifier $3\times$ that increases the beam size; A_1 and A_2 are two apertures to avoid that the light coming from the pumping lamps enter inside the detector; and finally $\lambda/4$ and P_2 symbolize the quarter-wave plate and the polarizer, respectively, that are used to determine the traces of the Stokes matrices. See also (Movilla et al., 2000)

Fig. 2.10. No experimental value appears in the central region of the curve because the beam size is not large enough to allow the accurate measurement of its width.

We see from Fig. 2.10 that the field essentially behaves as a uniformly polarized beam across its transversal section for low values of β. However, as β increases, the pumping produces non-uniform optical anisotropies inside the rod within the central regions, and the value of P_{G} reduces (non-uniform polarization distribution). Finally, P_{G} reaches a quasi-asymptotic behaviour for high pumping power, which means that depolarization is not complete. The same conclusion was also inferred by other authors analyzing a similar system (Kugler et al., 1997).

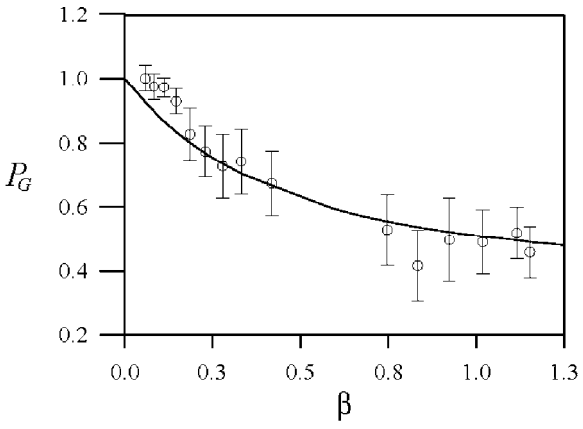

Fig. 2.10 P_{G} versus β. The circles are the experimental data and the continuos line plots the theoretical curve (cf. Eq.(2.68)) that best fits the experimental values. Ordinates include values greater than 1 because the experimental errors make P_G exceeds the limit value 1. See also (Movilla et al., 2000)

2.4.4 Classification Scheme of Partially Polarized Beams

The generalized degree of polarization, P_{G}, may be considered, in a sense, complementary to the parameters $\tilde{P}$ and $\tilde{\sigma}_p^2$ introduced in Chap. 1. To clarify this, let us again consider, for example, a radially polarized beam, whose polarization state is linear and oriented along radial lines from the beam axis. For these fields, $\tilde{P} = 1$ and $\tilde{\sigma}_p^2 = 0$, which are identical to the values associated to uniformly totally-polarized beams. To distinguish between both types of beams parameter P_{G} can be used: P_{G} equals zero for radially polarized fields but reaches its maximum value $P_{\mathrm{G}} = 1$ for uniformly totally polarized beams. Of course, in this example the radial polarization content can also be inferred from the parameters introduced in Sect. 1.5.

The triad of parameters P_{G}, $\tilde{P}$ and $\tilde{\sigma}_p^2$ provide, in addition, a global parametric characterization of the spatial distribution of the polarization state over the whole beam profile. On this basis, a rough but rather simple classification scheme of general (paraxial) partially polarized beams may formally be stated. Table 2.1 shows the sequence to be followed in order to classify a beam according with this scheme: thus, for example, the values $\tilde{\sigma}_p^2 = 0$, $\tilde{P} = 1$, $P_{\mathrm{G}} < 1$ would correspond to a non-uniformly totally polarized beam. We also see from Table 2.1 that, in certain cases, it is not necessary to determine all the three parameters.

Table 2.1 Classification scheme of partially polarized beams based on the parameters P_{G}, $\tilde{P}$ and $\tilde{\sigma}_{\mathrm{p}}^2$. The acronyms refer to the following types of fields: UP (uniformly polarized beams); UTP (uniformly totally polarized beams); UPP (uniformly partially polarized beams); NP (non-polarized beams); NUTP (non-uniformly totally polarized beams); NUPP (non-uniformly partially polarized beams)

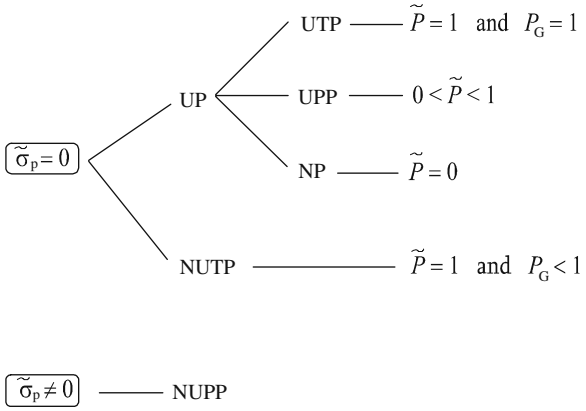

2.5 Beam Quality Parameter of Partially Polarized fields

In practice, it would be useful to handle a figure of merit providing a joint description of the focussing and collimation capabilities of a laser beam. To this purpose, the so-called beam quality parameter, Q, has been defined in the literature for partially-coherent scalar fields in terms of the second-order irradiance moments introduced in Sect. 2.2 (Lavi et al., 1988; Martínez-Herrero et al., 1992a, b; Martínez-Herrero and Mejías 1994; Mejías et al., 2002; Serna et al., 1991; Siegman, 1990, 1993a, b; Simon et al., 1988; Weber, 1992):

$$Q = \langle x^2 + y^2 \rangle \langle u^2 + v^2 \rangle - \langle xu + yv \rangle^2 = \langle r^2 \rangle \, \langle \eta^2 \rangle - \langle \boldsymbol{r} \cdot \boldsymbol{\eta} \rangle^2, \tag{2.69}$$

where, again, for simplicity, it has been assumed that $\langle x \rangle = \langle y \rangle = \langle u \rangle = \langle v \rangle = 0$. Since $\langle xu \rangle + \langle yv \rangle$ vanishes at the waist plane (see Sect. 2.2.1), the parameter Q can also be written in the form

$$Q = \langle r^2 \rangle_w \langle \eta^2 \rangle \tag{2.70}$$

where the subscript w means that the beam size is calculated at the waist plane. We thus see that this parameter contains simultaneous information of both the space and the spatial-frequency domains, characterizing the overall spatial structure of the beam at the near and at the far field. It should also be noticed that the squared root of Q is identical, a factor $k = 2\pi/\lambda$ apart, to the so-called beam propagation factor, M^2, introduced by Siegman (1990), namely,

$$M^2 = k\, Q^{1/2}. \tag{2.71}$$

The parameter Q exhibits two outstanding and practical properties:

(i) It remains invariant upon propagation through rotationally-symmetric first-order optical systems (even for beams without such symmetry and with non-zero crossed moments, $\langle xy \rangle$, $\langle xv \rangle$, $\langle yu \rangle$ or $\langle uv \rangle$).
(ii) It has a lower limit, given by the expression (uncertainty relation)

$$Q \geq 1/k^2, \tag{2.72}$$

or, equivalently,

$$M^2 \geq 1, \tag{2.73}$$

where the equalities are only reached by a Gaussian beam (best quality). It should also be remarked that the beam quality improves (better capabilities of the beam) when Q takes lower values, and, conversely, the quality deteriorates when the numerical value of Q increases.

These properties along with the simple measurement procedure explain why the beam propagation factor M^2 has been accepted as the current ISO beam quality standard (ISO, 1999, 2005).

A generalization of the quality parameter for the vectorial case can be achieved by extending, in a natural way, the former definition of Q, i.e., (Lü et al., 1995)

$$Q = \langle r^2 \rangle \langle \eta^2 \rangle - \langle \boldsymbol{r} \cdot \boldsymbol{\eta} \rangle^2, \tag{2.74}$$

where the second-order moments of the global vectorial beam now include both components, namely,

$$\langle r^2 \rangle = \frac{I_\mathrm{s}}{I} \langle r^2 \rangle_s + \frac{I_\mathrm{p}}{I} \langle r^2 \rangle_p, \tag{2.75}$$

$$\langle \eta^2 \rangle = \frac{I_s}{I} \langle \eta^2 \rangle_s + \frac{I_p}{I} \langle \eta^2 \rangle_p, \tag{2.76}$$

$$\langle \boldsymbol{r} \cdot \boldsymbol{\eta} \rangle = \frac{I_s}{I} \langle \boldsymbol{r} \cdot \boldsymbol{\eta} \rangle_\mathrm{s} + \frac{I_p}{I} \langle \boldsymbol{r} \cdot \boldsymbol{\eta} \rangle_\mathrm{p}, \tag{2.77}$$

In these equations

$$\langle \alpha\beta \rangle_i = \frac{1}{I_i} \frac{k^2}{4\pi^2} \iiint \alpha\beta \, \overline{E_i^* \, (\boldsymbol{r} + \boldsymbol{s}/2, z) \, E_i \, (\boldsymbol{r} - \boldsymbol{s}/2, z)} \exp(\mathrm{i} k \boldsymbol{s}.\boldsymbol{\eta}) \mathrm{d}\boldsymbol{s} \, \mathrm{d}\boldsymbol{r} \, \mathrm{d}\boldsymbol{\eta},$$

$$i = s, \, p; \quad \alpha, \beta = x, y, u, v \tag{2.78}$$

denote the second-order moments associated to the respective field components $I_\mathrm{i} = \iint \overline{|E_\mathrm{i}(\boldsymbol{r})|^2} \, d\boldsymbol{r}$, $i = \mathrm{s,p}$ and $I = I_\mathrm{s} + I_\mathrm{p}$. The presence of the factors I_i/I, $i = s$, p, arises from the different normalization constants (I and I_i) of the moments associated to the overall beam and to the field components, respectively. Note also that we are using sharp brackets to write the irradiance moments. Accordingly, $\boldsymbol{r} = (x, y)$ represents, as usual, the conventional position vector, with dimension of length.

As occurs in the scalar case, the parameter Q does not change when the beam freely propagates. Moreover, for any field, Q also satisfies the inequality

$$Q \geq 1/k^2, \tag{2.79}$$

where now the equality holds for uniformly totally-polarized Gaussian beams.

The parameter Q can also be written in terms of the beam qualities, Q_s and Q_p, associated to the electric field components. We have

$$Q = \left(\frac{I_s}{I} \right)^2 Q_s + \left(\frac{I_p}{I} \right)^2 Q_p + \left(\frac{I_s I_p}{I^2} \right) Q_{sp}, \tag{2.80}$$

where

$$Q_i = \langle r^2 \rangle_i \langle \eta^2 \rangle_i - \langle \boldsymbol{r} \cdot \boldsymbol{\eta} \rangle_i^2, i = s, p, \tag{2.81}$$

and

$$Q_{sp} = \langle r^2 \rangle_s \langle \eta^2 \rangle_p + \langle r^2 \rangle_p \langle \eta^2 \rangle_s - 2 \langle \boldsymbol{r} \cdot \boldsymbol{\eta} \rangle_s \langle \boldsymbol{r} \cdot \boldsymbol{\eta} \rangle_p, \tag{2.82}$$

For illustrative purposes, let us again consider the beam emerging from an optically pumped Nd:YAG rod (see the above section). It can be shown that the value of Q at the output plane of the rod is given by the simple formula (Lü et al., 1995; Mejías et al., 2002)

$$Q = \frac{1}{k^2} \left[1 + \beta + \ln(1 + \beta) \right]. \tag{2.83}$$

Accordingly, when β grows, the beam quality deteriorates. From the analytical expression of parameter β, it can be concluded that, in order to improve the beam quality of the output beam:

(i) the pumping power should decrease, and/or
(ii) the radius of the rod should increase, and/or
(iii) the transverse beam size should reduce.

This example shows how the beam quality parameter of the emerging field could be of simple practical use when designing laser devices.

2.6 Overall Parametric Characterization of PGSM Beams

We next apply the above parameters to provide a characterization of partially-polarized Gauss-Schell model (PGSM) beams, which were introduced in Chap. 1. More specifically, we investigate the behavior of the beam quality parameter and the different degrees of polarization (including P_G). For simplicity, the interest is focused on a particular class of PGSM beams, namely, those generated by PGSM sources that cannot be distinguished from ordinary GSM fields when polarization measurements are disregarded (i.e., when no anisotropic devices are inserted across the beam path).

Let us begin by writing the cross-spectral density matrix describing such fields at the waist plane (which takes a similar form to the corresponding BCP matrix)

$$\hat{W}(\boldsymbol{r}_1, \boldsymbol{r}_2) = \exp\left(-\frac{r_1^2 + r_2^2}{4\sigma^2} \right) \times \begin{pmatrix} A_s \exp\left[-\frac{(\boldsymbol{r}_1 - \boldsymbol{r}_2)^2}{2\mu^2} \right] & A_{sp} \exp\left[-\frac{(\boldsymbol{r}_1 - \boldsymbol{r}_2)^2}{2\mu_{sp}^2} \right] \\ A_{sp} \exp\left[-\frac{(\boldsymbol{r}_1 - \boldsymbol{r}_2)^2}{2\mu_{sp}^2} \right] & A_p \exp\left[-\frac{(\boldsymbol{r}_1 - \boldsymbol{r}_2)^2}{2\mu^2} \right] \end{pmatrix}, \tag{2.84}$$

where the parameters σ, μ, μ_{sp}, A_{s}, A_{p} and A_{sp} are analogous to those defined in Sect. 1.6. It should be remarked that they are linked through certain conditions derived from general properties of the cross-spectral density matrix (Gori et al., 2008).

For this kind of beams, the second-order irradiance moments become

$$\langle r^2\rangle = 2\langle r^2\rangle_s = 2\langle r^2\rangle_p = 2\langle r^2\rangle_{sp} = 2\sigma^2, \tag{2.85a}$$

$$\langle \eta^2\rangle = 2\langle \eta^2\rangle_s = 2\langle \eta^2\rangle_p = \frac{1}{2k^2\sigma^2\chi}, \tag{2.85b}$$

$$\langle \eta^2\rangle_{sp} = \frac{1}{4k^2\sigma^2\chi_{sp}}, \tag{2.85c}$$

where χ and χ_{sp} are given by the expressions

$$\frac{1}{\chi} = 4\sigma^2\left(\frac{1}{4\sigma^2} + \frac{1}{\mu^2}\right), \tag{2.86a}$$

$$\frac{1}{\chi_{sp}} = 4\sigma^2\left(\frac{1}{4\sigma^2} + \frac{1}{\mu_{sp}^2}\right), \tag{2.86b}$$

along with the condition $\chi_{sp} \geq \chi$. In Eqs. (2.85), the irradiance moments are defined by Eqs. (2.75), (2.76), (2.77), and (2.78), and

$$\langle r^2\rangle_{sp} = \frac{1}{I_{sp}}\frac{k^2}{4\pi^2}\iiint \left(x^2+y^2\right)\overline{E_s^*\left(\boldsymbol{r}+\boldsymbol{s}/2,z\right)E_p\left(\boldsymbol{r}-\boldsymbol{s}/2,z\right)}\exp\left(\mathrm{i}k\,\boldsymbol{s}\cdot\boldsymbol{\eta}\right)\mathrm{d}\boldsymbol{s}\,\mathrm{d}\boldsymbol{r}\,\mathrm{d}\boldsymbol{\eta}, \tag{2.87a}$$

$$\langle \eta^2\rangle_{sp} = \frac{1}{I_{sp}}\frac{k^2}{4\pi^2}\iiint \left(u^2+v^2\right)\overline{E_s^*\left(\boldsymbol{r}+\boldsymbol{s}/2,z\right)E_p\left(\boldsymbol{r}-\boldsymbol{s}/2,z\right)}\exp\left(\mathrm{i}k\,\boldsymbol{s}\cdot\boldsymbol{\eta}\right)\mathrm{d}\boldsymbol{s}\,\mathrm{d}\boldsymbol{r}\,\mathrm{d}\boldsymbol{\eta}, \tag{2.87b}$$

where

$$I_{sp} = \iint \overline{E_s(\boldsymbol{r})E_p^*(\boldsymbol{r})}\mathrm{d}\boldsymbol{r}. \tag{2.88}$$

Let us now introduce the quantity $\tilde{Q}_{sp}$ in the form

$$\tilde{Q}_{sp} = 4\langle r^2\rangle_{sp}\langle \eta^2\rangle_{sp}, \tag{2.89}$$

Note that $\tilde{Q}_{sp}$ involves the cross-correlation between the orthogonal s and p components of the field. No confusion should arise with regard to the function Q_{sp} given by Eq. (2.82), which did not consider any cross-correlation between components.

Both parameters, Q and $\tilde{Q}_{sp}$ are connected with the characteristic constants of the beam:

$$Q = \frac{1}{k^2 \chi}, \tag{2.90a}$$

$$\tilde{Q}_{sp} = \frac{1}{k^2 \chi_{sp}}, \tag{2.90b}$$

and satisfies $\tilde{Q}_{sp} \leq Q$ (remember that $\chi_{sp} \geq \chi$).

On the other hand, after some algebra, it can be shown that the standard degree of polarization of this class of fields turns out to be

$$P_{st} = \sqrt{\left(\frac{A_s - A_p}{A_s + A_p}\right)^2 + \frac{4A_{sp}^2}{\left(A_s + A_p\right)^2}}, \tag{2.91}$$

and, according with the equations given in Sect. 1.6, the local degree of polarization can be written in the form

$$P\left(\boldsymbol{r},z\right) = \sqrt{\left(\frac{A_s - A_p}{A_s + A_p}\right)^2 + \frac{4A_{sp}^2}{\left(A_s + A_p\right)^2} f^2\left(z\right) \exp\left[-a\left(z\right) r^2\right]},$$

where functions $f\left(z\right)$ and $a\left(z\right)$ are related with the spatial parameters Q and $\tilde{Q}_{sp}$ by the expressions

$$f\left(z\right) = \frac{4\sigma^4 + z^2 Q}{4\sigma^4 + z^2 \tilde{Q}_{sp}}, \tag{2.93a}$$

$$a\left(z\right) = \frac{4\sigma^2}{4\sigma^4 + z^2 Q}\left[f\left(z\right) - 1\right]. \tag{2.93b}$$

Note that function $f\left(z\right)$ increases as the beam propagates. In addition, its minimum value is reached at the waist plane, and we get

$$f\left(z = 0\right) = 1 \leq f\left(z\right) \leq f\left(z \to \infty\right) = \frac{Q}{\tilde{Q}_{sp}} = \frac{\chi_{sp}}{\chi}. \tag{2.94}$$

With regard to the generalized degree of polarization, P_G, it propagates for this type of beams according with the formula (Martínez-Herrero et al., 2004)

$$P_G\left(z\right) = \sqrt{\left(\frac{A_s - A_p}{A_s + A_p}\right)^2 + \frac{4A_{sp}^2}{\left(A_s + A_p\right)^2}\left(\frac{4\,k^2\sigma^4 + \frac{1}{k^2\chi_{sp}} + \frac{z^2}{\chi_{sp}}}{4\,k^2\sigma^4 + \frac{1}{k^2\chi} + \frac{z^2}{\chi}}\right)^2}. \tag{2.95}$$

We thus see that P_G decreases under free propagation, and for distances $z >> \lambda$ becomes

$$P_G(z) = \sqrt{\left(\frac{A_s - A_p}{A_s + A_p}\right)^2 + \frac{4A_{sp}^2}{\left(A_s + A_p\right)^2} \frac{1}{f^2(z)}}. \tag{2.96}$$

Close to the waist plane $z = 0$, the polarization parameters P_{st}, $P(0,z)$ and P_G are nearly identical for typical values of the beam parameters (width and divergence). Moreover, when $z >> \lambda$ (including the far field), the following relationship applies between the above three degrees of polarization:

$$\left[P_G^2(z) - \left(\frac{A_s - A_p}{A_s + A_p}\right)^2\right]\left[P^2(0,z) - \left(\frac{A_s - A_p}{A_s + A_p}\right)^2\right] = \left[P_{st}^2 - \left(\frac{A_s - A_p}{A_s + A_p}\right)^2\right]^2. \tag{2.97}$$

In particular, at the far-field they read

$$P_{st}(z \to \infty) = \sqrt{\left(\frac{A_s - A_p}{A_s + A_p}\right)^2 + \frac{4A_{sp}^2}{\left(A_s + A_p\right)^2}}, \tag{2.98a}$$

$$P(r, z \to \infty) = \sqrt{\left(\frac{A_s - A_p}{A_s + A_p}\right)^2 + \frac{4A_{sp}^2}{\left(A_s + A_p\right)^2}\left(\frac{Q}{\tilde{Q}_{sp}}\right)^2 \exp\left(-a_\infty r^2\right)}, \tag{2.98b}$$

$$P_G(z \to \infty) = \sqrt{\left(\frac{A_s - A_p}{A_s + A_p}\right)^2 + \frac{4A_{sp}^2}{\left(A_s + A_p\right)^2}\left(\frac{\tilde{Q}_{sp}}{Q}\right)^2}, \tag{2.98c}$$

where a_∞ represents the value of $a(z)$ at the far field.

For illustrative purposes, Fig. 2.11 computes the degrees of polarization $P_G(z)$, $P(\boldsymbol{r} = 0,z)$ and P_{st} in terms of the propagation distance z .

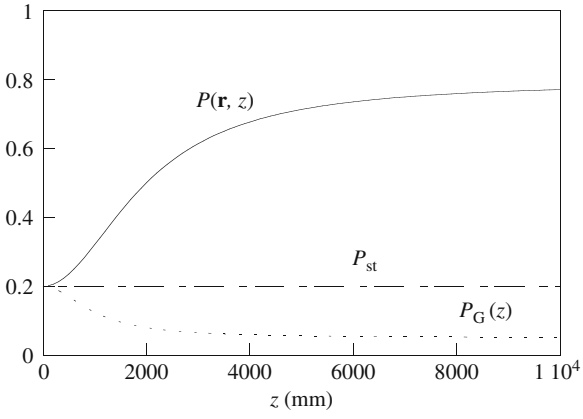

Fig. 2.11 Degrees of polarization $P(\boldsymbol{r} = 0,z)$, $P_G(z)$ and P_{st} versus the propagation distance z for a PGSM beam with the following characteristic parameters: $\sigma = 1$ mm. $\lambda = 633$ nm, $A_s = A_p = 0.5$, $A_{sp} = 0.1$, $\mu = 0.1$ mm and $\mu_{sp} = 0.2$ mm. In the figure, $P_{st} = 0.2$ (dotted line). See also (Martínez-Herrero et al., 2004)

To end this short survey, let us summarize a number of general properties derived for this class of beams:

(i) The local degree of polarization (squared) is a Gaussian function across the transverse profile (in accordance with previous theoretical and experimental results reported, for example, in (Gori et al., 2001; Piquero et al., 2002)).
(ii) Since the local and the generalized degree of polarization change upon free propagation according with the function $f(z)$, the overall polarization structure can then be determined at any plane z from the measurements of parameters Q and $\tilde{Q}_{sp}$ at the waist.
(iii) The parameters P_{st}, $P(\boldsymbol{r}=0,z)$, and $P_G(z)$ are nearly identical when $\mu_{sp} \sim \mu$.
(iv) If $A_{sp}^2 = A_s A_p$, then $P_{st} = P(\boldsymbol{r},z) = P_G(z) = 1$, and the beam is uniformly totally polarized at any transverse plane z.
(v) If $A_{sp} = 0$ then $P_{st} = P(\boldsymbol{r},z) = P_G(z) = \text{constant} < 1$. In other words, the beam is uniformly partially polarized. Moreover, for the particular case $A_s = A_p$, the three degrees of polarization,P_{st}, $P(\boldsymbol{r},z)$, and $P_G(z)$, are zero: The beam is unpolarized at every plane z.
(vi) If $A_s = A_p = A_0$ (as occurs in Fig. 2.11), the degrees of polarization are related at any plane z through the simple expression:

$$P_G(z)\,P(0,z) = P_{st}^2 = \frac{A_{sp}^2}{A_0^2}, \tag{2.99}$$

This means that the left-hand member of this equation is invariant upon free propagation, and it is also independent of the coherence characteristics of the field. In addition, we have in this case

$$\tilde{P} = P_{st} = \frac{A_{sp}}{A_0}, \tag{2.100}$$

and we see that the weighted degree of polarization (see Chap. 1) is independent of z as well. In particular, in Fig. 2.11 one has $\tilde{P} = P_{st} = 0.2$.

2.7 Beam Quality Improvement: General Considerations

Attention will now be devoted to the improvement of the beam quality parameter. Because of the invariance property of parameter Q in the scalar case, no rotationally-symmetric ABCD system could be employed to improve the quality of a partially coherent scalar beam. However, as it will next be apparent, such possibility arises when the vectorial behavior is taken into account. In the present section we will determine, for partially polarized beams, the optimized value of the beam quality parameter that can be attained by using rotationally-symmetric ABCD systems.

To begin with, note first that Q is invariant under rotation around the mean propagation direction. We can then choose, for convenience, a reference coordinate

system with respect to which

$$I_s = I_p \tag{2.101}$$

The angle θ between the new coordinate system and the former one is

$$\theta = \frac{1}{2}\left[\text{arctg}\left(\frac{I_s - I_p}{2\,\text{Re}\left\{I_{sp}\right\}}\right)\right], \tag{2.102}$$

where I_{sp} was defined in Eq. (2.88). In terms of this new coordinate system, the beam quality Q reads

$$Q = \frac{1}{4}\left(Q_s + Q_p + Q_{sp}\right). \tag{2.103}$$

Without loss of generality, let us assume, for simplicity, that the s-component reaches its waist at the plane where the irradiance moments are determined or measured. Accordingly, we can write at such plane.

$$\langle \boldsymbol{r} \cdot \boldsymbol{\eta} \rangle_s = 0, \tag{2.104}$$

and Q becomes

$$Q = \frac{1}{4}\left(Q_s + Q_p + \left\langle r^2 \right\rangle_s \left\langle \eta^2 \right\rangle_p + \left\langle r^2 \right\rangle_p \left\langle \eta^2 \right\rangle_s\right). \tag{2.105}$$

Let us now introduce the following functions (Martínez-Herrero et al., 2005):

$$F_1 = Q_s + \left\langle r^2 \right\rangle_s \left\langle \eta^2 \right\rangle_p, \tag{2.106}$$

$$F_2 = Q_p + \left\langle r^2 \right\rangle_p \left\langle \eta^2 \right\rangle_s, \tag{2.107}$$

Since Q_s, Q_p, $<r^2>_i$ and $<\eta^2>_i, i = s, p$, are positive quantities, we get

$$F_1 + F_2 \geq 2\sqrt{F_1 F_2}, \tag{2.108}$$

so that

$$Q \geq \frac{1}{2}\sqrt{F_1 F_2}, \tag{2.109}$$

In addition, functions F_1 and F_2 can be written in the form

$$F_i = G_i + J_i, \qquad i = 1,2, \tag{2.110}$$

with

$$G_1 = Q_s, \tag{2.111a}$$

$$J_1 = \left\langle r^2 \right\rangle_s \left\langle \eta^2 \right\rangle_p, \tag{2.111b}$$

$$G_2 = Q_p, \tag{2.111c}$$

$$J_2 = \left\langle r^2 \right\rangle_p \left\langle \eta^2 \right\rangle_s. \tag{2.111d}$$

Accordingly, we have

$$F_i = G_i + J_i \geq 2\sqrt{G_i J_i}, i = 1,2, \tag{2.112}$$

and therefore

$$Q^2 \geq \frac{1}{4} F_1 F_2 \geq \sqrt{G_1 J_1 G_2 J_2}. \tag{2.113}$$

Finally, since

$$\begin{aligned} G_1 J_1 G_2 J_2 &= Q_s Q_p \left\langle r^2 \right\rangle_s \left\langle \eta^2 \right\rangle_s \left\langle r^2 \right\rangle_p \left\langle \eta^2 \right\rangle_p = Q_s^2 Q_p \left\langle r^2 \right\rangle_p \left\langle \eta^2 \right\rangle_p \\ &\geq Q_s^2 Q_p \left(\left\langle r^2 \right\rangle_p \left\langle \eta^2 \right\rangle_p - \langle \boldsymbol{r} \cdot \boldsymbol{\eta} \rangle_p^2 \right) = Q_s^2 Q_p^2, \end{aligned} \tag{2.114}$$

it follows

$$Q^2 \geq Q_s Q_p. \tag{2.115}$$

This implies that the lower bound for the Q parameter of the partially polarized beam is the geometric mean of Q_s and Q_p. The equality is only reached when the second-order moments associated to each transverse field component are identical (recall we have chosen the coordinate system to make I_s equal to I_p). This, in turns, would imply that $Q_s = Q_p$.

We will next determine the lowest value of Q (best quality) that can be obtained by handling separate rotationally-symmetric first-order systems acting over each s- and p-component, along with the conditions to be fulfilled in order to optimize the overall beam quality (Martínez-Herrero et al., 2005).

The analysis is carried out by minimizing the function (see Eq. (2.115))

$$S(\chi, \beta) = 4\left[Q - \sqrt{Q_s Q_p} \right] = \left(\sqrt{Q_s} - \sqrt{Q_p} \right)^2 + \beta a + \chi b - 2\sqrt{Q_s Q_p}, \tag{2.116}$$

where

$$a \equiv \left\langle r^2 \right\rangle_s, \tag{2.117a}$$

$$b \equiv \left\langle \eta^2 \right\rangle_s, \tag{2.117b}$$

$$\chi \equiv \left\langle r^2 \right\rangle_p, \tag{2.117c}$$

$$\beta \equiv \left\langle \eta^2 \right\rangle_p. \tag{2.117d}$$

Note that

$$ab = Q_s \geq 1/k^2, \tag{2.118}$$

and

$$\chi\beta - \gamma^2 = Q_{\mathrm{p}} \geq 1/k^2, \tag{2.119}$$

where $\gamma = \langle \boldsymbol{r} \cdot \boldsymbol{\eta} \rangle_p$. In the calculations, we take a, b, Q_s and Q_p as known (measurable) parameters, and χ, β and γ as variables to be determined. Since they are linked through Eq. (2.119), the optimization procedure reduces to finding the minima of the following function

$$T(\chi,\gamma) = \left(\sqrt{Q_s} - \sqrt{Q_p}\right)^2 + \frac{a}{\chi}\left(Q_p + \gamma^2\right) + b\chi - 2\sqrt{Q_s Q_p} \tag{2.120}$$

Thus, by solving the equations

$$\frac{\partial T}{\partial \chi} = 0, \tag{2.121a}$$

$$\frac{\partial T}{\partial \gamma} = 0, \tag{2.121b}$$

we get that the critical points are given by

$$\chi_c = a\sqrt{Q_p/Q_s}, \tag{2.122}$$

$$\gamma_c = 0, \tag{2.123}$$

where the values χ_c, γ_c can be shown to represent a minimum of the function $T(\chi,\gamma)$. Equations (2.122) and (2.123) give the conditions to optimize the beam quality of the field. To get more insight into their physical meaning, let us write them in the more appropriate form

$$\left\langle r^2 \right\rangle_p = \left\langle r^2 \right\rangle_s \sqrt{Q_p/Q_s}, \tag{2.124}$$

$$\left\langle \eta^2 \right\rangle_p = \left\langle \eta^2 \right\rangle_s \sqrt{Q_p/Q_s}, \tag{2.125}$$

along with

$$\langle \boldsymbol{r} \cdot \boldsymbol{\eta} \rangle_p = 0. \tag{2.126}$$

Note that these three equations should be fulfilled at the plane where $\langle \boldsymbol{r} \cdot \boldsymbol{\eta} \rangle_s$ vanishes. They provide a precise relationship between the main second-order spatial parameters of the transverse field components. In addition, after substitution of Eqs. (2.124), (2.125), and (2.126) into Eq. (2.106), we find the optimized value of Q we are looking for:

$$(Q)_{optim} = \frac{1}{4}\left(\sqrt{Q_s} + \sqrt{Q_p}\right)^2. \tag{2.127}$$

Moreover, it can be shown at once that (Martínez-Herrero et al., 2005):

$$\min\left\{Q_s, Q_p\right\} \leq Q_{optim} \leq \max\left\{Q_s, Q_p\right\}, \tag{2.128}$$

i.e., Q_{optim} is always an intermediate value between Q_s and Q_p. Accordingly, when $Q_s = Q_p$, Q cannot be further improved: We have in such case (cf. Eqs. (2.124), (2.125), and (2.126))

$$\left\langle r^2 \right\rangle_p = \left\langle r^2 \right\rangle_s, \tag{2.129a}$$

$$\left\langle \eta^2 \right\rangle_p = \left\langle \eta^2 \right\rangle_s, \tag{2.129b}$$

$$\left\langle \boldsymbol{r} \cdot \boldsymbol{\eta}^2 \right\rangle_p = \left\langle \boldsymbol{r} \cdot \boldsymbol{\eta}^2 \right\rangle_s = 0, \tag{2.129c}$$

along with $I_s = I_p$ (see Eq. (2.101)).

In summary, the beam quality Q of the global field can be improved by means of rotationally-symmetric ABCD systems just to reach the value given by Eq. (2.127).

These conditions suggest a general procedure to optimize Q: the first two equalities (Eqs. (2.124) and (2.125)) show that the beam waists and divergences associated to the transverse field components should be exactly compensated, and Eq. (2.126) indicates that the waist planes of both components should match.

Taking this into account, a possible experimental scheme would involve a Mach-Zehnder-type (MZT) device, whose configuration resembles that of a classical Mach-Zehnder interferometer but now with a polarizer in each arm (Movilla et al., 2001). Thus, the field components can be controlled in a separate way in the optimization process.

For convenience, the transmission axes of the polarizers should match the reference coordinate system with respect to which $I_s = I_p$. Such a choice avoids interference between the emerging beams, because the transmission axes are then orthogonal.

To get the optimization conditions a two-step method can be followed: The initial beam can be made to propagate through a first MZT device with free propagation

paths in its arms in order to compensate for the different waist positions of the transverse beam components. The output of this interferometer is then made to travel through a second MZT arrangement that contains magnifiers to compensate for the corresponding beam sizes. Since a magnifier behaves as an ABCD optical system that increases the beam size, this also leads to a compensation for the difference in Rayleigh lengths z_{R} associated to each initial field components,

$$(z_R)_i = \left[\frac{\left(\langle r^2 \rangle_i\right)_w}{\langle \eta^2 \rangle_i} \right]^{1/2}, i = s,p, \tag{2.130}$$

where the subscript w refers to the waist plane. It should be pointed out that, when the waists of the field components are reached at the same plane, conditions (2.124) and (2.125) are met simultaneously.

To go further into the meaning of the optimization conditions, let us finally analyze two simple but general examples.

We first consider a beam whose moments associated to the s and p components are different but whose qualities Q_{s} and Q_{p} are identical. For simplicity, it is also assumed that $\langle \boldsymbol{r} \cdot \boldsymbol{\eta} \rangle_s = \langle \boldsymbol{r} \cdot \boldsymbol{\eta} \rangle_p = 0$. We then have

$$Q_s = \left\langle r^2 \right\rangle_s \left\langle \eta^2 \right\rangle_s = \left\langle r^2 \right\rangle_p \left\langle \eta^2 \right\rangle_p = Q_p \tag{2.131}$$

where $\langle r^2 \rangle_s \neq \langle r^2 \rangle_p$ and $\langle \eta^2 \rangle_s \neq \langle \eta^2 \rangle_p$. In this case, the global quality parameter Q reads

$$Q = \frac{Q_s}{4} \left(2 + q + \frac{1}{q} \right), \tag{2.132}$$

where

$$q \equiv \frac{\langle r^2 \rangle_s}{\langle r^2 \rangle_p} = \frac{\langle \eta^2 \rangle_p}{\langle \eta^2 \rangle_s}. \tag{2.133}$$

After using suitable MZT arrangements, we reach the optimized value

$$Q_{optim} = Q_s. \tag{2.134}$$

Remember that, in the present case, $Q_s = Q_p$. The relative quality improvement, $\Delta_{rel}Q$, defined in the form

$$\Delta_{rel}Q = \frac{Q - Q_{optim}}{Q}, \tag{2.135}$$

would then take the value

$$\Delta_{rel}Q = \frac{(1-q)^2}{(1+q)^2}. \tag{2.136}$$

In particular, when the second-order moments are identical, $q = 1$ so that $\Delta_{rel} Q = 0$. In the limit cases $q >> 1$ or $q << 1$ (very different beam sizes at the waist), we would get $\Delta_{rel} Q \approx 1$, which means strong beam quality improvement.

As a second example of interest, let us now focus our attention on those beams whose irradiance moments fulfil the relations

$$\langle r^2 \rangle_s = \langle r^2 \rangle_p, \tag{2.137a}$$

$$\langle \eta^2 \rangle_s \neq \langle \eta^2 \rangle_p, \tag{2.137b}$$

$$\langle \boldsymbol{r} \cdot \boldsymbol{\eta} \rangle_s = \langle \boldsymbol{r} \cdot \boldsymbol{\eta} \rangle_p = 0. \tag{2.137c}$$

It follows at once that $Q_s \neq Q_p$. Furthermore, the global quality parameter reads

$$Q = (1 + p) \frac{Q_s}{2}, \tag{2.138}$$

where

$$p \equiv \frac{\langle \eta^2 \rangle_p}{\langle \eta^2 \rangle_s}, \tag{2.139}$$

and the optimized value of Q becomes

$$Q_{optim} = (1 + p + 2\sqrt{p}) \frac{Q_s}{4}. \tag{2.140}$$

In this case we have

$$\Delta_{rel} Q = \frac{Q - Q_{optim}}{Q} = \frac{\left(1 - \sqrt{p}\right)^2}{2\,(1 + p)}. \tag{2.141}$$

For identical far-field divergences of the transverse field components (i.e., $p = 1$), it follows $\Delta_{rel} Q = 0$, as it should be expected. When the divergences drastically differ ($p >> 1$ or $p << 1$) then $\Delta_{rel} Q \approx 1/2$ which is half the change attained in the first example.

2.8 Beam Quality Improvement After Propagation Through Optical Phase Devices

In this section we investigate the influence of several optical devices on the quality parameter of light beams. More specifically, the possibility of beam quality improvement is examined when the field propagates through three kinds of phase components: Anisotropic pure-phase plates, quartic phase plates and spiral phase elements. It should be remarked that, due to the phase behavior of such

devices, no power losses would appear (in the ideal case) at the output of these components.

2.8.1 Propagation Through Anisotropic Pure-Phase Plates

Anisotropic pure-phase (APP) plates are analyzed in order to improve the quality parameter of an important class of partially coherent, partially polarized beams. In particular, we are interested on the determination of the phase transmittance of the APP plate that the beam should travel along to get the best quality keeping the same total power.

Within the framework of the paraxial approach, let us then consider a beam whose cross-spectral density matrix $\hat{W}$ contains diagonal elements of the form

$$\hat{W}_{ii}\left(\boldsymbol{r}_1,\boldsymbol{r}_2\right) = A_i\left(\boldsymbol{r}_1,\boldsymbol{r}_2\right)\exp\left\{i\left[\alpha_i\left(\boldsymbol{r}_2\right) - \alpha_i\left(\boldsymbol{r}_1\right)\right]\right\}, \; i = s,p, \tag{2.142}$$

where $\boldsymbol{r}_1$ and $\boldsymbol{r}_2$ are position vectors at a transverse plane, and A_i, α_i, i = s,p, are real functions, which should satisfy the relations

$$A_i\left(\boldsymbol{r}_1,\boldsymbol{r}_2\right) = A_i\left(\boldsymbol{r}_2,\boldsymbol{r}_1\right), \; i = s,p, \tag{2.143a}$$

$$A_i\left(\boldsymbol{r},\boldsymbol{r}\right) \geq 0, \; i = s,p, \tag{2.143b}$$

For simplicity, we will again choose our reference coordinate system in such a way that $I_s = I_p$, where now

$$I_i = \iint \hat{W}_{ii}(\boldsymbol{r},\boldsymbol{r})d\boldsymbol{r}, \quad i = s,p. \tag{2.144}$$

The class of fields we are considering includes those beams whose amplitude at any plane z can be written as an incoherent superposition of Hermite-Gauss modes. In particular, partially polarized Gaussian Schell-model sources belong to this family.

The APP plate can be represented, in the same reference system as before, by the Jones matrix

$$\hat{T}\left(\boldsymbol{r}\right) = \begin{pmatrix} \exp\left[i\Delta_s\left(\boldsymbol{r}\right)\right] & 0 \\ 0 & \exp\left[i\Delta_p\left(\boldsymbol{r}\right)\right] \end{pmatrix}. \tag{2.145}$$

Accordingly, the diagonal elements of $\hat{W}$ at the output of the APP plate are

$$\hat{W}_{ss}^{out}\left(\boldsymbol{r}_1,\boldsymbol{r}_2\right) = A_s\left(\boldsymbol{r}_1,\boldsymbol{r}_2\right)\exp\left\{i\left[\varphi_s\left(\boldsymbol{r}_2\right) - \varphi_s\left(\boldsymbol{r}_1\right)\right]\right\}, \tag{2.146a}$$

$$\hat{W}_{pp}^{out}\left(\boldsymbol{r}_1,\boldsymbol{r}_2\right) = A_p\left(\boldsymbol{r}_1,\boldsymbol{r}_2\right)\exp\left\{i\left[\varphi_p\left(\boldsymbol{r}_2\right) - \varphi_p\left(\boldsymbol{r}_1\right)\right]\right\}, \tag{2.146b}$$

where

$$\varphi_s(\boldsymbol{r}) = \alpha_s(\boldsymbol{r}) + \Delta_s(\boldsymbol{r}), \tag{2.147a}$$

$$\varphi_p(\boldsymbol{r}) = \alpha_p(\boldsymbol{r}) + \Delta_p(\boldsymbol{r}). \tag{2.147b}$$

Application of the definitions of the irradiance moments gives for the beam quality parameter Q^{out} at the output plane of the APP plate (Martínez-Herrero et al., 2003a)

$$Q^{out} = \langle r^2 \rangle G + F, \tag{2.148}$$

where $\langle r^2 \rangle$ is evaluated at the input plane,

$$\begin{aligned} G = \frac{1}{k^2 I}\Bigg[& \iint \left(\frac{\partial^2 A_s}{\partial x_1 \partial x_2} + \frac{\partial^2 A_s}{\partial y_1 \partial y_2} \right)_{x_1 = x_2 = x; y_1 = y_2 = y} dxdy + \\ & + \iint \left(\frac{\partial^2 A_p}{\partial x_1 \partial x_2} + \frac{\partial^2 A_p}{\partial y_1 \partial y_2} \right)_{x_1 = x_2 = x; y_1 = y_2 = y} dxdy \Bigg], \end{aligned} \tag{2.149}$$

is a function that depends only on the amplitude behavior of the input beam (therefore, G does not change after the APP plate), and

$$\begin{aligned} F = & \frac{\langle r^2 \rangle}{k^2 I} \left(\iint \left| \vec{\nabla} \varphi_s \right|^2 A_s dxdy + \iint \left| \vec{\nabla} \varphi_p \right|^2 A_p dxdy \right) \\ & - \left[\frac{1}{kI} \iint \left(\boldsymbol{r} \cdot \vec{\nabla} \varphi_s \right) A_s dxdy + \frac{1}{kI} \iint \left(\boldsymbol{r} . \vec{\nabla} \varphi_p \right) A_p dxdy \right]^2 \end{aligned} \tag{2.150}$$

It should be noted that the value of F involves information of both the phase of the input beam and the phase delay between the s and p components introduced by the plate. Furthermore, since the APP plate does not alter the value of G, the beam quality parameter at the output will depend only on F, which is always nonnegative (see (Martínez-Herrero et al., 2003a)). Accordingly, the best quality (lowest value of Q^{out}) will be obtained when $F = 0$. It can be shown (Martínez-Herrero et al., 2003a) that this occurs when

$$\alpha_s(\boldsymbol{r}) + \Delta_s(\boldsymbol{r}) = \alpha_p(\boldsymbol{r}) + \Delta_p(\boldsymbol{r}) = ar^2, \tag{2.151}$$

where a is a real-valued constant. In other words, for the beams we have considered here, the quality parameter would become optimized provided that either

(i) The phases of the s and p-components of the output field are identical, i.e., $a = 0$, or

(ii) The phase of the output field shows a quadratic dependence on the radial coordinate.

It should be noted that the quadratic phase factor $a\,r^2$ can be understood as the insertion of a lens (which does not change the quality parameter). Consequently, Eq. (2.151) indicates that, in order to optimize the quality, we have to remove the phase terms represented by the functions α_i, $i = s, p$. This is consistent with the results obtained in the previous section.

The physical meaning of Eq. (2.151) can be illustrated by means of a simple example: Let us consider a pure uniformly totally-polarized Gaussian beam propagating through a ground glass. The output field would belong to the type of beams studied here. The quality parameter of the output beam would be drastically affected by the action of the glass. To restore the original beam-quality value, it would obviously suffice to insert a plate that is phase conjugated with regard to the ground glass. But this is just what (2.151) shows.

In general, when the phase terms are completely removed, the APP plate behaves as a phase-conjugated filter (Pepper, 1985) matched to the phase transmittance of the light field. Equation (2.151) then assures that the quality parameter of the output field has the highest quality one can get by using pure-phase transmittances.

2.8.2 *Propagation of Radially and Azimuthally Polarized Beams Through Quartic Phase Plates*

We now analyze the change suffered by the beam quality of a radially (or azimuthally) polarized field, caused by quartic phase distortions, as occurs, for example, in strongly pumped laser rods used in high-power solid-state lasers (see Sect. 2.4).

For the sake of convenience, we will use planar polar coordinates, r and θ. The transverse field would then read

$$\boldsymbol{E}(r,\theta) = \left(E_s(r,\theta), E_p(r,\theta)\right), \tag{2.152}$$

and the electric field amplitude of a coherent radially (or azimuthally) polarized beam becomes

$$\boldsymbol{E}_R(r,\theta) = f(r)\,(\cos\theta, \sin\theta)\,, \tag{2.153a}$$

$$\boldsymbol{E}_\theta(r,\theta) = f(r)\,(-\sin\theta, \cos\theta)\,, \tag{2.153b}$$

where the subscripts R and θ stand for radial and azimuthal polarization, respectively. For both types of fields, the powers associated with the transverse

components are identical. Furthermore, the overall second-order moments are given by

$$\langle r^2 \rangle = \frac{1}{P} \int_0^\infty r^2 \, |f(r)|^2 \, r \, dr, \tag{2.154a}$$

$$\langle \eta^2 \rangle = \frac{1}{k^2 P} \int_0^\infty \left(\left| \frac{df}{dr} \right|^2 + \frac{1}{r^2} \, |f(r)|^2 \right) r \, dr, \tag{2.154b}$$

$$\langle \boldsymbol{r} \cdot \boldsymbol{\eta} \rangle = \frac{1}{2i \, k \, P} \int_0^\infty r \left(f^* \frac{df}{dr} - f \frac{df^*}{dr} \right) r \, dr, \tag{2.154c}$$

where

$$P = \int_0^\infty |f(r)|^2 \, r \, dr \tag{2.155}$$

Note that the above expressions do not depend on the coordinate θ. Let us now compare these formulae with the corresponding equations for *scalar* fields rotationally-symmetric around the z-axis. It should be remarked that, in the scalar case, we have to apply the scalar definition of the beam quality parameter (Lavi et al., 1988; Martínez-Herrero et al., 1992a, b; Siegman, 1990, 1993a, b; Simon et al., 1988; Serna et al., 1991; Weber, 1992). It can be shown that the only but important difference between both cases arises from the term $|f|^2/r^2$ in Eq. (2.154b). More specifically,

$$Q_{vectorial} = Q_{scalar} + \langle r^2 \rangle \, g, \tag{2.156}$$

where

$$g = \frac{1}{k^2 P} \int_0^\infty \frac{|f(r)|^2}{r^2} r \, dr. \tag{2.157}$$

We see that the second term of the right-hand side of Eq. (2.156) does not appear in the scalar case. Since this term is positive, it then follows that the value of the vectorial beam quality is always greater than the corresponding value of the scalar parameter.

Let us now consider that the radially (or azimuthally) polarized beam propagates through a strongly pumped laser rod. For the sake of simplicity, we assume in the calculations that changes in the beam diameter along the rod are not significant (this is the same assumption accepted in Sect. 2.4).

We know that, at high pump power, combined thermal lensing and birefringence generate a spherically aberrated lens, or, equivalently, an induced phase plate, $\exp[ik\Delta(r)]$ with

$$\Delta(r) = \alpha \frac{r^2}{2} + \beta \frac{r^4}{4}, \tag{2.158}$$

where α and β are, respectively, the quadratic and quartic coefficients describing the physical characteristics of the global process (Montmerle et al., 2006). Note that the values of α and β depend on the polarization of the incident field (radial or azimuthal): The low-order spherical aberration (SA) can be strongly reduced by using non-homogeneous pumping distribution. However, when the low-order SA vanishes, high-order spherical aberrations could rapidly increase. Consequently, in terms of beam quality preservation, a compromise should be established between low and high-order SA.

Here our interest is focused on the beam quality changes generated by the quartic term of Eq. (2.158). It can be found that the increment ΔQ, induced by SA, is given by

$$\Delta Q = Q_{out} - Q_{inp} = 2\beta \left(A \langle r^2 \rangle - \langle r^4 \rangle \langle \boldsymbol{r} \cdot \boldsymbol{\eta} \rangle \right) + \beta^2 \left(\langle r^2 \rangle \langle r^6 \rangle - \langle r^4 \rangle^2 \right), \tag{2.159}$$

where the subscripts *inp* and *out* refer to the input and output values of Q before and after crossing the rod, and

$$\langle r^n \rangle = \frac{1}{P} \int_0^\infty r^n \, |f(r)|^2 \, r \, dr, \quad n = 2,4,6 \tag{2.160}$$

$$A = \frac{i}{2kP} \int_0^\infty r^3 \left(f \frac{df^*}{dr} - f^* \frac{df}{dr} \right) r \, dr. \tag{2.161}$$

The sign of ΔQ (i.e., degradation or improvement of the beam quality) would depend on the spatial shape of the irradiance profile of the propagating beam. It should also be noted that the second term of the right-hand side of Eq. (2.159) is positive for every $f(r)$, whereas the sign of the first term depends on both, the transverse irradiance and the phase distribution of the output field.

Comparison between the beam quality change in the scalar and vectorial cases, shows that ΔQ is the same for both, rotationally-symmetric scalar beams and radially (or azimuthally) polarized fields. It should, however, be remarked that the ratio $\Delta Q/Q$ differs: In fact,

$$\left(\frac{\Delta Q}{Q} \right)_{vectorial} < \left(\frac{\Delta Q}{Q} \right)_{scalar}. \tag{2.162}$$

The above analysis can be illustrated by means of two simple examples. Let us first consider a radially or azimuthally polarized beam whose input amplitude $f(r)$ reads

$$f(r) = f_0(r)\,\exp\left(ikbr^2\right), \tag{2.163}$$

where b and f_0 are real quantities. In particular, beams whose amplitude is written in the form (Deng, 2006; Zhou, 2006)

$$f_{0n}(r) = r\,L_n^1\left(\frac{2r^2}{\omega_0^2}\right)\exp\left(-\frac{r^2}{\omega_0^2}\right), n = 1,2\ldots., \tag{2.164}$$

belong to this family (L_n^1 denoting the generalized Laguerre polynomials (Siegman, 1986)). For such fields we obtain (Martínez-Herrero et al., 2008)

$$\langle \boldsymbol{r}\cdot\boldsymbol{\eta}\rangle = 2\,b\,\langle r^2\rangle, \tag{2.165a}$$

$$A = 2\,b\,\langle r^4\rangle, \tag{2.165b}$$

and ΔQ reduces to

$$\Delta Q = \beta^2\left(\langle r^2\rangle\langle r^6\rangle - \langle r^4\rangle^2\right). \tag{2.166}$$

But ΔQ is positive. Consequently, for this kind of fields, the beam quality will always be degraded after passing through highly pumped laser rods. Figure 2.12 illustrates that the value ΔQ strongly increases for high values of the order n.

Let us finally write ΔQ in the form

$$\Delta Q = \frac{16}{k^2}\left(\frac{k\beta\langle r^2\rangle^2}{4}\right)^2\left[\frac{\langle r^6\rangle}{\langle r^2\rangle^3} - \left(\frac{\langle r^4\rangle}{\langle r^2\rangle^2}\right)^2\right]. \tag{2.167}$$

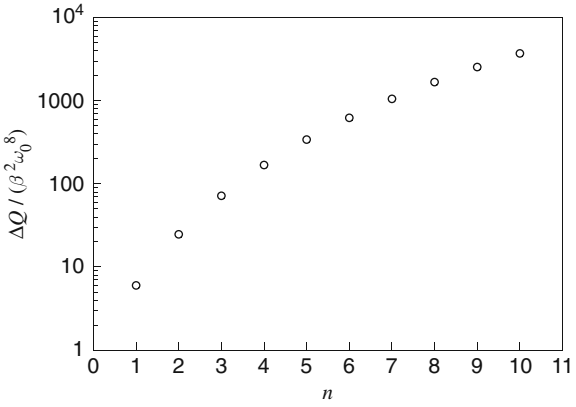

Fig. 2.12 Dimensionless ratio $\left(\Delta Q/\beta^2\omega_0^8\right)$ for the set of radially (or azimuthally) polarized beams whose amplitude is given by Eq. (2.164). The abscisses show the order n of the generalized Laguerre polynomials L_n^1. See also (Martínez-Herrero et al., 2008)

Since the factor $(k\beta\langle r^2\rangle^2/4)$ closely resembles the quartic phase term, we see that this factor explicitly shows the influence of the spherical aberration on the beam quality degradation.

As a second example we now consider a radially (or azimuthally) polarized beam whose incident amplitude $f(r)$ reads

$$f(r) = [I(r)]^{1/2} \exp\left[i\, k\varphi(r)\right], \tag{2.168}$$

where

$$\varphi(r) = \frac{ar^4}{4} + \frac{br^2}{2}, \tag{2.169}$$

and $I(r)$ denotes the irradiance. Equation (2.161) now becomes

$$A = \frac{1}{P} \int_0^\infty r^3 \frac{d\varphi(r)}{dr} I(r)\, r\, dr, \tag{2.170}$$

along with

$$\langle \boldsymbol{r} \cdot \boldsymbol{\eta} \rangle = \frac{1}{P} \int_0^\infty r \frac{d\varphi(r)}{dr} I(r)\, r\, dr. \tag{2.171}$$

After simple calculations, we obtain

$$\Delta Q = \left(\langle r^6\rangle\langle r^2\rangle - \langle r^4\rangle^2\right)\left(2\beta a + \beta^2\right). \tag{2.172}$$

Two conclusions can finally be derived from this expression:

(i) When $a = 0$ (as occurs in the above Laguerre-Gauss example), we have $\Delta Q > 0$, for any b and $I(r)$.
(ii) When $a = -\beta$, we then get $\Delta Q < 0$, for any b and $I(r)$. In other words, for this kind of polarized beams, a quartic phase plate could improve the beam quality.

2.8.3 Propagation Through Spiral Phase Elements

Attention will now be focused on the so-called spiral phase elements (SPEs) (Machavariani et al., 2007; Niv et al., 2005; Oemrawsingh et al., 2004; Oron et al., 2000; Xie and Zhao, 2008). The increasing interest on this kind of optical devices arises from their use in connection with certain depleted-center beams employed in a number of applications (Kuga et al., 1997; McCelland and Scheinfein, 1991; Molina-Terriza et al., 2007; Sato et al., 1994; Torner et al., 2005) such as, for instance, trapping of microscopic particles, focusing of atomic beams, and digital

spiral imaging, all of them well described in certain cases by means of the spiral spectrum of the light field.

We will next provide an introductory analysis about the changes suffered by the beam quality parameter of partially polarized, partially coherent fields travelling along SPEs.

The so-called spiral spectrum of a beam has revealed to be a useful tool to handle some type of situations. Let us introduce the spiral spectrum decomposition of the vector $\boldsymbol{E}(R,\theta)$ at a transverse plane (say, $z = 0$) in the form

$$\boldsymbol{E}(R,\theta) = \sum_n \boldsymbol{E}_n(R)\exp(in\theta), \tag{2.173}$$

where R and θ denote the planar polar coordinates, and

$$\boldsymbol{E}_n(R) = \frac{1}{2\pi}\int_0^{2\pi} \boldsymbol{E}(R,\theta)\exp(-in\theta)d\theta. \tag{2.174}$$

As in the previous section, for the sake of simplicity, we again choose the s- and p-axis in such a way that $I_s = I_p = I$.

By using Eq. (2.173), we get that the main second-order irradiance moments of a light beam can be written in terms of its spiral spectrum as follows (Martínez-Herrero and Manjavacas, 2009)

$$\left\langle r^2\right\rangle = \frac{\pi}{I}\sum_n \int_0^\infty \overline{|\boldsymbol{E}_n(R)|^2}R^3 dR, \tag{2.175a}$$

$$\left\langle \eta^2\right\rangle = \frac{\pi}{k^2 I}\sum_n \int_0^\infty \overline{\left|\boldsymbol{E}_n'(R)\right|^2}RdR + \frac{\pi}{k^2 I}\sum_n n^2\int_0^\infty \overline{|\boldsymbol{E}_n(R)|^2}\frac{1}{R}dR, \tag{2.175b}$$

$$\begin{aligned}\langle \boldsymbol{r}\cdot\boldsymbol{\eta}\rangle = \frac{\pi}{ikI}\sum_n \int_0^\infty \Big[&\overline{E_{ns}'(R)E_{ns}^*(R) - E_{ns}'^*(R)E_{ns}(R)} \\ &+ \overline{E_{np}'(R)E_{np}^*(R) - E_{np}'^*(R)E_{np}(R)}\Big]RdR\end{aligned} \tag{2.175c}$$

where the prime means derivation with respect to R. Application of Eq. (2.175b) requires that the irradiance of the field on the propagation axis decays with R^{m}, with $\mathrm{m} > 1$. Otherwise, the far-field moment $< \eta^2 >$ diverges. This comes from the singularity in the center, $R = 0$. It is also clear from these equations that the second-order moments can be understood as the sum of the corresponding moments associated to the spiral spectrum components.

Let us now assume that the light beam passes through a spiral phase element. This device will add a spiral phase $\varphi = p\theta$ to the field amplitude. Accordingly, the above irradiance moments at the input and output planes of the SPE are linked by

the following equations:

$$\left\langle r^2 \right\rangle_{out} = \left\langle r^2 \right\rangle_{inp}, \tag{2.176a}$$

$$\langle \boldsymbol{r} \cdot \boldsymbol{\eta} \rangle_{out} = \langle \boldsymbol{r} \cdot \boldsymbol{\eta} \rangle_{inp}, \tag{2.176b}$$

$$\left\langle \eta^2 \right\rangle_{out} = \left\langle \eta^2 \right\rangle_{inp} + M_p, \tag{2.176c}$$

where

$$M_p = \frac{\pi}{k^2 I} \sum_n \left(p^2 + 2np \right) \int_0^\infty \overline{|\mathbf{E}_n(R)|^2} \frac{1}{R} dR. \tag{2.177}$$

As expected, the beam width and the average curvature radii remain unchanged. However, the SPE alters the far-field divergence. Moreover, since the SPE introduces a change on the spiral spectrum of the field, the polarization behavior is also modified upon free propagation.

In addition, the output quality parameter, Q_{out}, reads

$$Q_{out} = Q_{inp} + \left\langle r^2 \right\rangle_{inp} M_p \tag{2.178}$$

Taking this into account, we finally obtain for the ratio $\frac{Q_{out} - Q_{inp}}{Q_{inp}}$ the value

$$\frac{\Delta Q}{Q_i} \equiv \frac{Q_{out} - Q_{inp}}{Q_{inp}} = \frac{\left\langle r^2 \right\rangle_{inp} M_p}{Q_{inp}}. \tag{2.179}$$

We thus conclude that, depending on the characteristics of the spiral spectrum of the specific light field, the SPE could improve or deteriorate the beam quality parameter. Here we do not proceed further into this subject, which deserves more study in the future. Application to some examples of interest can be found, for instance, in (Martínez-Herrero and Manjavacas, 2009).

2.9 Global Beam Shaping with Non-uniformly Polarized Beams

As is well known, in a number of applications one needs to obtain a prescribed beam profile at a certain transverse plane. Consequently, optical devices should be designed in order to modify at will the irradiance distributions of the laser beam. Drilling, welding, surface treatment, laser fusion experiments, information recording or optical data processing are examples in which appropriate transversal profiles are required.

This topic, namely, the implementation of particular distributions of irradiance (beam shaping) has been extensively investigated in the literature, and a large number of methods have been reported. They are based on refraction, reflection of beams over prescribed surfaces, diffraction, absorption, and transmission through pure phase plates or liquid-crystal layers, to mention only some of them. The majority of these techniques have been studied within the framework of the scalar theory of light, without taking into account its vectorial nature. Comparatively, there are not many papers that consider the polarization properties for beam shaping. In such cases, the techniques were focused on modifying the irradiance distribution at each point of the transverse section of the beam.

Here we consider a different approach, based on the global parameters introduced in this chapter. In fact, we are interested on a global shaping, which involves the control of the overall characteristics of the light field. For illustrative purposes, in the present section we show a simple example of application. Attention will be restricted on two parameters, the beam quality and the so-called kurtosis (Amarande, 1996; Martínez-Herrero et al., 1995a; Martínez-Herrero and Mejías 1997a), associated to the sharpness of the beam profile. To modify these parameters, several optical devices have already been proposed, such as binary phase plates (Siegman, 1993b), quartic phase plates (Martínez-Herrero et al., 1992b, Martínez-Herrero and Mejías 1993a; Siegman, 1993a), aberrated lenses (Alda et al., 1997; Piquero et al., 1994) and axicons (Luo and Lu, 2003). Next we briefly analyze a procedure that takes the vectorial character of light into account.

The method is essentially based on the generation of a non-uniformly totally polarized field by means of a Mach-Zehnder-type interferometric system.

To begin with, let us assume a beamlike field propagating along the z-axis. For the sake of simplicity, we consider in this example the two-dimensional x-z case, i.e., we write the field components as follows

$$\boldsymbol{E}(x,z) = \left(E_s(x,z),E_p(x,z)\right). \tag{2.180}$$

The so-called kurtosis parameter, K, is then defined in terms of higher-order irradiance moments in the form (Martínez-Herrero et al., 1995a)

$$K = \frac{\langle x^4 \rangle}{\langle x^2 \rangle^2} \tag{2.181}$$

with

$$\langle x^n \rangle = \frac{I_s}{I} \langle x^n \rangle_s + \frac{I_p}{I} \langle x^n \rangle_p \ ; n = 2,4, \tag{2.182}$$

where I_s, I_p and I were defined earlier. This parameter provides information about the sharpness or flatness of the beam profile. As a matter of fact, any beam can be classified as leptokurtic ($K > 3$), platykurtic ($K < 3$) or mesokurtic ($K = 3$). Since the kurtosis value of a Gaussian beam equals 3, leptokurtic and platykurtic profiles

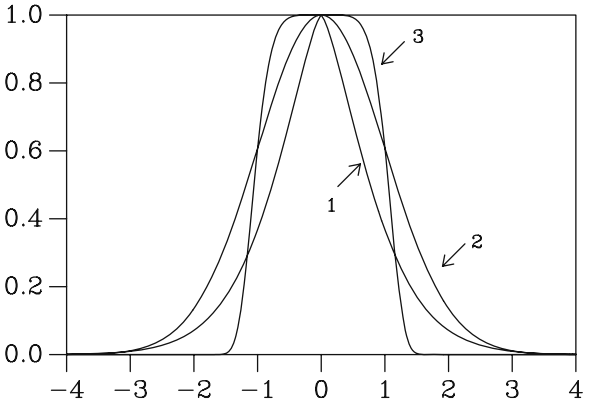

Fig. 2.13 Plots of three kinds of functions with regard to their values of the kurtosis: (*1*) leptokurtic ($K > 3$); (*2*) mesokurtic ($K = 3$); and (*3*) platykurtic ($K < 3$)

imply (globally) sharper and flatter beams, respectively, than the Gaussian case (see Fig. 2.13).

Let us now consider a Mach-Zehnder-type arrangement, in which two different amplitude filters are placed at each arm of the interferometer (see Fig. 2.14).

The transmittances of the filters are chosen to be the functions

$$t_i(x) = \exp\left[-g_i(x)\right], i = 1{,}2, \tag{2.183}$$

where $g_i(x)$, $i = 1{,}2$, denote the real-valued functions

$$g_1(x) = \frac{1}{2}\,(a\,x)^{2m}\,, \tag{2.184a}$$

and

$$g_2(x) = \frac{1}{2}\,(b\,x)^{2n}\,, \tag{2.184b}$$

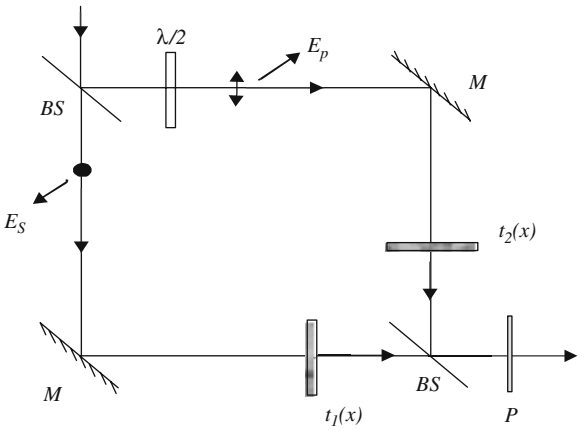

Fig. 2.14 Interferometric setup for global beam shaping. E_S and E_P are the field components of the beam, orthogonal to the propagation direction, λ/2 is a suitably rotated half-wave plate used to get the p-component, $t_1(x)$ and $t_2(x)$ are the amplitude transmittances, *M* denotes the mirrors, *BS* indicates the position of the beam splitters of the Mach-Zehnder arrangement, and *P* represents the linear polarizer that controls the parameters *Q* and *K* of the output beam

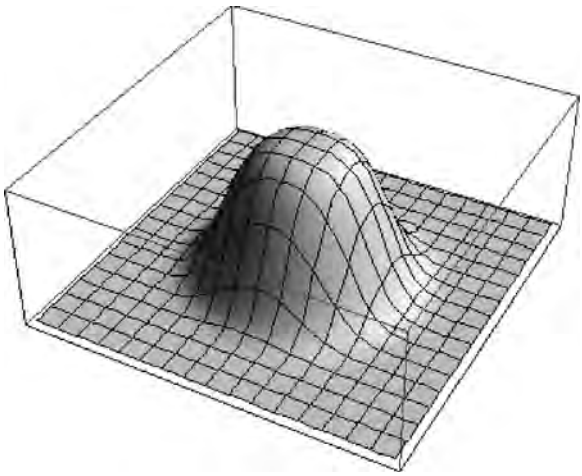

Fig. 2.15 Plot of a superGaussian transmittance (3D case) for $n = 2$

a and b being positive constants related to the aperture widths, and n and m are positive integers. As is well known, when n,$m > 1$ the transmittances are super-Gaussian functions. In such case, diffraction effects are expected to be negligible enough because these filters should be considered as soft-edge apertures (see, for example, Fig. 2.15).

If, for simplicity, the incident beam on the MZT device is assumed to be a plane wave, linearly polarized along the s-axis, it can be shown (Ramírez-Sánchez and Piquero, 2006) that the beam quality, Q, and the kurtosis parameter of the beam at the output of the interferometer (just before the polarizer P) read

$$Q = \frac{1}{2\,k^2}\left[ma\,\Gamma\left(2-\frac{1}{2m}\right)+n\,b\,\Gamma\left(2-\frac{1}{2n}\right)\right]\frac{\left[\frac{a^{-3}}{m}\Gamma\left(\frac{3}{2m}\right)+\frac{b^{-3}}{n}\Gamma\left(\frac{3}{2n}\right)\right]}{\left[\frac{a^{-1}}{m}\Gamma\left(\frac{1}{2m}\right)+\frac{b^{-1}}{n}\Gamma\left(\frac{1}{2n}\right)\right]^2}, \tag{2.185}$$

$$K = \left[\frac{a^{-1}}{2m}\Gamma\left(\frac{1}{2m}\right)+\frac{b^{-1}}{2n}\Gamma\left(\frac{1}{2n}\right)\right]\frac{\left[\frac{a^{-5}}{m}\Gamma\left(\frac{5}{2m}\right)+\frac{b^{-5}}{n}\Gamma\left(\frac{5}{2n}\right)\right]}{\left[\frac{a^{-3}}{m}\Gamma\left(\frac{3}{2m}\right)+\frac{b^{-3}}{n}\Gamma\left(\frac{3}{2n}\right)\right]^2}, \tag{2.186}$$

where Γ denotes the gamma function. From these expressions, it follows that the minimum value of Q (optimized quality) is reached when $a = b$ and $m = n$, as it should be expected. In such a case, throughout the wavefront, the output beam is linearly polarized with azimuth 45°.

In order to modify, in a continuous and controlled way, the parameters Q and K, a dichroic linear polarizer can be placed at the output plane of the MZT system. For different angles θ between the transmission axis of the polarizer and the x-axis, a global beam shaping can be implemented. In particular, when θ is equal to 0° or 90°, Q and K do not depend on the widths a and b, as expected. In such cases,

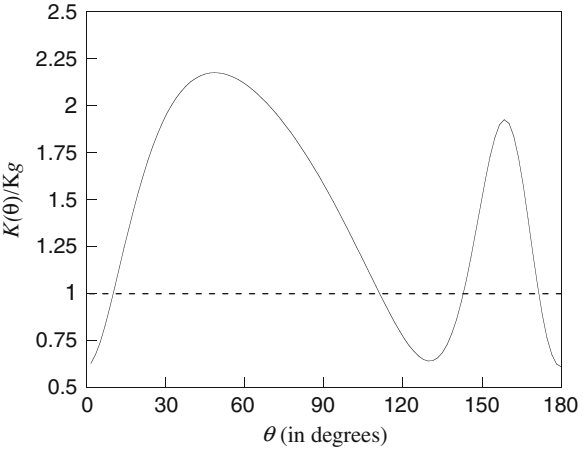

Fig. 2.16 Ratio K/K_g after the polarizer (at the output of the Mach-Zehnder arrangement) versus the angle θ that defines the orientation of the transmission axis of P. See also (Ramírez-Sánchez and Piquero, 2006)

the analytical expressions for the beam quality and the kurtosis at the output of the polarizer take the following simple forms:

$$Q = \frac{n^2}{k^2} \frac{\Gamma(3/2n)\Gamma(2 - 1/2n)}{\Gamma^2(1/2n)}, \tag{2.187}$$

$$K = \frac{\Gamma(5/2n)\Gamma(1/2n)}{\Gamma^2(3/2n)}. \tag{2.188}$$

Figure 2.16 computes the ratio K/K_g versus the angle θ, for the values $n = 0.6$, $m = 10$ and $a = b = 1$ mm^{-1}, K_g being the kurtosis of a Gaussian beam ($K_g = 3$). In this figure, the ratio ranges from 0.61 to 2.17, and the kurtosis exhibits maxima and minima. This means that the overall beam profile changes from leptokurtic to platykurtic and viceversa, becoming sharper or flatter depending on the orientation of the polarizer.

References

Abramochkin, E., Losevsky, N., Volostnikov, V. (1997): Generation of spiral-type laser beams, Opt. Commun. 141, 59–64.

Alda, J., Alonso, J., Bernabeu, E. (1997): Characterization of aberrated laser beams, J. Opt. Soc. Am. A 14, 2737–2747.

Alieva, T., Bastiaans, M. J. (2004): Evolution of the vortex and the asymmetrical parts of orbital angular momentum in separable first-order optical systems, Opt. Lett. 29, 1587–1589.

Allen, L., Padgett, M. J., Babiker, M. (1999): The orbital angular momentum of light, Prog. Opt. 39, 291-372.

Amarande, S. A. (1996): Beam propagation factor and the kurtosis parameter of flattened Gaussian beams, Opt. Commun. 129, 311–317.

Bastiaans, M. J. (1989): Propagation laws for the second-order moments of the Wigner distribution function in first-order optical systems, Optik 82, 173–181.

Bekshaev, A. Y., Soskin, M. S., Vasnetsov, M. V. (2003): Optical vortex symmetry breakdown and decomposition of the orbital angular momentum of light beams, J. Opt. Soc. Am. A 20, 1635–1643.

Born, M., Wolf, E. (1999): *Principles of Optics*, 7th ed. (Cambridge University Press, Cambridge).

Deng, D. M. (2006): Nonparaxial propagation of radially polarized light beams, J. Opt. Soc. Am. B 23, 1228–1234.

Encinas-Sanz, F., Serna, J., Martínez, C. Martínez-Herrero, R., Mejías, P. (1998): Time-varying beam quality factor and mode evolution TEA CO2 laser pulses, IEEE J. Quantum Electron., 34, 1835–1838.

Friberg, A. T. (1993): ed., *Selected Papers on Coherence and Radiometry* (SPIE Milestone Series, MS 69).

Giesen, A., Morin, M. (1998): eds., *Proceedings of the 4th International Workshop on Laser Beam and Optics Characterization* (LBOC4) (VDI-TechnologieZentrum, Munich).

Giesen, A., Weber, H. (2002): eds., *Proceedings of the 7th International Workshop on Laser Beam and Optics Characterization* (LBOC7) (Proc. SPIE 4932, Boulder, Colorado).

Gori, F., Bagini, V., Santarsiero, M., Frezza, F., Schettini, G., Schirripa Spagnolo, G. (1994): Coherent and partially coherent twisting beams, Opt. Rev. 1, 143–145.

Gori, F., Santarsiero, M., Piquero, G., Borghi, R., Mondello, A., Simon, R. (2001): Partially polarized Gaussian Schell-model beams, J. Opt. A Pure Appl. Opt. 3, 1–9.

Gori, F., Santarsiero, M., Borghi, R., Ramírez-Sánchez, V. (2008): Realizability condition for electromagnetic Schell-model sources, J. Opt. Soc. Am. A 25, 1016–1021.

Hodgson, H., Weber, H. (1993): Influence of spherical aberration of the active medium on the performance of Nd:YAG lasers**,** IEEE J. Quantum Electron. 29, 2497–2507.

ISO Standard 11146 (1999): Lasers and laser related equipment test methods for laser beams parameters: Beam widths, divergence angle and beam propagation factor.

ISO/DIS 12005 (2003): Optics and optical instruments-Lasers and laser related equipment-test methods for laser beam parameters: Polarization.

ISO 11146 (2005): Laser and laser related equipment-test methods for laser beam widths, divergence angles and beam propagation ratios, Parts 1, 2 and 3. International Organization for Standardization, Geneva, Switzerland.

Kudryashov, A. V., Paxton, A. H., Ilchenko, V. S., Giesen, A., Nickel, D., Davis, S. J., Heaven, M. C., Schriempf, J. T. (2006): eds., *Proceedings of the 8th International Workshop on Laser Beam and Optics Characterization* (LBOC8) (Proc. SPIE 6110, San Jose, CA).

Kuga, T., Torii, Y., Shiokawa, N., Hirano, T., Shimizu, Y., Sasada, H. (1997): Novel optical trap of atoms with a doughnut beam, Phys. Rew. Lett. 78, 4713–4716.

Kugler, N., Dong, N., Lü, Q., Weber, H. (1997): Investigation of the misalignment sensitivity of a birefringence: compensated two-rod Nd:YAG laser system, Appl. Opt. 36, 9359–9366.

Laabs, H., Weber, H. (2000): eds., *Proceedings of the 5th International Workshop on Laser Beam and Optics Characterization* (LBOC5) (VDI-TechnologieZentrum, Erice).

Lavi, S., Prochaska, R., Keren, E. (1988): Generalized beam parameters and transformation law for partially coherent light, Appl. Opt. 27, 3696–3703.

Lü, Q., Dong, S., Weber, H. (1995): Analysis of TEM_{00} laser beam quality degradation caused by a birefringent Nd:YAG rod, Opt. Quantum Electron. 27, 777–783.

Luo, S., Lu, B. (2003): M2 factor and kurtosis parameter of super-Gaussian beams passing through an axicon, Optik 114, 193–8.

Machavariani, G., Lumer, Y., Moshe, I., Jackel, S. (2007): Effect of the spiral phase element on the radial-polarization (0,1) * LG beam, Opt. Commun. 271, 190–196.

Mandel, L., Wolf, E. (1995): *Optical Coherence and Quantum Optics* (Cambridge University Press, Cambridge).

Marchand, E. W., Wolf, E. (1974): Walther′s definitions of generalized radiance, J. Opt. Soc. Am. 64(9), 1273–1274.

Martínez-Herrero, R., Mejías, P. M., Sánchez, M., Neira, J. L. H. (1992a): Third-and fourth-order parametric characterization of partially coherent beams propagating through ABCD optical systems, Opt. Quantum Electron. 24, 1021–1026.

Martínez-Herrero, R., Mejías, P. M., Piquero, G. (1992b): Quality improvement of partially coherent symmetric-intensity beams caused by quartic phase distorsions, Opt. Lett. 17, 1650–1651.

Martínez-Herrero, R., Mejías, P. M. (1993a): Quality improvement of symmetric-intensity beams propagating through pure phase plates, Opt. Commun. 95, 18–20.

Martínez-Herrero, R., Mejías, P. M. (1993b): Second-order spatial characterization of hard-edge diffracted beams, Opt. Lett. 18, 1669–1671.

Martínez-Herrero, R., Mejías, P. M. (1994): On the spatial parametric characterization of general light beams, *Current Trends in Optics*, Dainty, J. ed., Vol II (Academic Press, London, 105).

Martínez-Herrero, R., Piquero, G., Mejías, P. M. (1995a): On the propagation of the kurtosis parameter of general beams, Opt. Commun. 115, 225–232.

Martínez-Herrero, R., Mejías, P. M., Hodgson, N., Weber, H. (1995b): Beam-quality changes generated by thermally-induced spherical aberration in laser cavities, IEEE J. Quantum Electron. 31, 2173–2176.

Martínez-Herrero, R., Mejías, P. M., Arias, M. (1995c): Parametric characterization of coherent, lowest-order Gaussian beams propagating through hard-edge apertures, Opt. Lett. 20, 124–126.

Martínez-Herrero, R., Mejías, P. M. (1997a): On the fourth-order spatial characterization of laser beams: new invariant, Opt. Commun. 140, 57–60.

Martínez-Herrero, R., Mejías, P. M., Movilla, J. M. (1997b): Spatial characterization of partially polarized beams, Opt. Lett. 22, 206–208.

Martínez-Herrero, R., Mejías, P. M., Piquero, G. (2003a): Anisotropic pure-phase plates for quality improvement of partially coherent, partially polarized beams, J. Opt. Soc. Am. A 20, 577–581.

Martínez-Herrero, R., Mejías, P. M., Bosch, S., Carnicer, A. (2003b): Spatial width and power-content ratio of hard-edge diffracted beams, J. Opt. Soc. Am. A 20, 388–391.

Martínez-Herrero, R., Piquero, G., Mejías, P. M. (2004): Parametric characterization of the spatial structure of partially coherent and partially polarized beams, J. Opt. A: Pure Appl. Opt. 6, S67–S71.

Martínez-Herrero, R., Mejías, P. M., Movilla, J. M. (2005): Beam-quality optimization of partially polarized fields, J. Opt. Soc. Am. A 22, 1442–1446.

Martínez-Herrero, R., Mejías, P. M. (2006a): On the control of the spatial orientation of the transverse profile of a light beam, Opt. Express 14, 1086–1093.

Martínez-Herrero, R., Mejías, P. M. (2006b): On the spatial orientation of the transverse irradiance profile of partially coherent beams, Opt. Express 14, 3294–3303.

Martínez-Herrero, R., Mejías, P. M. (2007): Invariant parameters for characterizing nonuniformly partially polarized beams, Opt. Spectrosc. 103, 886–889.

Martínez-Herrero, R., Mejías, P. M., Piquero, G. (2008): Beam quality changes of radially and azimuthally polarized fields propagating through quartic phase, Opt. Commun. 281, 756–759.

Martínez-Herrero, R., Manjavacas, A. (2009): Overall second-order parametric characterization of light beams propagating through spiral phase elements, Opt. Commun. 282, 473–477.

McCelland, J. J., Scheinfein, M. R. J. (1991): Laser focusing of atoms: a particle-optics approach, J. Opt. Soc. Am. B 8, 1974–1986.

Mejías, P. M., Weber, H., Martínez-Herrero, R. (1993): González-Ureña, A., eds. *Proceedings of the 1st Workshop on Laser Beam Characterization* (LBOC1) (SEDO, Madrid).

Mejías, P. M., Martínez-Herrero, R. (1995): Time-resolved spatial parametric characterization of pulsed light beams, Opt. Lett. 20, 660–662.

Mejías, P. M., Martínez-Herrero, R., Piquero, G., Movilla, J. M. (2002): Parametric characterization of the spatial structure of non-uniformly polarizad laser beams, Prog. Quantum Electron. 26, 65–130.

Molina-Terriza, G., Rebane, L., Torres, J. P., Torner, L., Carrasco, S. (2007): Probing canonical geometrical objects by digital spiral Imaging, J. Eur. Opt. Soc. Rap. Public 2, 07014–07019.

Montmerle, B. A., Gilbert, M., Thro, P. Y., Weulersse, J. M. (2006): Thermal lensing and spherical aberration in high-power transversally pumped laser rods, Opt. Commun. 259, 223–235.

Morin, M., Giesen, A. (1996): eds., *Proceedings of the 3th International Workshop on Laser Beam Characterization* (LBOC3) (Proc. SPIE 2870, Quebec).
Movilla, J. M., Piquero, G., Martínez-Herrero, R., Mejías, P. M. (1998): Parametric characterization of non-uniformly polarized beams, Opt. Commun. 149, 230–234.
Movilla, J. M., Piquero, G., Martínez-Herrero, R., Mejías, P. M. (2000): On the measurement of the generalized degree of polarization, Opt. Quantum Electron. 32, 1333–1342.
Movilla, J. M., Martínez-Herrero, R., Mejías, P. M. (2001): Quality improvement of partially polarized beams, Appl. Opt. 40, 6098–6101.
Nemes, G., Siegman, A. E. (1994): Measurement of all ten second-order moments of an astigmatic beam by the use of rotating simple astigmatic (anamorphic) optics, J. Opt. Soc. Am. A 11, 2257–2264.
Niv, A., Biener, G., Kleiner, V., Hasman, E. (2005): Spiral phase elements obtained by use of discrete space-variant subwavelength gratings, Opt.Commun. 251, 306–314.
Oemrawsingh, S. S. R.; van Houwelingen, J. A. W.; Eliel, E. R., Woerdman, J. P., Verstegen, E. J. K., Kloosterboer, J. G., Hooft, G. W. (2004): Production and characterization of spiral phase plates for optical wavelengths, Appl. Opt. 43, 688–694.
Oron, R., Davidson, N., Friesem, A. A., Hasman, E. (2002): Continuous-phase elements can improve laser beam quality, Opt. Lett. 25, 939–941.
Pepper, D. M. (1985): Nonlinear optical phase conjugation, *Laser Handbook*, M. L. Stitch, M. L., and M. Bass, M., eds., Vol 4 (North-Holland, Amsterdam, 433–485).
Perina, J. (1971): *Coherence of Light* (Van Nostrand Reinhold Company, London).
Piquero, G., Mejías, P. M., Martínez-Herrero, R. (1994): Sharpness changes of Gaussian beams induced by spherically aberrated lenses, Opt. Commun. 107, 179–183.
Piquero, G., Gori, F., Romanini, P., Santarsiero, M., Borghi, R., Mondello, A. (2002): Synthesis of partially polarized Gaussian Schell-model sources, Opt. Commun. 208, 9–16.
Ramírez-Sánchez, V., Piquero, G. (2006): Global beam shaping with non-uniformly polarized beams: a proposal, Appl. Opt. 45, 8902–8906.
Sato, S., Harada, Y., Waseda, Y. (1994): Optical trapping of microscopic metal particles, Opt. Lett. 19, 1807–1809.
Serna, J., Martínez-Herrero, R., Mejías, P. M. (1991): Parametric characterization of general partially coherent beams propagating through ABCD optical systems, J. Opt. Soc. Am. A 8, 1094–1098.
Serna, J., Mejías, P. M., Martínez-Herrero, R. (1992a): Rotation of partially coherent beams propagating through free space, Opt. Quantum Electron. 24, S873–S880.
Serna, J., Mejías, P. M., Martínez-Herrero, R. (1992b): Beam quality changes of Gaussian Schell-model fields propagating through Gaussian apertures, Appl. Opt. 31, 4330–4331.
Siegman, A. E. (1986): *Lasers*, (University Science Books, California).
Siegman, A. E. (1990): New developments in laser resonators, *Optical Resonators*, Holmes, D. A., ed., Proc. SPIE, Vol1224, 2–14.
Siegman, A. E. (1993a): Analysis of laser beam quality degradation caused by spherical aberration, Appl. Opt. 32, 5893–5901.
Siegman, A. E. (1993b): Binary phase plates cannot improve laser beam quality, Opt. Lett. 18, 675–677.
Simon, R, Mukunda, N., Sudarshan, E. C. G. (1988): Partially coherent beams and a generalized ABCD-law, Opt. Commun. 65, 322–328.
Simon, R., Mukunda, N. (1993): Twisted Gaussian-Schell-model beams, J. Opt. Soc. Am. A 10, 95–109.
Torner, L., Torres, J., Carrasco, S. (2005): Digital spiral imaging, Opt. Express 13, 873–881.
Vasnetsov, M. V., Torres, J. P., Petrov, D. V., Torner, L. (2003): Observation of the orbital angular momentum spectrum of a light beam, Opt. Lett. 28, 2285–2287.
Walther, A. (1968): Radiometry and coherence, J. Opt. Soc. Am. 58, 1256–1259.
Weber, H. (1992): Propagation of higher-order intensity moments in quadratic-index media, Opt. Quantum Electron. 24, 1027–1049.

Weber, H., Reng, N., Lüdtke, J., Mejías, P. M. (1994): eds., *Proceedings of the 2nd Workshop on Laser Beam Characterization* (LBOC2) (FLI, Berlín).

WLT (2001): eds., *Proceedings of the 6th International Workshop on Laser Beam and Optics Characterization* (LBOC6) (WLT, Munich).

Wolf, E. (2007): *Introduction to the Theory of Coherence and Polarization of Light* (Cambridge University Press, Cambridge).

Xie, Q., Zhao, D. (2008): Optical vortices generated by multi-level achromatic spiral phase plates for broadband beams, Opt. Commun. 281, 7–11.

Zhou, G. Q. (2006): Analytical vectorial structure of Laguerre-Gaussian beam in the far field, Opt. Lett. 31, 2616–2618.

Chapter 3
Polarization and Coherence of Random Electromagnetic Fields

3.1 Introduction

In recent years, the study of the coherence properties of partially polarized electromagnetic fields is a subject of increasing interest and active research (see, for instance, Dennis, 2007; Ellis and Dogariu, 2004; Gori, 2008; Gori et al., 2006a, b, 2007, 2009; Korotkova and Wolf, 2005a, b; Lahiri and Wolf, 2009; Li et al., 2006; Mujat and Dogariu, 2003; Ponomarenko and Wolf, 2003; Pu et al., 2007; Réfrégier and Goudail, 2005; Réfrégier and Roueff, 2006, 2007a, b; Réfrégier, 2008a, b; Réfrégier and Luis, 2008; Roychowdhury and Wolf, 2005; Santarsiero and Borghi, 2006; Santarsiero, 2007; Setälä et al., 2004, 2006a, b; Tervo, 2003; Tervo et al., 2003, 2004; Wolf, 2003; Wolf and Roychowdhury, 2005; Wolf et al., 2006; Zhao and Wolf, 2008). As is well known, the scalar theory was clearly established many years ago (Beran and Parrent, 1967; Born and Wolf, 1999; Mandel and Wolf, 1995; Perina, 1971; Wolf, 2007b), and the concept of complete coherence of light was shown to be equivalent to a factorization condition of the cross-spectral density function of the field. Furthermore, in the scalar approach, a degree of coherence of unit modulus means maximum fringe visibility in Young's interference experiments. However, such behavior is no longer so simple in the vectorial regime. Moreover, the properties of polarization, factorization and visibility allow defining and characterizing different types of vectorial beams. This subject will be analyzed in a detailed way along the present chapter.

In addition, since we are interested on intrinsic coherence features of light fields, we will concentrate throughout the chapter on the so-called reversible optical devices, whose action can analytically be described by means of unitary matrices. To properly define this kind of optical element and clarify its role in the topic under study, let us briefly discuss a simple example: We consider a field linearly polarized along the x-axis at one pinhole in a standard Young interferometer, and linearly polarized along the y-axis at the other. As is explained in the textbooks, even though these fields have the same power and are completely correlated, no fringes are observed at the superposition plane because the field has orthogonal polarization states at the pinholes. However, on placing a $\pi/2$ rotator at one of the pinholes, interference fringes with unit visibility will be seen. A similar result is obtained by covering both pinholes with linear polarizers whose transmission axis makes 45°

R. Martínez-Herrero et al., *Characterization of Partially Polarized Light Fields*, Springer Series in Optical Sciences 147, DOI 10.1007/978-3-642-01327-0_3,

with the x-axis. There is, however, an essential difference between both procedures. In the first case, the original polarization state of the incident beam can be restored by means of a $-\pi/2$ rotator, but, in the second case, some fundamental information about the field is destroyed in an unrecoverable way. We refers to the first class of element (rotator) as reversible optical device: it generates a reversible transformation, which can be implemented by using anisotropic non-absorbing elements. The second type of device (polarizer) produces an irreversible transformation because certain field components are lost.

The chapter is then arranged as follows. In the next section, several important definitions and results are briefly reported for scalar light. In Sect. 3.3, the above definitions and experiments are discussed for the vectorial case. A number of recently introduced coherence parameters are considered, and some relations between them are analyzed. Section 3.4 is devoted to the study of the maximum fringe visibility one can attain in a Young interferometer by placing reversible optical devices at the pinholes. Sections 3.5 and 3.6 investigate two special types of random electromagnetic beams, namely, fields with position-independent stochastic behavior (Martínez-Herrero and Mejías, 2008a, b) and the so-called mean-square coherent light (Réfrégier, 2008b). Finally, Sect. 3.7 summarizes, in a comparative way, the main coherence and polarization properties of several families of vectorial fields investigated in this chapter.

3.2 Scalar Framework

Let us consider a random wide-sense stationary scalar light field, characterized by its cross-spectral density function, $W(\boldsymbol{r}_1,\boldsymbol{r}_2)$, defined in the usual way

$$W(\boldsymbol{r}_1,\boldsymbol{r}_2) = \overline{E^*(\boldsymbol{r}_1)\,E(\boldsymbol{r}_2)}, \tag{3.1}$$

where E represents realizations of the field amplitude at points $\boldsymbol{r}_1$ and $\boldsymbol{r}_2$, and the overbar denotes again the average over the ensemble of realizations. As in the previous chapter, the explicit dependence on the angular frequency, ω, has been omitted.

In order to compare the scalar case with the vectorial regime, we will next introduce the key definition and the main properties of the so-called spectral degree of coherence, and we will briefly review the concept of complete coherence for scalar fields. The relation between coherence and visibility in a Young's interference arrangement is also discussed within the scalar framework.

3.2.1 Spectral Degree of Coherence

As is well known in many textbooks, the coherence features in the space-frequency domain can be inferred from the spectral degree of coherence (SDC), given by the expression (Born and Wolf, 1999; Mandel and Wolf, 1995; Perina, 1971; Wolf, 2007b)

$$\mu\left(\boldsymbol{r}_1,\boldsymbol{r}_2\right)=\frac{W\left(\boldsymbol{r}_1,\boldsymbol{r}_2\right)}{\sqrt{W\left(\boldsymbol{r}_1,\boldsymbol{r}_1\right)W\left(\boldsymbol{r}_2,\boldsymbol{r}_2\right)}}. \tag{3.2}$$

This function takes complex values and exhibits the following general properties

i) $$\mu^*\left(\boldsymbol{r}_1,\boldsymbol{r}_2\right)=\mu\left(\boldsymbol{r}_2,\boldsymbol{r}_1\right). \tag{3.3a}$$

ii) $$\left|\mu\left(\boldsymbol{r}_1,\boldsymbol{r}_2\right)\right|\leq 1, \tag{3.3b}$$

iii) The modulus of the SDC does not change upon propagation through a deterministic position-dependent complex transmittance $t(\boldsymbol{r})$.

The particular but important case of complete coherence is defined in the scalar case by the equality

$$\left|\mu\left(\boldsymbol{r}_1,\boldsymbol{r}_2\right)\right|=1. \tag{3.4}$$

In other words, in the space-frequency domain, a fully coherent scalar field at a certain spatial domain Ω fulfils

$$\left|W\left(\boldsymbol{r}_1,\boldsymbol{r}_2\right)\right|=\sqrt{W\left(\boldsymbol{r}_1,\boldsymbol{r}_1\right)W\left(\boldsymbol{r}_2,\boldsymbol{r}_2\right)}\ \text{at}\ \Omega. \tag{3.5}$$

The above expressions involve two meaningful equivalent properties for complete coherence:

i) The CSD is factorizable, i.e.,

$$W\left(\boldsymbol{r}_1,\boldsymbol{r}_2\right)=F^*\left(\boldsymbol{r}_1\right)F\left(\boldsymbol{r}_2\right), \tag{3.6}$$

where $F\left(\boldsymbol{r}\right)$ is a deterministic function,

ii) The amplitude $E\left(\boldsymbol{r}\right)$ of the field can be written in the form

$$E\left(\boldsymbol{r}\right)=\alpha g\left(\boldsymbol{r}\right)\ \text{at}\ \Omega, \tag{3.7}$$

where α denotes a position-independent random variable, which takes values over the ensemble or realizations of the field, and $g\left(\boldsymbol{r}\right)$ is a deterministic function. We thus see that, in the fully-coherent scalar case, the stochastic behaviour does not depend on the position at the beam cross-section.

Let us finally note that the equality (3.7) should be understood in the mean-square sense, that is, the ensemble average of the quantity $|E-\alpha g|^2$ equals zero at each point $\boldsymbol{r}\in\Omega$.

3.2.2 Young's Interference Experiment

Let us now consider the typical Young's interference arrangement, sketched in Fig. 3.1. A light field, characterized by its cross-spectral density, illuminates an opaque screen Π_0 that contains two pinholes at points P_1 and P_2. As usual, we also understand that the pinholes are small enough to allow the field amplitude can be assumed to be constant throughout each pinhole. In addition, the field emerging from P_1 and P_2 is modelled as spherical wavefronts.

The light field at a point P of the observation plane Π is then given, to a good approximation, by the expression

$$E(P) = \frac{E(P_1)}{|\boldsymbol{R} - \boldsymbol{r}_1|} \exp(-ik\,|\boldsymbol{R} - \boldsymbol{r}_1|) + \frac{E(P_2)}{|\boldsymbol{R} - \boldsymbol{r}_2|} \exp(-ik\,|\boldsymbol{R} - \boldsymbol{r}_2|)\,, \tag{3.8}$$

where $\boldsymbol{R}$ and $\boldsymbol{r}_i$, $i = 1,2$, are the position vectors of points P and $P_{\,\mathrm{i}}$, respectively. Accordingly, the power spectrum at P, $I(P)$, reads

$$\begin{aligned} I(P) = \overline{|E(P)|^2} &= \frac{I(P_1)}{|\boldsymbol{R} - \boldsymbol{r}_1|^2} + \frac{I(P_2)}{|\boldsymbol{R} - \boldsymbol{r}_2|^2} \\ &+ 2\frac{\sqrt{I(P_1)\,I(P_2)}}{|\boldsymbol{R} - \boldsymbol{r}_1|\,|\boldsymbol{R} - \boldsymbol{r}_2|}\,|\mu(\boldsymbol{r}_1,\boldsymbol{r}_2)|\cos[\phi(\boldsymbol{r}_1,\boldsymbol{r}_2) + \delta]\,, \end{aligned} \tag{3.9}$$

where $I(P_i) = \overline{|E(P_i)|^2}$, $i = 1,2$, $\phi(\boldsymbol{r}_1,\boldsymbol{r}_2)$ represents the phase of the SDC, and

$$\delta = k\,(|\boldsymbol{R} - \boldsymbol{r}_1| - |\boldsymbol{R} - \boldsymbol{r}_2|)\,. \tag{3.10}$$

We immediately see from Eq. (3.9) that the third term of its right-hand side vanishes (i.e., no interference is observed at Π) if $|\mu(\boldsymbol{r}_1,\boldsymbol{r}_2)| = 0$.

When the SDC differs from zero, maximum and minimum values of I will be reached at those points of the observation plane given by the conditions (see Fig. 3.2)

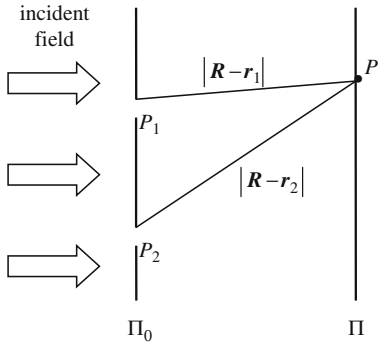

Fig. 3.1 Young's interference arrangement: Notation

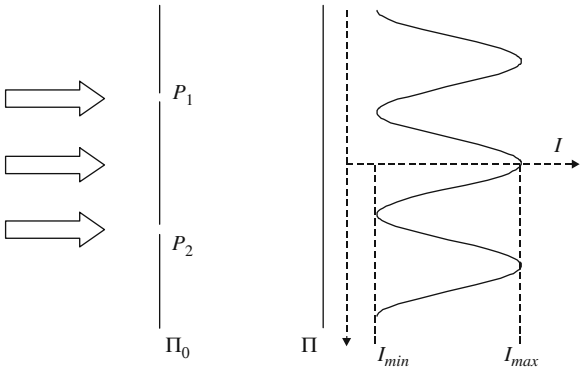

Fig. 3.2 Illustrating the interference pattern at the observation plane Π of a Young interference arrangement

$$I_{max} = \tilde{I}(P_1) + \tilde{I}(P_2) + 2\sqrt{\tilde{I}(P_1)\,\tilde{I}(P_2)}\,|\mu(\boldsymbol{r}_1,\boldsymbol{r}_2)|\,, \tag{3.11a}$$

$$I_{min} = \tilde{I}(P_1) + \tilde{I}(P_2) - 2\sqrt{\tilde{I}(P_1)\,\tilde{I}(P_2)}\,|\mu(\boldsymbol{r}_1,\boldsymbol{r}_2)|\,, \tag{3.11b}$$

where

$$\tilde{I}(P_i) = \frac{I(P_i)}{|\boldsymbol{R} - \boldsymbol{r}_i|^2},\ i = 1,2. \tag{3.12}$$

The visibility of the interference fringes, namely,

$$\mathcal{V} = \frac{I_{\max} - I_{\min}}{I_{\max} + I_{\min}}, \tag{3.13}$$

will then read

$$\mathcal{V} = \frac{2\sqrt{\tilde{I}(P_1)\,\tilde{I}(P_2)}}{\tilde{I}(P_1) + \tilde{I}(P_2)}\,|\mu(\boldsymbol{r}_1,\boldsymbol{r}_2)|\,. \tag{3.14}$$

Therefore, $\mathcal{V}$ is proportional to $|\mu|$ in the Young interferometer. Moreover, maximum visibility will be achieved by those fields whose modulus of the SDC equals 1 (fully-coherent scalar beams). In particular $\mathcal{V} = 1$ when $\tilde{I}(P_1) = \tilde{I}(P_2)$. It is also interesting to note that function $|\mu|$ (and, consequently, the ability of light to interfere) is not altered by placing deterministic transmittances at P_i, $i = 1,2$. This directly follows from property iii) of the SDC.

As a final conclusion, let us remark that, according with the results reported in this section, maximum visibility, factorization of the cross-spectral density (see Eq. (3.6)) and position-independent stochastic behaviour are equivalent properties for completely coherent scalar fields.

3.3 Vectorial Framework: Key Definitions

As we pointed out in the introduction, the study of partially polarized, partially coherent beamlike fields reveals to be more involved than the scalar case. The effects produced by coherence and polarization features are interconnected, and well-known scalar definitions, properties and fundamental experiments should be revisited in the vectorial regime. Thus, we will next consider the standard Young interferometric arrangement, and introduce a number of parameters, recently proposed in the literature (Gori et al., 2007; Martínez-Herrero and Mejías, 2007a; Réfrégier and Goudail, 2005; Setälä et al., 2004; Tervo et al., 2003; Wolf, 2003), in order to describe the coherence of the illuminating random electromagnetic beam. Certain analytical relations between the above parameters will also be shown. Supplementary results concerning optimization of the fringe visibility in the Young experiment will be investigated in subsequent sections.

3.3.1 Young's Experiment Revisited

Let us consider a random wide-sense stationary electromagnetic light beam. In the spectral domain, the field is represented by an statistical ensemble whose realizations $\boldsymbol{E}(\boldsymbol{r})$ are described by two components, $E_s(\boldsymbol{r})$ and $E_p(\boldsymbol{r})$, which are orthogonal to the propagation direction z (we assume again the paraxial approach). As we pointed out in the previous chapter, the behavior of the field at some transverse plane can be obtained from the cross-spectral density tensors (CDTs) $\hat{W}_{ij}$,i,j = 1,2, given by

$$\hat{W}_{ij} \equiv \hat{W}\left(\boldsymbol{r}_i,\boldsymbol{r}_j\right) = \overline{\boldsymbol{E}^{\dagger}\left(\boldsymbol{r}_i\right)\boldsymbol{E}\left(\boldsymbol{r}_j\right)},\ i,j = 1,2. \tag{3.15}$$

The deterministic optical devices that could modify the polarization state of the field will be characterized by position-dependent Jones matrices. When such optical elements are reversible (Gori et al., 2007), the Jones matrices become unitary.

Another example of unitary matrices arises from a transformation into orthogonal curvilinear coordinate systems (for instance, the standard s- and p-field representation into radial and azimuthal components) From now on, $\hat{U}(\boldsymbol{r})$ will symbolize a unitary transformation, characterizing both, a reversible optical element and a transformation into curvilinear coordinates.

It is interesting to note that the degree of polarization of the field is invariant under this kind of operations, on the contrary to that occurs with regard to the Stokes parameters, which are modified by unitary transformations.

Let us now revisit the Young arrangement shown in Fig. 3.3, in which two reversible devices have been placed in front on the pinholes at P_1 and P_2. The action of such optical elements on the incident field, $E(r)$, is represented by the unitary matrices $\hat{U}_1$ and $\hat{U}_2$.

Accordingly, the field at a point P of the superposition region, would be given by

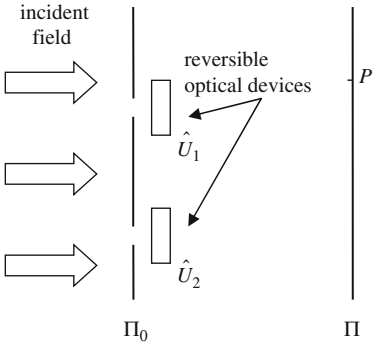

Fig. 3.3 Young's scheme in the vectorial case

$$\boldsymbol{E}(P) = \frac{\boldsymbol{E}(P_1)\,\hat{U}_1}{|\boldsymbol{R}-\boldsymbol{r}_1|}\exp\left(-ik\,|\boldsymbol{R}-\boldsymbol{r}_1|\right) + \frac{\boldsymbol{E}(P_2)\,\hat{U}_2}{|\boldsymbol{R}-\boldsymbol{r}_2|}\exp\left(-ik\,|\boldsymbol{R}-\boldsymbol{r}_2|\right), \quad (3.16)$$

where $\boldsymbol{E}(P)$ and $\boldsymbol{E}(P_\mathrm{i})$ are the row vectors

$$\boldsymbol{E}(P) = \left(E_s(P), E_p(P)\right), \quad (3.17a)$$

$$\boldsymbol{E}(P_i) = \left(E_s(P_i), E_p(P_i)\right), \quad i = 1,2. \quad (3.17b)$$

The polarization matrix $\hat{W}(P,P)$ would provide the polarization characteristics of the field resulting from de superposition. We get

$$\hat{W}(P,P) = \frac{\hat{U}_1^\dagger \hat{W}_{11}\hat{U}_1}{|\boldsymbol{R}-\boldsymbol{r}_1|^2} + \frac{\hat{U}_2^\dagger \hat{W}_{22}\hat{U}_2}{|\boldsymbol{R}-\boldsymbol{r}_2|^2} + \frac{\hat{U}_1^\dagger \hat{W}_{12}\hat{U}_2 \mathrm{e}^{\mathrm{i}\delta}}{|\boldsymbol{R}-\boldsymbol{r}_1|\,|\boldsymbol{R}-r_2|} + \frac{\hat{U}_2^\dagger \hat{W}_{12}\hat{U}_1 \mathrm{e}^{-\mathrm{i}\delta}}{|\boldsymbol{R}-\boldsymbol{r}_1|\,|\boldsymbol{R}-\boldsymbol{r}_2|}, \quad (3.18)$$

where δ was defined by Eq. (3.10). Consequently, the power spectrum at P reads

$$\begin{aligned} I(P) &= \mathrm{Tr}\hat{W}(P,P) = \tilde{I}(P_1) + \tilde{I}(P_2) \\ &+ 2\left[\tilde{I}(P_1)\,\tilde{I}(P_2)\right]^{1/2} \frac{\left|\mathrm{Tr}\left(U_1^\dagger \hat{W}_{12} U_2\right)\right|}{\sqrt{\mathrm{Tr}\hat{W}_{11}\mathrm{Tr}\hat{W}_{22}}}\,\cos\left(\phi_{12}+\delta\right), \end{aligned} \quad (3.19a)$$

with

$$\tilde{I}(P_i) = \frac{\mathrm{Tr}\hat{W}_{ii}}{|\boldsymbol{R}-\boldsymbol{r}_i|^2}, \mathrm{i} = 1,2, \quad (3.19b)$$

and ϕ_{12} denotes the phase of $\mathrm{Tr}\left(U_1^\dagger \hat{W}_{12} U_2\right)$. The visibility of the interference fringes becomes in this case

$$\mathcal{V} = \frac{2\sqrt{\tilde{I}(P_1)\,\tilde{I}(P_2)}}{\tilde{I}(P_1) + \tilde{I}(P_2)} \frac{\left|\mathrm{Tr}\left(U_1^{\dagger}\hat{W}_{12}U_2\right)\right|}{\sqrt{\mathrm{Tr}\hat{W}_{11}\mathrm{Tr}\hat{W}_{22}}}. \tag{3.20}$$

From this expression we see that, in the vectorial case, the visibility is proportional to $\left|\mathrm{Tr}\left(U_1^{\dagger}\hat{W}_{12}U_2\right)\right|$. This factor depends on the stochastic behavior of the field through $\hat{W}_{12}$ as well as on the deterministic reversible optical elements represented by the unitary matrices U_{i},i = 1,2. The influence of these devices is crucial in this type of interference scheme as is shown by means of the following illustrative example.

Let us assume that the cross-spectral density tensor associated to a field that illuminate the plane Π_0 is given by the matrix

$$\hat{W}_{ij} = a\begin{pmatrix} 1 & 0 \\ 0 & 0 \end{pmatrix}, \mathrm{i} = 1,2, \tag{3.21}$$

where a is a constant. We first consider the case $\hat{U}_1 = \hat{U}_2 = \hat{I}$ (no device is placed in front of the pinholes). For those regions of the observation plane close to the z-axis, application of Eq. (3.20) shows that $\mathcal{V} = 1$, i.e., the visibility is optimized.

Let us now consider that $\hat{U}_1 = \hat{I}$, but

$$\hat{U}_2 = \begin{pmatrix} 0 & 1 \\ -1 & 0 \end{pmatrix}. \tag{3.22}$$

Equation (3.20) shows that, in this case, $\mathcal{V} = 0$. In other words, a reversible optical device (anisotropic $\pi/2$-rotation phase plate) can alter substantially the visibility of the interference fringes in an standard Young experiment. In this sense, remember that, in the scalar case, no deterministic phase transmittance can change the visibility of this type of fringes.

3.3.2 Degrees of Coherence of Random Electromagnetic Fields

To characterize the state of coherence of a (paraxial) random electromagnetic field by means of scalar quantities, several parameters have been proposed in the literature as a measure for its degree of coherence.

i) *Wolf's spectral degree of coherence*, μ_w .
It is defined as follows (Wolf, 2003)

$$\mu_w = \frac{\mathrm{Tr}\hat{W}_{12}}{\sqrt{\mathrm{Tr}\hat{W}_{11}\mathrm{Tr}\hat{W}_{22}}}, \tag{3.23}$$

whose modulus satisfies the relation

$$0 \leq |\mu_w| \leq 1. \tag{3.24}$$

As is quite apparent from Eq. (3.20), $|\mu_w|$ is directly connected with the visibility in the standard Young interference experiment when no optical devices are placed at the pinholes (i.e., $\hat{U}_1 = \hat{U}_2 = \hat{I}$). In addition, note that μ_w only depends on the diagonal elements of matrix $\hat{W}_{12}$ in a given reference frame.

ii) *Electromagnetic degree of coherence*, μ^2_{STF} .
It was introduced in (Setälä et al., 2004) (see also (Tervo et al., 2003)) as follows:

$$\mu^2_{STF} = \frac{\mathrm{Tr}\left(\hat{W}_{12}\hat{W}^{\dagger}_{12}\right)}{\mathrm{Tr}\hat{W}_{11}\mathrm{Tr}\hat{W}_{22}}, \tag{3.25}$$

which takes nonnegative values. More specifically,

$$0 \leq \mu^2_{STF} \leq 1. \tag{3.26}$$

From the definition, it can be shown that deterministic unitary transformations do not alter μ^2_{STF} .

iii) *Intrinsic degrees of coherence*, μ_S and μ_I .
They can be defined as the singular values of the so-called normalized cross-spectral density matrix, $\hat{M}_{12}$, namely,

$$\hat{M}_{12} = \hat{W}_{11}^{-1/2}\,\hat{W}_{12}\hat{W}_{22}^{-1/2}. \tag{3.27}$$

These parameters were introduced in the space-time domain (Réfrégier and Goudail, 2005; Réfrégier and Roueff, 2007a; Réfrégier, 2008b). Here we keep the same notation, although, in this chapter, the space-frequency formalism is being considered.

To go further into the analytical properties of the intrinsic degrees of coherence, note first that $\hat{W}_{ii}$, $i = 1, 2$, are nonnegative definite Hermitian matrices. Therefore, there exist unitary matrices, $\hat{V}_i$,i = 1,2, and nonnegative numbers, α_i and β_i , with $\alpha_i \geq \beta_i$, such that the following equality applies:

$$\hat{W}_{ii} = \hat{V}_i^{\dagger}\hat{D}_i\hat{V}_i, i = 1,2, \tag{3.28}$$

where

$$\hat{D}_i = \begin{pmatrix} \alpha_i & 0 \\ 0 & \beta_i \end{pmatrix}, i = 1,2. \tag{3.29}$$

Note that, for totally polarized fields, $\beta_i = 0$. Taking Eq. (3.28) into account, we define $\hat{W}_{ii}^{-1/2}$ in the form

$$\hat{W}_{ii}^{-1/2} = \hat{V}_i^{\dagger}\hat{D}_i^{-1/2}\hat{V}_i, i = 1,2, \tag{3.30}$$

where, for partially polarized fields,

$$\hat{D}_i^{-1/2} = \begin{pmatrix} \alpha_i^{-1/2} & 0 \\ 0 & \beta_i^{-1/2} \end{pmatrix}, i = 1,2. \tag{3.31}$$

A relation similar to Eqs. (3.24) and (3.26) is satisfied by the intrinsic degrees of coherence:

$$0 \leq \mu_j \leq 1, j = S,I. \tag{3.32}$$

Furthermore, it can be shown that $\mu_S = \mu_I = 1$ if and only if $\hat{M}_{12}$ is a unitary matrix.

When we consider reversible optical elements, characterized by unitary matrices $\hat{U}(\boldsymbol{r})$, the matrix $\hat{M}_{12}^{\text{out}}$ at the output of such devices becomes

$$\hat{M}_{12}^{\text{out}} = \hat{U}_1^{\dagger} \hat{M}_{12} \hat{U}_2, \tag{3.33}$$

where $\hat{M}_{12}$ denotes the input matrix, and the subscripts 1 and 2 refer, as usual, to the points $\boldsymbol{r}_1$ and $\boldsymbol{r}_2$. It then follows that μ_S and μ_I are invariant under this kind of reversible elements.

Finally, as a particular but illustrative example, let us consider those fields whose cross-spectral density tensor reads

$$\hat{W}_{ij} = f\left(\boldsymbol{r}_i, \boldsymbol{r}_j\right) \hat{\phi}, i,j = 1,2, \tag{3.34}$$

where $f\left(\boldsymbol{r}_i, \boldsymbol{r}_j\right)$ is a nonnegative definite function, with $f^*(\boldsymbol{r}_1, \boldsymbol{r}_2) = f(\boldsymbol{r}_2, \boldsymbol{r}_1)$, and $\hat{\phi}$ denotes a nonnegative definite Hermitian matrix with constant elements. It can be shown that, for this class of fields,

$$|\mu_W|^2 = \mu_S^2 = \mu_I^2 = \frac{|f(\boldsymbol{r}_1, \boldsymbol{r}_2)|^2}{f(\boldsymbol{r}_1, \boldsymbol{r}_1) f(\boldsymbol{r}_2, \boldsymbol{r}_2)}, \tag{3.35a}$$

together with

$$\mu_{STF}^2 = |\mu_W|^2 \frac{\text{Tr}\hat{\phi}^2}{\left(\text{Tr}\hat{\phi}\right)^2}. \tag{3.35b}$$

In particular, when $\text{Det}\, \hat{\phi} = 0$ (totally polarized beams), we have

$$|\mu_W|^2 = \mu_{STF}^2 = \mu_S^2 = \mu_I^2. \tag{3.36}$$

It is interesting to remark that the complex degree of coherence, μ, of a scalar field whose CSD takes the form

$$W(\boldsymbol{r}_1, \boldsymbol{r}_2) = f(\boldsymbol{r}_1, \boldsymbol{r}_2), \tag{3.37}$$

would read

$$|\mu(\boldsymbol{r}_1,\boldsymbol{r}_2)|^2 = \frac{|f(\boldsymbol{r}_1,\boldsymbol{r}_2)|^2}{f(\boldsymbol{r}_1,\boldsymbol{r}_1) f(\boldsymbol{r}_2,\boldsymbol{r}_2)}, \tag{3.38}$$

which is completely analogous to Eq. (3.35a), obtained for random electromagnetic beams. In other words, the visibility attained in the standard Young experiment would take the same functional form for the fields defined by Eq. (3.34) (vectorial case) and (3.37) (scalar case). Consequently, in a sense we could refer to the beams given by Eq. (3.34) as pseudo-scalar fields.

3.3.3 Relation Between Degrees of Coherence of Electromagnetic Fields

We will next see that, under some conditions, certain relationships can de established between the degrees of coherence introduced before. More specifically, we are going to show the following proposition for partially coherent, partially polarized beams (Martínez-Herrero and Mejías, 2007b):

Proposition *A suitable local (i.e., position-dependent) unitary transformation can be found to get* $|\mu_W|^2 = 1$ *at points* $\boldsymbol{r}_1$ *and* $\boldsymbol{r}_2$ if and only if

1) the degree of polarization, P, is identical at these two points, and
2) $\mu^2_{STF} = \frac{1+P^2}{2}$ *, and*
3) the intrinsic degrees of coherence are equal to 1.

Proof We will first show that any field with $|\mu_W|^2 = 1$ at $\boldsymbol{r}_1$ and $\boldsymbol{r}_2$ satisfies conditions 1–3.

To begin with, note that the equality $|\mu_W|^2 = 1$ implies that

$$\left|\mathrm{Tr}\,\overline{\boldsymbol{E}_1^\dagger \boldsymbol{E}_2}\right|^2 = \left(\mathrm{Tr}\,\overline{\boldsymbol{E}_1^\dagger \boldsymbol{E}_1}\right)\left(\mathrm{Tr}\,\overline{\boldsymbol{E}_2^\dagger \boldsymbol{E}_2}\right), \tag{3.39}$$

where $\boldsymbol{E}_1$ and $\boldsymbol{E}_2$ denote the value of the field at $\boldsymbol{r}_1$ and $\boldsymbol{r}_2$, respectively. In addition, the trace of matrix $\hat{W}_{ij},i,j = 1,2$, can be understood as the inner product $\overline{\boldsymbol{E}(\boldsymbol{r}_i)\boldsymbol{E}^\dagger(\boldsymbol{r}_i)}$, $i = 1,2$. Consequently, application of the Cauchy-Schwarz inequality to (3.39) yields

$$\boldsymbol{E}(\boldsymbol{r}_1) = a\boldsymbol{E}(\boldsymbol{r}_2), \tag{3.40}$$

in the mean-square sense, where a is a deterministic constant. Taking this into account, we get

$$\hat{W}_{11} = |a|^2 \hat{W}_{22}, \tag{3.41a}$$

$$\hat{W}_{12} = a^* \hat{W}_{22}. \tag{3.41b}$$

Accordingly, we conclude

1) $P(\boldsymbol{r}_1) = P(\boldsymbol{r}_2)$,

2) $\mu^2_{STF} = \dfrac{\mathrm{Tr}\hat{W}^2_{22}}{\left(\mathrm{Tr}\hat{W}_{22}\right)^2} = \dfrac{1+P^2}{2}$, (3.42)

3) Matrix $\hat{M}_{12}$ becomes

$$\hat{M}_{12} = \frac{a^*}{|a|}\hat{W}_{22}^{-1/2}\hat{W}_{22}\hat{W}_{22}^{-1/2} = \frac{a^*}{|a|}\hat{I}, \tag{3.43}$$

which implies

$$\hat{M}_{12}\hat{M}_{12}^{\dagger} = \hat{I}, \tag{3.44}$$

and, therefore, the intrinsic degrees of coherence μ_S and μ_I equals 1. The first part ($\Rightarrow$) of the proof is thus completed.

Let us now demonstrate the converse part. We first recall (see Eq. (3.28)) that the nonnegative definiteness of matrices $\hat{W}_{ii}$, $i = 1,2$, implies that two unitary matrices exist, $\hat{V}_i$,$i = 1,2$, fulfilling

$$\hat{W}_{ii} = \hat{V}_i^{\dagger}\hat{D}_i\hat{V}_i,\ i = 1,2, \tag{3.45}$$

where $\hat{D}_i$ was defined in Eq. (3.29). Let us assume that the values of the degree of polarization of the field at $\boldsymbol{r}_1$ and $\boldsymbol{r}_2$ are identical (condition 1 of the proposition). From the expression of $P(\boldsymbol{r}_1)$ in terms of $\hat{W}_{ii}$, $i = 1,2$, we obtain

$$\frac{\alpha_1 - \beta_1}{\alpha_1 + \beta_1} = \frac{\alpha_2 - \beta_2}{\alpha_2 + \beta_2}, \tag{3.46}$$

so that

$$\frac{\beta_1}{\alpha_1} = \frac{\beta_2}{\alpha_2} \equiv b, \text{ with } b \leq 1. \tag{3.47}$$

We can then write

$$\hat{W}_{11} = \alpha_1 \hat{V}_1^{\dagger}\hat{D}\hat{V}_1, \tag{3.48a}$$

$$\hat{W}_{22} = \alpha_2 \hat{V}_2^{\dagger}\hat{D}\hat{V}_2, \tag{3.48b}$$

where

$$\hat{D} = \begin{pmatrix} 1 & 0 \\ 0 & b \end{pmatrix}. \tag{3.49}$$

Accordingly,

$$\hat{W}_{22} = \alpha_2 \hat{V}_2^\dagger \hat{V}_1 \hat{V}_1^\dagger \hat{D} \hat{V}_1 \hat{V}_1^\dagger \hat{V}_2 = \hat{N}^\dagger \hat{W}_{11} \hat{N}, \tag{3.50}$$

where

$$\hat{N} = m \hat{V}_1^\dagger \hat{V}_2, \tag{3.51}$$

with

$$m = \sqrt{\frac{\alpha_2}{\alpha_1}}. \tag{3.52}$$

We then have $\mathrm{Tr}\hat{W}_{22} = m^2 \mathrm{Tr}\hat{W}_{11}$. But $\frac{1+P^2}{2} = \frac{\mathrm{Tr}W_{11}^2}{(\mathrm{Tr}W_{11})^2}$. Consequently, application of condition 2 of the proposition gives

$$\mathrm{Tr}\left(\hat{W}_{12}\hat{W}_{12}^\dagger\right) = \mathrm{Tr}\left(m^2 \hat{W}_{11}^2\right). \tag{3.53}$$

On the other hand, condition 3 implies (since $\hat{M}_{12}$ is unitary)

$$\mathrm{Det}\left(\hat{W}_{12}\hat{W}_{12}^\dagger\right) = \left|\mathrm{Det}\hat{W}_{12}\right|^2 = \left|\mathrm{Det}\left(\hat{W}_{11}^{1/2}\hat{M}_{12}\hat{W}_{22}^{1/2}\right)\right|^2 = \mathrm{Det}\hat{W}_{11}\mathrm{Det}\hat{W}_{22}, \tag{3.54}$$

and, by using Eq. (3.51), we obtain

$$\mathrm{Det}\left(\hat{W}_{12}\hat{W}_{12}^\dagger\right) = \mathrm{Det}\left(|m|^2\, \hat{W}_{11}^2\right). \tag{3.55}$$

We thus conclude that the determinants and the traces of the nonnegative matrices $\hat{W}_{12}\hat{W}_{12}^\dagger$,$\hat{W}_{12}^\dagger\hat{W}_{12}$ and $|m|^2\, \hat{W}_{11}^2$ are identical. As a consequence, two 2×2 unitary matrices exist, $\hat{U}$ and $\hat{V}$, such that

$$\hat{W}_{12}\hat{W}_{12}^\dagger = |m|^2\, \hat{U}^\dagger \hat{W}_{11} \hat{U}, \tag{3.56a}$$

$$\hat{W}_{12}^\dagger\hat{W}_{12} = |m|^2\, \hat{V}^\dagger \hat{W}_{11} \hat{V}, \tag{3.56b}$$

and one gets

$$\hat{W}_{12} = m\hat{U}^\dagger \hat{W}_{11} \hat{V}. \tag{3.57}$$

We now place two reversible optical devices (at points $\boldsymbol{r}_1$ and $\boldsymbol{r}_2$) represented by the unitary matrices $\hat{R}_1$ and $\hat{R}_2$. Moreover, in particular, we choose

$$\hat{R}_1^\dagger = \hat{U}, \tag{3.58a}$$

$$\hat{R}_2^\dagger = \hat{V}, \tag{3.58b}$$

$\hat{U}$ and $\hat{V}$ being defined by Eqs. (3.56). The cross-spectral density tensors $\hat{W}_{ij}^{\text{out}}$, $i,j =$ 1,2 after these local transformations become

$$\hat{W}_{11}^{\text{out}} = \hat{U}\hat{W}_{11}\hat{U}^{\dagger}, \tag{3.59a}$$

$$\hat{W}_{22}^{\text{out}} = \hat{V}\hat{W}_{22}\hat{V}^{\dagger}, \tag{3.59b}$$

$$\hat{W}_{12}^{\text{out}} = \hat{U}\hat{W}_{12}\hat{V}^{\dagger}. \tag{3.59c}$$

But Eqs. (3.57) and (3.59c) implies

$$\hat{W}_{12}^{\text{out}} = m\hat{W}_{11}. \tag{3.60}$$

Accordingly, taking Eqs. (3.50), (3.59a) and (3.59b) into account, we finally get

$$|\mu_W|^2 = \frac{\left|\text{Tr}\hat{W}_{12}^{\text{out}}\right|^2}{\text{Tr}\hat{W}_{11}^{\text{out}}\text{Tr}\hat{W}_{22}^{\text{out}}} = \frac{|m|^2\left(\text{Tr}\hat{W}_{11}\right)^2}{|m|^2\left(\text{Tr}\hat{W}_{11}\right)^2} = 1, \tag{3.61}$$

and the proof of the proposition is completed, Q.E.D.

To get deeper insight into the physical meaning of the proposition, let us analyze a simple but illustrative example. We consider a random electromagnetic field whose CDTs at points $\boldsymbol{r}_1$ and $\boldsymbol{r}_2$ are given by the matrices

$$\hat{W}_{ii} = a_i\hat{I}, i = 1,2, \tag{3.62a}$$

$$\hat{W}_{12} = \sqrt{\frac{a_1 a_2}{2}}\begin{pmatrix} 1 & 1 \\ 1 & -1 \end{pmatrix}, \tag{3.62b}$$

where $a_i, i = 1,2$, are positive numbers proportional to the power. Equation (3.62a) shows that this field is unpolarized at $\boldsymbol{r}_1$ and $\boldsymbol{r}_2$, i.e., the degree of polarization at both points equals zero. From the above equation we also have

$$|\mu_W|^2 = 0, \tag{3.63a}$$

$$\mu_{STF}^2 = \frac{1}{2}, \tag{3.63b}$$

$$\mu_S = \mu_I = 1. \tag{3.63c}$$

In other words, direct superposition (upon free propagation) of the fields $\boldsymbol{E}(\boldsymbol{r}_1)$ and $\boldsymbol{E}(\boldsymbol{r}_2)$ in a Young interferometer gives zero fringe visibility.

However, since this field satisfies conditions 1–3 of the proposition, we could attain $|\mu_W|^2 = 1$ by propagating the field through reversible optical devices placed at points $\boldsymbol{r}_1$ and $\boldsymbol{r}_2$. More specifically, in Eqs. (3.58) the values of matrices $\hat{U}$ and $\hat{V}$ that represent such optical elements are

$$\hat{U} = \hat{I}, \tag{3.64a}$$

$$\hat{V} = \frac{\sqrt{2}}{2}\begin{pmatrix} 1 & 1 \\ 1 & -1 \end{pmatrix}. \tag{3.64b}$$

This means that the transformation should be applied only on the field incident on $\boldsymbol{r}_2$. In this example, the reversible device represented by $\hat{V}$ would involve a half-wave birefringent plate along with a $\frac{\pi}{4}-$ rotation of the coordinate axes.

Note that the CDTs $\hat{W}_{ij}^{\text{out}}$, $i,j = 1,2$, at the output of such device would read

$$\hat{W}_{11}^{\text{out}} = \hat{W}_{11}, \tag{3.65a}$$

$$\hat{W}_{22}^{\text{out}} = \hat{W}_{22}, \tag{3.65b}$$

$$\hat{W}_{12}^{\text{out}} = \sqrt{a_1 a_2}\hat{I}, \tag{3.65c}$$

so that $|\mu_W|^2 = 1$. Of course, since μ_{STF}^2, μ_s and μ_I are invariant under this kind of transformations, their values remain 1/2 and 1, respectively.

3.4 Maximum Visibility Under Unitary Transformations

Let us again consider the standard Young's interference experiment. It was shown in the previous section that the fringe visibility is given in terms of $|\mu_W|^2$, and its value can be controlled by using appropriate reversible optical devices at the pinholes, placed at points $\boldsymbol{r}_1$ and $\boldsymbol{r}_2$. We will next determine the maximum visibility we can get by using unitary transformations applied on such points. The main result is contained in the following proposition (Martínez-Herrero and Mejías, 2007a).

Proposition *Given a random electromagnetic beamlike field, characterized by its CDTs $\hat{W}_{ij}$, $i,j = 1,2$, the maximum fringe visibility, $|\mu_W|^2_{\max}$, one can obtain in a*

Young's scheme by applying local unitary transformations at the pinholes is given by

$$|\mu_W|^2_{\max} = \frac{(|\sigma_1| + |\sigma_2|)^2}{\mathrm{Tr}\hat{W}_{11}\mathrm{Tr}\hat{W}_{22}}, \tag{3.66}$$

where σ_i^2, $i = 1,2$, *denote the eigenvalues (both are nonnegative) of the matrix product* $\hat{W}_{12}\hat{W}_{12}^{\dagger}$, *and* $|\sigma_i|$, $i = 1,2$, *are the positive square roots of* σ_i^2.

Proof Let us consider a random light field, incident on a Young interferometer, whose CDT at the pinholes is $\hat{W}_{12}$. From the so-called singular-value decomposition of $\hat{W}_{12}$ (Brosseau, 1998), one can assure that there exist two unitary matrices, $\hat{U}$ and $\hat{V}$, such that

$$\hat{W}_{12} = \hat{U}^{\dagger}\hat{D}\hat{V}, \tag{3.67}$$

with

$$\hat{D} = \begin{pmatrix} |\sigma_1| & 0 \\ 0 & |\sigma_2| \end{pmatrix}, \tag{3.68}$$

were $|\sigma_1|$, $i = 1,2$, were defined above. Let us now introduce two unitary matrices $\hat{U}_i$, $i = 1,2$, representing reversible optical devices at $\boldsymbol{r}_1$ and $\boldsymbol{r}_2$. The CDT, $\hat{W}_{12}^{\mathrm{out}}$ at the output of such devices would read

$$\hat{W}_{ij}^{\mathrm{out}} = \hat{U}_i^{\dagger}\hat{W}_{ij}\hat{U}_j, i,j = 1,2, \tag{3.69}$$

and therefore

$$|\mu_W|^2 = \frac{\left|\mathrm{Tr}\hat{W}_{12}^{\mathrm{out}}\right|^2}{\mathrm{Tr}\hat{W}_{11}^{\mathrm{out}}\mathrm{Tr}\hat{W}_{22}^{\mathrm{out}}} = \frac{\left|\mathrm{Tr}\left(\hat{H}_1^{\dagger}\hat{D}\hat{H}_2\right)\right|^2}{\mathrm{Tr}\hat{W}_{11}\mathrm{Tr}\hat{W}_{22}}, \tag{3.70}$$

where

$$\hat{H}_1 = \hat{U}\hat{U}_1, \tag{3.71a}$$

$$\hat{H}_2 = \hat{V}\hat{U}_2. \tag{3.71b}$$

The numerator of Eq. (3.70) can also be written as follows

$$\mathrm{Tr}\left(\hat{H}_1^{\dagger}\hat{D}\hat{H}_2\right) = \mathrm{Tr}\left(\hat{H}_2\hat{H}_1^{\dagger}\hat{D}^{1/2}\,\hat{D}^{1/2}\right), \tag{3.72}$$

with

$$\hat{D}^{1/2} = \begin{pmatrix} \sqrt{|\sigma_1|} & 0 \\ 0 & \sqrt{|\sigma_2|} \end{pmatrix}. \tag{3.73}$$

But application of the Schwarz inequality gives

$$\left|\mathrm{Tr}\left(\hat{H}_2\hat{H}_1^{\dagger}\hat{D}^{1/2}\,\hat{D}^{1/2}\right)\right|^2 \leq \mathrm{Tr}\hat{D}\mathrm{Tr}\left(\hat{H}_2\hat{H}_1^{\dagger}\hat{D}^{1/2}\,\hat{D}^{1/2}\,\hat{H}_1\hat{H}_2^{\dagger}\right), \tag{3.74}$$

and the equality is reached when

$$\hat{H}_2\hat{H}_1^{\dagger}\hat{D}^{1/2} = \eta\hat{D}^{1/2}, \tag{3.75}$$

which implies

$$\left(\hat{H}_2\hat{H}_1^{\dagger} - \eta\hat{I}\right)\hat{D}^{1/2} = 0, \tag{3.76}$$

η being a complex number. We obtain that, when expression (3.74) transforms into an equality, $|\mu_W|^2$ becomes maximized, which is the result we are trying to get. Let us then assume that Det $\hat{D}^{1/2}$ differs from zero (the case Det $\hat{D}^{1/2} = 0$ will be analyzed below). Equation (3.75) would give

$$\hat{H}_2\hat{H}_1^{\dagger} = \eta\hat{I}. \tag{3.77}$$

Moreover, since $\hat{H}_i$, $i = 1,2$, are unitary matrices, we have from the above equation

$$\hat{H}_1^{\dagger} = \eta\hat{H}_2^{\dagger}, \tag{3.78a}$$

$$\hat{H}_2 = \eta\hat{H}_1, \tag{3.78b}$$

which implies $|\eta|^2 = 1$. Taking Eqs. (3.78) into account, we finally conclude that the maximum value of $|\mu_W|^2$ after local unitary transformations is given by the expression

$$|\mu_W|^2_{\max} = \frac{\left|\mathrm{Tr}\left(\hat{H}_1^{\dagger}\hat{D}\hat{H}_2\right)\right|^2}{\mathrm{Tr}\hat{W}_{11}\mathrm{Tr}\hat{W}_{22}} = \frac{\left(\mathrm{Tr}\hat{D}\right)}{\mathrm{Tr}\hat{W}_{11}\mathrm{Tr}\hat{W}_{22}} = \frac{(|\sigma_1| + |\sigma_2|)^2}{\mathrm{Tr}\hat{W}_{11}\mathrm{Tr}\hat{W}_{22}}, \tag{3.79}$$

in agreement with Eq. (3.66).

When Det $\hat{D}^{1/2} = 0$, one of the diagonal elements of matrix $\hat{D}^{1/2}$ vanishes. Accordingly, by using Eq. (3.76) and the fact that the product $\hat{H}_2\hat{H}_1^{\dagger}$ is a unitary matrix, we again obtain Eq. (3.66), and the proof is completed, Q.E.D.

Two direct consequences can be inferred from Eq. (3.79) (i.e., from the proposition):

i) We have seen that to reach the maximum attainable fringe visibility in a Young arrangement, we can choose reversible optical devices whose respective unitary matrices are

$$\hat{U}_1 = \hat{U}^{\dagger}, \tag{3.80a}$$

$$\hat{U}_2 = \hat{V}^{\dagger}, \tag{3.80b}$$

where $\hat{U}$ and $\hat{V}$ were introduced in Eq. (3.67). At the output of such elements $\hat{W}_{12}^{\text{out}} = \hat{D}$, and we conclude that this cross-spectral density tensor becomes a diagonal matrix.

ii) Let us now recall that, since σ_1^2 and σ_2^2 are the eigenvalues of $\hat{W}_{12}\hat{W}_{12}^{\dagger}$ we have

$$\text{Tr}\left(\hat{W}_{12}\hat{W}_{12}^{\dagger}\right) = \sigma_1^2 + \sigma_2^2, \tag{3.81a}$$

$$\text{Det}\left(\hat{W}_{12}\hat{W}_{12}^{\dagger}\right) = \sigma_1^2\sigma_2^2. \tag{3.81b}$$

Hence the quantity μ_{STF}^2 becomes (cf. Eq. (3.25))

$$\mu_{STF}^2 = \frac{\sigma_1^2 + \sigma_2^2}{\text{Tr}\hat{W}_{11}\text{Tr}\hat{W}_{22}}, \tag{3.82}$$

and $|\mu_{\text{W}}|_{\text{max}}^2$ finally reads

$$|\mu_{\text{W}}|_{\text{max}}^2 = \mu_{STF}^2 + \frac{\sqrt{4\text{Det}\hat{W}_{12}W_{12}^{\dagger}}}{\text{Tr}\hat{W}_{11}\text{Tr}\hat{W}_{22}}. \tag{3.83}$$

To analytically illustrate the above results, let us briefly consider two simple examples. In the first one, the CDTs representing the field at $\boldsymbol{r}_1$ and $\boldsymbol{r}_2$ are

$$\hat{W}_{11} = \hat{I}, \tag{3.84a}$$

$$\hat{W}_{12} = \begin{pmatrix} 1 & 1 \\ 1 & 0 \end{pmatrix}, \tag{3.84b}$$

$$\hat{W}_{22} = \begin{pmatrix} 2 & 1 \\ 1 & 1 \end{pmatrix}. \tag{3.84c}$$

In this case, one gets $\mu_{STF}^2 = 1/2$, $\mu_I = \mu_S = 1$, and $|\mu_{\text{W}}|^2 = 1/6$ without any optical device at the pinholes. The maximum attainable visibility (using reversible elements) is calculated from Eq. (3.83) and gives $|\mu_{\text{W}}|_{\text{max}}^2 = 5/6$.

In the second example, the matrices $\hat{W}_{ij}$, $i = 1,2$, are

$$\hat{W}_{11} = \hat{I}, \tag{3.85a}$$

$$\hat{W}_{12} = \begin{pmatrix} \frac{1}{\sqrt{2}} & 1 \\ 1 & \frac{1}{\sqrt{2}} \end{pmatrix}, \tag{3.85b}$$

$$\hat{W}_{22} = \begin{pmatrix} \frac{3}{2} & \sqrt{2} \\ \sqrt{2} & \frac{3}{2} \end{pmatrix}. \tag{3.85c}$$

We then obtain $\mu_{STF}^2 = 1/2$, $\mu_I = \mu_S = 1$, and $|\mu_W|^2 = 1/3$, but now $|\mu_W|^2_{\max} = 2/3$. We also see that the above fields show identical values for μ_{STF}^2,μ_S, and μ_I, but their attainable maximum visibility clearly differs.

It should be noticed that, although a light field at the output of a unitary-matrix optical device is modified, in general, with regard to its input value, the quantity $|\mu_W|^2_{\max}$ can, however, be understood as the intimate capability of such field to improve their fringe visibility in a suitably designed Young interference scheme.

This intrinsic characteristic is analytically provided by the scalar function g_{12}, defined for general partially coherent, partially polarized beamlike fields at two points, $\boldsymbol{r}_1$ and $\boldsymbol{r}_2$, in the form (Gori et al., 2007; Martínez-Herrero and Mejías, 2007a, 2008a, b)

$$g_{12} \equiv g\left(\boldsymbol{r}_1,\boldsymbol{r}_2\right) = \frac{\mathrm{Tr}\left(\hat{W}_{12}\hat{W}_{21}\right) + 2\left|\mathrm{Det}\hat{W}_{12}\right|}{\mathrm{Tr}\hat{W}_{11}\mathrm{Tr}\hat{W}_{22}}. \tag{3.86}$$

Its clear from its definition that function g_{12} equals $|\mu_W|^2_{\max}$ in a Young interferometric arrangement. However, we have used a different notation to remark that g_{12} is a function associated with the field itself, which allow to describing its behaviour and characteristics.

This function will again be considered in subsequent sections. Here we restrict ourselves to give a number of significant properties (Martínez-Herrero and Mejías, 2007a):

i) g_{12} remains invariant under local unitary transformations. This follows at once from its definition.

ii) $g_{12} = g_{21}$,

iii) $0 \le g_{12} \le 1$ (cf. Eq. (3.24)), (3.87)

iv) $g_{12} = \mu_{STF}^2 + \dfrac{1}{2}\,\mu_S\mu_I\sqrt{\left(1-P_1^2\right)\left(1-P_2^2\right)}$, (3.88)

where $P_i,i = 1,2$, denotes the respective degrees of polarization at $\boldsymbol{r}_1$ and $\boldsymbol{r}_2$. To show this property, let us recall that matrix $\hat{W}_{12}$ can be expressed in terms of $\hat{M}_{12}$ (see Eq. (3.27) as follows

$$\hat{W}_{12} = \hat{W}_{11}^{1/2}\hat{M}_{12}\hat{W}_{22}^{1/2}, \tag{3.89}$$

so that

$$\left|\mathrm{Det}\hat{W}_{12}\right| = \mathrm{Det}\hat{W}_{11}^{1/2}\mathrm{Det}\hat{W}_{22}^{1/2}\left|\mathrm{Det}\hat{M}_{12}\right|. \tag{3.90}$$

But the singular values of $\hat{M}_{12}$ are μ_S and μ_I, which satisfy

$$\left|\mathrm{Det}\hat{M}_{12}\right| = \mu_I \mu_S. \tag{3.91}$$

From the above equations and the definition of the degree of polarization we get

$$\begin{aligned}\left|\mathrm{Det}\hat{W}_{12}\right| &= \mu_I \mu_S \sqrt{\mathrm{Det}\hat{W}_{11}\mathrm{Det}\hat{W}_{22}} \\ &= \frac{1}{4}\mu_I \mu_S \mathrm{Tr}W_{11}\mathrm{Tr}W_{22}\sqrt{\left(1-P_1^2\right)\left(1-P_2^2\right)}.\end{aligned} \tag{3.92}$$

We then have

$$\frac{\sqrt{4\mathrm{Det}\hat{W}_{12}\hat{W}_{12}^{\dagger}}}{\mathrm{Tr}\hat{W}_{11}\mathrm{Tr}\hat{W}_{22}} = \frac{1}{2}\,\mu_I \mu_S \sqrt{\left(1-P_1^2\right)\left(1-P_2^2\right)}, \tag{3.93}$$

and Eq. (3.88) is finally obtained after the application of Eq. (3.83).

v) $\mu_{STF}^2 = 1$, at a region Ω, implies $g_{12} = 1$ for each pair of points of such region. Note, however, that the converse is not true.

To prove this, let us recall that the condition $\mu_{STF}^2 = 1$ implies that a deterministic row vector exists, $\boldsymbol{F}(\boldsymbol{r})$, such that (Setälä et al., 2004)

$$\hat{W}_{12} = \boldsymbol{F}_1^{\dagger}\boldsymbol{F}_2, \tag{3.94}$$

where $\boldsymbol{F}_i \equiv \boldsymbol{F}(r_i)$, $i = 1,2$. As a consequence, we get $P_1 = P_2 = 1$; $\mu_S = \mu_I = 1$, and (see Eq. (3.88)) $g_{12} = 1$.

Let us finally remark that Eq. (3.88) can also be considered as a simple analytical and physical link between all the four quantities $|\mu_W|^2_{\max}$, μ_{STF}^2, μ_I and μ_S. In this sense, note that the role of the degree of polarization reveals to be essential. This point will be further discussed in subsequent sections.

3.5 Position-Independent Stochastic Behavior of Random Electromagnetic Fields

In Sect. 3.2 it was mentioned that, for scalar fields, complete coherence at a certain region Ω means that

$$E(\boldsymbol{r}) = \alpha g(\boldsymbol{r}), \boldsymbol{r} \in \Omega \tag{3.95}$$

where $E(\boldsymbol{r})$ represents the stochastic process associated to the field, α is a position-independent random variable, and $g(\boldsymbol{r})$ is a deterministic function. It was concluded

that, in the scalar case, complete coherence is equivalent to a position-independent stochastic behavior throughout Ω. We will next investigate the generalization of this property to vectorial fields and discuss the consequences involved.

Let us then introduce a particular kind of fields whose associated electric-field vector is written in the form (Martínez-Herrero and Mejías, 2008a, b)

$$\boldsymbol{E}(\boldsymbol{r}) = \boldsymbol{E}_0 f(\boldsymbol{r})\, \hat{U}(\boldsymbol{r}), \tag{3.96}$$

where the equality should be understood in the mean-square sense. In this equation, $\boldsymbol{E}_0 = (\alpha, \beta)$ is a row vector whose components take random values over the stochastic ensemble, $f(\boldsymbol{r})$ is a deterministic function, and $\hat{U}(\boldsymbol{r})$ is a 2×2 deterministic unitary matrix. It should be noted that the randomness of the field $\boldsymbol{E}$ is only contained in $\boldsymbol{E}_0$, which does not depend on the location.

For convenience, we now write $\hat{A} = f\hat{U}$, so that

$$\hat{A}(\boldsymbol{r})\, \hat{A}^{\dagger}(\boldsymbol{r}) = \hat{A}^{\dagger}(\boldsymbol{r})\, \hat{A}(\boldsymbol{r}) = |f(\boldsymbol{r})|^2\, \hat{I}. \tag{3.97}$$

It then follows that the CDT for this class of fields can be written in the form

$$\hat{W}(\boldsymbol{r}_1,\boldsymbol{r}_2) = \hat{A}^{\dagger}(\boldsymbol{r}_1)\, \hat{\phi}\, \hat{A}(\boldsymbol{r}_2), \tag{3.98}$$

where

$$\hat{\phi} = \overline{\boldsymbol{E}_0^{\dagger}\, \boldsymbol{E}_0} = \begin{pmatrix} \overline{|\alpha|^2} & \overline{\alpha^*\beta} \\ \overline{\alpha\beta^*} & \overline{|\beta|^2} \end{pmatrix}. \tag{3.99}$$

Equation (3.98) provides the coherence and polarization structure of the beams given by Eq. (3.96). A way to implement such fields would start, for example, by considering a beam whose electric field vector takes the form $\boldsymbol{E}(\boldsymbol{r}) = \boldsymbol{E}_0\, f(\boldsymbol{r})$, where, as before, $\boldsymbol{E}_0 = (\alpha,\beta)$ represents a stochastic vector, and $f(\boldsymbol{r})$ denotes, for instance, a Gaussian amplitude. The next step would be to propagate this field through a position-dependent anisotropic nonabsorbing optical element characterized by a unitary matrix $\hat{U}$. This element should be reversible because, otherwise, matrix $\hat{U}$ would not be unitary. The final output beam would belong to the type of fields defined by Eq. (3.96). Another simple example are the fields whose CDT is factorizable, i.e., $\hat{W}(\boldsymbol{r}_1,\boldsymbol{r}_2) = \boldsymbol{F}^{\dagger}(\boldsymbol{r}_1)\boldsymbol{F}(\boldsymbol{r}_2)$, $\boldsymbol{F}$ being a row vector.

Let us now devote the remainder of the present section to report a number of interesting properties exhibited by the beams we are considering (Martínez-Herrero and Mejías, 2008a).

Property 1: The character of the field, expressed by Eq. (3.96), is not changed after the application of any local unitary transformation. In the same way, the field can be yet expressed in the form given by Eq. (3.96) after any local rotation of the coordinate axes (as occurs in a change to curvilinear coordinates).

Property 2: It can be shown that the intrinsic degrees of coherence, μ_S, μ_I, of this class of fields are equal to 1, but the converse is not true.

Property3: The (local) degree of polarization, $P(\boldsymbol{r})$, for this class of fields reads

$$P^2(\boldsymbol{r}) = 1 - \frac{4\,\mathrm{Det}\hat{\phi}}{(\mathrm{Tr}\hat{\phi})^2}, \tag{3.100}$$

where matrix $\hat{\phi}$ was defined above. Since the elements of $\hat{\phi}$ are position-independent, we conclude that, for these fields, P is constant throughout the region in which Eq. (3.98) applies. It should be noted that the converse property is not true.

Property 4: For the kind of fields we are analyzing, it can be shown that $\mu^2_{STF} = \frac{1+P^2}{2}$. Recall that any field with $\mu^2_{STF} = 1$ fulfils Eq. (3.98). In other words, any factorizable cross-spectral density tensor can be written in the form given by expression (3.98), with $\mathrm{Det}\hat{\phi} = 0$.

Property 5: It is well known that, for a general field, $\hat{W}(\boldsymbol{r},\boldsymbol{r})$ can be written in the form $\hat{W}(\boldsymbol{r},\boldsymbol{r}) = \hat{W}_{TP}(\boldsymbol{r},\boldsymbol{r}) + \hat{W}_{NP}(\boldsymbol{r},\boldsymbol{r})$, where $\hat{W}_{TP}(\boldsymbol{r},\boldsymbol{r})$ and $\hat{W}_{NP}(\boldsymbol{r},\boldsymbol{r})$ refer to a totally polarized field and to an unpolarized field, respectively. This important property can be generalized for the cross-spectral density matrix $\hat{W}(\boldsymbol{r}_1,\boldsymbol{r}_2)$ of the fields considered here.

To see this, note first that, since $\hat{\phi}$ is a Hermitian nonnegative definite matrix, we have (Martínez-Herrero and Mejías, 2008a).

$$\hat{\phi} = \begin{pmatrix} \phi_{11} & \phi_{12} \\ \phi_{12}^* & \phi_{22} \end{pmatrix} = \hat{\phi}_{TP} + \hat{\phi}_{NP}, \tag{3.101}$$

where $\hat{\phi}_{TP} = \begin{pmatrix} a_{11} & a_{12} \\ a_{12}^* & a_{22} \end{pmatrix}$; $\hat{\phi}_{NP} = q\hat{I}$, with $\mathrm{Det}\hat{\phi}_{TP} = 0$, and

$$a_{11} = \frac{1}{2}(\phi_{11} - \phi_{22}) + \frac{1}{2}\sqrt{(\mathrm{Tr}\hat{\phi})^2 - 4\,\mathrm{Det}\hat{\phi}}, \tag{3.102a}$$

$$a_{12} = \phi_{12}, \tag{3.102b}$$

$$a_{22} = \frac{1}{2}(\phi_{22} - \phi_{11}) + \frac{1}{2}\sqrt{(\mathrm{Tr}\hat{\phi})^2 - 4\,\mathrm{Det}\hat{\phi}}, \tag{3.102c}$$

$$q = \frac{1}{2}(\phi_{22} + \phi_{11}) - \frac{1}{2}\sqrt{(\mathrm{Tr}\hat{\phi})^2 - 4\,\mathrm{Det}\hat{\phi}}. \tag{3.102d}$$

Taking Eqs. (3.102) into account, the CDT of the fields characterized by Eq. (3.98) reads

$$\hat{W}(\boldsymbol{r}_1,\boldsymbol{r}_2) = \hat{A}^\dagger(\boldsymbol{r}_1)\,\hat{\phi}_{TP}\,\hat{A}(\boldsymbol{r}_2) + \hat{A}^\dagger(\boldsymbol{r}_1)\,\hat{\phi}_{NP}\,\hat{A}(\boldsymbol{r}_2). \tag{3.103}$$

The first term of the right-hand side of Eq. (3.103) represents the CDT of a totally polarized field, whereas the second term corresponds to an unpolarized field. It is important to remark that expansion (3.103) is no longer valid for a general field.

Property 6: Let us assume we perform the local unitary transformations $\hat{U}^\dagger(\boldsymbol{r}_1)$ and $\hat{U}^\dagger(\boldsymbol{r}_2)$ at two points $\boldsymbol{r}_1$ and $\boldsymbol{r}_2$, respectively, where $\hat{U}^\dagger$ refers here to the matrix

that defines the field we are considering (see Eq. (3.96)). Since $\hat{U}^{\dagger}\hat{U} = \hat{I}$, the light field, after the transformations, becomes $\boldsymbol{E}^{\text{out}}(\boldsymbol{r}_{\text{i}}) = f(\boldsymbol{r}_{\text{i}})\boldsymbol{E}_0$, i = 1, 2. Accordingly, the resulting field, $\boldsymbol{E}_{\text{Y}}(\boldsymbol{R})$, at the observation plane of a Young's interferometer (the pinholes placed at $\boldsymbol{r}_1$ and $\boldsymbol{r}_2$) would read

$$\boldsymbol{E}_Y(\boldsymbol{R}) = \boldsymbol{E}^{\text{out}}(\boldsymbol{r}_1) + \boldsymbol{E}^{\text{out}}(\boldsymbol{r}_2)\,\exp(\text{i}\delta)\,. \tag{3.104}$$

where $\boldsymbol{R}$ gives the position of the superposition point, and δ is the path difference between the interfering waves. It is simple to see that the fringe visibility $\mathcal{V}$ around $\boldsymbol{R}$ becomes

$$\mathcal{V} = \frac{I_{\max} - I_{\min}}{I_{\max} + I_{\min}} = \frac{2\,|f(\boldsymbol{r}_1)|\,|f(\boldsymbol{r}_2)|}{|f(\boldsymbol{r}_1)|^2 + |f(\boldsymbol{r}_2)|^2}. \tag{3.105}$$

From this expression, it is clear that we would get the same visibility as that obtained for scalar coherent fields with powers $|f(\boldsymbol{r}_1)|^2$ and $|f(\boldsymbol{r}_2)|^2$. In the particular case $|f(\boldsymbol{r}_1)| = |f(\boldsymbol{r}_2)|$, the fringe visibility equals 1.

Let us now consider the scalar function g_{12}, defined in the previous section for general partially-coherent partially-polarized beams. For the special type of fields introduced here, we will next show that the following proposition applies (Martínez-Herrero and Mejías, 2008b):

Proposition *Function g_{12} equals 1 for any pair of points of a certain region Ω* if and only if *the field belongs to the class of fields described by Eqs. (3.96) and (3.98) over Ω.*

Proof Let us assume that, for a certain random electromagnetic field,

$$g_{12} = 1, \text{ for any pair of points } \boldsymbol{r}_1, \boldsymbol{r}_2 \in \Omega. \tag{3.106}$$

This implies that there exist two unitary matrices, $\hat{U}_1$ and $\hat{U}_2$, such that

$$|\mu_W|^2 = \frac{\left|\text{Tr}\hat{W}_{12}^{\text{out}}\right|^2}{\text{Tr}\hat{W}_{11}^{\text{out}}\text{Tr}\hat{W}_{22}^{\text{out}}} = 1 \tag{3.107}$$

where

$$\hat{W}_{ij}^{\text{out}} = \hat{U}_i^{\dagger}\hat{W}_{ij}\hat{U}_j,\ i,j = 1, 2. \tag{3.108}$$

As we know, matrices $\hat{U}_1$ and $\hat{U}_2$ could be understood as representing the action of reversible optical devices at two pinholes in a Young arrangement. In Eq. (3.108), $\hat{W}_{ij}$ would then refer to the CDT evaluated at the pinholes, and the superscript out would indicate the CDT associated to the field after passing through the unitary-matrix elements. It follows from Eq. (3.107) that

$$\left|\text{Tr}\hat{W}_{12}^{\text{out}}\right|^2 = \left|\text{Tr}\overline{\boldsymbol{E}_1^{\text{out}\dagger}\boldsymbol{E}_2^{\text{out}}}\right|^2 = \overline{\left|\boldsymbol{E}_1^{\text{out}}\right|^2}\,\overline{\left|\boldsymbol{E}_2^{\text{out}}\right|^2}, \text{ for any } \boldsymbol{r}_1, \boldsymbol{r}_2 \in \Omega \tag{3.109}$$

where

$$\boldsymbol{E}_i^{\text{out}} = \boldsymbol{E}_i \hat{U}_i, \text{i} = 1,2, \tag{3.110}$$

and $\boldsymbol{E}_{\text{i}}$, i = 1, 2, are row vectors at the pinholes (prior to the passage through the optical devices). But Eq. (3.109) implies that $\boldsymbol{E}_1^{\text{out}}$ and $\boldsymbol{E}_2^{\text{out}}$ are proportional (in the mean square sense). Accordingly, we have

$$\boldsymbol{E}^{\text{out}}(\boldsymbol{r}_1) = \rho(\boldsymbol{r}_1,\boldsymbol{r}_2)\boldsymbol{E}^{\text{out}}(\boldsymbol{r}_2), \boldsymbol{r}_1,\boldsymbol{r}_2 \in \Omega, \tag{3.111}$$

where ρ is a scalar function. Applying this equation to three points in the region Ω, we get

$$\rho_{12} \equiv \rho(\boldsymbol{r}_1,\boldsymbol{r}_2) = \rho(\boldsymbol{r}_1,\boldsymbol{r}_3)\rho(\boldsymbol{r}_3,\boldsymbol{r}_2) \equiv \rho_{13}\rho_{32}, \tag{3.112}$$

and setting $\boldsymbol{r}_1 = \boldsymbol{r}_2$ one obtains

$$\rho_{12} = 1 = \rho_{13}\rho_{31}, \tag{3.113}$$

which implies

$$\rho_{ab} = \rho_{ba}^{-1}. \tag{3.114}$$

Equation (3.112) can then be written in the form

$$\rho_{12} = \frac{\rho_{13}}{\rho_{23}}. \tag{3.115}$$

But the left-hand side of this equation does not depend on $\boldsymbol{r}_3$, and therefore the $\boldsymbol{r}_3$-dependence of the ratio $\frac{\rho_{13}}{\rho_{23}}$ must cancel. We then write

$$\rho_{12} = \frac{g(\boldsymbol{r}_1)}{f(\boldsymbol{r}_2)}, \tag{3.116}$$

where f and g denote deterministic functions. After substituting Eq. (3.116) into Eq. (3.115), we get

$$\rho_{12} = \frac{g(\boldsymbol{r}_1)}{f(\boldsymbol{r}_2)} = \rho_{21}^{-1} = \frac{f(\boldsymbol{r}_1)}{g(\boldsymbol{r}_2)}, \boldsymbol{r}_1,\boldsymbol{r}_2 \in \Omega, \tag{3.117}$$

which implies $f = g$ in Ω. Therefore,

$$\boldsymbol{E}^{\text{out}}(\boldsymbol{r}_1) = \frac{f(\boldsymbol{r}_1)}{f(\boldsymbol{r}_2)}\boldsymbol{E}^{\text{out}}(\boldsymbol{r}_2) \Rightarrow \frac{\boldsymbol{E}^{\text{out}}(\boldsymbol{r}_1)}{f(\boldsymbol{r}_1)} = \frac{\boldsymbol{E}^{\text{out}}(\boldsymbol{r}_2)}{f(\boldsymbol{r}_2)} = \ldots = \boldsymbol{E}_0, \qquad \boldsymbol{r}_1,\boldsymbol{r}_2 \in \Omega \tag{3.118}$$

where $\boldsymbol{E}_0$ is a random vector, and we finally obtain

$$\boldsymbol{E}^{\text{out}}(\boldsymbol{r}) = f(\boldsymbol{r})\boldsymbol{E}_0 \text{ (in the mean square sense), for any } \boldsymbol{r} \in \Omega, \tag{3.119}$$

Consequently, the CDT associated to $\boldsymbol{E}^{out}$ reads

$$\hat{W}^{\text{out}}(\boldsymbol{r}_1,\boldsymbol{r}_2) = f^*(\boldsymbol{r}_1)f(\boldsymbol{r}_2)\hat{\phi}, \tag{3.120}$$

so that matrix $\hat{W}$ becomes

$$\hat{W}(\boldsymbol{r}_1,\boldsymbol{r}_2) = f^*(\boldsymbol{r}_1)f(\boldsymbol{r}_2)\hat{U}_1\ \hat{\phi}\ \hat{U}_2^{\dagger}. \tag{3.121}$$

Comparing this expression with Eq. (3.98), we conclude that the stochastic process $\boldsymbol{E}(\boldsymbol{r})$ associated to a beam satisfying Eq. (3.106) corresponds to the kind of fields defined by Eq. (3.96). The first part of the proof is thus demonstrated.

The converse property is simple to show: Since the CDT of any field given by Eq. (3.96) takes the form (3.98), substitution of this expression into Eq. (3.86) gives $g_{12} = 1$, and the proof is completed, Q.E.D.

From this general property, we also conclude that the possibility of optimizing the fringe visibility in a Young's interference arrangement is intimately connected with a position-independent stochastic behavior of the field. Thus, the beams defined by Eqs. (3.96) and (3.98) are the only fields that attain optimized visibility by using reversible unitary optical devices at the pinholes. Accordingly, the value $g_{12} = 1$ fully characterizes this kind of fields.

Corollary *For the class of fields defined by Eq. (3.96), the local degree of polarization, P_S, is uniform (i.e., position-independent) across the superposition region Ω_S in a Young interference arrangement* (Martínez-Herrero and Mejías, 2008b). This applies once the fringe visibility has been optimized.

To show this property note first that, in terms of the CDT, the value of P_S at the superposition region reads

$$P_s^2(\boldsymbol{R}) = 1 - \frac{4\text{Det}\hat{W}_s(\boldsymbol{R},\boldsymbol{R})}{\left[\text{Tr}\hat{W}_s(\boldsymbol{R},\boldsymbol{R})\right]^2} \tag{3.122}$$

where $\boldsymbol{R}$ is the position vector of a point inside Ω_S, and $\hat{W}_s(\boldsymbol{R},\boldsymbol{R})$ denotes the CDT at $\boldsymbol{R}$. We then have

$$\hat{W}_s(\boldsymbol{R},\boldsymbol{R}) = \hat{W}^{out}(\boldsymbol{r}_1,\boldsymbol{r}_1) + \hat{W}^{out}(\boldsymbol{r}_2,\boldsymbol{r}_2) + \hat{W}^{out}(\boldsymbol{r}_1,\boldsymbol{r}_2)\exp(i\delta) + \hat{W}^{out}(\boldsymbol{r}_2,\boldsymbol{r}_1)\exp(-i\delta), \tag{3.123}$$

where, as usual, $\boldsymbol{r}_1$ and $\boldsymbol{r}_2$ are the position vectors of the pinholes, $\hat{W}^{out}$ is given by Eq. (3.120) (after passing through appropriate reversible devices) and $\delta = k(|\boldsymbol{R}-\boldsymbol{r}_2| - |\boldsymbol{R}-\boldsymbol{r}_1|)$ is the path difference in free space. For the sake of simplicity, in Eq. (3.123) we have omitted the factors $1/|\boldsymbol{R}-\boldsymbol{r}_1| \approx 1/|\boldsymbol{R}-\boldsymbol{r}_2| \approx 1/D$, where D is the distance between the plane of the pinholes and the observation plane.

Taking Eq. (3.120) into account, $\hat{W}_S(\boldsymbol{R},\boldsymbol{R})$ reads

$$\hat{W}_S(\boldsymbol{R},\boldsymbol{R}) = |f(\boldsymbol{r}_1) + f(\boldsymbol{r}_2)\exp(i\delta)|^2\,\hat{\phi}, \tag{3.124}$$

and, finally,

$$P_s^2(\boldsymbol{R}) = 1 - \frac{4Det\hat{\phi}}{(Tr\hat{\phi})^2}, \tag{3.125}$$

which is independent of $\boldsymbol{R}$, and the corollary is demonstrated, Q.E.D.

As a complementary conclusion, note that the value of P_S^2 given by Eq. (3.125) is just the same to that of the degree of polarization of the incident field at the pinholes (see property 3). It should be mentioned in this connection that, in general, the polarization of the field changes upon propagation (James, 1994). The invariance of the polarization when light propagates is a topic that is currently being investigated (Du and Zhao, 2008; Gori, 2008; Gori et al., 2009; Martínez-Herrero and Mejías, 2007c; Santarsiero, 2007; Wolf, 2007a; Zhao and Wolf, 2008) and deserves further study in the future.

3.6 Mean-Square Coherent Light: Maximum Young's Fringe Visibility Through Reversible Devices

It was recently introduced in the literature (Réfrégier, 2008b) the so-called mean-square coherent (MSC) field, defined as light that is able to interfere with Young's fringes of unit visibility, when its electromagnetic field propagates through appropriate nonsingular deterministic Jones matrices. In other words, the original state of these fields could be suitably modified at the pinholes by means of certain optical devices in order to maximize the visibility.

In this section, we are interested on this kind of light passing through reversible optical elements (implemented by means of anisotropic nonabsorbing devices), which are represented by unitary matrices. More specifically, we are interested on the following problem: Given the values P_1 and P_2, arbitrary but fixed, of the degree of polarization of the field at the pinholes in a Young interferometer, we will try to find the maximum attainable visibility under unitary transformations when the illuminating beam is mean-square coherent light.

Let us then consider a MSC field in a spatial domain Ω, impinging on a Young interference arrangement where the two pinholes are placed at points $\boldsymbol{r}_1$ and $\boldsymbol{r}_2$ inside Ω. Since light is mean-square coherent, it is known that the intrinsic degrees of coherence (μ_S,μ_I) of the field $\boldsymbol{E}(\boldsymbol{r}_1)$ and $\boldsymbol{E}(\boldsymbol{r}_2)$ at the pinholes are equal to one. Taking this into account, it follows at once that, for MSC fields, the parameter g_{12} (see Eq. (3.86) becomes

$$g_{12} = \mu_{STF}^2 + \frac{1}{2}\sqrt{(1-P_1^2)(1-P_2^2)}, \tag{3.126}$$

where P_1 and P_2 denote the values of the degree of polarization at the pinholes. As we showed in the previous section, the maximum value $g_{12} = 1$ is reached by the set of electromagnetic fields whose random character is position-independent. Note, in this sense, that this type of fields for which $g_{12} = 1$ constitutes a subclass of mean-square coherent light.

Taking in mind the meaning of g_{12}, one sees that obtaining maximum visibility at the superposition plane (under unitary transformations at the pinholes) is equivalent to determine the highest value of g_{12} for MSC fields with degrees of polarization $P(\boldsymbol{r}_1) = P_1$ and $P(\boldsymbol{r}_2) = P_2$. But (see Eq. (3.126)) this problem reduces to maximize μ^2_{STF} for MSC light with fixed degrees of polarization at two points. After some calculations (see below), it can finally be shown that (Martínez-Herrero and Mejías, 2009)

$$\left[g(\boldsymbol{r}_1,\boldsymbol{r}_2)\right]_{\max} = \frac{1}{2}\left[1 + P(\boldsymbol{r}_1)P(\boldsymbol{r}_2) + \sqrt{(1 - P^2(\boldsymbol{r}_1))(1 - P^2(\boldsymbol{r}_2))}\right] \tag{3.127}$$

In particular, $\left[g(\boldsymbol{r}_1,\boldsymbol{r}_2)\right]_{\max}$ equals one (optimization) when $P(\boldsymbol{r}_1) = P(\boldsymbol{r}_2)$, as expected. This happens, as we pointed out before, for the electromagnetic fields with position-independent stochastic behavior (Martínez-Herrero and Mejías, 2008a, b).

Proof of Eq. (3.127) For a general MSC field in a domain Ω, it has recently been shown (Réfrégier, 2008b) that its CDT can be written in the form

$$\hat{W}(\boldsymbol{r}_1,\boldsymbol{r}_2) = \lambda_1 \boldsymbol{\Psi}_1^{\dagger}(\boldsymbol{r}_1)\boldsymbol{\Psi}_1(\boldsymbol{r}_2) + \lambda_2 \boldsymbol{\Psi}_2^{\dagger}(\boldsymbol{r}_1)\boldsymbol{\Psi}_2(\boldsymbol{r}_2), \tag{3.128}$$

with $\lambda_1,\lambda_2 > 0$ and where $\boldsymbol{\Psi}_1(\boldsymbol{r})$ and $\boldsymbol{\Psi}_2(\boldsymbol{r})$ are nonproportional, nonzero, deterministic row vectors. Moreover, it is not difficult to show that this CDT can also be expressed in the alternative factorizable form

$$\hat{W}(\boldsymbol{r}_1,\boldsymbol{r}_2) = \hat{H}^{\dagger}(\boldsymbol{r}_1)\hat{H}(\boldsymbol{r}_2), \tag{3.129}$$

where $\hat{H}$ is a 2×2 matrix, namely,

$$\hat{H}(\boldsymbol{r}) = \begin{pmatrix} \sqrt{\lambda_1}\Psi_{11}(\boldsymbol{r}) & \sqrt{\lambda_1}\Psi_{12}(\boldsymbol{r}) \\ \sqrt{\lambda_2}\Psi_{21}(\boldsymbol{r}) & \sqrt{\lambda_2}\Psi_{22}(\boldsymbol{r}) \end{pmatrix}, \tag{3.130}$$

with $\mathrm{Det}\,\hat{H} \neq 0$, and $\boldsymbol{\Psi}_i = (\Psi_{i1},\Psi_{i2})$, $i = 1,2$. Taking into account the singular value decomposition of matrix $\hat{H}$ we can write

$$\hat{H}(\boldsymbol{r}) = \hat{V}^{\dagger}(\boldsymbol{r})\hat{D}(\boldsymbol{r})\hat{U}(\boldsymbol{r}). \tag{3.131}$$

where $\hat{U}$ and $\hat{V}$ are unitary matrices, and

$$\hat{D}(\boldsymbol{r}) = \begin{pmatrix} \alpha(\boldsymbol{r}) & 0 \\ 0 & \beta(\boldsymbol{r}) \end{pmatrix}, \tag{3.132}$$

$\alpha(\boldsymbol{r}) > \beta(\boldsymbol{r})$ taking nonnegative values. Furthermore, in terms of the diagonal elements, the degree of polarization of the MSC field at each point $\boldsymbol{r}$ is given by

$$P(\boldsymbol{r}) = \frac{\alpha^2(\boldsymbol{r}) - \beta^2(\boldsymbol{r})}{\alpha^2(\boldsymbol{r}) + \beta^2(\boldsymbol{r})}. \tag{3.133}$$

By using Eq. (3.131), the CDT becomes

$$\hat{W}(\boldsymbol{r}_1,\boldsymbol{r}_2) = \hat{U}^\dagger(\boldsymbol{r}_1)\hat{D}(\boldsymbol{r}_1)\hat{V}(\boldsymbol{r}_1)\hat{V}^\dagger(\boldsymbol{r}_2)\hat{D}^\dagger(\boldsymbol{r}_2)\hat{U}(\boldsymbol{r}_2). \tag{3.134}$$

Then

$$\mathrm{Tr}\left[\hat{W}(\boldsymbol{r}_1,\boldsymbol{r}_2)\hat{W}^\dagger(\boldsymbol{r}_1,\boldsymbol{r}_2)\right] = \mathrm{Tr}\left[\hat{D}^2(\boldsymbol{r}_1)\hat{S}(\boldsymbol{r}_1,\boldsymbol{r}_2)\hat{D}^2(\boldsymbol{r}_2)\hat{S}^\dagger(\boldsymbol{r}_1,\boldsymbol{r}_2)\right], \tag{3.135}$$

where

$$\hat{S}(\boldsymbol{r}_1,\boldsymbol{r}_2) = \hat{V}(\boldsymbol{r}_1)\hat{V}^\dagger(\boldsymbol{r}_2), \tag{3.136}$$

which implies that $\hat{S}$ is unitary. Taking this into account, after some algebra we obtain

$$\begin{aligned} &\mathrm{Tr}\left[\hat{W}(\boldsymbol{r}_1,\boldsymbol{r}_2)\hat{W}^\dagger(\boldsymbol{r}_1,\boldsymbol{r}_2)\right] = \\ &= \cos^2\theta\left[\alpha^2(\boldsymbol{r}_1)\alpha^2(\boldsymbol{r}_2) + \beta^2(\boldsymbol{r}_1)\beta^2(\boldsymbol{r}_2)\right] + \sin^2\theta\left[\alpha^2(\boldsymbol{r}_1)\beta^2(\boldsymbol{r}_2) + \beta^2(\boldsymbol{r}_1)\alpha^2(\boldsymbol{r}_2)\right], \end{aligned} \tag{3.137}$$

with $\theta(\boldsymbol{r}_1,\boldsymbol{r}_2)$ defined through the relations

$$|S_{11}| = \cos\theta(\boldsymbol{r}_1,\boldsymbol{r}_2) = |S_{22}|\,, \tag{3.138a}$$

$$|S_{12}| = \sin\theta(\boldsymbol{r}_1,\boldsymbol{r}_2) = |S_{21}|\,, \tag{3.138b}$$

where S_{ij}, $i,j = 1,2$, denotes the elements of matrix $\hat{S}(\boldsymbol{r}_1,\boldsymbol{r}_2)$. Application of Eq. (3.133) allows to write

$$1 + P(\boldsymbol{r}_1)P(\boldsymbol{r}_2) = \frac{2\alpha^2(\boldsymbol{r}_1)\alpha^2(\boldsymbol{r}_2) + 2\beta^2(\boldsymbol{r}_1)\beta^2(\boldsymbol{r}_2)}{\mathrm{Tr}\hat{W}(\boldsymbol{r}_1,\boldsymbol{r}_1)\mathrm{Tr}\hat{W}(\boldsymbol{r}_2,\boldsymbol{r}_2)}, \tag{3.139}$$

and

$$1 - P(\boldsymbol{r}_1)P(\boldsymbol{r}_2) = \frac{2\alpha^2(\boldsymbol{r}_1)\beta^2(\boldsymbol{r}_2) + 2\beta^2(\boldsymbol{r}_1)\alpha^2(\boldsymbol{r}_2)}{\mathrm{Tr}\hat{W}(\boldsymbol{r}_1,\boldsymbol{r}_1)\mathrm{Tr}\hat{W}(\boldsymbol{r}_2,\boldsymbol{r}_2)}. \tag{3.140}$$

By using Eqs. (3.137), (3.139) and (3.140), we get

$$\mu^2_{STF} = \frac{\mathrm{Tr}(\hat{W}_{12}\hat{W}^{\dagger}_{12})}{\mathrm{Tr}(\hat{W}_{11})\mathrm{Tr}(\hat{W}_{22})} = \frac{1}{2}\left[1 + P(\boldsymbol{r}_1)P(\boldsymbol{r}_2)\cos 2\theta(\boldsymbol{r}_1,\boldsymbol{r}_2)\right], \tag{3.141}$$

so that

$$g(\boldsymbol{r}_1,\boldsymbol{r}_2) = \frac{1}{2}\left[1 + P(\boldsymbol{r}_1)P(\boldsymbol{r}_2)\cos 2\theta(\boldsymbol{r}_1,\boldsymbol{r}_2) + \sqrt{(1 - P^2(\boldsymbol{r}_1))(1 - P^2(\boldsymbol{r}_2))}\right]. \tag{3.142}$$

Equation (3.141) provides an analytical expression of μ^2_{STF} for a general MSC light. Moreover, Eq. (3.142) gives the value $|\mu_W|^2_{\max}$ for this type of fields. Accordingly, the maximal value of g_{12} one can attain in a Young interferometer (when the illuminating field is MSC light passing through reversible optical elements at the pinholes) is given by the expression

$$\left[g(\boldsymbol{r}_1,\boldsymbol{r}_2)\right]_{\max} = \frac{1}{2}\left[1 + P(\boldsymbol{r}_1)P(\boldsymbol{r}_2) + \sqrt{(1 - P^2(\boldsymbol{r}_1))(1 - P^2(\boldsymbol{r}_2))}\right], \tag{3.143}$$

and Eq. (3.127) is shown, Q.E.D.

It should also be noted that, in Eq. (3.142), function $\cos 2\theta(\boldsymbol{r}_1,\boldsymbol{r}_2)$ does not depend on the local degree of polarization.

To complete the description of the particular set of MSC fields we are considering, let us now derive a general expression for their CDT. Note first that $\left[g_{12}\right]_{\max}$ is attained when $\theta = 0$. Accordingly, $\hat{S}$ becomes a diagonal matrix:

$$\hat{S}(\boldsymbol{r}_1,\boldsymbol{r}_2) = \hat{V}(\boldsymbol{r}_1)\hat{V}^{\dagger}(\boldsymbol{r}_2) = \begin{pmatrix} \exp i\left[\varphi(\boldsymbol{r}_2) - \varphi(\boldsymbol{r}_1)\right] & 0 \\ 0 & \exp i\left[\phi(\boldsymbol{r}_2) - \phi(\boldsymbol{r}_1)\right] \end{pmatrix}. \tag{3.144}$$

Consequently, the unitary matrix $\hat{V}$ can be expressed as follows

$$\hat{V}(\boldsymbol{r}) = \hat{M}(\boldsymbol{r})\hat{Q}, \tag{3.145}$$

where $\hat{M}(\boldsymbol{r})$ represents a diagonal matrix whose nonzero elements are complex exponentials, and $\hat{Q}$ denotes a position-independent unitary matrix. Thus, the general (factorizable) form of the CDT of the MSC fields that maximizes g_{12} reads (see Eq. (3.134))

$$\hat{W}(\boldsymbol{r}_1,\boldsymbol{r}_2) = \hat{U}^{\dagger}(\boldsymbol{r}_1)\hat{D}_0(\boldsymbol{r}_1)\hat{D}^{\dagger}_0(\boldsymbol{r}_2)\hat{U}(\boldsymbol{r}_2), \tag{3.146}$$

where

$$\hat{D}_0(\boldsymbol{r}) = \begin{pmatrix} \alpha(\boldsymbol{r})\exp i\varphi(\boldsymbol{r}) & 0 \\ 0 & \beta(\boldsymbol{r})\exp i\phi(\boldsymbol{r}) \end{pmatrix}. \tag{3.147}$$

An interesting consequence of Eq. (3.146) refers to the field vector $\boldsymbol{E}(\boldsymbol{r})$ associated with this kind of MSC light. We have (in the mean-square sense)

$$\boldsymbol{E}(\boldsymbol{r}) = \boldsymbol{E}_0 \hat{D}_0^{\dagger}(\boldsymbol{r})\hat{U}(\boldsymbol{r}), \tag{3.148}$$

where $\boldsymbol{E}_0 = (u,v)$ is a 1×2 vector whose components take complex random values fulfilling $< |u|^2 >=< |v|^2 >$ and $< u^* v >= 0$. From Eq. (3.148), it follows that $\boldsymbol{E}(\boldsymbol{r})$ can be written in the form

$$\boldsymbol{E}(\boldsymbol{r}) = \varepsilon_1 \tilde{\boldsymbol{\Psi}}_1(\boldsymbol{r}) + \varepsilon_2 \tilde{\boldsymbol{\Psi}}_2(\boldsymbol{r}), \tag{3.149}$$

where ε_i, $i = 1, 2$, are also complex random variables satisfying $< \varepsilon_1^* \varepsilon_2 >= 0$, and

$$\tilde{\boldsymbol{\Psi}}_1(\boldsymbol{r}) \propto \alpha(\boldsymbol{r})\exp i\varphi(\boldsymbol{r})\,(U_{11}(\boldsymbol{r}),U_{12}(\boldsymbol{r}))\,, \tag{3.150a}$$

$$\tilde{\boldsymbol{\Psi}}_2(\boldsymbol{r}) \propto \beta(\boldsymbol{r})\exp i\phi(\boldsymbol{r})\,(U_{21}(\boldsymbol{r}),U_{22}(\boldsymbol{r}))\,, \tag{3.150b}$$

the symbol $\propto$ denoting proportionality, and U_{ij}, $i,j = 1,2$ being the matrix elements. Since $\hat{U}$ is unitary, we finally conclude that vectors $\tilde{\boldsymbol{\Psi}}_1$ and $\tilde{\boldsymbol{\Psi}}_2$ should be orthogonal. This is a crucial difference with regard to general MSC light. In that case, the vectors $\boldsymbol{\Psi}_1$ and $\boldsymbol{\Psi}_2$, introduced in Eq. (3.128), are nonproportional, non-orthogonal vector fields.

3.7 Comparing Special Types of Random Electromagnetic Fields

Let us finally summarize and compare the main characteristics of several families of random electromagnetic fields studied in the present chapter. We remark certain similarities and differences with regard to the attainable fringe visibility, the factorization of the CDT, and the stochastic structure (in the mean-square sense) of the associated vector field. Recall that all these properties are considered as equivalent features of the field in the scalar approach, but they describe different classes of light in the vectorial regime.

The sets of fields we are comparing exhibit the following coherence and polarization characteristics in a region D:

$\{T\}$: Set of fields with $\mu^2_{STF} = 1$ (Setälä et al., 2004; Tervo et al., 2003). The CDT of this kind of beams is factorizable in the form $\hat{W}(\boldsymbol{r}_1,\boldsymbol{r}_2) = \boldsymbol{F}^{\dagger}(\boldsymbol{r}_1)\boldsymbol{F}(\boldsymbol{r}_2)$, where $\boldsymbol{F}$ is a deterministic row vector. These fields are totally polarized, with

position-independent stochastic character and maximum attainable visibility in a Young scheme.

$\{V\}$: Set of fields with $g_{12} = |\mu_W|^2_{\max} = 1$ (Gori et al., 2007; Martínez-Herrero and Mejías, 2007a) (maximum attainable visibility under local unitary transformations in a Young interferometer). The CDT of these fields is factorizable in the sense expressed by Eq. (3.98) of Sect. 3.5, with position-independent stochastic behaviour. The vector field reads (cf. Eq. (3.96) of Sect. 3.5)

$$\boldsymbol{E}(\boldsymbol{r}) = \boldsymbol{E}_0 f(\boldsymbol{r}) \hat{U}(\boldsymbol{r}), \tag{3.151}$$

where $\boldsymbol{E}_0 = (u,v)$ is a row vector whose components take complex random values, f is a deterministic complex function, and $\hat{U}$ denotes a unitary matrix.

$\{R\}$ (MSC light): Set of partially polarized fields with $\mu_S = \mu_I = 1$ (Réfrégier, 2008b). The CDT of these fields is factorizable as a product of two matrices, as shown in Eq. (3.129). The vector field reads (in the mean-square sense)

$$\boldsymbol{E}(\boldsymbol{r}) = \varepsilon_1 \boldsymbol{\Psi}_1(\boldsymbol{r}) + \varepsilon_2 \boldsymbol{\Psi}_2(\boldsymbol{r}), \tag{3.152}$$

where ε_1 and ε_2 are complex random variables, with $< \varepsilon_1^* \varepsilon_2 >= 0$, and $\boldsymbol{\Psi}_1$ and $\boldsymbol{\Psi}_2$ denote deterministic vectors, which, in general, are not orthogonal.

$\{R^*\}$: Set of MSC fields that, for fixed values of the degree of polarization at the pinholes, maximize the Young fringe visibility under unitary transformations (Martínez-Herrero and Mejías, 2009). The CDT is also factorizable as a matricial product in the particular form given by Eq. (3.146). The vector field becomes

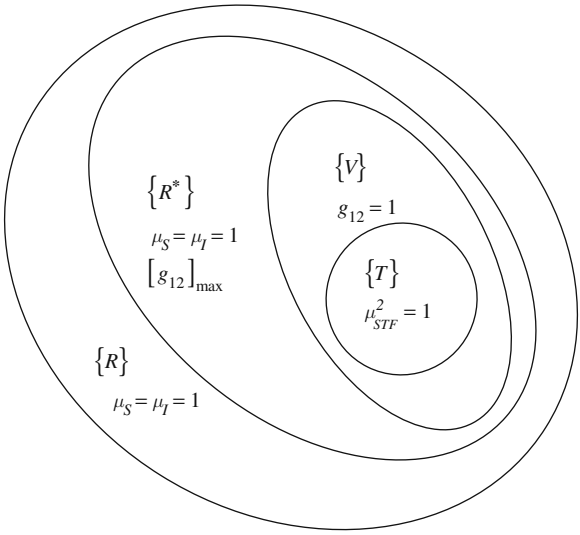

Fig. 3.4 Illustrating the relation $\{T\} \subset \{V\} \subset \{R^*\} \subset \{R\}$. See also (Martínez-Herrero and Mejías, 2009)

$$\boldsymbol{E}(\boldsymbol{r}) = \boldsymbol{E}_0 \hat{D}_0^{\dagger}(\boldsymbol{r})\hat{U}(\boldsymbol{r}) = \varepsilon_1 \tilde{\boldsymbol{\Psi}}_1(\boldsymbol{r}) + \varepsilon_2 \tilde{\boldsymbol{\Psi}}_2(\boldsymbol{r}), \tag{3.153}$$

where $\hat{D}_0$ is a diagonal matrix, and $\tilde{\boldsymbol{\Psi}}_1$ and $\tilde{\boldsymbol{\Psi}}_2$ are orthogonal vectors.

Taking into account all these characteristics, a hierarchy between these sets of electromagnetic fields can finally be established on the basis of inclusive relations, namely,

$$\{T\} \subset \{V\} \subset \left\{R^*\right\} \subset \{R\} \tag{3.154}$$

This layer structure is illustrated in Fig. 3.4.

References

Beran, M. J., Parrent, G. B. (1967): *Theory of Partial Coherence* (Prentice Hall, Englewood Cliffs, NJ).

Born, M., Wolf, E. (1999): *Principles of Optics*, 7th ed. (Cambridge University Press, Cambridge).

Brosseau, C. (1998): *Fundamentals of Polarized Light* (Wiley, New York).

Dennis, M. (2007): A three-dimensional degree of polarization based on Rayleigh scattering, J. Opt. Soc. Am. A 24, 2065–2069.

Du, X., Zhao, D. (2008): Criterion for keeping completely unpolarized or completely polarized stochastic electromagnetic Gaussian Schell-model beams on propagation, Opt. Express 16, 16172–16180.

Ellis, J., Dogariu, A. (2004): Complex degree of mutual polarization, Opt. Lett. 29, 536–538.

Gori, F., Santarsiero, M., Borghi, R. (2006a): Vector mode analysis of a Young interferometer, Opt. Lett. 31, 858–860.

Gori, F., Santarsiero, M., Borghi, R., Wolf, E. (2006b): Effects of coherence on the degree of polarization in a Young interference pattern, Opt. Lett. 31, 688–690.

Gori, F., Santarsiero, M., Borghi, R. (2007): Maximizing Young′s fringe visibility through reversible optical transformations, Opt. Lett.32, 588–590.

Gori, F. (2008): Partially correlated sources with complete polarization, Opt. Lett. 33, 2818–2820.

Gori, F., Tervo, J., Turunen, J. (2009): Correlation matrices of completely unpolarized beams, Opt. Lett. 34, 1447–1449.

James, D. F. V. (1994): Change of polarization of light beams on propagation in free space, J. Opt. Soc. Am. A 11, 1641–1643.

Korotkova, O., Wolf, E. (2005a): Effects of linear non-image-forming devices on spectra and on coherence and polarization properties of stochastic electromagnetic beams: part I: general theory, J. Mod. Opt. 52, 2659–2671.

Korotkova, O., Wolf, E. (2005b): Effects of linear non-image-forming devices on spectra and on coherence and polarization properties of stochastic electromagnetic beams: part II: examples, J. Mod. Opt. 52, 2673–2685.

Lahiri, M., Wolf, E. (2009): Cross-spectral density matrices of polarized light beams, Opt. Lett. 34, 557–559.

Li, Y., Lee, H., Wolf, E. (2006): Spectra, coherence and polarization in Young's interference pattern formed by stochastic electromagnetic beams, Opt. Commun. 265, 63–72.

Mandel, L., Wolf, E. (1995): *Optical Coherence and Quantum Optics* (Cambridge University Press, Cambridge).

Martínez-Herrero, R., Mejías, P. M. (2007a): Maximum visibility under unitary transformations in two-pinhole interference for electromagnetic fields, Opt. Lett. 32, 1471–1473.

Martínez-Herrero, R., Mejías, P. M. (2007b): Relation between degrees of coherence for electromagnetic fields, Opt. Lett. 32, 1504–1506.

Martínez-Herrero, R., Mejías, P. M. (2007c): Electromagnetic fields that remain totally polarized under propagation, Opt. Commun. 279, 20–22.
Martínez-Herrero, R., Mejías, P. M. (2008a): On the vectorial fields with position-independent stochastic behavior, Opt. Lett. 33, 195–197.
Martínez-Herrero, R., Mejías, P. M. (2008b): Equivalence between optimum Young′s fringe visibility and position-independent stochastic behavior of electromagnetic fields, J. Opt. Soc. Am. A 25, 1902–1905.
Martínez-Herrero, R., Mejías, P. M. (2009): Maximizing Young's fringe visibility under unitary transformations for mean-square coherent light, Opt. Express 17, 603–610.
Mujat, M., Dogariu, A. (2003): Polarimetric and spectral changes in random electromagnetic fields, Opt. Lett. 28, 2153–2155.
Perina, J. (1971): *Coherence of Light* (Van Nostrand Reinhold Company, London).
Ponomarenko, S. A., Wolf, E. (2003): The spectral degree of coherence of fully spatially coherent electromagnetic beams, Opt. Commun. 227, 73–74.
Pu, J. X., Korotkova, O., Wolf, E. (2007): Polarization-induced spectral changes on propagation of stochastic electromagnetic beams, Phys. Rev. E 75, 056610.
Réfrégier, P., Goudail, F. (2005): Invariant degrees of coherence of partially polarized light, Opt. Express 13, 6051–6060.
Réfrégier, P., Roueff, A. (2006): Linear relations of partially polarized and coherent electromagnetic fields, Opt. Lett. 31, 2827–2829.
Réfrégier, P., Roueff, A. (2007a): Intrinsic coherence: a new concept in polarization and coherence theory, Opt. Photon News 18(2), 30–35.
Réfrégier, P., Roueff, A. (2007b): Visibility interference fringes optimization on a single beam in the case of partially polarized and partially coherent light, Opt. Lett. 32, 1366–1368.
Réfrégier, P. (2008a): Irreversible effects of random modulation on coherence properties of partially polarized light, Opt. Lett. 33, 636–638.
Réfrégier, P. (2008b): Mean-square coherent light, Opt. Lett. 33, 1551–1553.
Réfrégier, P., Luis, A. (2008): Irreversible effects of random unitary transformations on coherence properties of partially polarized electromagnetic fields, J. Opt. Soc. Am. A 25, 2749–2757.
Roychowdhury, H., Wolf, E. (2005): Young's interference experiment with light of any state of coherence and polarization, Opt. Commun. 252, 268–274.
Santarsiero, M. (2007): Polarization invariance in a Young interferometer, J. Opt. Soc. Am. A 24, 3493–3499.
Santarsiero, M., Borghi, R. (2006): Measuring spatial coherence by using a reversed-wavefront Young interferometer, Opt. Lett. 31, 861–863.
Setälä, T., Tervo, J., Friberg, A. T. (2004): Complete coherence in the space-frequency domain, Opt. Lett. 29, 328–330.
Setälä, T., Tervo, J., Friberg, A. T. (2006a): Contrasts of Stokes parameters in Young′s interference experiment and electromagnetic degree of coherence, Opt. Lett. 31, 2669–2671.
Setälä, T., Tervo, J., Friberg, A. T. (2006b): Stokes parameters and polarization contrasts in Young's interference experiment, Opt. Lett. 31, 2208–2210.
Tervo, J. (2003): Azimuthal polarization and partial coherence, J. Opt. Soc. Am. A 20, 1974–1980.
Tervo, J, Setäla, T., Friberg, A. T. (2003): Degree of coherence for electromagnetic fields, Opt. Express 11, 1137–1143.
Tervo, J., Setälä, T., Friberg, A. T. (2004): Theory of partially coherent electromagnetic fields in the space-frequency domain, J. Opt. Soc. Am. A 21, 2205–2215.
Wolf, E. (2003): Unified theory of coherence and polarization of random electromagnetic beams, Phys. Lett. A 312, 263–267.
Wolf, E. (2007a): Polarization invariance in beam propagation, Opt. Lett. 32, 3400–3401.
Wolf, E. (2007b): *Introduction to the Theory of Coherence and Polarization of Light* (Cambridge University Press, Cambridge).
Wolf, E., Roychowdhury, H. (2005): Young′s interference experiment with light of any state of coherence and of polarization, Opt. Commun. 252, 268–274.

Wolf, E., Yajun, L., Hungte, L. (2006): Spectra, coherence and polarization in Young′s interference pattern formed by stochastic electromagnetic beams, Opt. Commun. 265, 63–72.
Zhao, D. M., Wolf, E. (2008): Light beams whose degree of polarization does not change on propagation, Opt. Commun. 281, 3067–3070.

Chapter 4
Non-Paraxial Electromagnetic Beams

4.1 Introduction

In the previous chapters, we have considered electromagnetic beams whose longitudinal field component (along the propagation direction) is negligible. In other words, the electric field vector was assumed to be transverse to the z-axis and, consequently, it was represented by means of two components. This paraxial approach and the subsequent quasi-transversality assumption have provided in the above chapters a considerable simplification in both, the calculations and the characterization of this kind of beams.

However, in high-resolution microscopy, particle trapping, high-density recording and tomography, to mention only some recent applications, the light beam is strongly-focused and raises waist sizes smaller than the wavelength. In such cases, the paraxial approximation is no longer valid, and a non-paraxial treatment is required. This is a topic of considerable current interest, which has been extensively investigated in the last decade (see, for example, (Agrawal and Lax, 1983; Alonso, 2004; Alonso et al., 2006a, b; April, 2008; Belkebir et al., 2006; Borghi et al., 2002; Borghi and Santarsiero, 2003, 2004; Chaumet, 2006; Chen et al., 2002; Ciattoni et al., 2002; Deng, 2006; Dorn et al., 2003; Duan and Lü, 2005a, b; Hall, 1996; Lekner, 2003; Mejías et al., 2002; Mei and Zhao, 2008; Seshadri, 1998, 2008; Sheppard and Saghafi, 1999; Sheppard, 2000; Tervo and Turunen, 2001; Varga and Török, 1996, 1998; Volpe and Petrov, 2004; Zhou, 2006, 2008)).

In the present chapter, attention will be focused on two main subjects, namely, to get exact solutions of the Maxwell equations behaving as highly non-paraxial beams, and to investigate the analytical structure, field magnitude and polarization features of the associated field distributions.

Up to now, different vectorial formulations of non-paraxial electromagnetic beams have been explored in the literature (for example, in terms of the Hertz vectors (Varga and Török, 1996, 1998; Sheppard, 2000), or by using the complex-source-point mode (Sheppard and Saghafi, 1999)). Among them, several types of representations based on the angular plane-wave spectrum have been reported in recent years (Chaumet, 2006; Guo et al., 2006; Martínez-Herrero et al., 2001, 2006; Zhou, 2006). Such kind of decomposition has revealed to be particularly useful because it allows separate the contribution of the propagating and evanescent waves.

R. Martínez-Herrero et al., *Characterization of Partially Polarized Light Fields*, Springer Series in Optical Sciences 147, DOI 10.1007/978-3-642-01327-0_4,

In the next sections, we will show that, when the contribution of the evanescent waves is negligible, the electric field solution can be written as the sum of two terms: one of them is transverse to the propagation direction; another one exhibits a non-zero longitudinal component and its associated magnetic field is also transverse. This analytical structure differs from alternative proposals reported in the literature, also based on the angular spectrum (see, for instance (Chaumet, 2006) and references therein). Moreover, our formalism enables us to incorporate the presence of evanescent waves (Arnoldus and Foley, 2002; Chaumet, 2006; Ciattoni et al., 2002; Martínez-Herrero et al., 2008a, b; Petrov, 1999; Setala et al., 1999; Shchegrov and Carney, 1999), which are receiving increasing attention due to the possibility of subwavelength resolution, beyond the diffraction limit.

This chapter is arranged as follows. In the next section, the formalism and the key definitions to be handled in the rest of the chapter are introduced. It will be obtained a general expression with separate contributions of TE, TM and evanescent terms. In Sect. 4.3, the particular but important case of radially or azimuthally polarized fields at some transverse plane is analyzed in detail. The concept of closest field is discussed in Sect. 4.4. The field components of the evanescent part of the field are considered in Sect. 4.5 for several illustrative cases in which this kind of waves are significant. Finally, some results concerning the polarization features of partially coherent beams at the near- and far-field are reported in Sect. 4.6.

4.2 Formalism and Key Definitions

After defining the angular plane-wave spectrum of the electromagnetic field, we will introduce a general solution of the Maxwell equations as a sum of propagating and evanescent waves. The TE- and TM-decomposition of the propagating field are also discussed, as well as the relative significance of the longitudinal field component compared with the magnitude of the global field.

4.2.1 Angular Plane-Wave Spectrum

Let us consider monochromatic electromagnetic beams propagating into free space. For the sake of simplicity, in this chapter we will consider propagation in vacuum (the results, however, can be generalized to beams travelling along homogeneous isotropic dielectric media, free of losses). The behavior of the field is described by means of the Maxwell equations, which take a particularly simple form in the Gauss system:

$$\nabla \times \boldsymbol{H} + \mathrm{i}k\boldsymbol{E} = 0, \tag{4.1a}$$

$$\nabla \times \boldsymbol{E} - \mathrm{i}k\boldsymbol{H} = 0, \tag{4.1b}$$

$$\nabla \cdot \boldsymbol{E} = 0, \tag{4.1c}$$

$$\nabla \cdot \boldsymbol{H} = 0, \tag{4.1d}$$

where $\boldsymbol{E}$ and $\boldsymbol{H}$ contain the spatial structure of the electric and magnetic fields, respectively. Recall that, in SI-units, Eqs. (4.1a) and (4.1b) would read $\nabla \times \boldsymbol{H} + \mathrm{i}\omega\varepsilon_0\boldsymbol{E} = 0$ and $\nabla \times \boldsymbol{E} - \mathrm{i}\omega\mu_0\boldsymbol{H} = 0$, respectively, where ε_0 and μ_0 represent the permittivity and the permeability of the vacuum.

As is well known, the fields $\boldsymbol{E}$ and $\boldsymbol{H}$ can be expressed in terms of their angular plane-wave spectrum,

$$\boldsymbol{E}(x,y,z) = \int \tilde{\boldsymbol{E}}(u,v,z) \exp\left[\mathrm{i}k(xu + yv)\right] du dv, \tag{4.2a}$$

$$\boldsymbol{H}(x,y,z) = \int \tilde{\boldsymbol{H}}(u,v,z) \exp\left[\mathrm{i}k(xu + yv)\right] du dv, \tag{4.2b}$$

where $\tilde{\boldsymbol{E}}$ and $\tilde{\boldsymbol{H}}$ denote the spatial Fourier transform of $\boldsymbol{E}$ and $\boldsymbol{H}$, respectively. Although x, y and z should be considered, in principle, as equivalent directions, for simplicity, in the present chapter we choose z as the direction of propagation of the beam (see Fig. 4.1). In terms of the angular plane-wave spectrum associated to the electric and magnetic fields, the Maxwell equations become

$$\boldsymbol{L} \times \tilde{\boldsymbol{H}} + \mathrm{i}k\tilde{\boldsymbol{E}} = 0, \tag{4.3a}$$

$$\boldsymbol{L} \times \tilde{\boldsymbol{E}} - \mathrm{i}k\tilde{\boldsymbol{H}} = 0, \tag{4.3b}$$

$$\boldsymbol{L} \cdot \tilde{\boldsymbol{E}} = 0, \tag{4.3c}$$

$$\boldsymbol{L} \cdot \tilde{\boldsymbol{H}} = 0, \tag{4.3d}$$

where

$$\boldsymbol{L} \equiv (\mathrm{i}ku, \mathrm{i}kv, \partial/\partial z). \tag{4.4}$$

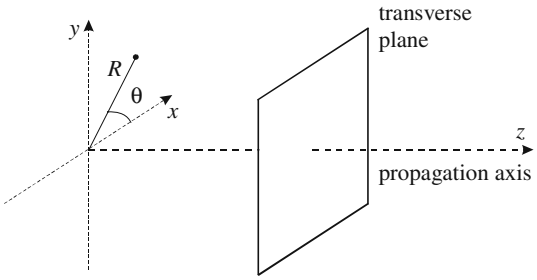

Fig. 4.1 Cartesian and cylindrical coordinate systems: Notation

Instead of using Cartesian coordinates, for the sake of convenience we will next handle cylindrical coordinates R, θ and z, i.e.,

$$x = R\cos\theta, \tag{4.5a}$$
$$y = R\sin\theta, \tag{4.5b}$$

along with polar coordinates, ρ and ϕ, related to the transverse Cartesian Fourier-transform variables u, v by the equations

$$u = \rho\cos\phi, \tag{4.6a}$$
$$v = \rho\sin\phi. \tag{4.6b}$$

Taking this into account, a general solution of Eqs. (4.3) can formally be written in the form

$$\tilde{\boldsymbol{E}}(\rho,\phi,z) = \tilde{\boldsymbol{E}}_0(\rho,\phi)\exp(ikz\xi), \tag{4.7}$$

with the conditions

$$\tilde{\boldsymbol{E}}_{0\boldsymbol{x}}\sigma_x + \tilde{\boldsymbol{E}}_{0y}\sigma_y + \tilde{\boldsymbol{E}}_{0z}\sigma_z = 0, \tag{4.8}$$

and

$$\tilde{\boldsymbol{H}}(\rho,\phi,z) = (\boldsymbol{\sigma}\times\tilde{\boldsymbol{E}}_0)\exp(ikz\xi), \tag{4.9}$$

where

$$\xi = (1-\rho^2)^{1/2}, \quad \rho \le 1, \tag{4.10a}$$

$$\xi = \mathrm{i}(\rho^2-1)^{1/2}, \quad \rho > 1, \tag{4.10b}$$

and

$$\boldsymbol{\sigma} = (\sigma_x,\sigma_y,\sigma_z) = (\rho\cos\phi,\rho\sin\phi,\xi). \tag{4.11}$$

It should be remarked that condition (4.8) is a direct consequence of the Maxwell equation $\nabla\cdot\boldsymbol{E} = 0$. In addition, it is clear from Eq. (4.10b) that the third component of $\boldsymbol{\sigma}$ would be, in general, a complex number whose physical meaning will be apparent later.

Based on the plane-wave spectrum given by Eq. (4.7), we obtain for the electric field solution of the Maxwell equations the expression

$$\boldsymbol{E}(R,\theta,z) = \int_0^\infty\int_0^{2\pi}\tilde{\boldsymbol{E}}_0(\rho,\phi)\exp[\mathrm{i}k\rho R\cos(\theta-\phi)]\exp(\mathrm{i}kz\xi)\rho d\,\rho d\phi, \tag{4.12}$$

where $\tilde{\boldsymbol{E}}_0$ should fulfil Eq. (4.8).

4.2.2 Propagating and Evanescent Waves

To get deeper insight into this general solution, we write the field $\boldsymbol{E}(R,\theta,z)$, given by Eq. (4.12), as the sum of two terms:

$$\boldsymbol{E}(R,\theta,z) = \boldsymbol{E}_{pr}(R,\theta,z) + \boldsymbol{E}_{ev}(R,\theta,z), \tag{4.13}$$

where

$$\boldsymbol{E}_{pr}(R,\theta,z) = \int_0^1 \int_0^{2\pi} \tilde{\boldsymbol{E}}_0(\rho,\phi) \exp\left[\mathrm{i}k\rho R\cos(\theta-\phi)\right] \exp(\mathrm{i}kz\xi)\rho d\,\rho d\phi, \tag{4.14a}$$

$$\boldsymbol{E}_{ev}(R,\theta,z) = \int_1^{\infty} \int_0^{2\pi} \tilde{\boldsymbol{E}}_0(\rho,\phi) \exp\left[\mathrm{i}k\rho R\cos(\theta-\phi)\right] \exp(\mathrm{i}kz\xi)\rho d\,\rho d\phi. \tag{4.14b}$$

The first term, $\boldsymbol{E}_{\mathrm{pr}}$, should be understood as a superposition of plane waves with propagation directions specified by ρ and ϕ. The field $\boldsymbol{E}_{\mathrm{pr}}$ would then represent the contribution of the propagating waves (some authors (Sherman et al., 1976) refer to this term as the homogeneous part of the angular spectrum). The second term of Eq. (4.13), $\boldsymbol{E}_{\mathrm{ev}}$, should be considered as a superposition of inhomogeneous waves that decay at different rates along the longitudinal axis. In practice, the evanescent part of the exact solution is significant enough in the highly nonparaxial case at the neighbourhood of the initial plane (see Sect. 4.5). Otherwise, $\boldsymbol{E}_{\mathrm{ev}}$ is negligible. We will next focus our attention on the propagating term of the exact solution.

4.2.3 TE- and TM-Decomposition of the Propagating Field

Let us now write the vector angular spectrum $\tilde{\boldsymbol{E}}_0$ of the field (recall Eq. (4.7)) in the form (Martínez-Herrero et al., 2001)

$$\tilde{\boldsymbol{E}}_0(\rho,\phi) = a(\rho,\phi)\boldsymbol{e}_1(\phi) + b(\rho,\phi)\boldsymbol{e}_2(\rho,\phi), \tag{4.14c}$$

where $\boldsymbol{e}_1$ and $\boldsymbol{e}_2$ are unitary vectors,

$$\boldsymbol{e}_1 = (\sin\phi, -\cos\phi, 0), \tag{4.15a}$$

$$\boldsymbol{e}_2 = \left(\sqrt{1-\rho^2}\cos\phi, \sqrt{1-\rho^2}\sin\phi, -\rho\right). \tag{4.15b}$$

and

$$a(\rho,\phi) = \tilde{\boldsymbol{E}}_0 \cdot \boldsymbol{e}_1, \tag{4.16a}$$

$$b(\rho,\phi) = \tilde{\boldsymbol{E}}_0 \cdot \boldsymbol{e}_2, \tag{4.16b}$$

Functions $a(\rho,\phi)$ and $b(\rho,\phi)$ can be understood as the projection of $\tilde{\boldsymbol{E}}_0$ onto the vectors $\boldsymbol{e}_1$ and $\boldsymbol{e}_2$, respectively. These vectors should then be considered as reference axes with respect to which the vector $\tilde{\boldsymbol{E}}_0$ is decomposed. In addition, for the propagating field $\boldsymbol{E}_{\rm pr}$, condition (4.8) reduces to

$$\tilde{\boldsymbol{E}}_0(\rho,\phi)\cdot\boldsymbol{s}(\rho,\phi)=0, \tag{4.17}$$

where

$$\boldsymbol{s}(\rho,\phi)=\left(\rho\cos\phi,\rho\sin\phi,\sqrt{1-\rho^2}\right),\ \text{with}\ \rho\in[0,1], \tag{4.18}$$

is a unitary vector describing the propagation direction of each planewave. It can be shown at once that $\boldsymbol{s}$, $\boldsymbol{e}_1$ and $\boldsymbol{e}_2$ are a triad of a mutually orthogonal system of unit vectors (see Fig. 4.2). Moreover, the choice of these three vectors characterizes the formalism used in this chapter.

We conclude finally that the propagating electric-field solution of the Maxwell equations can be written as follows

$$\boldsymbol{E}(\boldsymbol{r})=\int_0^1\int_0^{2\pi}a(\rho,\phi)\boldsymbol{e}_1(\phi)\exp(\mathrm{i}k\boldsymbol{s}\cdot\boldsymbol{r})\rho d\rho d\phi+\int_0^1\int_0^{2\pi}b(\rho,\phi)\boldsymbol{e}_2(\rho,\phi)\exp(\mathrm{i}k\boldsymbol{s}\cdot\boldsymbol{r})\rho d\,\rho d\phi. \tag{4.19}$$

The first term of the right-hand side of this equation, namely,

$$\boldsymbol{E}_{\rm TE}(\boldsymbol{r})=\int_0^1\int_0^{2\pi}a(\rho,\phi)\boldsymbol{e}_1(\phi)\exp(\mathrm{i}k\boldsymbol{s}\cdot\boldsymbol{r})\rho d\,\rho d\phi, \tag{4.20}$$

represents a field transverse to the propagation axis z (in other words, the z-component vanishes). We refer to this term as the transverse-electric field, $\boldsymbol{E}_{\rm TE}$.

On the other hand, associated to the second term of Eq. (4.19)

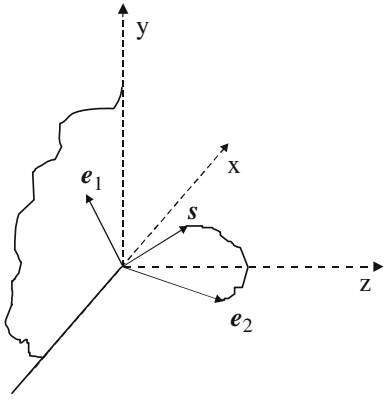

Fig. 4.2 Mutually-orthogonal unitary vectors $\boldsymbol{s}$, $\boldsymbol{e}_1$ and $\boldsymbol{e}_2$. This figure illustrates that vector $\boldsymbol{e}_1$ is contained in the transverse plane x-y and is orthogonal to the plane formed by vectors $\boldsymbol{e}_2$ and $\boldsymbol{s}$, which, in turns, contains the z-axis (note that these two vectors have longitudinal components)

$$\boldsymbol{E}_{\mathrm{TM}}(\boldsymbol{r}) = \int_0^1 \int_0^{2\pi} b(\rho,\phi)\boldsymbol{e}_2(\rho,\phi)\exp\left(ik\boldsymbol{s}\cdot\boldsymbol{r}\right)\rho d\,\rho d\phi. \tag{4.21}$$

We call $\boldsymbol{E}_{\mathrm{TM}}$ the transverse-magnetic term of the field solution (4.19). In a similar way, the TE- and TM-terms associated to the global magnetic field $\boldsymbol{H} = \boldsymbol{H}_{\mathrm{TE}} + \boldsymbol{H}_{\mathrm{TM}}$ are given by (see Eq. (4.9))

$$\boldsymbol{H}_{TE}(R,\theta,z) = \int_0^1 \int_0^{2\pi} a(\rho,\phi)\boldsymbol{e}_2(\rho,\phi) \exp\left[ikR\rho\cos\left(\phi-\theta\right)\right]\exp\left[ikz\sqrt{1-\rho^2}\right]\rho d\,\rho d\phi, \tag{4.22}$$

$$\boldsymbol{H}_{TM}(R,\theta,z) = \int_0^1 \int_0^{2\pi} b(\rho,\phi)\boldsymbol{e}_1(\phi)\exp\left[ikR\rho\cos\left(\phi-\theta\right)\right]\exp\left[ikz\sqrt{1-\rho^2}\right]\rho d\,\rho d\phi. \tag{4.23}$$

where, for the sake of clarity, we have expanded the exponential function inside the integrals. Note first that $\boldsymbol{H}_{\mathrm{TM}}$ is transverse to the z-axis. In addition, orthogonality between $\boldsymbol{e}_1$ and $\boldsymbol{e}_2$ implies that $\boldsymbol{E}_{\mathrm{TE}}$ and $\boldsymbol{E}_{\mathrm{TM}}$ are orthogonal at the far field. It should finally be remarked that the well-known paraxial approximation follows from the substitutions (Fresnel approach)

$$\exp\left[ikz\sqrt{1-\rho^2}\right] \approx \exp\left(ikz\right)\exp\left[-ikz\left(\frac{\rho^2}{2}\right)\right], \tag{4.24}$$

$$\boldsymbol{e}_2 \approx (\cos\phi, \sin\phi, 0), \tag{4.25}$$

in the corresponding expressions.

Let us finally consider the behavior of the electric field at a point defined by the coordinates R, θ, z ($z > 0$) in the far zone, i.e., far away from the initial plane $z = 0$. The observation direction is given by the unit vector $\boldsymbol{u} = (u_{\mathrm{x}}, u_{\mathrm{y}}, u_{\mathrm{z}})$, where

$$u_x = \frac{R\cos\theta}{L}, \tag{4.26a}$$

$$u_y = \frac{R\sin\theta}{L}, \tag{4.26b}$$

$$u_z = \frac{z}{L}, \tag{4.26c}$$

and

$$L^2 = R^2 + z^2. \tag{4.27}$$

The asymptotic behavior $kL \to \infty$ of the integral that appear in Eqs. (4.20) and (4.21), for a fixed direction $\boldsymbol{u}$, can be obtained by using the procedure stated in Mandel and Wolf (1995) and Wolf and Foley (1998). We finally arrive to the following expressions for TE- and TM-fields at the far zone:

$$\boldsymbol{E}_{TE}(R,\theta,z) \approx \frac{-2\pi i}{k}\frac{z}{L}a\left(\frac{R}{L},\theta\right)\frac{\exp(ikL)}{L}\boldsymbol{e}_1(\phi), \tag{4.28a}$$

$$\boldsymbol{E}_{TM}(R,\theta,z) \approx \frac{-2\pi i}{k}\frac{z}{L}b\left(\frac{R}{L},\theta\right)\frac{\exp(ikL)}{L}\boldsymbol{e}_2\left(\frac{R}{L},\phi\right), \tag{4.28b}$$

where, for simplicity, a quadratic-phase factor has been disregarded. We see that $\boldsymbol{E}_{\mathrm{TE}}$ and $\boldsymbol{E}_{\mathrm{TM}}$ are orthogonal at the far field, as expected. In addition, these fields exhibit non-uniform polarization distributions. The global field, $\boldsymbol{E} = \boldsymbol{E}_{\mathrm{TE}} + \boldsymbol{E}_{\mathrm{TM}}$, can then be written as follows

$$\boldsymbol{E}(R,\theta,z) \approx \frac{-2\pi i}{k}\frac{z}{L}\frac{\exp(ikL)}{L}\left[a\left(\frac{R}{L},\theta\right)\boldsymbol{e}_1(\phi) + b\left(\frac{R}{L},\theta\right)\boldsymbol{e}_2\left(\frac{R}{L},\phi\right)\right]. \tag{4.29}$$

Since $\boldsymbol{e}_1$ and $\boldsymbol{e}_2$ are mutually orthogonal, the polarization features at the far field are determined by the amplitude and the phase of functions a and b. In general, the field would be elliptically polarized, with the characteristic parameters of the polarization ellipse depending on the chosen observation direction.

4.2.4 Significance of the Longitudinal Field Component

It could be useful to quantify the relative significance of the TM-component of a field with regard to the global field $\boldsymbol{E}$. A simple parameter would be given by the ratio

$$\eta_{TM} = \frac{\int_0^{\infty}\int_0^{2\pi} |\boldsymbol{E}_{TM}|^2 \, RdRd\theta}{\int_0^{\infty}\int_0^{2\pi} |\boldsymbol{E}|^2 \, RdRd\theta}, \tag{4.30}$$

where, as before, $\boldsymbol{E}$ represents the global field. It is not difficult to show that η_{TM} takes the same value at any transverse plane z. In terms of the functions a and b, η_{TM} reads

$$\eta_{TM} = \frac{\int_0^1 \int_0^{2\pi} |b|^2 \, \rho d \, \rho d\phi}{\int_0^1 \int_0^{2\pi} \left(|a|^2 + |b|^2\right) \rho d \, \rho d\phi}, \tag{4.31}$$

It is clear that

$$0 \leq \eta_{TM} \leq 1, \tag{4.32}$$

with the values $\eta_{TM} = 0$ for a pure TE-field, and $\eta_{TM} = 1$ for a pure TM-field. This parameter is also related with the relative weight of the longitudinal component of the field, E_z, namely,

$$E_z(R, \theta, z) = -\int_0^1 \int_0^{2\pi} \rho b(\rho,\phi) \exp\left[ikR\rho \cos(\phi - \theta)\right] \exp\left[ikz\sqrt{1-\rho^2}\right] \rho d \, \rho d\phi. \tag{4.33}$$

Analytically, the significance of E_z can be described in a similar way to that used concerning the TM-component. Thus, a parameter η_z could be introduced in the form

$$\eta_z = \frac{\int_0^\infty \int_0^{2\pi} |E_z|^2 \, RdRd\theta}{\int_0^\infty \int_0^{2\pi} |E|^2 \, RdRd\theta}, \tag{4.34}$$

which, in terms of functions a and b, becomes

$$\eta_z = \frac{\int_0^1 \int_0^{2\pi} |b|^2 \, \rho^3 d\rho d\phi}{\int_0^1 \int_0^{2\pi} \left(|a|^2 + |b|^2\right) \rho d \, \rho d\phi}. \tag{4.35}$$

From Eq. (4.31), it follows at once

$$\eta_z = <\rho^2>_b \, \eta_{TM}, \tag{4.36}$$

where

$$<\rho^2>_b = \frac{\int_0^1 \int_0^{2\pi} |b|^2 \, \rho^3 d\rho d\phi}{\int_0^1 \int_0^{2\pi} |b|^2 \, \rho d \, \rho d\phi} \tag{4.37}$$

characterizes the size of the region where $|b(\rho,\phi)|^2$ is important. Since we are assuming that the evanescent waves are negligible, the value of $<\rho^2>_b$ would be less than 1. Equation (4.36) establishes a link between the relative significance of E_z and $\boldsymbol{E}_{\mathrm{TM}}$ compared with the global field. In those cases in which the quantity $<\rho^2>_b$ is small, the longitudinal component will be small as well, and we are concerned with the paraxial regime. On the contrary, higher values of η_z occur for pure TM-fields ($\eta_{TM} = 1$) and $<\rho^2>_b$ approaching 1 (highly non-paraxial case).

4.3 Propagation of Non-paraxial Beams with Radial or Azimuthal Polarization Distribution at a Transverse Plane

The interest will now be focused on a particular kind of beams, namely, those fields whose polarization distribution at a certain transverse plane is either radial or azimuthal. As was pointed out in the first two chapters, radially and azimuthally polarized light beams have attained considerable interest during the last years (see, for example, (Deng, 2006; Deng and Guo, 2007; Diehl et al., 2006; Dorn et al., 2003; Machavariani et al., 2008; Martínez-Herrero and Mejías, 2008; Nesterov et al., 1999; Niu et al., 2005; Yan and Yao, 2008; Yew and Sheppard, 2007; Zhang et al., 2008) and the references also quoted in Chaps. 1 and 2). The intrinsic non-uniform character of the polarization distribution over the beam cross-section forces to apply a vectorial treatment. Here we will use the formalism proposed before, based on the angular plane-wave spectrum of the light beam, and we will express the field in cylindrical coordinates, in which the electric field vector is decomposed into radial, azimuthal and longitudinal (along z) components. This is the most natural choice because of the peculiar polarization structure of this class of fields.

We will investigate along the subsequent sections how they propagate into free space. The final Sect. 4.3.6 will be devoted to the interesting case of radially polarized fields that retain this character at any transverse plane under free propagation.

4.3.1 Radial and Azimuthal Components

It was obtained in Sect. 4.2 that, in the absence of evanescent waves, the electric-field solution of the Maxwell equations can be written in terms of the angular spectrum as follows

$$\boldsymbol{E}(R,\theta,z) = \int_0^1 \int_0^{2\pi} [a(\rho,\phi)\boldsymbol{e}_1(\phi) + b(\rho,\phi)\boldsymbol{e}_2(\rho,\phi)] \times \exp\left[ikR\rho\cos(\phi-\theta)\right] \exp\left[ikz\sqrt{1-\rho^2}\right] \rho d\,\rho d\phi. \tag{4.38}$$

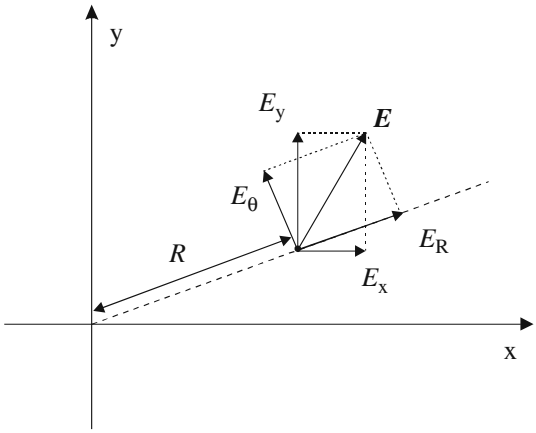

Fig. 4.3 Notation used to introduce the radial and azimuthal field components in terms of the Cartesian components (cf. Eqs. (4.39)). The z-axis is orthogonal to the plane of the figure

For the sake of convenience, at each point of a transverse plane $z =$ constant, instead of using Cartesian components, E_x and E_y, (defined with respect to some laboratory axes), we will consider the radial and azimuthal components of the field, E_R and E_θ, given by (see Fig. 4.3)

$$E_R(R,\theta,z) = \cos\theta\ E_x(R,\theta,z) + \sin\theta\ E_y(R,\theta,z), \tag{4.39a}$$

$$E_\theta(R,\theta,z) = -\sin\theta\ E_x(R,\theta,z) + \cos\theta\ E_y(R,\theta,z), \tag{4.39b}$$

and the longitudinal component E_z remaining unaltered. By using Eqs. (4.38) and (4.39), general expressions for the radial and azimuthal components of any free-propagating field can be obtained, namely (Martínez-Herrero and Mejías, 2008)

$$E_R(R,\theta,z) = \int_0^1 \int_0^{2\pi} \left[-a(\rho,\phi)\sin(\theta-\phi) + \tilde{b}(\rho,\phi)\cos(\theta-\phi)\right] \times \exp\left[\mathrm{i}k\rho R\cos(\theta-\phi)\right] \exp\left(\mathrm{i}kz\sqrt{1-\rho^2}\right) \rho\, d\,\rho d\phi, \tag{4.40a}$$

and

$$E_\theta(R,\theta,z) = -\int_0^1 \int_0^{2\pi} \left[a(\rho,\phi)\cos(\theta-\phi) + \tilde{b}(\rho,\phi)\sin(\theta-\phi)\right] \times \exp\left[\mathrm{i}k\rho R\cos(\theta-\phi)\right] \exp\left(\mathrm{i}kz\sqrt{1-\rho^2}\right) \rho\, d\,\rho d\phi, \tag{4.40b}$$

where

$$\tilde{b}(\rho,\phi) \equiv b(\rho,\phi)\sqrt{1-\rho^2}. \tag{4.41}$$

Taking the above equations into account, a radially (azimuthally) polarized field at some transverse plane is then defined as that field whose E_θ (E_R) component equals zero at such plane. We will next study these two cases separately.

4.3.2 Radial Case: Free-Space Propagation

Let us analyze the propagation into free space of a field with radially polarized structure at the transverse plane $z = 0$. To begin with, recall that the component E_θ of the radially polarized field (RPF) should vanish at $z = 0$, so that (cf. Eq. (4.40b))

$$\int_0^1 \int_0^{2\pi} [\, a(\rho,\phi)\cos(\theta-\phi) + \tilde{b}(\rho,\phi)\sin(\theta-\phi)\,] \exp[ik\rho R\cos(\theta-\phi)]\,\rho d\,\rho d\phi = 0, \tag{4.42}$$

which can also be expressed in the form

$$\int_0^{2\pi} d\phi \int_0^1 a(\rho,\phi)\frac{\partial}{\partial\rho}\{\exp[ikR\rho\cos(\theta-\phi)]\}\,\rho d\rho + \int_0^1 d\rho \int_0^{2\pi} \tilde{b}(\rho,\phi)\frac{\partial}{\partial\phi}\{\exp[ikR\rho\cos(\theta-\phi)]\}\,d\phi = 0. \tag{4.43}$$

After elementary integration, the first term of Eq. (4.43) (we refer to it as I_1) becomes

$$I_1 = \int_0^{2\pi} d\phi \left\{\left[\rho a \exp[ikR\rho\cos(\theta-\phi)]\right]\right\}_{\rho=0}^{\rho=1} - \int_0^{2\pi}\int_0^1 \left[\frac{\partial \rho a}{\partial\rho}\right]\exp[ikR\rho\cos(\theta-\phi)]\,d\rho d\phi. \tag{4.44}$$

Since we have assumed that the contribution of the evanescent waves is negligible, the function $a(\rho = 1,\phi)$ should be equal to zero, for any ϕ. Otherwise, the limit $\rho = 1$ of the integration interval for the evanescent wave would contribute in a

significant way to the global field. Accordingly, Eq. (4.44) reduces to

$$I_1 = -\int_0^{2\pi}\int_0^1 \left[\frac{\partial \rho a}{\partial \rho}\right] \exp\left[ikR\rho\cos(\theta-\phi)\right] d\rho d\phi. \tag{4.45}$$

In an analogous way, the second term, I_2, of the left-hand side of Eq. (4.43) can be written in the form

$$I_2 = -\int_0^{2\pi}\int_0^1 \left[\frac{\partial \tilde{b}}{\partial \phi}\right] \exp\left[ikR\rho\cos(\theta-\phi)\right] d\rho d\phi, \tag{4.46}$$

and Eq. (4.42) reads

$$\int_0^{2\pi}\int_0^1 \left[\frac{\partial \rho a}{\partial \rho} + \frac{\partial \tilde{b}}{\partial \phi}\right] \exp\left[ikR\rho\cos(\theta-\phi)\right] d\rho d\phi = 0. \tag{4.47}$$

This equation would then be fulfilled provided functions $a(\rho,\phi)$ and $\tilde{b}(\rho,\phi)$ satisfies the condition

$$\frac{\partial \rho a}{\partial \rho} + \frac{\partial \tilde{b}}{\partial \phi} = 0. \tag{4.48}$$

The general solution to this equation would be given by writing functions a and $\tilde{b}$ in the form

$$a(\rho,\phi) = -\frac{1}{\rho}\frac{\partial F(\rho,\phi)}{\partial \phi}, \tag{4.49}$$

$$\tilde{b}(\rho,\phi) = \frac{\partial F(\rho,\phi)}{\partial \rho}, \tag{4.50}$$

where F represents any mathematically well-behaved function in the region we are considering. Taking Eqs. (4.38) and (4.50) into account, a general propagation expression is obtained for a field with radially polarized structure at plane $z = 0$ (Martínez-Herrero and Mejías, 2008):

$$\boldsymbol{E}_{rad}(R,\theta,z) = \int_0^1\int_0^{2\pi}\left[-\frac{1}{\rho}\frac{\partial F(\rho,\phi)}{\partial \phi}\boldsymbol{e}_1(\phi) + \frac{1}{\sqrt{1-\rho^2}}\frac{\partial F(\rho,\phi)}{\partial \rho}\boldsymbol{e}_2(\rho,\theta)\right]\times \exp\left[ikR\rho\cos(\theta-\phi)\right]\exp\left(ikz\sqrt{1-\rho^2}\right)\rho d\,\rho d\phi. \tag{4.51}$$

To go further into the analysis of this equation, let us now consider the following Fourier series expansion of function $F(\rho,\phi)$

$$F(\rho,\phi) = \sum_m \exp(im\phi) f_m(\rho), \;\; m = 0, \pm 1, \pm 2, \ldots \tag{4.52}$$

where

$$f_m(\rho) = \frac{1}{2\pi} \int_0^{2\pi} F(\rho,\phi) \exp(-im\phi) d\phi, \tag{4.53}$$

From Eqs. (4.51), (4.52) and (4.53), it can be shown after some algebra that the Cartesian components of the field $\boldsymbol{E}_{\mathrm{rad}}$ can be expressed as follows

$$(E_{rad})_x(R,\theta,z) = \sum_m i \exp(im\theta) [A_m(R,z)\cos\theta + iB_m(R,z)\sin\theta], \tag{4.54a}$$

$$(E_{rad})_y(R,\theta,z) = \sum_m \exp(im\theta) [B_m(R,z)\cos\theta + iA_m(R,z)\sin\theta], \tag{4.54b}$$

$$(E_{rad})_z(R,\theta,z) = \sum_m \exp(im\theta) C_m(R,z), \tag{4.54c}$$

where

$$A_m(R,z) = \frac{\pi}{(-i)^m} \int_0^1 \exp\left(ikz\sqrt{1-\rho^2}\right) \times$$
$$\left\{-mf_m(\rho)\left[J_{m-1}(kR\rho) + J_{m+1}(kR\rho)\right] + \rho f'_m(\rho)\left[J_{m+1}(kR\rho) - J_{m-1}(kR\rho)\right]\right\} d\rho, \tag{4.55a}$$

$$B_m(R,z) = \frac{\pi}{(-i)^m} \int_0^1 \exp\left(ikz\sqrt{1-\rho^2}\right) \times$$
$$\left\{mf_m(\rho)\left[J_{m-1}(kR\rho) - J_{m+1}(kR\rho)\right] + \rho f'_m(\rho)\left[J_{m+1}(kR\rho) + J_{m-1}(kR\rho)\right]\right\} d\rho, \tag{4.55b}$$

$$C_m(R,z) = \frac{-2\pi}{(-i)^m} \int_0^1 \frac{\rho^2 f'_m(\rho)}{\sqrt{1-\rho^2}} J_m(kR\rho) \exp\left(ikz\sqrt{1-\rho^2}\right) d\rho, \tag{4.55c}$$

J_{m} being the Bessel function of order m, and the prime denoting derivation with respect to ρ. Equations (4.54) can finally be rearranged in a physically more

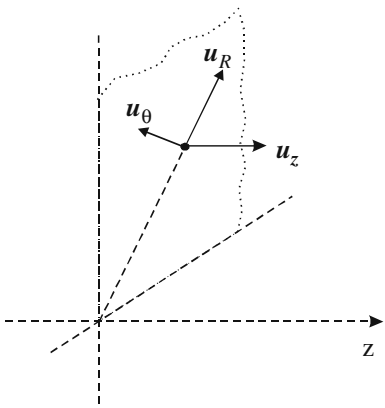

Fig. 4.4 Mutually orthogonal unitary vectors $\boldsymbol{u}_\mathrm{R}$, $\boldsymbol{u}_\theta$ and $\boldsymbol{u}_\mathrm{z}$. Note that $\boldsymbol{u}_\mathrm{R}$ and $\boldsymbol{u}_\theta$ are contained in a plane transverse to the propagation axis z

understandable and compact form (Martínez-Herrero and Mejías, 2008)

$$\boldsymbol{E}_{rad}(R,\theta,z) = \left[\sum_m i\exp(im\theta)A_m(R,z)\right]\boldsymbol{u}_R(\theta) + \left[\sum_m \exp(im\theta)B_m(R,z)\right]\boldsymbol{u}_\theta(\theta) + \\ + \left[\sum_m \exp(im\theta)C_m(R,z)\right]\boldsymbol{u}_z \tag{4.56}$$

where $\boldsymbol{u}_\mathrm{R}$ and $\boldsymbol{u}_\theta$ are unitary vectors in the radial and azimuthal directions (see Fig. 4.4), i.e.,

$$\boldsymbol{u}_R = (\cos\theta, \sin\theta, 0), \tag{4.57a}$$

$$\boldsymbol{u}_\theta = (-\sin\theta, \cos\theta, 0), \tag{4.57b}$$

$$\boldsymbol{u}_z = (0,0,1). \tag{4.57c}$$

Equation (4.56) shows how propagates into free space a field whose vectorial structure is radially polarized at some initial transverse plane z (this is consistent with the fact of that $B_m(R,z=0)=0$, for any m). Furthermore, since the function B_m depends, in general, on the propagation distance z, the azimuthal content (second term of the right-hand side of Eq. (4.56)) does not vanish, and the field will not, in general, retain its radially-polarized character upon propagation.

A number of properties of this kind of fields can be inferred immediately from Eq. (4.56). More specifically, on the propagation axis z ($R=0$), the field components reduce to

$$(E_{rad})_x(0,z) = iA_1(0,z) + iA_{-1}(0,z), \tag{4.58a}$$

$$(E_{rad})_y(0,z) = -A_1(0,z) + A_{-1}(0,z), \tag{4.58b}$$

$$(E_{rad})_z(0,z) = -2\pi \int_0^1 \frac{f'_{m=0}(\rho)}{\sqrt{1-\rho^2}} \rho^2 \exp\left(ikz\sqrt{1-\rho^2}\right) d\rho, \tag{4.58c}$$

and the following conclusions are easily obtained:

i) The transverse field of this type of beams is zero at the origin ($R = 0$, $z = 0$).
ii) Those fields with $f_{\mathrm{m}=0} = 0$ in the expansion (4.52) do not exhibit longitudinal component on the z-axis.
iii) When $f_{\mathrm{m}=1} = f_{\mathrm{m}=-1} = 0$, the transverse field vanishes at any axial point.
iv) When $f_{\mathrm{m}=1} = 0$ and $f_{\mathrm{m}=-1} \neq 0$ (or vice versa), the transverse field is circularly polarized on the propagation axis z.

Let us finally discuss the special but important case of RPFs whose function $F(\rho,\phi)$ does not depend on the coordinate ϕ. This implies $a(\rho,\phi) = 0$ (in accordance with Eq. (4.49)), and $f_m(\rho) = \delta_{m0} f_0(\rho)$ (δ_{m0} denotes here the Kronecker's delta). In addition, it follows from Eq. (4.55) that $B_0(R,z)$ equals zero for such fields. Taking all this into account, one concludes that this class of fields are radially polarized not only at the initial plane $z = 0$ but also at any other transverse plane $z =$ constant. In other words, these fields retain their radially-polarized character upon free propagation. Furthermore, since $a(\rho,\phi)$ vanishes, they are pure TM fields, in the sense described in Sect. 4.2 of this chapter. Moreover, since function $\tilde{b}$ does not depend on ϕ, the angular plane-wave spectrum of these fields is independent of ϕ as well. It should be remarked that these results are in agreement with previous works (Pääkkönen et al., 2002; Tervo, 2003). Note finally that the longitudinal component of this kind of beams differs from zero on the z-axis, in contrast with the fields satisfying $f_{\mathrm{m}=0} = 0$ and behaving as radially polarized only at plane $z = 0$, for which E_z vanishes at the origin ($R = z = 0$).

4.3.3 Azimuthal Case: Free-Space Propagation

In this section we are going to analyze the free-space propagation of a field $\boldsymbol{E}_{\mathrm{azim}}$ with azimuthally-polarized structure at some initial plane $z = 0$. Now the radial component E_{R} should vanish (see Eq. (4.39a)), and we can write

$$\int_0^1 \int_0^{2\pi} \left[-a(\rho,\phi)\sin(\theta-\phi) + \tilde{b}(\rho,\phi)\cos(\theta-\phi)\right] \exp\left[ik\rho R\cos(\theta-\phi)\right] \rho d\,\rho d\phi = 0. \tag{4.59}$$

From this equation, by following a similar procedure to that used for RPFs (see Eqs. (4.43), (4.44), (4.45), (4.46), (4.47) and (4.48)), we obtain after some calculations (compare with Eq. (4.48)).

$$\frac{\partial a}{\partial \phi} - \frac{\partial \rho \tilde{b}}{\partial \rho} = 0, \tag{4.60}$$

whose solution can be given in the form

$$a(\rho,\phi) = \frac{\partial G}{\partial \rho}, \tag{4.61a}$$

$$\tilde{b}(\rho,\phi) = \frac{1}{\rho}\frac{\partial G}{\partial \phi}, \tag{4.61b}$$

where $G(\rho,\phi)$ denotes any function with the appropriate mathematical requirements. Substitution of Eq. (4.61) into Eq. (4.38), gives the propagation law

$$\begin{aligned} \boldsymbol{E}_{azim}(R,\theta,z) = \int_0^1 \int_0^{2\pi} \left[\frac{\partial G}{\partial \rho}\boldsymbol{e}_1(\phi) + \frac{1}{\rho}\frac{1}{\sqrt{1-\rho^2}}\frac{\partial G}{\partial \phi}\boldsymbol{e}_2(\rho,\theta) \right] \times \\ \exp\left[ikR\rho\cos(\theta-\phi)\right]\exp\left(ikz\sqrt{1-\rho^2}\right)\rho d\,\rho d\phi. \end{aligned} \tag{4.62}$$

Following a parallel method to that applied in the radially polarized case, we write $G(\rho,\phi)$ in series form

$$G(\rho,\phi) = \sum_m \exp(im\,\phi) g_m(\rho), \tag{4.63}$$

and Eq. (4.62) is transformed into the expression (Martínez-Herrero and Mejías, 2008):

$$\begin{aligned} \boldsymbol{E}_{azim}(R,\theta,z) = \left[\sum_m \exp(im\,\theta) U_m(R,z)\right]\boldsymbol{u}_R(\theta) + \left[\sum_m i\exp(im\,\theta) V_m(R,z)\right]\boldsymbol{u}_\theta(\theta) + \\ + \left[\sum_m \exp(im\,\theta) W_m(R,z)\right]\boldsymbol{u}_z, \end{aligned} \tag{4.64}$$

where

$$\begin{aligned} U_m(R,z) = \frac{\pi}{(-i)^m}\int_0^1 \exp\left(ikz\sqrt{1-\rho^2}\right) \times \\ \left\{\rho g_m'(\rho)\left[J_{m-1}(kR\rho) + J_{m+1}(kR\rho)\right] + m g_m(\rho)\left[J_{m-1}(kR\rho) - J_{m+1}(kR\rho)\right]\right\} d\rho, \end{aligned} \tag{4.65a}$$

$$V_m(R,z) = \frac{\pi}{(-i)^m} \int_0^1 \exp\left(ikz\sqrt{1-\rho^2}\right) \times$$
$$\left\{\rho g'_m(\rho)\left[J_{m+1}(kR\rho) - J_{m-1}(kR\rho)\right] - m g_m(\rho)\left[J_{m-1}(kR\rho) + J_{m+1}(kR\rho)\right]\right\} d\rho, \tag{4.65b}$$

$$W_m(R,z) = \frac{-2m\pi}{(-i)^{m-1}} \int_0^1 \frac{\rho^2 g_m(\rho)}{\sqrt{1-\rho^2}} J_m(kR\rho) \exp\left(ikz\sqrt{1-\rho^2}\right) d\rho, \tag{4.65c}$$

the prime denoting again derivation with respect to ρ. Equation (4.64) provides a general propagating law for the vector $\boldsymbol{E}$ associated to azimuthally polarized fields (APFs). It should be remarked that, in spite of $U_m(R,0) = 0$, the field $\boldsymbol{E}_{\text{azim}}$ would not retain, in general, its azimuthally-polarized character upon propagation: $U_{\text{m}}(R,z)$ does not vanish when $z \neq 0$, and a radial field-component would also contribute.

A number of properties follow at once from Eq. (4.64). They should be understood as the azimuthal analogy of the properties exhibited by RPFs. We get on the z-axis

$$(E_{azim})_x(0,z) = U_1(0,z) + U_{-1}(0,z), \tag{4.66a}$$

$$(E_{azim})_y(0,z) = iU_1(0,z) - iU_{-1}(0,z), \tag{4.66b}$$

$$(E_{azim})_z(0,z) = 0. \tag{4.66c}$$

The third equation explicitly shows that, for any APF, the longitudinal component equals zero on the propagation axis. Moreover, Eqs. (4.66a) and (4.66b) imply that any APF is zero along the z-axis if $g_1 = g_{-1} = 0$. In addition, when $g_{\text{m}=1} = 0$ and $g_{\text{m}-1} \neq 0$ (or vice versa), the APF is circularly polarized on the z-axis.

To end this section, let us consider those fields that remain azimuthally polarized at any transverse plane after propagation. It can be shown that, when $G(\rho,\phi)$ does not depend on ϕ, the field $\boldsymbol{E}_{\text{azim}}$ becomes

$$\boldsymbol{E}_{azim}(R,\theta,z) = V_0(R,z)\boldsymbol{u}_\theta(\theta), \tag{4.67}$$

where

$$V_0(R,z) = 2\pi i \int_0^1 \frac{dG(\rho)}{d\rho} J_1(kR\rho) \exp\left(ikz\sqrt{1-\rho^2}\right) \rho d\rho. \tag{4.68}$$

It follows at once from Eq. (4.67) that this class of field remains azimuthally polarized upon free propagation. Moreover, it is a pure TE-field (the longitudinal component is zero everywhere), and the function $a(\rho,\phi)$, characterizing its angular

spectrum, does nor depend on ϕ. This recovers earlier results reported, for example, in Tervo (2003) (see also references therein).

It should finally be remarked that the longitudinal components of the fields behaving as azimuthally polarized only at a plane (say, $z = 0$) do not vanish when $R \neq 0$ (see Eq. (4.64)). This characteristic reveals an important difference with respect to the APFs given by Eq. (4.67).

4.3.4 Application to a Particular Set of Fields

We will next study a certain kind of fields whose radial and azimuthal components are given by simple analytical functions. This makes easier the application of the results derived before.

Let us then consider a particular example of function F introduced in Eqs. (4.49) and (4.50) (Martínez-Herrero and Mejías, 2008):

$$F(\rho,\phi) = \delta(\rho - a)\exp(ip\phi),\ \ a \in (0,1), \tag{4.69}$$

where now δ denotes the Dirac delta function, a is a dimensionless constant, and $p = 1, 2, 3,\ldots$ These two parameters, a and p, generate the beams belonging to this family, which provides radially polarized fields at the initial plane $z = 0$. After substituting Eq. (4.69) into the general propagation law for RPFs (Eq. (4.56)), we get the amplitude of the radial and azimuthal components at any transverse plane z

$$E_R \propto -\left[\tilde{R}J_p(\tilde{R}) + i\tilde{z}\frac{dJ_p}{d\tilde{R}}\right]\exp\left(ikz\sqrt{1-a^2}\right)\exp(ip\theta), \tag{4.70a}$$

$$E_\theta \propto p\tilde{z}\frac{J_p(\tilde{R})}{\tilde{R}}\exp\left(ikz\sqrt{1-a^2}\right)\exp(ip\theta), \tag{4.70b}$$

where the symbol $\propto$ means proportionality, and $\tilde{R}$ and $\tilde{z}$ are dimensionless variables,

$$\tilde{R} = kaR, \tag{4.71a}$$

$$\tilde{z} = \frac{ka^2}{\sqrt{1-a^2}}z. \tag{4.71b}$$

Both expressions (4.70a) and (4.70b) involve the same value of the proportionality constant. As is quite apparent from Eq. (4.58), the case $p = 1$ gives a purely-transverse circularly polarized field on the propagation axis. On the other hand, when $p \neq 1$, the transverse components E_x and E_y vanish. The field is purely longitudinal on the z-axis (it should be noted that, on such axis, to speak about radial or azimuthal components of a field does not make sense).

Figure 4.5 illustrates the squared modulus of this class of fields at the initial plane $z = 0$ for the values $p = 1$, 2 and 3.

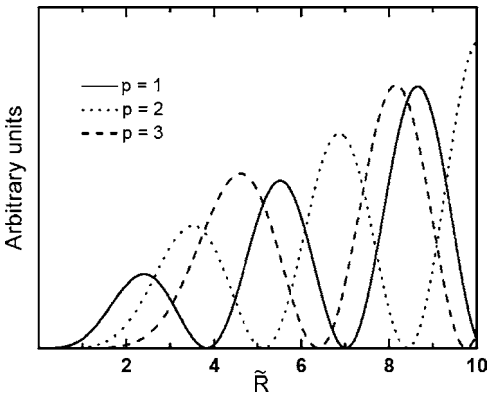

Fig. 4.5 Squared modulus of the radial component of the field defined by Eqs. (4.69) and (4.70) in terms of $\tilde{R}$ at the transverse plane $z = 0$. *Continuous line*: $p = 1$; *dotted line*: $p = 2$; *dashed line*: $p = 3$. Ordinates are given in arbitrary units. Note that, at plane $z = 0$, the azimuthal component E_θ vanishes. After Martínez-Herrero and Mejías (2008), with permission

It is also clear from Eqs. (4.70) that this set of fields does not retain the radially-polarized character under free propagation. However, the existence of zeros of functions $J_p(\tilde{R})$ implies the appearance of concentric circular dark rings around the z-axis: the azimuthal field component vanishes along these circumferences.

Figures 4.6 and 4.7 show the magnitude of the radial and azimuthal-components at a transverse plane for two distances of propagation: $z = 2\ \lambda$ and $z = 40\ \lambda$ from the initial plane. In both cases $a = 1/2$ and $p = 1$. It is clear from the figures that the propagated field behaves essentially as radially polarized except within a small region around the z-axis whose radius approaches λ, in which the magnitude of the azimuthal component is similar to that of the radial one (Fig. 4.6) or even higher (Fig. 4.7) for longer propagation distances. Furthermore, Fig. 4.7 also shows the existence of circular dark rings, associated with negligible radial field component.

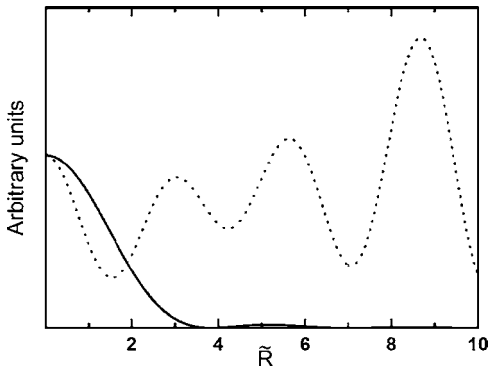

Fig. 4.6 Squared modulus of the radial field component, $|E_R|^2$ (*dotted line*), and azimuthal component, $|E_\theta|^2$ (*continuous line*) in terms of $\tilde{R}$, at plane $z = 2\ \lambda$. The curves are computed for $p = 1$. It should be remarked that, on the propagation axis, the field is circularly polarized, which implies $|E_R|^2 = |E_\theta|^2$ at $\tilde{R} = 0$, in agreement with the behavior shown in the figure. After Martínez-Herrero and Mejías (2008), with permission

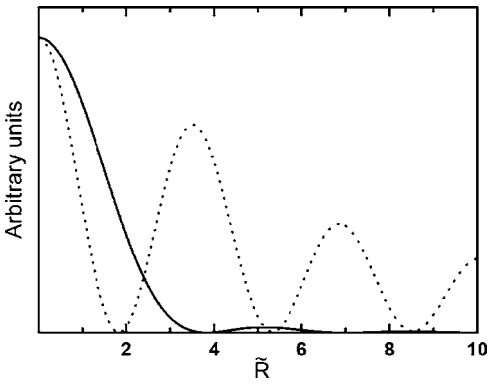

Fig. 4.7 The same as in Fig. 4.6, but now computed at the transverse plane $z = 40\ \lambda$. After Martínez-Herrero and Mejías (2008), with permission

To compare the relative importance of the radial and azimuthal components of the field upon propagation, we represent in Fig. 4.8 the ratio (Martínez-Herrero and Mejías, 2008)

$$q = \frac{|E_\theta|^2}{|E_R|^2 + |E_\theta|^2}, \tag{4.72}$$

computed far away from the initial plane (in other words, we consider $z \to \infty$). Peaks indicate the presence of a pure azimuthally-polarized field at certain rings, whereas, in the valleys ($q = 0$), the field is radially polarized. It should also be noted that the size of all the above rings increases for higher values of parameter p.

Figures 4.9 and 4.10 plot the radial and azimuthal field components at the same transverse plane to that of Figs. 4.6 and 4.7, but now for the value $p = 2$. The main qualitative difference with regard to the case $p = 1$ appears on the propagation axis

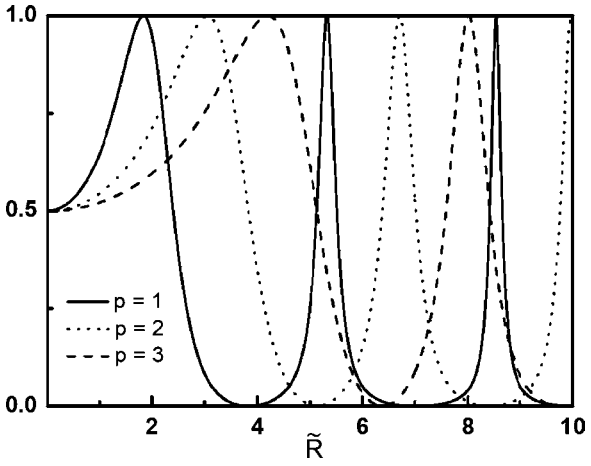

Fig. 4.8 Ordinates plot the ratio q in terms of $\tilde{R}$ in the limit $z \to \infty$. The curves correspond to the cases $p = 1$ (*continuous line*); $p = 2$ (*dotted line*); and $p = 3$ (*dashed line*). Note that, from the definition (4.72), we always have $0 \leq q \leq 1$. After Martínez-Herrero and Mejías (2008), with permission

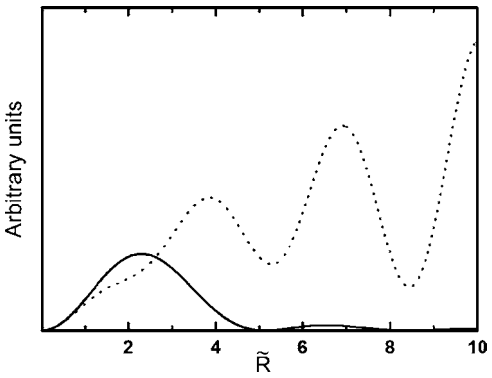

Fig. 4.9 The same as in Fig. 4.6 but now with $p = 2$. On the axis ($\tilde{R} = 0$) the transverse field components vanish, and the field only exhibits a longitudinal component. After Martínez-Herrero and Mejías (2008), with permission

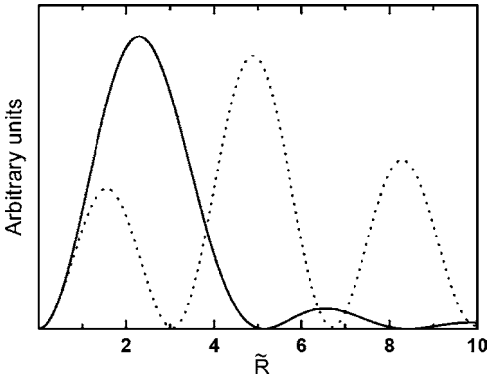

Fig. 4.10 The same as in Fig. 4.9 but now computed at plane $z = 40\ \lambda$. Again, the transverse components of the field vanish on the propagation axis. After Martínez-Herrero and Mejías (2008), with permission

($\tilde{R} = 0$): the transverse components vanish and the field is now purely longitudinal, as expected from Eq. (4.70a).

4.3.5 Radially-Polarized Fields at Any Transverse Plane

Let us now consider radially-polarized fields that retain this character at any transverse plane upon propagation. In short, we refer to them as RPM fields (radially-polarized-maintained fields). It is interesting to mention that doughnut-like beams with radial polarization are relevant as light sources used in superresolution processes. Possible applications include microfluidics and improved capacity of DVD systems.

It was shown at the end of Sect. 4.3.2 that functions $a(\rho,\phi)$ and $b(\rho,\phi)$ become for RPM fields

$$a(\rho,\phi) = 0, \tag{4.73}$$

$$b(\rho,\phi) = b(\rho). \tag{4.74}$$

By taking this into account, we get from Eq. (4.56) the following general propagation law for this kind of fields (Martínez-Herrero et al., 2008a)

$$\boldsymbol{E}(R,\theta,z) = \mathrm{i}A_0(R,z)\boldsymbol{u}_R + C_0(R,z)\boldsymbol{u}_z, \tag{4.75}$$

where $\boldsymbol{u}_\mathrm{R}$ and $\boldsymbol{u}_\mathrm{z}$ have been defined before (see Eq. (4.24) and (4.25)), and

$$A_0(R,z) = 2\pi \int_0^1 b(\rho)\sqrt{1-\rho^2}J_1(kR\rho)\exp\left(ikz\sqrt{1-\rho^2}\right)\rho d\rho, \tag{4.76a}$$

$$C_0(R,z) = -2\pi \int_0^1 \rho b(\rho)J_0(kR\rho)\exp\left(ikz\sqrt{1-\rho^2}\right)\rho d\rho, \tag{4.76b}$$

J_0 and J_1 being the Bessel functions of the first kind of order 0 and 1, respectively. Equations (4.74), (4.75), and (4.76) allow us to determine the vector amplitude of this type of fields at any z. Note that functions $A_0(R, z)$ and $C_0(R, z)$ are given in terms of the angular plane-wave spectrum $b(\rho)$ that characterizes the particular RPM field. Furthermore, from Eqs. (4.75) and (4.76), a number of simple but general consequences can be obtained at once:

i) The transverse part of a RPM field is radially polarized at any plane transverse to the propagation direction z (as expected).
ii) On the axis z ($R = 0$), any RPM field only has longitudinal component (i.e., the field is linearly polarized along z). This agrees with the rotationally-symmetric polarization structure of the RPM beams.
iii) When $R \neq 0$, the ellipse that describes the electric field vector associated to a RPM field is contained in the plane defined by $\boldsymbol{u}_\mathrm{R}$ and the z axis.
iv) The characteristics of the polarization ellipse depend on R and z, but are independent of θ.

It should be remarked that the general propagation law (4.75) is valid for non-paraxial fields as well as for paraxial beams. Let us compare both cases.

In Sect. 4.2, we pointed out that the paraxial regime analytically follows from the Fresnel approximation (see Eqs. (4.24) and (4.25)). However, to get deeper insight into the physical meaning of this approach, it would now be better to consider directly the angular spectrum that characterizes an RPM field. Let us then introduce the (squared) width of the angular spectrum, ψ^2, in the form

$$\psi^2 = \frac{\int (u^2+v^2)\left|\tilde{\boldsymbol{E}}\right|^2 dudv}{\int \left|\tilde{\boldsymbol{E}}\right|^2 dudv}, \tag{4.77}$$

where $\tilde{\boldsymbol{E}}$ represents again the spatial Fourier transform of the field $\boldsymbol{E}$. Note that ψ^2 does not depend on z. In the particular case of RPM fields, it can be shown that ψ^2 becomes

$$\psi^2 = \frac{\int_0^1 |b(\rho)|^2 \rho^3 d\rho}{\int_0^1 |b(\rho)|^2 \rho d\rho} = <\rho^2>_b , \tag{4.78}$$

where $<\rho^2>_b$ was defined in Eq. (4.37) (it estimates the size of the region where $|b(\rho)|^2$ is significant). We see that the parameter ψ^2 gives the (squared) width of the function $|b(\rho)|^2$ and, consequently, could be understood as a measure of the size of the angular spectrum (far field). Therefore, its value is inversely proportional to the size σ (measured in λ-units) of the region at a transverse (near field) plane z where $|\boldsymbol{E}|^2$ is important. As expected, paraxiality is then related with small values of ψ^2, whereas greater ψ^2 refers to the non-paraxial case.

Let us finally evaluate the significance of the longitudinal field component E_z with respect to the total field $\boldsymbol{E}_{\mathrm{R}}$. This can be done by calculating the ratio (cf. Eq. (4.34))

$$(\eta_z)_R = \frac{\int_0^\infty \int_0^{2\pi} |\boldsymbol{E}_z|^2 RdRd\theta}{\int_0^\infty \int_0^{2\pi} |\boldsymbol{E}_R|^2 RdRd\theta}, \tag{4.79}$$

It can be shown that $(\eta_z)_R$ and ψ^2 are related through the equation (Martínez-Herrero et al., 2008a)

$$(\eta_z)_R = \frac{\psi^2}{1-\psi^2}. \tag{4.80}$$

The quantity $(\eta_z)_R$ can then be considered as a measure (averaged over the transverse cross-section) of the squared ratio between the major and the minor axes of the polarization ellipse. Accordingly, since ψ^2 drastically reduces in the paraxial case, such ellipse would closely resemble a segment along the radial (transverse) direction. This behavior will be illustrated in the examples shown in the next section.

We will finally apply the propagation equation (4.75) to a kind of fields whose angular spectrum is confined on a ring and is defined by the functions (Martínez-Herrero et al., 2008a)

$$a(\rho,\phi) = 0, \tag{4.81a}$$

$$b(\rho) = B\,\delta(\rho - q), \tag{4.81b}$$

where B and q are constants ($q < 1$), and $\delta(.)$ denotes the Dirac delta function. In this case, A_0 and C_0 are proportional to simple analytical functions:

$$A_0(R,z) \propto J_1(kR\rho)\exp\left(ikz\sqrt{1-q^2}\right), \tag{4.82a}$$

$$C_0(R,z) \propto J_0(kR\rho)\exp\left(ikz\sqrt{1-q^2}\right). \tag{4.82b}$$

After substituting these expressions into Eq. (4.75), several special features of the polarization structure of these fields can be obtained (apart from the general characteristics of RPM fields derived above):

i) The polarization state does not depend on the transverse plane z, so that, for a fixed radial distance, it remains invariant upon free propagation. This result is consistent with the invariance properties of this kind of beams.
ii) The longitudinal component of the field equals zero for distances $R_{\mathrm{m}} = j_{\mathrm{m}0}/qk$, where $j_{\mathrm{m}0}$ denotes the zeros of J_0.
iii) The transverse field vanishes (i.e., the field only exhibits longitudinal component) for radial distances $R_{\mathrm{n}} = j_{\mathrm{n}1}/qk$, where $j_{\mathrm{n}1}$ are the zeros of J_1.

4.4 Closest Field

We will next introduce the concept of (exact) field solutions *closest* (in an algebraic sense) to a vector function at a certain plane (Martínez-Herrero et al., 2001). In particular, we study, in a detailed way, the field magnitude and the transverse polarization structure of the closest field associated to the well-known uniformly totally-polarized Gaussian model. Other examples will also be analyzed in Sect. 4.4.4.

4.4.1 Definition and Meaning

Let us assume that we try to represent a certain field at a plane, say, $z = 0$, by means of an easy-to-use vectorial function $\boldsymbol{f}(x, y)$. This could be inferred, for instance, either from a theoretical analysis or from experimental data. We define the so-called closest solution to $\boldsymbol{f}$ as the electric-field solution of the Maxwell equations that is best fitted, in an algebraic sense, to the vector $\boldsymbol{f}$. To understand what this means let us first write $\boldsymbol{f}$ in terms of its angular plane-wave spectrum, $\tilde{\boldsymbol{f}}$, namely

$$\boldsymbol{f}(x,y) = \int_0^1 \int_0^{2\pi} \tilde{\boldsymbol{f}}(\rho,\phi) \exp\left[ik\rho(x\cos\phi + y\sin\phi)\right]\rho d\rho d\phi. \tag{4.83}$$

where the evanescent waves have again been neglected. Function $\boldsymbol{f}$, given by Eq. (4.83), would then represent an electric field solution at plane $z = 0$ provided its associated vectorial spectrum belongs to the (two-dimensional) subspace $\mathcal{A}$ generated by $\boldsymbol{e}_1$ and $\boldsymbol{e}_2$. It should be remarked that, in general, an arbitrary function $\tilde{\boldsymbol{f}}(\rho,\phi)$ does not fulfil this condition. From an algebraic point of view, the vector $\boldsymbol{v}(\rho,\phi)$ (belonging to $\mathcal{A}$) closest to $\tilde{\boldsymbol{f}}(\rho,\phi)$ is given by

$$\boldsymbol{v}(\rho,\phi) = (\tilde{\boldsymbol{f}} \cdot \boldsymbol{e}_1)\boldsymbol{e}_1 + (\tilde{\boldsymbol{f}} \cdot \boldsymbol{e}_2)\boldsymbol{e}_2. \tag{4.84}$$

Accordingly, we define the electric-field vector, $\boldsymbol{E}_{\mathrm{f}}$, solution of the Maxwell equations, closest to $\boldsymbol{f}$ at the initial plane as

$$\boldsymbol{E}_{\mathrm{f}}(\boldsymbol{r}) = \int_0^1 \int_0^{2\pi} \left[(\tilde{\boldsymbol{f}} \cdot \boldsymbol{e}_1)\boldsymbol{e}_1 + (\tilde{\boldsymbol{f}} \cdot \boldsymbol{e}_2)\boldsymbol{e}_2\right] \exp(ik\boldsymbol{r} \cdot \boldsymbol{s})\rho d\rho d\phi, \tag{4.85}$$

where $\boldsymbol{r} = (x, y, z)$ is again the position vector, and $\boldsymbol{s}$ was defined in Eq. (4.18). It is clear from this equation that the first (second) term inside the integral would represent the TE (TM) contribution of the field closest to $\boldsymbol{f}(x, y)$.

Moreover, the associated magnetic field closest to $\boldsymbol{f}$ takes the form (see Eqs. (4.22) and (4.23))

$$\boldsymbol{H}_{\mathrm{f}}(\mathrm{r}) = \int_0^1 \int_0^{2\pi} \left[(\tilde{\boldsymbol{f}} \cdot \boldsymbol{e}_1)\boldsymbol{e}_2 - (\tilde{\boldsymbol{f}} \cdot \boldsymbol{e}_2)\boldsymbol{e}_1\right] \exp(ik\boldsymbol{r} \cdot \boldsymbol{s})\rho d\rho d\phi. \tag{4.86}$$

4.4.2 Application to the Uniformly-Polarized Gaussian Model

To illustrate the concept of closest field, let us now consider a typical uniformly totally polarized Gaussian beam, which is the most widely-used model of a paraxial electromagnetic field. At the initial plane $z = 0$, the electric-field vector, $\boldsymbol{E}_G(x,y)$, would take the form

$$\boldsymbol{E}_G(x,y) = G(x,y)\boldsymbol{E}_0 = G(x,y)(a,ib,0). \tag{4.87}$$

where the (real) constants a and b describe the transverse polarization state and $G(x,y)$ represents the Gaussian field amplitude at $z = 0$. The values $a = 1$, $b = 0$ and $a = b = 1$ correspond, respectively, to the linearly and circularly polarized cases.

It is important to note that, in this paraxial model, the longitudinal field component along the z-axis vanishes.

In terms of the angular spectrum, $\tilde{G}(u,v)$, the function $G(x,y)$ can be written as follows

$$\begin{aligned} G(x,y) &= \int \tilde{G}(u,v)\exp\left[ik(xu+yv)\right]dudv = \\ &= C\int_0^1\int_0^{2\pi}\exp\left(-\frac{\rho^2}{D^2}\right)\exp\left[ik(x\rho\cos\phi + y\rho\sin\phi)\right]\rho\mathrm{d}\rho\mathrm{d}\phi \end{aligned} \tag{4.88}$$

where C is a proportionality constant, and D is another constant (proportional to the divergence at the far field) closely connected with a parameter ω_0 through the relation $D = 1/k\omega_0$. Recall that, according with the current ISO standard that characterizes the transverse size of the field at the waist (ISO, 2005), the diameter of the irradiance profile of the present beam would be $4\omega_0$. Note also that, in this model, the contribution of the evanescent waves is assumed to be negligible.

Under free propagation, the field represented by Eq. (4.87) does not satisfy the condition $\nabla\cdot\boldsymbol{E}_{\mathrm{G}} = 0$, so it cannot be considered as an exact solution of the complete Maxwell equations. It can, however, be useful to get exact solutions through its associated closest solution.

To see this, let us first note that function $\tilde{\boldsymbol{f}}(\rho,\phi)$ introduced above (see Eq. (4.83)) reads now

$$\tilde{\boldsymbol{f}}(\rho,\phi) = C\exp\left(-\frac{\rho^2}{D^2}\right)(a,ib,0). \tag{4.89}$$

Accordingly, the field closest to this Gaussian model will be obtained after applying (4.85), and we get

$$\boldsymbol{E}_{closest} = (\boldsymbol{E}_{\mathrm{TE}})_G + (\boldsymbol{E}_{\mathrm{TM}})_G \tag{4.90}$$

where

$$(\boldsymbol{E}_{\mathrm{TE}})_G = C\int_0^1\int_0^{2\pi}(a\sin\phi - \mathrm{i}b\cos\phi)\exp\left(-\frac{\rho^2}{D^2}\right)\boldsymbol{e}_1\exp(ik\boldsymbol{r}\cdot\boldsymbol{s})\rho d\rho d\phi, \tag{4.91a}$$

$$(\boldsymbol{E}_{\mathrm{TM}})_G = C\int_0^1\int_0^{2\pi}(a\cos\phi + \mathrm{i}b\sin\phi)\sqrt{1-\rho^2}\exp\left(-\frac{\rho^2}{D^2}\right)\boldsymbol{e}_2\exp(\mathrm{i}k\boldsymbol{r}\cdot\boldsymbol{s})\rho d\rho d\phi. \tag{4.91b}$$

It is important to remark that $\boldsymbol{E}_{closest}$, $(\boldsymbol{E}_{\mathrm{TE}})_G$ and $(\boldsymbol{E}_{\mathrm{TM}})_G$ are three free-propagating electric-field exact solutions of the Maxwell equations (without taking the evanescent waves into account). Proceeding in a similar way for the magnetic field we have

$$\boldsymbol{H}_{closest} = (\boldsymbol{H}_{\mathrm{TE}})_G + (\boldsymbol{H}_{\mathrm{TM}})_G, \tag{4.92}$$

where

$$(\boldsymbol{H}_{\mathrm{TE}})_G = C\int_0^1\int_0^{2\pi}(a\sin\phi - \mathrm{i}b\cos\phi)\exp\left(-\frac{\rho^2}{D^2}\right)\boldsymbol{e}_2\exp(\mathrm{i}k\boldsymbol{r}\cdot\boldsymbol{s})\rho d\rho d\phi, \tag{4.93a}$$

$$(\boldsymbol{H}_{\mathrm{TM}})_G = -C\int_0^1\int_0^{2\pi}(a\cos\phi + \mathrm{i}b\sin\phi)\sqrt{1-\rho^2}\exp\left(-\frac{\rho^2}{D^2}\right)\boldsymbol{e}_1\exp(\mathrm{i}k\boldsymbol{r}\cdot\boldsymbol{s})\rho d\rho d\phi. \tag{4.93b}$$

The vector solution given by Eq. (4.91a) represents a field orthogonal to the propagation direction. Consequently, $(\boldsymbol{E}_{\mathrm{TE}})_G$ is a non-paraxial field whose polarization is always transverse to the z-axis upon free propagation. The other field solution, $(\boldsymbol{E}_{\mathrm{TM}})_G$, is not transverse and exhibits a longitudinal component, but its associated magnetic field, $(\boldsymbol{H}_{\mathrm{TM}})_G$, is orthogonal to the z-axis. Although the third non-paraxial solution, $\boldsymbol{E}_{closest}$ has been obtained from the combination of the above fields, $(\boldsymbol{E}_{\mathrm{TE}})_G+(\boldsymbol{E}_{\mathrm{TM}})_G$, its irradiance and polarization structure clearly differs from the other two solutions, as we will see later.

The integrals appearing in Eq. (4.91) are not, in general, analytically solvable, but they provide, however, a suitable procedure to numerically propagate this class of non-paraxial electromagnetic fields. Furthermore, to obtain other families of solutions associated to an arbitrary amplitude $f(x,y)$ at the initial plane, it would suffice to replace the function $\exp(-\rho^2/D^2)$, inside the integrals in Eq. (4.91), by the corresponding angular spectrum associated with $f(x,y)$.

As we pointed out before, Eq. (4.91) do not include the contribution of the evanescent part of spectrum. In highly non-paraxial regimes, in which ω_0 is a fraction of λ, this type of waves could play a significant role (see Sect. 4.5). However, in the present section we will consider beams whose diameters at the waist are greater than 4λ (in other words, $\omega_0 \geq \lambda$). Moreover, the irradiance and the polarization distributions associated to the exact vector solutions will be calculated for propagation distances longer than $d = \omega_0{}^2/\lambda$, which is the so-called diffraction length (Ciattoni et al., 2002). Accordingly, for the beam size and the propagation distances considered in the computations, the influence of the evanescent waves would be negligible. It should also be mentioned that the solution given by Eqs. (4.90) and (4.91) is similar to the Gaussian vectorial wave proposed in Varga and Török (1996).

Let us now investigate the relative magnitude of the Cartesian components of the non-paraxial electric fields obtained from the Gaussian model. More specifically, we consider the ratios (Martínez-Herrero et al., 2006)

$$\frac{\boldsymbol{\varepsilon}_{\mathrm{i}}}{\boldsymbol{\varepsilon}_{\mathrm{j}}} = \frac{\int |E_i|^2\, d\boldsymbol{r}}{\int \left|E_j\right|^2 d\boldsymbol{r}}, \quad i,j = x,y,z, \tag{4.94}$$

where the integrals extend throughout the beam cross-section. In Eq. (4.94), $\boldsymbol{E}$ represents either the combination $(\boldsymbol{E}_{\mathrm{TE}})_{\mathrm{G}}$ + $(\boldsymbol{E}_{\mathrm{TM}})_{\mathrm{G}}$ (Fig. 4.11a) or $(\boldsymbol{E}_{\mathrm{TE}})_{\mathrm{G}}$ and $(\boldsymbol{E}_{\mathrm{TM}})_{\mathrm{G}}$ (Fig. 4.11b). It should be noticed that the above ratios do not change upon free propagation. Consequently, they have the same value at any transverse plane.

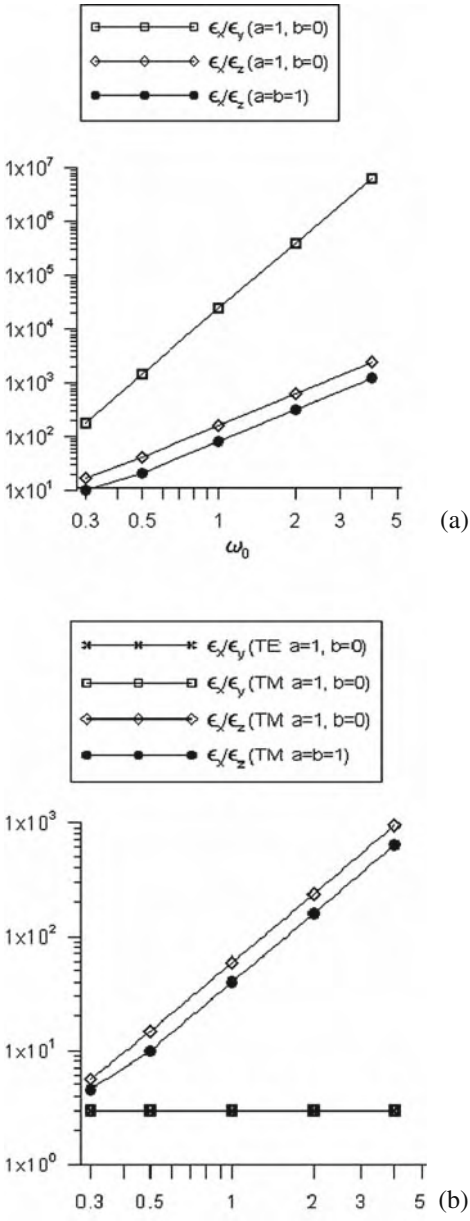

Fig. 4.11 Ratio $\frac{|E_i|^2}{|E_j|^2}$, i,j = x,y,z (integrated across the transverse beam profile) associated with the Cartesian components of the global field $(\boldsymbol{E}_{\mathrm{TE}})_{\mathrm{G}} + (\boldsymbol{E}_{\mathrm{TM}})_{\mathrm{G}}$ (Fig. 4.11a); and $(\boldsymbol{E}_{\mathrm{TE}})_{\mathrm{G}}$ and $(\boldsymbol{E}_{\mathrm{TM}})_{\mathrm{G}}$ (Fig. 4.11b). The abcises are given in terms of the parameter ω_0 (in units of λ). After Martínez-Herrero et al. (2006), with permission

Furthermore, although Fig. 4.11 computes the cases $a = 1$, $b = 0$ (linearly polarized) and $a = b = 1$ (circularly polarized), the conclusions can, however, be applied in a straightforward way to the general elliptically polarized case.

From Figs. 4.11a and 4.11b, we see that the integrated magnitude of the longitudinal component, ε_z, is almost negligible with respect to ε_x (as occurs in the

paraxial regime) for ω_0 higher than, say, 4λ. This behavior is valid in the two cases we are considering (linear and circularly polarized). In general, the vectorial (non-paraxial) effects are always enhanced for small enough values of ω_0. This enables us to establish an approximate limit for the paraxial approach. In fact, the value $\omega_0 \approx 4\lambda$ could be selected as a tentative limit for the validity of the paraxial Gaussian model. This value of the initial beam size agrees with that obtained in Simon et al. (1987) by using a completely different formalism.

We now compare the ratio ε_x / ε_y in Fig. 4.11a (it refers to the combined field $(\boldsymbol{E}_{TE})_G + (\boldsymbol{E}_{TM})_G$) with the corresponding values in Fig. 4.11b for the vector fields $\boldsymbol{E}_{TE}$ and $\boldsymbol{E}_{TM}$. We see in the figure that the ratio ε_x / ε_y is nearly 3 for both, the TE- and the TM-solution, and for any ω_0 (remember that here we are considering the linearly polarized case $a = 1$, $b = 0$).

The combination $(\boldsymbol{E}_{TE})_G + (\boldsymbol{E}_{TM})_G$ shows, however, a quite different behavior: the ratio ε_x / ε_y strongly increases with ω_0 and, in the paraxial regime (i.e., $\omega_0 > 4\lambda$), ε_y is negligible compared with ε_x, as expected. This means that the phases of the y-components of $\boldsymbol{E}_{TE}$ and $\boldsymbol{E}_{TM}$ cause a destructive interference for this component of the global field $(\boldsymbol{E}_{TE})_G + (\boldsymbol{E}_{TM})_G$. On the contrary, the phases associated to the x-components of the vector fields $\boldsymbol{E}_{TE}$ and $\boldsymbol{E}_{TM}$ are arranged in such a way that produce a constructive superposition of these field amplitudes, which, in turn, generates higher values of ε_x for the combined field. Also note that these phase interference effects increase as ω_0 approaches the paraxial limit.

Let us finally consider the spatial distributions associated to the squared modulus of the fields $\boldsymbol{E}_{TE}$, $\boldsymbol{E}_{TM}$ and $(\boldsymbol{E}_{TE})_G + (\boldsymbol{E}_{TM})_G$ at the transverse plane $z = \lambda$, which correspond to the diffraction length d. It should be remarked that the conclusions would remain valid, a scale factor apart, at any transverse plane.

Figures 4.12a and 4.12b show (the hachures in the curves show descents from the contours), that the bell-shaped rotationally-symmetric structure of the transverse profile of a Gaussian beam is no longer valid for the $\boldsymbol{E}_{TE}$ and $\boldsymbol{E}_{TM}$ fields in the case $a = 1$, $b = 0$. Note also that, although Fig. 4.12a is qualitatively similar to the distribution plotted in Fig. 4.12b, their contour lines and numerical values are not the same.

On the other hand, the transverse profile of the global field $(\boldsymbol{E}_{TE})_G + (\boldsymbol{E}_{TM})_G$ resembles the bell-shaped distribution of a Gaussian field, and behaves almost rotationally-symmetric close to the center (see Fig. 4.12c). We therefore conclude that both terms, $\boldsymbol{E}_{TE}$ and $\boldsymbol{E}_{TM}$, should be combined in order that the profile of the resulting exact solution looks like the Gaussian model at a transverse plane.

The behavior of the transverse x-y profile clearly differs in the case $a = b = 1$ (circularly polarized Gaussian model). The three exact solutions, $\boldsymbol{E}_{TE}$, $\boldsymbol{E}_{TM}$, $(\boldsymbol{E}_{TE})_G + (\boldsymbol{E}_{TM})_G$, always exhibit a bell-shaped rotationally-symmetric structure, which closely resembles a typical Gaussian profile around the peak. We thus conclude that this family of exact fields would provide a good fit to the spatial cross-section of the Gaussian model.

Figure 4.13 plots finally the spatial structure of the longitudinal component. It shows a two-lobe shape for $a = 1$, $b = 0$ (see Fig. 4.13a), but the shape corresponds to a doughnut-type distribution in the case $a = b = 1$ (see Fig. 4.13b). It should be noted that, in this example, ε_z would be negligible for ω_0 higher than 4λ.

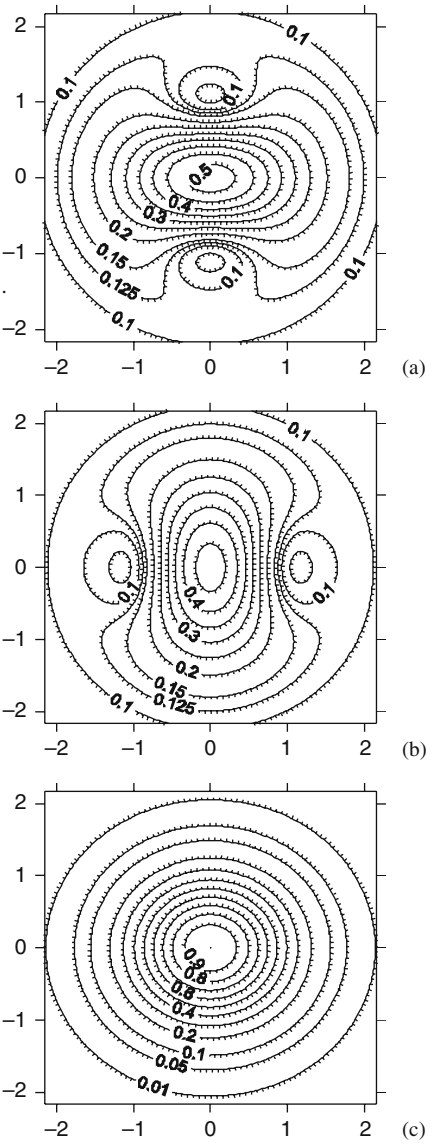

Fig. 4.12 The curves give the square root of the spatial profile at plane $z = \lambda$ associated with the transverse components of the electric-field solutions: (a) $\left[|(\boldsymbol{E}_{TE})_x|^2 + \left|(\boldsymbol{E}_{TE})_y\right|^2\right]^{1/2}$; (b) $\left[|(\boldsymbol{E}_{TM})_x|^2 + \left|(\boldsymbol{E}_{TM})_y\right|^2\right]^{1/2}$; (c) $\left[|(\boldsymbol{E}_{TE})_x + (\boldsymbol{E}_{TM})_x|^2 + \left|(\boldsymbol{E}_{TE})_y + (\boldsymbol{E}_{TM})_y\right|^2\right]^{1/2}$. After Martínez-Herrero et al. (2006), with permission

4.4.3 Transverse Polarization Structure of the Closest Field Associated to the Gaussian Model

To complete the study of the closest field associated to the Gaussian model, we will next spatially describe the transverse polarization distribution at a plane $z =$ constant.

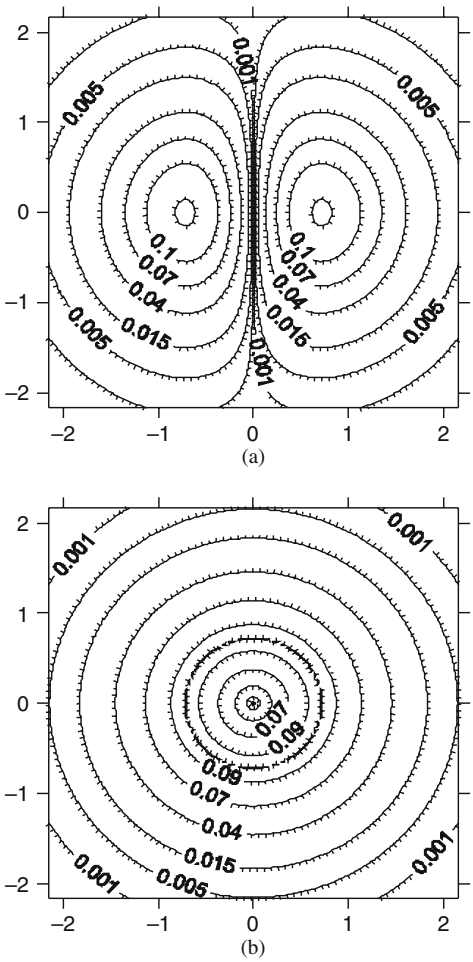

Fig. 4.13 Squared root of the spatial profile at plane $z = \lambda$, associated with the longitudinal z-component in the case $a = 1, b = 0$ (Fig. 4.13a) and $a = b = 1$ (Fig. 4.13b). It has been considered the value $\omega_0 = \lambda$, and the sides of the figures are given in units of λ. The hachures in Fig. 4.13b indicate a doughnut-type spatial shape of the z-component profile. After Martínez-Herrero et al. (2006), with permission

Let us first consider the x- and y-components of the closest field at plane $z = \lambda$, i.e., for very short propagation distances. Recall that $(\boldsymbol{E}_{\mathrm{TM}})_{\mathrm{G}}$ and $(\boldsymbol{E}_{\mathrm{TE}})_{\mathrm{G}} + (\boldsymbol{E}_{\mathrm{TM}})_{\mathrm{G}}$ have the same longitudinal z-component.

From the application of Eq. (4.91), one obtains the spatial distributions we are looking for. They are plotted in Figs. 4.14 and 4.15 for the cases $a = 1$, $b = 0$ and $a = b = 1$, respectively. We see that the polarization diagrams of the TE- and TM-solutions exhibit a non-uniform spatial structure. The diagrams associated with $(\boldsymbol{E}_{\mathrm{TE}})_{\mathrm{G}} + (\boldsymbol{E}_{\mathrm{TM}})_{\mathrm{G}}$ have not been represented because the polarization states across the central region of plane $z = \lambda$ are almost identical to those of a typical uniformly totally-polarized Gaussian field. This occurs when $\omega_0 \approx 4\lambda$, in agreement with the paraxial limit adopted on the basis of the ratio (4.94).

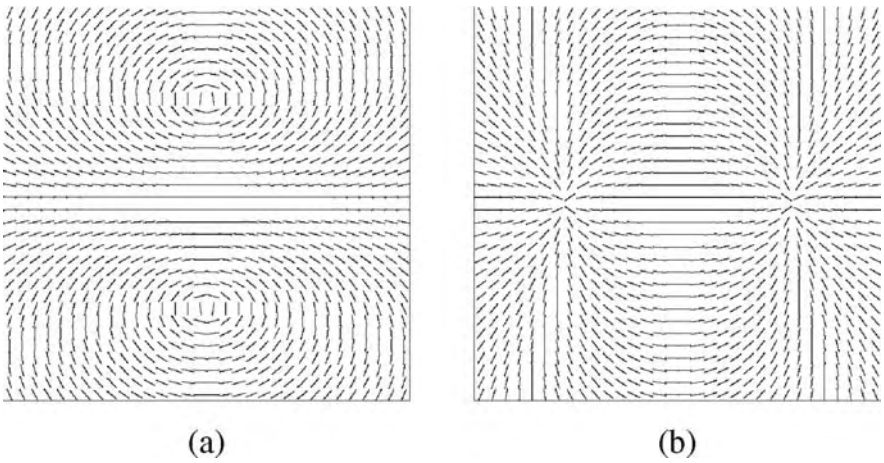

Fig. 4.14 Spatial distribution of the transverse polarization across the beam profile of $\boldsymbol{E}_{\mathrm{TE}}$ (Fig. 4.14a) and $\boldsymbol{E}_{\mathrm{TM}}$ (Fig. 4.14b) in the case $a = 1$, $b = 0$. The diagrams are represented at plane $z = \lambda$ for $\omega_0 = \lambda$. The sides of the figures range from –4λ to +4λ. After Martínez-Herrero et al. (2006), with permission

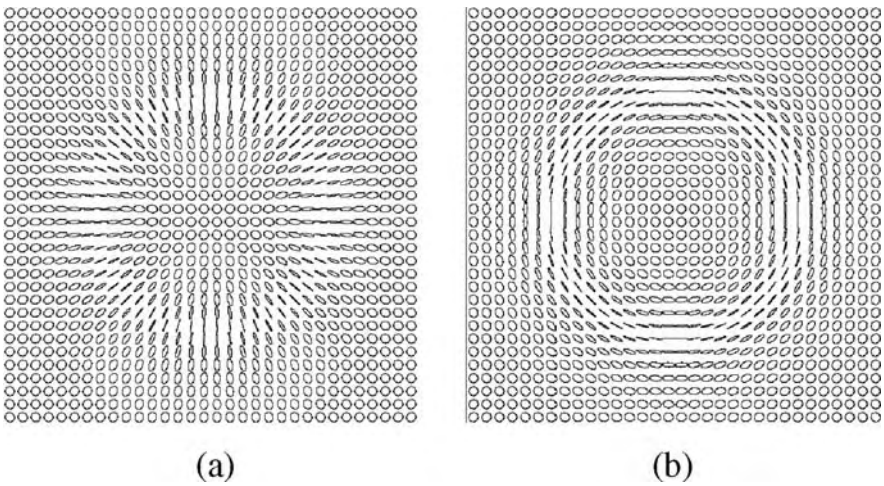

Fig. 4.15 The same as in Fig. 4.14 but now for the values $a = b = 1$. After Martínez-Herrero et al. (2006), with permission

The behavior of the transverse polarization associated with the fields $\boldsymbol{E}_{\mathrm{TE}}$ and $\boldsymbol{E}_{\mathrm{TM}}$ is plotted in Figs. 4.16 and 4.17, calculated at the transverse plane $z = 500\ \lambda$. Note first a "curl-like" structure close to the center in Fig. 4.17a (it also appears in Fig. 4.17b). The right- or left-handed shape of this central region depends on the associate values $b = \pm 1$ in Eq. (4.87). Another characteristic refers to the nearly identical polarization structure outside the central region for both cases, $a = 1$,

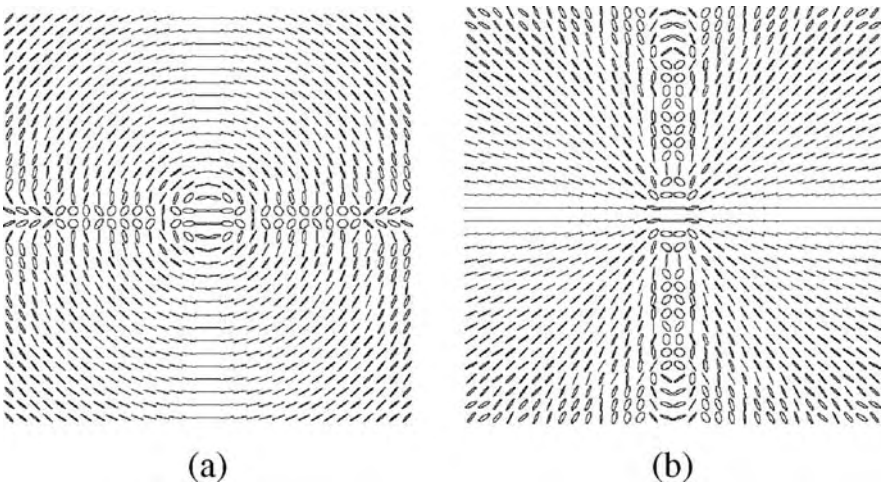

Fig. 4.16 Spatial distributions of the transverse polarization across the beam profile associated to $\boldsymbol{E}_{\mathrm{TE}}$ (Fig. 4.16a) and $\boldsymbol{E}_{\mathrm{TM}}$ (Fig. 4.16b) in the case $a = 1$, $b = 0$. The diagrams are now plotted at plane $z = 500\lambda$. Again, $\omega_0 = \lambda$. The sides of the figures range from –128λ to +128λ. After Martínez-Herrero et al. (2006), with permission

$b = 0$ and $a = b = 1$. This is closely related with the transverse polarization of *any* TE- and TM-beam far away from the initial plane $z = 0$ (see Fig. 4.18): the local polarization states are always linear and show a rotationally-symmetric spatial distribution. This behavior appears for shorter distances when we move away from the paraxial approximation).

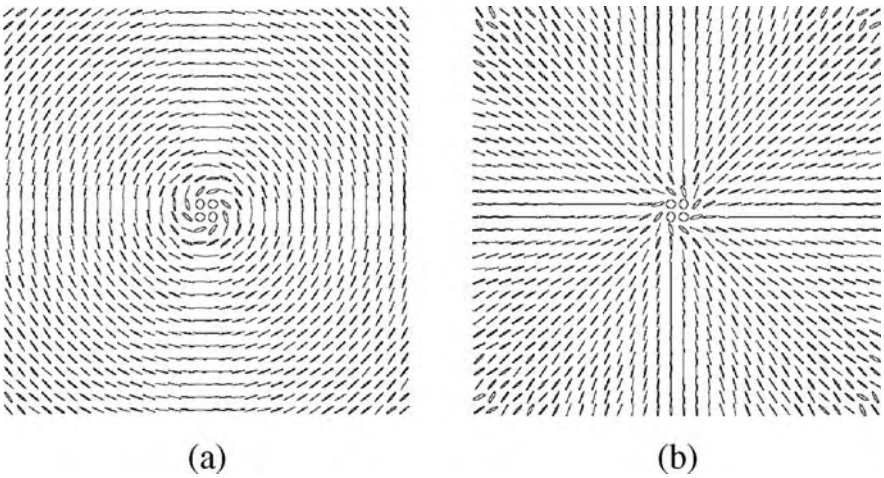

Fig. 4.17 The same as in Fig. 4.16 but now for the values $a = b = 1$. After Martínez-Herrero et al. (2006), with permission

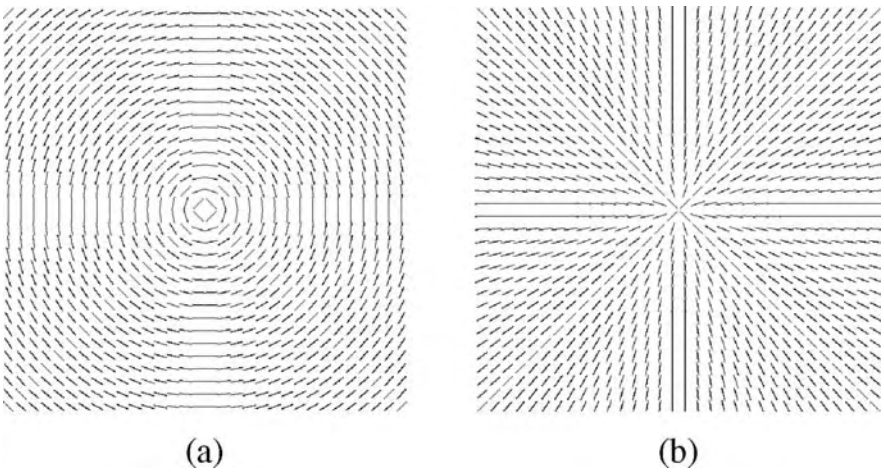

Fig. 4.18 Far-field spatial distribution of the transverse polarization of a TE-field (Fig. 4.18a) and a TM-field (Fig. 4.18b). After Martínez-Herrero et al. (2006), with permission

Summarizing the above results, we conclude that the combination $(\boldsymbol{E}_{\mathrm{TE}})_{\mathrm{G}} + (\boldsymbol{E}_{\mathrm{TM}})_{\mathrm{G}}$ (global closest field) exhibits a transverse part that closely resembles the beam profile and the transverse polarization distribution of the typical uniformly totally-polarized Gaussian model. Accordingly, the field $(\boldsymbol{E}_{\mathrm{TE}})_{\mathrm{G}} + (\boldsymbol{E}_{\mathrm{TM}})_{\mathrm{G}}$ offers an alternative *exact* solution instead of the (approximate) Gaussian field. The price to be paid is the contribution of a (usually small) longitudinal z-component.

4.4.4 Other Examples

We are now interested on the closest field associated to a vector $\boldsymbol{f}(x,y)$ whose transverse components are zero, i.e., $\boldsymbol{f}$ only has longitudinal component z. Accordingly, the corresponding Fourier-transform would read

$$\tilde{\boldsymbol{f}}(\rho,\phi) = (0,0,f_0(\rho,\phi)). \tag{4.95}$$

In addition,

$$\tilde{\boldsymbol{f}} \cdot \boldsymbol{e}_1 = 0, \tag{4.96}$$

and therefore the closest field is a pure TM-beam whose electric and magnetic vector take the form

$$(\boldsymbol{E}_{TM})_{closest} = -\int_0^1 \int_0^{2\pi} \rho f_0(\rho,\phi)\boldsymbol{e}_2 \exp(ik\boldsymbol{r}\cdot\boldsymbol{s})\rho d\rho d\phi, \tag{4.97a}$$

$$(\boldsymbol{H}_{TM})_{closest} = -\int_0^1 \int_0^{2\pi} \rho f_0(\rho,\phi)\boldsymbol{e}_1 \exp(ik\boldsymbol{r}\cdot\boldsymbol{s})\rho d\rho d\phi, \tag{4.97b}$$

In the particular but interesting case in which $f_0(\rho,\phi)$ is independent of ϕ, i.e., $f_0(\rho,\phi) = f_0(\rho)$, the field $\boldsymbol{E}_{\mathrm{TM}}$ transforms into the expression

$$\boldsymbol{E}_{TM}(R,\theta,z) = iF_R(R,z)\boldsymbol{u}_R(\theta) + F_z(R,z)\boldsymbol{u}_z, \tag{4.98}$$

where, for convenience, we have used cylindrical coordinates, and $\boldsymbol{u}_{\mathrm{R}}$ and $\boldsymbol{u}_{\mathrm{z}}$ are again the unit vectors in the radial and longitudinal directions, respectively. In the above equation,

$$F_R(R,z) = -2\pi \int_0^1 \rho f_0(\rho)\sqrt{1-\rho^2}J_1(kR\rho)\exp\left(ikz\sqrt{1-\rho^2}\right)\rho d\rho, \tag{4.99a}$$

$$F_z(R,z) = 2\pi \int_0^1 \rho^2 f_0(\rho)J_0(kR\rho)\exp\left(ikz\sqrt{1-\rho^2}\right)\rho d\rho, \tag{4.99b}$$

We readily conclude from Eq. (4.98) that, in the present case, the closest field $(\boldsymbol{E}_{TM})_{closest}$ exhibits rotational symmetry around the z-axis (as expected), and the polarization at any beam cross-section is always radial. Furthermore, on the propagation axis z ($R = 0$), the closest field reduces to

$$(\boldsymbol{E}_{TM})_{closest}(R=0,z) = F_z(0,z)\boldsymbol{u}_z, \tag{4.100}$$

and the electric field only shows a longitudinal component.

As a final example, let us now consider a vectorial function whose angular spectrum is

$$\tilde{\boldsymbol{f}} = \rho L_n^1\left(\frac{2\rho^2}{D^2}\right)\exp\left(-\frac{\rho^2}{D^2}\right)(\cos\phi,\sin\phi,0), \tag{4.101}$$

where L_n^1 denotes the generalized Laguerre polynomials (Siegman, 1986), $D = 1/k\omega_0$ is again a constant proportional to the far-field divergence of the beam, and ω_0 is the 1/e irradiance beam radius of the Gaussian factor at the near field. More specifically, we now focus our attention on vector fields closest (best fitted) to the vectorial function $\tilde{\boldsymbol{f}}$ defined by Eq. (4.101). We have (Martínez-Herrero et al., 2008a)

$$a(\rho,\phi) = \tilde{\boldsymbol{f}}\cdot\boldsymbol{e}_1 = 0, \tag{4.102a}$$

$$b(\rho,\phi) = \tilde{\boldsymbol{f}}\cdot\boldsymbol{e}_2 = \rho\sqrt{1-\rho^2}L_n^1\left(\frac{2\rho^2}{D^2}\right)\exp\left(-\frac{\rho^2}{D^2}\right). \tag{4.102b}$$

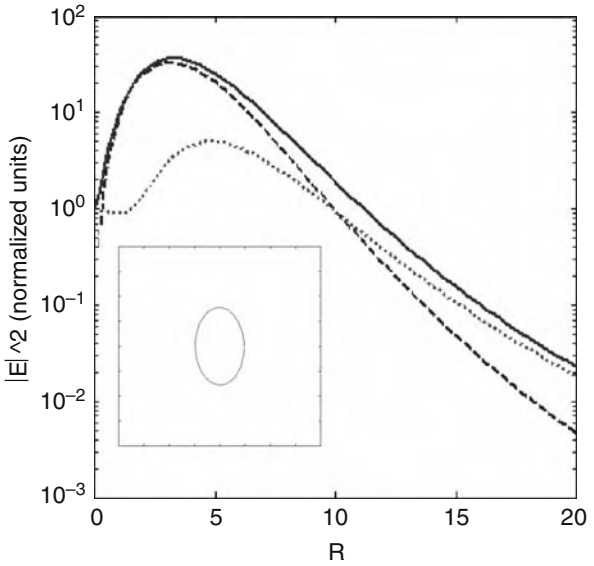

Fig. 4.19 Squared modulus of the electric field at a plane $z = 10\lambda$ for the beam given by Eq. (4.102), with $\omega_0 = 0.3\lambda$ and n = 1. In abcises, the radial distance R is represented in units of λ. Ordinates are plotted in logarithmic scale (the value on the z-axis is normalised to unity). The *continuous line* shows the global field, the *dashed line* plots the radial component (along $\boldsymbol{u}_R$), and the *dotted line* plots the longitudinal component (along $\boldsymbol{u}_z$). The longitudinal component E_z predominates for two ranges of radial distances, $R << \lambda$ and $R >> \lambda$. However, for intermediate distances, $R \approx 10\ \lambda$, the modulus of the radial and the longitudinal components of the field takes almost identical values. The *inset* of this figure illustrates the polarization ellipse that describes the electric field at a radial distance $R = 0.2\ \lambda$: Abcises and ordinates represent the radial and the longitudinal components, respectively. After Martínez-Herrero et al. (2008a), with permission

From these equations, we see that this beam is a RPM field. In addition, by using Eq. (4.75), the beam defined by Eq. (4.102) can be calculated at different transverse planes upon free propagation. Figure 4.19 shows the vectorial structure of these fields in the non-paraxial regime (ω_0 less than λ). It can be summarized as follows:

i) At radial distances close enough to the axis z, the longitudinal field component E_z predominates.
ii) At radial distances far enough from the z-axis, the polarization is essentially longitudinal.
iii) In comparison with the case of Gaussian-model non-paraxial beams, analyzed in the previous section, the longitudinal component E_z has revealed to be much more significant for these RPM fields.
iv) The above general characteristics are also valid for longer propagation distances z.

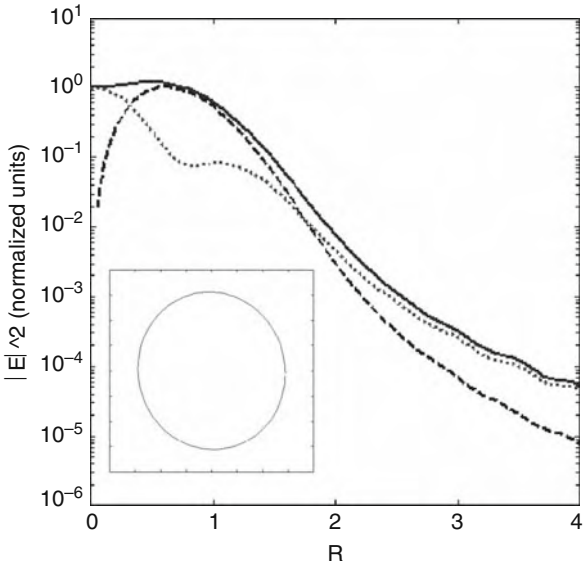

Fig. 4.20 The same as in Fig. 4.19 but now with $z = \lambda$. In the inset the polarization ellipse corresponds to a radial distance $R = 0.3\ \lambda$. After Martínez-Herrero et al. (2008a) with permission.

An example of the polarization ellipse close to the z-axis ($R \sim 0$) is plotted in the inset of Fig. 4.19.

Figure 4.20 (very short propagation distances) exhibits a similar polarization behavior to that observed in the case plotted in Fig. 4.19. Figure 4.21 illustrates the highly non-paraxial case $\omega_0 = 0.1\ \lambda$: The general characteristics shown in Fig. 4.19 are also preserved, in a qualitative way, in the present case.

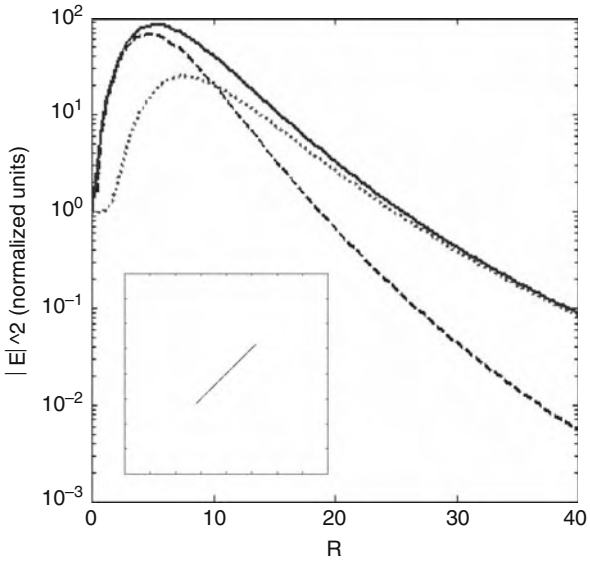

Fig. 4.21 The same as in Fig. 4.19 but now with $\omega_0 = 0.1\lambda$. In the inset the polarization ellipse has been plotted for $R = 10\ \lambda$. After Martínez-Herrero et al. (2008a), with permission

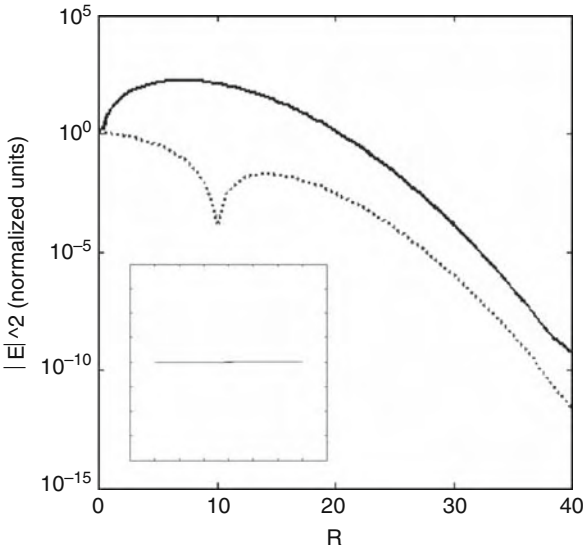

Fig. 4.22 The same as in Fig. 4.19 but now with $\omega_0 = \lambda$. Continuous and dashed lines are indistinguishable. In the inset the polarization ellipse has been shown for $R = 10\ \lambda$. After Martínez-Herrero et al. (2008a), with permission

Figure 4.22 considers the paraxial regime ($\omega_0 = 5\ \lambda$). At each point of the transverse plane, the polarization ellipse essentially behaves as a line along the radial direction, perpendicular to the z-axis. Accordingly, compared with the non-paraxial regime, the magnitude of the longitudinal component, $|E_z|$, is now negligible (as expected).

4.5 Evanescent Waves Associated to Highly Non-paraxial Beams

In Sect. 4.2 the field was decomposed into propagating and evanescent waves (cf. Eqs. (4.13) and (4.14)).Attention will now be devoted to the study of the spatial and vectorial structure of the evanescent field in those cases in which the evanescent term is not negligible. Thus, after introducing the key equations to be used in the rest of this section, a number of numerical examples are shown. They could be considered as the generalization, including the evanescent wave, of the closest field associated to the typical paraxial Gaussian model.

4.5.1 Formalism

Let us extend the formalism handled in Sect. 4.2. We first write the field solution associated to the evanescent term in the alternative equivalent form (see Eqs. (4.13) and (4.14b))

$$\boldsymbol{E}_{ev} = \int_1^{\infty}\int_0^{2\pi} [a(\rho,\phi)\boldsymbol{e}_1(\phi) + b_{ev}(\rho,\phi)\boldsymbol{e}_{ev}(\rho,\phi)] \exp[\mathrm{i}k\boldsymbol{s}_{ev}\cdot\boldsymbol{r})]\,\rho d\rho d\phi, \quad (4.103)$$

where the unit vector $\boldsymbol{e}_1$ was defined earlier, and (Martínez-Herrero et al., 2008b)

$$\boldsymbol{e}_{ev} = \frac{1}{\sqrt{2\rho^2-1}}(\mathrm{i}(\rho^2-1)^{1/2}\cos\phi, \mathrm{i}(\rho^2-1)^{1/2}\sin\phi, -\rho) \quad (4.104a)$$

$$\boldsymbol{s}_{ev} = (\rho\cos\phi, \rho\sin\phi, \mathrm{i}\sqrt{(\rho^2-1)}), \text{ with } \rho\in[1,\infty], \quad (4.104b)$$

are formally vectors with complex components. The structure of $\boldsymbol{s}_{\mathrm{ev}}$ assures the fulfilment of condition (4.8) when $\rho \in [1,\infty]$. For this range of values of ρ, vectors $\boldsymbol{e}_1$ and $\boldsymbol{e}_{\mathrm{ev}}$ are now the two-dimensional reference basis. It should be remarked that the choice of vectors $\boldsymbol{e}_1$, $\boldsymbol{e}_2$ and $\boldsymbol{e}_{\mathrm{ev}}$ characterizes, in fact, the formalism considered in the present chapter. Concerning the notation used to denote inner products when vectors $\boldsymbol{e}_{\mathrm{ev}}$ and $\boldsymbol{s}_{\mathrm{ev}}$ are involved, recall that $\boldsymbol{a}\cdot\boldsymbol{b}$ should be understood as $a_x b_x^* + a_y b_y^* + a_z b_z^*$ (cf. Chap. 1).

The global field $\boldsymbol{E}(R,\theta,z)$ would then read

$$\begin{aligned}\boldsymbol{E}(R,\theta,z) = &\int_0^1\int_0^{2\pi} a(\rho,\phi)\boldsymbol{e_1}(\phi)\exp[\mathrm{i}k\boldsymbol{s}\cdot\boldsymbol{r})]\rho d\rho d\phi\\ &+\int_0^1\int_0^{2\pi} b(\rho,\phi)\boldsymbol{e_2}(\rho,\phi)\exp[\mathrm{i}k\boldsymbol{s}\cdot\boldsymbol{r})]\rho d\rho d\phi\\ &+\int_1^{\infty}\int_0^{2\pi} [a(\rho,\phi)\boldsymbol{e_1}(\phi) + b_{ev}(\rho,\phi)\boldsymbol{e_{ev}}(\rho,\phi)]\exp[\mathrm{i}k\boldsymbol{s_{ev}}\cdot\boldsymbol{r})]\rho d\rho d\phi.\end{aligned} \quad (4.105)$$

We see that functions $a(\rho,\phi)$, $b(\rho,\phi)$ and $b_{\mathrm{ev}}(\rho,\phi)$ contain the complete information about the Fourier spectrum of the $\boldsymbol{E}(R,\theta,z)$ (see Eq. (4.7)). In fact, these functions can be easily obtained from $\tilde{\boldsymbol{E}}_0$ as follows:

$$a(\rho,\phi) = \tilde{\boldsymbol{E}}_0\cdot\boldsymbol{e}_1, \quad (4.106a)$$

$$b(\rho,\phi) = \tilde{\boldsymbol{E}}_0\cdot\boldsymbol{e}_2, \quad (4.106b)$$

$$b_{\mathrm{ev}}(\rho,\phi) = \tilde{\boldsymbol{E}}_0\cdot\boldsymbol{e}_{\mathrm{ev}}. \quad (4.106c)$$

In particular, the evanescent part reveals to be a superposition of inhomogeneous waves whose constant phase surfaces are planes orthogonal to the (non-unitary) transverse vector $\boldsymbol{s}_0$, namely,

$$\boldsymbol{s}_0 = (\rho\cos\phi, \rho\sin\phi, 0), \tag{4.107}$$

and whose constant-amplitude planes are perpendicular to the z-axis. We see that the formal structure of the evanescent term of our global field solution is similar to that of the propagating wave.

In summary, Eq. (4.105) gives a general exact solution of the Maxwell equations, which is valid for both, paraxial and highly-focused beams. The angular spectrum $\tilde{\boldsymbol{E}}_0$ at some initial plane defines each particular field. Furthermore, the magnitude and the polarization features of the transverse profile of any vectorial beam could be calculated from this equation. In particular, its third term provides a simple but general way to determine the evanescent field associated to the exact solution. It should also be noted that the separate contribution of TE-, TM- and evanescent parts of the electric field enables to compare the relative weight of these terms (for instance, by comparing the respective square modulus, integrated throughout the beam profile). This can be used to find the ranges of the propagation distance and of the beam size for which the evanescent waves are significant. Recall that the evanescent term involves the sum $(\tilde{\boldsymbol{E}}_0 \cdot \boldsymbol{e}_1)\boldsymbol{e}_1 + (\tilde{\boldsymbol{E}}_0 \cdot \boldsymbol{e}_{\mathrm{ev}})\boldsymbol{e}_{\mathrm{ev}}$, which can be understood as the projection vector $\tilde{\boldsymbol{E}}_0$ onto the subspace generated by $\boldsymbol{e}_1$ and $\boldsymbol{e}_{\mathrm{ev}}$. A similar interpretation led to the concept of "closest" field to a given vector solution, introduced in the previous section for the propagating term $\boldsymbol{E}_{\mathrm{pr}}$ of the global solution.

4.5.2 Numerical Examples

We will next analyze the evanescent structure of the vectorial field closest (in the algebraic sense) to the polarized Gaussian field. Again, we consider the vector plane-wave spectrum associated to a pure-transverse linearly-polarized Gaussian beam, namely,

$$\tilde{\boldsymbol{f}}(\rho,\phi) = C\exp\left(-\frac{\rho^2}{D^2}\right)(1,0,0), \tag{4.108}$$

where C and D were introduced in Sect. 4.4. To obtain an exact non-paraxial solution based on the paraxial Gaussian model, alternative procedures have been reported in the literature. For example (see, Chaumet, 2006), one may consider that the x- and y-components of the field at the initial plane $z = 0$ exhibits a Gaussian structure. The angular spectrum associated to each transverse component would then be determined by using the inverse Fourier transform, and the plane-wave spectrum of the longitudinal component E_{z} would analytically be derived from the condition (4.8). The global $\boldsymbol{E}(\boldsymbol{r}) = (E_{\mathrm{x}}, E_{\mathrm{y}}, E_{\mathrm{z}})$ (including the evanescent part) would finally propagate into the $z > 0$ half-space according with well-known integral expressions (Chaumet, 2006). The transverse components of such a solution would therefore show a Gaussian profile at plane z = 0.

Here we use another procedure: We start from the Gaussian spectrum given by Eq. (4.108) and write the inner products $\tilde{\boldsymbol{f}} \cdot \boldsymbol{e}_1 = a(\rho,\phi)$; $\tilde{\boldsymbol{f}} \cdot \boldsymbol{e}_2 = b(\rho,\phi)$; and $\tilde{\boldsymbol{f}} \cdot \boldsymbol{e}_{\mathrm{ev}} = b_{\mathrm{ev}}(\rho,\phi)$. We have (Martínez-Herrero et al., 2008b)

$$a(\rho,\phi) = C \sin\phi \exp(-\rho^2/D^2), \tag{4.109a}$$

$$b(\rho,\phi) = C \cos\phi \sqrt{1-\rho^2} \exp(-\rho^2/D^2), \tag{4.109b}$$

$$b_{\mathrm{ev}}(\rho,\phi) = -\frac{\mathrm{i}}{\sqrt{2\rho^2-1}} C \cos\phi (\rho^2-1)^{1/2} \exp(-\rho^2/D^2). \tag{4.109c}$$

Consequently, an exact field solution is derived by substituting functions a, b and b_{ev} into Eq. (4.105). The resulting expression should be understood as the generalization, including the evanescent term, of the closest field associated to the (paraxial) Gaussian field. Also note that, although we have considered the Gaussian case, the procedure can immediately be extended to a general function $\tilde{\boldsymbol{f}}(\rho,\phi)$.

Since in the present section, however, the interest is focused on the evanescent field, we have to choose parametric values for which the evanescent contribution is significant.

Figure 4.23 allows us to evaluate this point. In the figure we represent the ratio

$$\Delta = \frac{|I_{pr} - I_{ev}|}{I_{pr}} \tag{4.110}$$

for the highly non-paraxial case $\omega_0 = 0.1\lambda$ at different propagation distances (in units of λ) from the initial plane $z = 0$, where

$$I_{pr} = \int_0^1 \int_0^{2\pi} \left[|a(\rho,\phi)|^2 + |b(\rho,\phi)|^2 \right] \rho d\rho d\phi, \tag{4.111a}$$

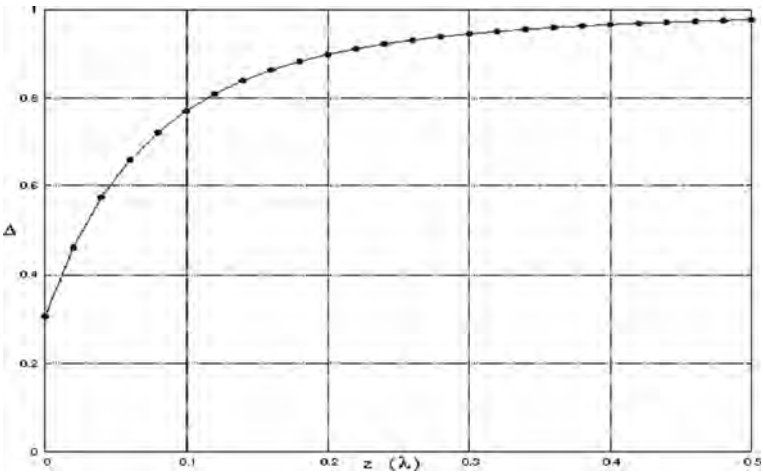

Fig. 4.23 Ratio Δ in terms of the propagation distance z for the field defined by Eq. (4.108), with $\omega_0 = 0.1\lambda$ (highly non-paraxial case). After Martínez-Herrero et al. (2008a), with permission

$$I_{ev} = \int_1^{\infty} \int_0^{2\pi} \left[|a(\rho,\phi)|^2 + |b_{ev}(\rho,\phi)|^2 \right] \exp\left(-2kz\sqrt{\rho^2 - 1} \right) \rho d\rho d\phi, \qquad (4.111b)$$

Therefore, I_{pr} and I_{ev} provide the (integrated) squared modulus of the propagating and evanescent electric fields, respectively. Accordingly, the ratio Δ gives direct information about the importance of the propagating-field solution: Δ ranges from $0.3(I_{\mathrm{ev}} \approx 0.7 I_{\mathrm{pr}})$ to 1 (the evanescent wave vanishes). For the present example, the evanescent field is significant enough for propagation distances not longer than, say, 0.5 λ. Of course, if the waist size ω_0 increases, the relative weight of $\boldsymbol{E}_{\mathrm{ev}}$ would drastically reduce, as expected. For instance, when ω_0 approaches 0.2λ, the distance for noticeable evanescent field does not exceed 0.1λ.

Let us now describe the evanescent spatial structure involved in the closest-field solution associated to the Gaussian model (Martínez-Herrero et al., 2008b).

Figures 4.24, 4.25 and 4.26 plot the transverse distributions of the squared modulus of the electric field components of (i) propagating waves (Fig. 4.24); (ii) evanescent waves (Fig. 4.25); and (iii) global field (Fig. 4.26).

In all the cases the angular spectrum is defined by Eqs. (4.109), and we have chosen the values $\omega_0 = 0.1\lambda$ and $z = 0.1\lambda$. Abcises and ordinates are associated to

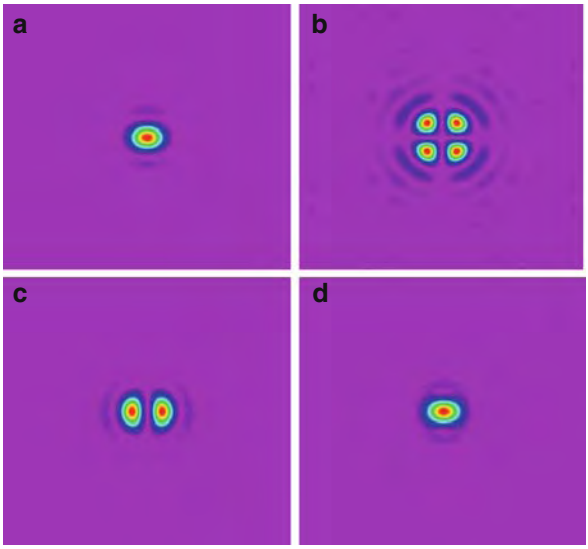

Fig. 4.24 Transverse distributions (pseudocolor) of the squared modulus of the propagating waves for the field defined by Eqs. (4.109). In the figure, $\omega_0 = 0.1\lambda$ and the field magnitude is calculated after propagating a distance $z = 0.1\lambda$. Abcises are parallel to the lines of writing and ordinates are orthogonal to them. (**a**) plot of $(|E_x|^2)_{pr}$; (**b**) $(|E_y|^2)_{pr}$; (**c**) $(|E_z|^2)_{pr}$; (**d**) $(|E_x|^2 + |E_y|^2 + |E_z|^2)_{pr}$. Integration throughout the transverse plane gives the values (**a**) 0.69; (**b**) 0.035; (**c**) 0.085; (**d**) 0.81. These values have been normalised with respect to that of Fig. 4.26d (see below). After Martínez-Herrero et al. (2008a), with permission

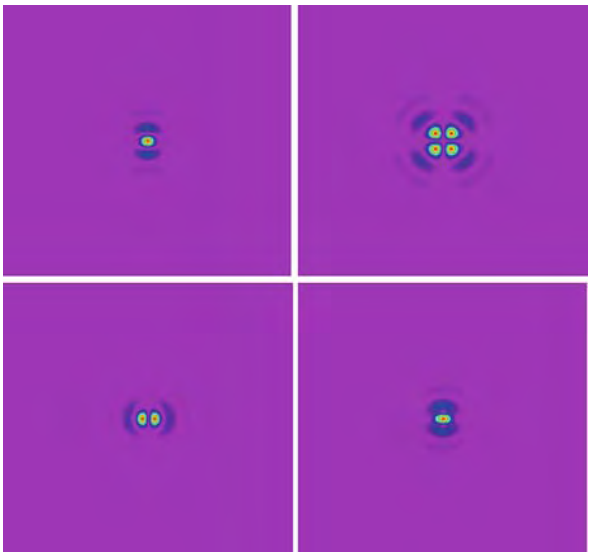

Fig. 4.25 The same as in Fig. 4.24 but now referred to the evanescent waves: (**a**) plot of $\left(|E_x|^2\right)_{ev}$; (**b**) $\left(\left|E_y\right|^2\right)_{ev}$; (**c**) $\left(|E_z|^2\right)_{ev}$; (**d**) $\left(|E_x|^2+\left|E_y\right|^2+|E_z|^2\right)_{ev}$. After integrating throughout the transverse plane, we get the values (**a**) 0.14; (**b**) 0.025; (**c**) 0.025; (**d**) 0.19. After Martínez-Herrero et al. (2008a), with permission

the conventional Cartesian axes x and y, respectively. The length of the side of each square frame is 8 λ. The center of the figures always exhibit peak values. Moreover, integration over the entire plane has been normalised to 1 in Fig. 4.26d. The rest of the plots are then calculated with respect to this value. For instance, in Fig. 4.25d the integration gives the value 0.19. This means that the overall evanescent field

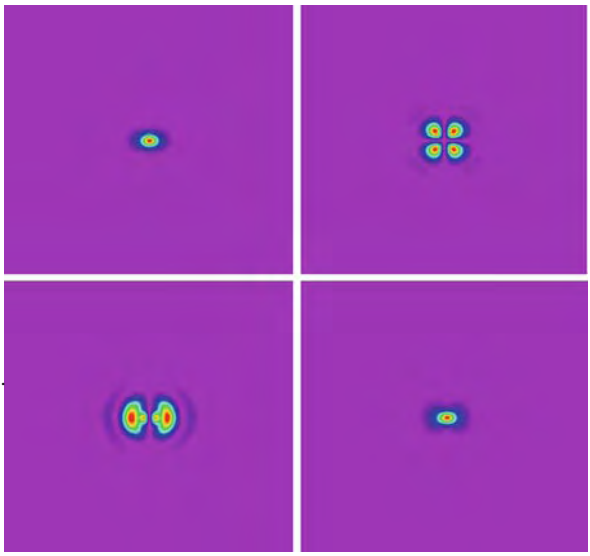

Fig. 4.26 The same as in Fig. 4.24 but now referred to the global field (propagating + evanescent waves): (**a**) plot of $\left(|E_x|^2\right)_{pr+ev}$; (**b**) $\left(\left|E_y\right|^2\right)_{pr+ev}$; (**c**) $\left(|E_z|^2\right)_{pr+ev}$; (**d**) $\left(|E_x|^2+\left|E_y\right|^2+|E_z|^2\right)_{pr+ev}$. After integrating throughout the transverse plane, we obtain the values (**a**) 0.83; (**b**) 0.06; (**c**) 0.11; (**d**) 1. After Martínez-Herrero et al. (2008a), with permission

contributes to the global field (propagating + evanescent waves) in a percentage of 19% (and similarly for the rest of figures).

In addition, Fig. 4.24a shows that $\left(|E_x|^2\right)_{pr}$ is important on a region whose transverse size along the x-axis is nearly λ. This value reduces to 0.5λ for $\left(|E_x|^2\right)_{ev}$ in Fig. 4.25a. Consequently, it should be expected that the size of the region over which is significant enough the squared modulus of the x-component of the global field approaches the intermediate value 0.7λ, in agreement with Fig. 4.26a. An analogous conclusion is derived for the other figures.

From the comparison of Figs. 4.24 and 4.25, a qualitative similarity (a scale factor apart) is also observed between the spatial distributions of the propagating and evanescent fields. Note that no approach has been used to evaluate the electric-field solution represented in the above figures.

For comparative purposes, let us finally consider the closest field associated to a typical circularly-polarized Gaussian beam. In such a case, instead of Eq. (4.108), the vector function $\tilde{\boldsymbol{f}}(\rho,\phi)$ should be

$$\tilde{\boldsymbol{f}}(\rho,\phi) = C \exp\left(-\frac{\rho^2}{D^2}\right)(1,i,0). \tag{4.112}$$

The features of the associated closest-field solution are plotted in Figs. 4.27, 4.28 and 4.29 (Martínez-Herrero et al., 2008b). In the figures, all the graphics (c) and (d) exhibit rotational symmetry, as expected. It should be remarked the different spatial structure shown by the evanescent part with respect to the former case, illustrated in Figs. 4.25 and 4.28. Note also the similar contributions (percentages) involved in the linear and circular cases, associated to the longitudinal z-components (figures (c)) and to the global waves (figures (d)).

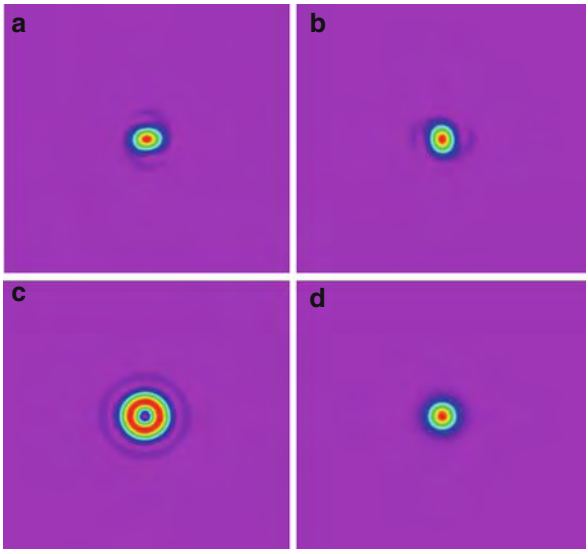

Fig. 4.27 The same as in Fig. 4.24 but now for the closest field associated to a circularly polarized Gaussian beam (cf. Eq. (4.112)). Integration over the complete transverse plane has been normalised with respect to the value of Fig. 4.29d (see below). (**a**) plot of $\left(|E_x|^2\right)_{pr}$; (**b**) $\left(\left|E_y\right|^2\right)_{pr}$; (**c**) $\left(|E_z|^2\right)_{pr}$; (**d**) $\left(|E_x|^2 + \left|E_y\right|^2 + |E_z|^2\right)_{pr}$. After integrating throughout the transverse plane, we get the values (**a**) 0.362; (**b**) 0.362; (**c**) 0.085; (**d**) 0.81. After Martínez-Herrero et al. (2008a), with permission

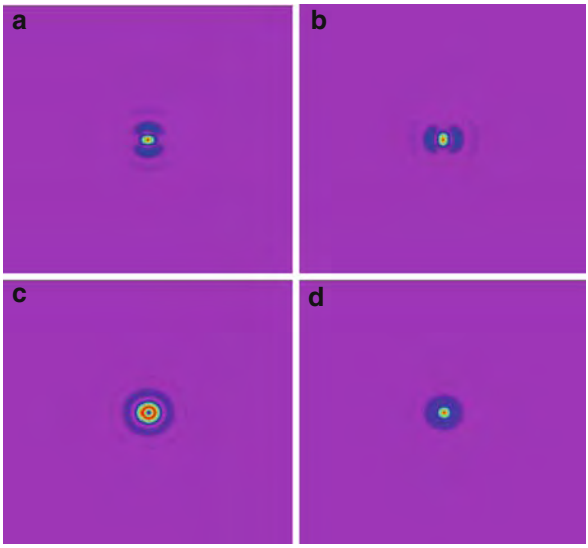

Fig. 4.28 The same as in Fig. 4.27 but now referred to the evanescent waves: (**a**) plot of $(|E_x|^2)_{ev}$; (**b**) $(|E_y|^2)_{ev}$; (**c**) $(|E_z|^2)_{ev}$; (**d**) $(|E_x|^2 + |E_y|^2 + |E_z|^2)_{ev}$. After integrating throughout the transverse plane, we obtain the values (**a**) 0.082; (**b**) 0.082; (**c**) 0.025; (**d**) 0.19. After Martínez-Herrero et al. (2008a), with permission

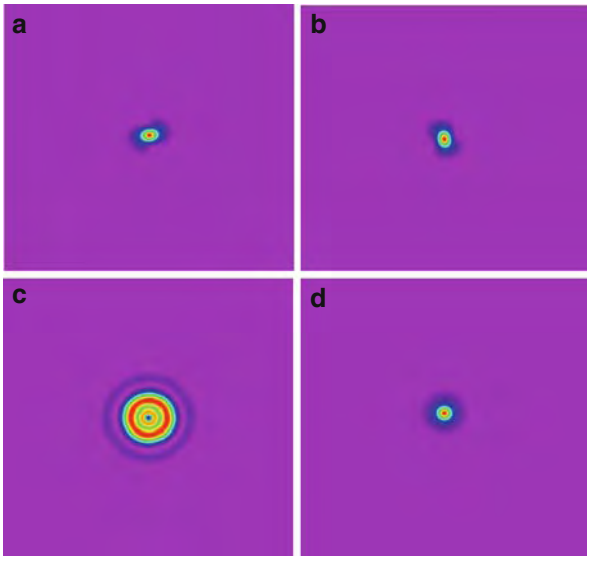

Fig. 4.29 The same as in Fig. 4.27 but now referred to the combined field (propagating + evanescent waves): (**a**) plot of $(|E_x|^2)_{pr+ev}$; (**b**) $(|E_y|^2)_{pr+ev}$; (**c**) $(|E_z|^2)_{pr+ev}$; (**d**) $(|E_x|^2 + |E_y|^2 + |E_z|^2)_{pr+ev}$. After integrating throughout the transverse plane, we get the values (**a**) 0.445; (**b**) 0.445; (**c**) 0.11; (**d**) 1. After Martínez-Herrero et al. (2008a), with permission

4.6 Partially Coherent Electromagnetic TE-Fields

The last section of this chapter examines non-paraxial fields with a partially coherent behavior. Previous studies (see, for example Tervo (2003)) have extended the vectorial case to cover partially coherent fields. In those papers, the field was propagated from a source plane, and changes in the degree of polarization were analyzed upon

propagation. Here we restrict ourselves to non-paraxial TE-fields, and the attention will be devoted to investigate the connection between their polarization and coherence features. Note that, in general, the polarization state would involve the three field components. It should then be expected that a pure transversal character will play a significant role in the polarization behavior of a non-paraxial field.

To begin with, let us first recall that the longitudinal component of TE-fields (in the sense defined in Sect. 4.2) should vanish, and their spectral density tensor (SDT) reduces to a 2×2 matrix, $\hat{W}(\boldsymbol{r},\boldsymbol{r})$. We then have

$$W_{\mathrm{ij}}\left(\boldsymbol{r},\boldsymbol{r}\right)=\overline{E_{\mathrm{i}}^{*}\left(\boldsymbol{r}\right)E_{\mathrm{j}}\left(\boldsymbol{r}\right)},\ \mathrm{i,j}=\mathrm{s,p}. \tag{4.113}$$

Neglecting the contribution of the evanescent waves, the SDT of a non-paraxial partially coherent TE-field would be written at a transverse plane z in the form (Martínez-Herrero and Moreu, 2006)

$$\begin{aligned}\hat{W}_{\mathrm{TE}}\left(R,\theta,z\right)=&\int_{0}^{1}\int_{0}^{1}\int_{0}^{2\pi}\int_{0}^{2\pi}\Gamma_{\mathrm{TE}}\left(\rho_1,\rho_2,\phi_1,\phi_2\right)\boldsymbol{e}_1^{t}\left(\phi_1\right)\boldsymbol{e}_1\left(\phi_2\right)\times\\&\times\exp\left\{ikR\left[\rho_2\cos\left(\theta-\phi_2\right)-\rho_1\cos\left(\theta-\phi_1\right)\right]\right\}\times\\&\times\exp\left\{ikz\left[\left(1-\rho_2^2\right)^{1/2}-\left(1-\rho_2^2\right)^{1/2}\right]\right\}\rho_1\rho_2 d\rho_1 d\rho_2 d\phi_1 d\phi_2\end{aligned} \tag{4.114}$$

where R, θ, z are the cylindrical coordinates that give the position of a point at the transverse plane, the superscript t denotes the transposed vector, and

$$\Gamma_{TE}\left(\rho_1,\rho_2,\phi_1,\phi_2\right)=\overline{a^{*}\left(\rho_1,\phi_1\right)a\ \left(\rho_2,\phi_2\right)}. \tag{4.115}$$

In Eq. (4.115) $a(\rho,\phi)$ represents a stochastic process, which is related to the field $\boldsymbol{E}_{\mathrm{TE}}$ through the equality (in the mean square sense)

$$\boldsymbol{E}_{\mathrm{TE}}=\int_{0}^{1}\int_{0}^{2\pi}a\left(\rho,\phi\right)\boldsymbol{e}_1\left(\phi\right)\exp\left(ik\boldsymbol{r}\cdot\boldsymbol{s}\right)\rho d\,\rho d\phi. \tag{4.116}$$

Associated to the plane-wave spectrum of the field, the SDT would read

$$\left(\hat{W}_{\mathrm{TE}}\right)_{pw}=\overline{\left|a\ \left(\rho,\phi\right)\right|^{2}}\boldsymbol{e}_1^{t}\left(\phi\right)\boldsymbol{e}_1\left(\phi\right), \tag{4.117}$$

where the subscript pw refers to the plane-wave spectrum. By recalling the expression that gives the local degree of polarization in terms of $\hat{W}$, namely,

$$P\left(\boldsymbol{r}\right)=\left(1-\frac{4\mathrm{Det}\hat{W}(\boldsymbol{r},\boldsymbol{r})}{\left(\mathrm{Tr}\hat{W}(\boldsymbol{r},\boldsymbol{r})\right)^{2}}\right)^{1/2}, \tag{4.118}$$

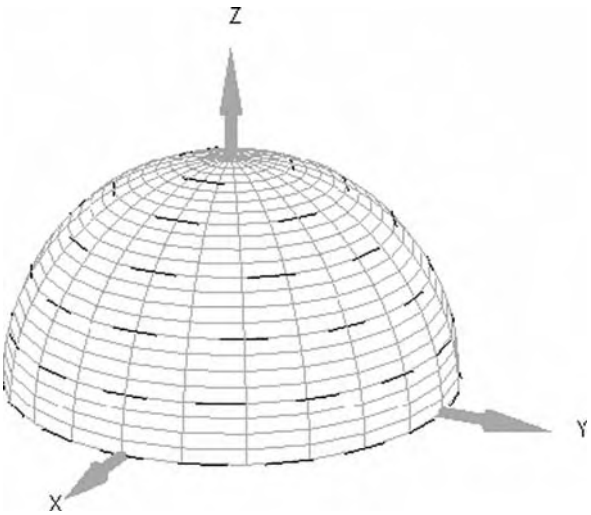

Fig. 4.30 Polarization diagram associated to the plane-wave spectrum of a TE field. Every point on the sphere represents a direction characterized by its ρ and ϕ coordinates. The segments illustrate directions of polarization for some (ρ,ϕ) values. After Martínez-Herrero and Moreu (2006), with permission

one sees that matrix $(\hat{W}_{\mathrm{TE}})_{pw}$, involves a non-uniformly totally polarized behavior. This is illustrated in Fig. 4.30.

Let us now consider the spatial distribution of the polarization state at a transverse plane z (near field). We first assume rotational symmetry of the function Γ_{TE}, i.e.,

$$\Gamma_{TE}\left(\rho_1,\rho_2,\phi_1,\phi_2\right) = \Gamma_0\left(\rho_1,\rho_2\right) \tag{4.119}$$

where $\Gamma_0\left(\rho_1,\rho_2\right)$ is an integrable function in the region [0,1]×[0,1]. Making use of this expression, we get after substitution into Eq. (4.114)

$$\hat{W}_{\mathrm{TE}}\left(R,\theta,z\right) = \boldsymbol{e}_0^t\left(\theta\right)\,\boldsymbol{e}_0\left(\theta\right) f\left(R,z\right) \tag{4.120}$$

where $\boldsymbol{e}_0$ denotes the two-dimensional unit vector,

$$\boldsymbol{e}_0\left(\theta\right) = \left(\sin\theta, -\cos\theta\right) \tag{4.121}$$

and

$$\begin{aligned} f\left(R,z\right) = -4\pi^2 \int_0^1 \int_0^1 \Gamma_0\left(\rho_1,\rho_2\right) J_1\left(kR\rho_1\right) J_1\left(kR\rho_2\right) \times \\ \times \exp\left\{ikz\left[\left(1-\rho_2^2\right)^{1/2} - \left(1-\rho_1^2\right)^{1/2}\right]\right\} \rho_1\rho_2 d\rho_1 d\rho_2, \end{aligned} \tag{4.122}$$

J_1 being, as usual, the first-order Bessel function. Thus, rotational symmetry of function Γ_{TE} involves a (non-uniformly) totally polarized behavior (azimuthally polarized) at the near field.

As a second case of interest, we now assume that Γ_{TE} is factorizable and takes the form

$$\Gamma_{TE}\left(\rho_1,\rho_2,\phi_1,\phi_2\right) = A^*\left(\rho_1,\phi_1\right) A\left(\rho_2,\phi_2\right) \tag{4.123}$$

so that matrix $\hat{W}_{\mathrm{TE}}$ becomes

$$\hat{W}_{TE}\left(R,\theta,z\right) = \boldsymbol{F}^{\dagger}\left(R,\theta,z\right) \boldsymbol{F}\left(R,\theta,z\right) \tag{4.124}$$

where the deterministic vector $\boldsymbol{F}\left(R,\theta,z\right)$ is given by the expression

$$\begin{aligned} \boldsymbol{F}\left(R,\theta,z\right) = & \int_0^1 \int_0^{2\pi} A\left(\rho,\phi\right) \boldsymbol{e}_1\left(\phi\right) \exp\left[ikR\rho\cos\left(\theta-\phi\right)\right] \\ & \exp\left[ikz\left(1-\rho^2\right)^{1/2}\right] \mathrm{d}\rho\mathrm{d}\phi. \end{aligned} \tag{4.125}$$

Since $\hat{W}_{\mathrm{TE}}$ is factorizable, the local degree of polarization equals 1 at any transverse plane z.

Let us now consider the other extreme case, i.e., we assume that function Γ_{TE} reads

$$\Gamma_{TE}\left(\rho_1,\rho_2,\phi_1,\phi_2\right) = I\left(\rho_1,\phi_1\right) \delta\left(\rho_1-\rho_2\right) \delta\left(\phi_1-\phi_2\right), \tag{4.126}$$

where the symbol δ denotes again the Dirac delta function and $I\left(\rho,\phi\right)$ is proportional to the beam irradiance associated to each plane-wave spectral component. One obtains that the SDT is constant (independent on coordinates R, θ and z), and takes the form

$$\hat{W}_{\mathrm{TE}} = \int_0^1 \int_0^{2\pi} I\left(\rho,\phi\right) \boldsymbol{e}_1^t\left(\phi\right) \boldsymbol{e}_1\left(\phi\right) \rho d\rho d\phi. \tag{4.127}$$

Accordingly, the local degree of polarization is also constant, and satisfies

$$0 \leq P < 1. \tag{4.128}$$

In order to show that P cannot be equal to 1, it would suffice to note that the following inequality occurs between the elements of a matrix $\hat{W}_{\mathrm{TE}}$ given by Eq. (4.127):

$$\left|\left(\hat{W}_{\mathrm{TE}}\right)_{12}\right|^2 < \left(\hat{W}_{\mathrm{TE}}\right)_{11}\left(\hat{W}_{\mathrm{TE}}\right)_{22}, \text{ for any } I\left(\rho,\phi\right). \tag{4.129}$$

In the case we are analysing, the field, at any transverse plane, could be either uniformly partially polarized or unpolarized. This second type of behavior arises

when function I is independent of the coordinate ϕ (note that $\boldsymbol{e}_1$ does not depend on ρ).

To study an intermediate case, let us use the following modal expansion of function Γ_{TE} (Martínez-Herrero, 1979)

$$\Gamma_{TE}\left(\rho_1,\rho_2,\phi_1,\phi_2\right) = \sum_n \lambda_n^2 A_n^*\left(\rho_1,\phi_1\right) A_n\left(\rho_2,\phi_2\right) \tag{4.130}$$

where $A_n(\rho,\phi)$ represents a set of integrable mutually-orthonormal functions in the region $\rho \in [0,1]$, $\phi \in [0,2\pi]$, and $\lambda_n{}^2$ are non-negative numbers.

The SDT becomes in this case (Martínez-Herrero and Moreu, 2006)

$$\hat{W}_{TE}\left(R,\theta,z\right) = \sum_n \lambda_n^2 \boldsymbol{F}_n^{\dagger}\left(R,\theta,z\right) \boldsymbol{F}_n\left(R,\theta,z\right), \tag{4.131}$$

where

$$\begin{aligned} \boldsymbol{F}_n\left(R,\theta,z\right) = \int_0^1 \int_0^{2\pi} & A_n\left(\rho,\phi\right) \boldsymbol{e}_1\left(\phi\right) \exp\left[ikR\rho\cos\left(\theta-\phi\right)\right] \\ & \exp\left[ikz\left(1-\rho^2\right)^{1/2}\right] \rho d\rho d\phi, \end{aligned} \tag{4.132}$$

and one observes, in general, non-uniform partial polarization at the near field.

This result can be illustrated in a simple way by considering a field defined by the following function Γ_{TE}:

$$\Gamma_{TE}\left(\rho_1,\rho_2,\phi_1,\phi_2\right) = \exp\left[-D^2\left(\rho_1^2+\rho_2^2\right)\right]\cos\left(\phi_1-\phi_2\right). \tag{4.133}$$

By using Eqs. (4.131), (4.132), and (4.133), it can be shown that the local degree of polarization becomes (Martínez-Herrero and Moreu, 2006)

$$P\left(R,z\right) = \left\{\frac{4I_0\left(R,z\right) I_2\left(R,z\right)}{\left[I_0\left(R,z\right)+I_2\left(R,z\right)\right]^2}\right\}^{1/2}, \tag{4.134}$$

where

$$I_n\left(R,z\right) = \pi^2 \left| \int_0^1 \exp\left(-\rho^2 D\right) J_n\left(kR\rho\right) \exp\left[ikz\left(1-\rho^2\right)^{1/2}\right] \rho d\rho \right|^2, n = 0,2, \tag{4.135}$$

$J_0 J_2$ being the zero and second-order Bessel functions, respectively. The transverse behavior of P at plane $z = 0$ is plotted in Fig. 4.31.

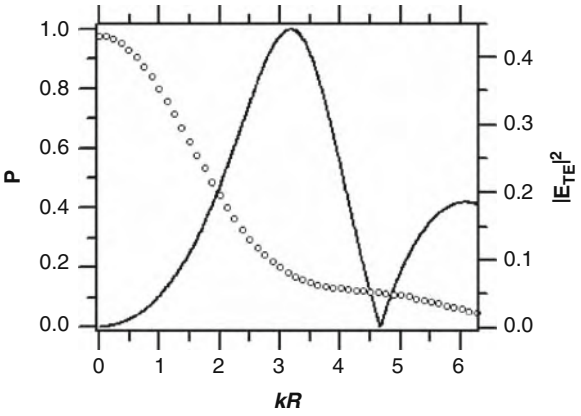

Fig. 4.31 Local degree of polarization (continuous line) at plane $z = 0$, for a field given by Eq (4.133), with $D = 1$. The ordinates scale of the right-hand side of this figure refers to the normalized squared modulus of the TE-field (dotted line). After Martínez-Herrero and Moreu (2006), with permission

From this figure, it is clear the non-uniformly partially-polarized behavior at the initial plane. Moreover, P does not depend on θ, and reaches maximum and minimum values at certain distances from the z-axis.

Note finally that, in this example, function $\Gamma_{\mathrm{TE}}(\rho,\rho,\phi,\phi)$ is rotationally symmetric, even though $\Gamma_{\mathrm{TE}}(\rho_1,\rho_2,\phi_1,\phi_2)$ is not.

References

Agrawal, G. P., Lax, M. (1983): Free-space wave propagation beyond the paraxial approximation, Phys. Rev. A 27, 1693–1695.

Alonso, M. A. (2004): Wigner functions for nonparaxial, arbitrarily polarized electromagnetic wave fields in free space, J. Opt. Soc. Am. A 21, 2233–2243.

Alonso, M. A., Borghi, R., Santarsiero, M. (2006a): Nonparaxial fields with maximum joint spatial-directional localization. I. Scalar case, J. Opt. Soc. Am. A 23, 691–700.

Alonso, M. A., Borghi, R., Santarsiero, M. (2006b): Nonparaxial fields with maximum joint spatial-directional localization. II. Vectorial case, J. Opt. Soc. Am. A 23, 701–712.

April, A. (2008): Nonparaxial TM and TE beams in free space, Opt. Lett. 33, 1563–1565.

Arnoldus, H. F., Foley, J. T. (2002): Traveling and evanescent fields of an electric point dipole, J. Opt. Soc. Am. A 19, 1701–1711.

Belkebir, K., Chaumet, P. C., Sentetac, A. (2006): Influence of multiple scatering on three-dimensional imaging with optical diffraction tomography, J. Opt. Soc. Am. A 23, 586–595.

Borghi, R., Ciattoni, A., Santarsiero, M. (2002): Exact axial electromagnetic field for vectorial Gaussian and flattened Gaussian boundary distribution, J. Opt. Soc. Am. A 19, 1207–1211.

Borghi, R., Santarsiero, M. (2003): Summing lax series for nonparaxial beam propagation, Opt. Lett 28, 774–776.

Borghi, R., Santarsiero, M. (2004): Nonparaxial propagation of spirally polarized optical beams, J. Opt. Soc. Am. A 21, 2029–2037.

Chaumet, P. C. (2006): Fully vectorial highly nonparaxial beam close to the waist, J. Opt. Soc. Am. A 23, 3197–3202.

Chen, C. G., Konkola, P. T., Ferrera, J., Heilman, R. K., Schattenburg, M. L. (2002): Analyses of vector Gaussian beam propagation and the validity of paraxial and spherical approximation, J. Opt. Soc. Am. A 19, 404–412.

Ciattoni, A., Crosignani, B., Di Porto, P. (2002): Vectorial analytical description of propagation of a highly nonparaxial beam, Opt. Commun. 202, 17–20.
Deng, D. M. (2006): Nonparaxial propagation of radially polarized light beams, J. Opt. Soc. Am. B 23, 1228–1234.
Deng, D. M., Guo, Q. (2007): Analytical vectorial structure of radially polarized light beams, Opt. Lett. 32, 2711–2713.
Diehl, D. W., Schoonover, R. W., Visser, T. D. (2006): The structure of focused radially polarized fields, Opt. Express 14, 3030–3038.
Dorn, R., Quabis, S., Lenchs, G. (2003): Sharper focus for a radially polarized light beam, Phys. Rev. Lett. 91, 233901 (1–4).
Duan, K., Lü, B. (2005a): Polarization properties of vectorial nonparaxial Gaussian beam in the far field, Opt. Lett. 30, 308–310.
Duan, K., Lü, B. (2005b): Wigner-distribution-function matrix and its application to partially coherent vectorial nonparaxial beams, J. Opt. Soc. Am. B 22, 1585–1593.
Guo, H. M., Chen, J. B., Zhuang, S. L. (2006): Vector plane wave spectrum of an arbitrary polarized electromagnetic wave, Opt. Express 14, 2095–2100.
Hall, D. G. (1996): Vector-beam solutions of Maxwell's waves equation, Opt. Lett. 21, 9–11.
ISO 11146 (2005): Laser and laser related equipment – Test methods for laser beam widths, divergence angles and beam propagation ratios, Parts 1, 2 and 3 (International Organization for Standardization, Geneva, Switzerland).
Lekner, J. (2003): Polarization of tightly focused laser beams, J. Opt. A: Pure Appl. Opt. 5, 6–14.
Machavariani, G., Lumer, Y., Moshe, I., Meir, A., Jackel, S. (2008): Spatially-variable retardation plate for efficient generation of radially- and azimuthally-polarized beams, Opt. Commun. 281, 732–738.
Mandel, L., Wolf, E. (1995): *Optical Coherence and Quantum Optics* (Cambridge University Press, Cambridge).
Martínez-Herrero, R. (1979): Expansion of complex degree of coherente, Il Nuevo Cimento B, 54, 205–210.
Martínez-Herrero, R., Mejías, P. M. (2008): Propagation of light fields with radial or azimuthal polarization distribution at a transverse plane, Opt. Express 16, 9021–9033.
Martínez-Herrero, R., Mejías, P. M., Bosch, S. (2008a): On the vectorial structure of non-paraxial radially polarized light fields, Opt. Commun. 281, 3046–3050.
Martínez-Herrero, R., Mejias, P. M., Carnicer, A. (2008b): Evanescent field of vectorial highly non-paraxial beams, Opt. Express 16, 2845–2858.
Martínez-Herrero, R., Mejías, P. M., Bosch, S., Carnicer, A. (2001): Vectorial structure of nonparaxial electromagnetic beams, J. Opt. Soc. Am. A 18, 1678–1680.
Martínez-Herrero, R., Mejías, P. M., Bosch, S., Carnicer, A. (2006): Structure of the transverse profile of Gaussian-model non-paraxial electromagnetic beams, J. Opt. A: Pure Appl. Opt. 8, 524–530.
Martínez-Herrero, R., Moreu, A. F. (2006): On the polarization of non-paraxial transverse fields, Opt. Commun. 267, 20–23.
Mei, Z. R., Zhao, D. M. (2008): Non-paraxial propagation of controllable dark-hollow beams, J. Opt. Soc. Am. A 25, 537–542.
Mejías, P. M., Martínez-Herrero, R., Piquero, G., Movilla, J. M. (2002): Parametric characterization of the spatial structure of non-uniformly polarized laser beams, Prog. Quantum Electron. 26, 65–130.
Nesterov, A. V., Niziev, V. G., Yakunin, V. P. (1999): Generation of high-power radially polarized beam, J. Phys. D 32, 2871–2875.
Niu, C. H., Gu, B. Y., Dong, B. Z., Zhang, Y. (2005): A new method for generating axially-symmetric and radially-polarized beams, J. Phys. D 38, 827–832.
Pääkkönen, P., Tervo, J., Vahimaa, P., Turunen, J., Gori, F. (2002): General vectorial decomposition of electromagnetic fields with application to propagation-invariant and rotating fields, Opt. Express 10, 949–959.

Petrov, N. I. (1999): Nonparaxial focusing of wave beams in a graded-index medium, Quantum Electron. 29, 249–255.
Seshadri, S. R. (1998): Electromagnetic Gaussian beam, J. Opt. Soc. Am. A 15, 2712–2719.
Seshadri, S. R. (2008): Fundamental electromagnetic Gaussian beam beyond the paraxial approximation, J. Opt. Soc. Am. A 25, 2156–2164.
Setala, T., Friberg, A. T., Kaivola, M. (1999): Decomposition of the point-dipole field into homogeneous and evanescent parts, Phys. Rev. E 59, 1200–1206.
Shchegrov, A. V., Carney, P. S. (1999): Far-field contribution to the electromagnetic Green's tensor from evanescent modes, J. Opt. Soc. Am. A 16, 2583–2584.
Sherman, G. C., Stamnes, J. J., Lalor, E. (1976): Asymptotic approximations to angular-spectrum representations, J. Math. Phys. 17, 760–776.
Sheppard, C. J. R. (2000): Polarization of almost-planes waves, J. Opt. Soc. Am. A 17, 335–341.
Sheppard, C. J. R., Saghafi, S. (1999): Electromagnetic Gaussian beams beyond the paraxial approximation, J. Opt. Soc. Am. A 16, 1381–1386.
Siegman, A. E. (1986): *Lasers* (University Science Books, California).
Simon, R., Sudarshan, E. C. G., Mukunda, N. (1987): Cross polarization in laser beams, Appl. Opt. 26, 1589–1593.
Tervo, J. (2003): Azimuthal polarization and partial coherence, J. Opt. Soc. Am. A 20, 1974–1980.
Tervo, J., Turunen, J. (2001): Self-imaging of electromagnetic fields, Opt. Express 9, 622–630.
Varga, P., Török, P. (1996): Exact and approximate solutions of Maxwell's equation and the validity of the scalar wave approximation, Opt. Lett. 21, 1523–1525.
Varga, P., Török, P. (1998): The Gaussian wave solution of Maxwell's equations and the validity of the scalar wave approximation, Opt. Commun. 152, 108–118.
Volpe, G., Petrov, D. (2004): Optical tweezers with cylindrical vector beams produced by optical fibers, Opt. Commun. 237, 89–95.
Wolf, E., Foley, J. T. (1998): Do evanescent waves contribute to the far field?, Opt. Lett. 23, 16–18.
Yan, S. H., Yao, B. L. (2008): Accurate description of a radially polarized Gaussian beam, Phys. Rev. A 77, 023827(1–4).
Yew, E. Y. S., Sheppard, C. J. R. (2007): Tight focusing of radially polarized Gaussian and Bessel-Gauss beams, Opt. Lett. 32, 3417–3419.
Zhang, Z., Pu, J., Wang, X. (2008): Tight focusing of radially and azimuthally polarized vortex beams through a uniaxial birefringent crystal, Appl. Opt. 47, 1963–1967.
Zhou, G. Q. (2006): Analytical vectorial structure of Laguerre-Gaussian beam in the far field, Opt. Lett. 31, 2616–2618.
Zhou, G. Q. (2008): The analytical vectorial structure of non-paraxial Gaussian beam close to the source, Opt. Express 16, 3504–3514.

Index

R. Martínez-Herrero et al., *Characterization of Partially Polarized Light Fields*, Springer Series in Optical Sciences 147, DOI 10.1007/978-3-642-01327-0_BM2,